

Knowledge-Based Optimization of  
Cell Culture Production Media  
Wissensbasierte Optimierung von  
Zellkulturproduktionsmedien

DISSERTATION

Von der Fakultät Energie-, Verfahrens- und Biotechnik der Universität Stuttgart  
zur Erlangung der Würde eines Doktors der Naturwissenschaften  
(Doctor rerum naturalium, Dr. rer. nat.) genehmigte Abhandlung

Vorgelegt von

**Natascha Sigrid Helga Ursula Verhagen**

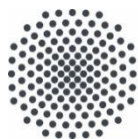
aus Stuttgart

*Hauptberichter:* Prof. Dr.-Ing. Ralf Takors

*Mitberichter:* Prof. Dr. Roland Kontermann

Tag der mündlichen Prüfung: 17.05.2021

Institut für Bioverfahrenstechnik der Universität Stuttgart



**Universität Stuttgart**

2021



*Ein Gelehrter in einem Laboratorium ist nicht nur ein  
Techniker, er steht auch vor den Naturvorgängen wie  
ein Kind vor einer Märchenwelt. (Marie Curie)*



## Danksagung

Diese Dissertation ist das Resultat vieler Menschen in meinem (Arbeits-)Leben, die mich auf die eine oder andere Weise, kürzer oder länger, begleitet und unterstützt haben.

Ich bedanke mich bei meinem Doktorvater Herr Prof. Dr. Ralf Takors, der mir die Möglichkeit gegeben hat, dieses interessante Thema an seinem Institut zu bearbeiten. Für sein Vertrauen in meine Fähigkeiten und die Freiheiten beim Ausgestalten dieser Arbeit danke ich ihm sehr. Ebenso bedanke ich mich bei Herrn Prof. Dr. Kontermann, der sich bereit erklärt hat als Zweitprüfer zur Verfügung zu stehen und Herrn Prof. Dr. Lausen, der den Vorsitz übernimmt.

Ich danke meinen Projektpartnern von Evonik, Boehringer Ingelheim und Xell AG für die angenehme Kooperation und die anregenden Diskussionen in diesem BMBF-Projekt.

Großer Dank geht an meine Kollegen Attila und Mira, die mich in die fabelhafte Welt der Analytik eingeführt haben. Attila danke ich außerdem für seine Anmerkungen zu meiner Arbeit.

Im Bereich der Zellkulturtechnik bedanke ich mich herzlich bei Max und Lisa, die mir von Anfang an geholfen haben und mich herzlich in ihr abgelegenes Zellkulturbüro aufgenommen haben. Meinem Masterstudenten Janik und meiner wissenschaftlichen Hilfskraft Eva danke ich für ihre tatkräftige Unterstützung.

Vielen Dank an die zwei besten Ingenieure, die immer ein offenes Ohr für meine Probleme hatten: Alexander und Andreas. Großer Dank geht außerdem an Silke Reu, Martin, Andrea, Martina und Branka, ohne die der Institutsalltag nicht funktionieren würde. Maria, Alex und Andi danke ich für die vielen leckeren gemeinsamen Mittagessen und Kaffeepausen. Großer Dank auch der grünen Hölle, die mich in ihren „elitären“ Kreis des Cake Friday aufgenommen hat. Allen anderen Kollegen danke ich für die angenehme Arbeitsatmosphäre und die Hilfsbereitschaft.

Der größte Dank gilt meiner Familie und meinen Freunden, ganz besonders meinen Eltern Armin und Beate, meiner Schwester Jasmin, Tamara und Tobias. Ich danke ihnen dafür, dass sie mich immer in meinem Weg bestärkt haben und nie einen Zweifel daran hatten, dass ich es nicht schaffen könnte.



The experimental work in this dissertation was conducted under the supervision of Prof. Dr.-Ing. Ralf Takors at the Institute of Biochemical Engineering (University of Stuttgart, Germany) within the time span of 2016-2020.

The project was supported by a grant from the Bundesministerium für Bildung und Forschung (BMBF, Funding Number 031L0077A).

Parts of this work have been published in peer-reviewed journals.

**Verhagen N**, Wijaya AW, Teleki A, et al. Comparison of L-tyrosine containing dipeptides reveals maximum ATP availability for L-prolyl-L-tyrosine in CHO cells. *Eng Life Sci.* 2020;1-11.

**Verhagen N**, Teleki A, Heinrich C, Schilling M, Unsöld A, Takors R. S-adenosylmethionine and methylthioadenosine boost cellular productivities of antibody forming Chinese hamster ovary cells. *Biotechnology and Bioengineering.* 2020;1–9.

**Verhagen N**, Zieringer J and Takors R. Methylthioadenosine (MTA) boosts cell-specific productivities of Chinese hamster ovary cultures: dosage effects on proliferation, cell cycle and gene expression. *FEBS Open Bio.* 2020; 1-14

Excerpts of this research have additionally been presented at international conferences as posters.

**Verhagen, N**, Teleki A, Takors, R (05/2018)

Unraveling the functioning and mechanism of medium additives in CHO cell cultures. *DECHEMA Himmelfahrtstagung 2018. Magdeburg, Germany.*

**Verhagen, N**, Teleki A, Takors, R (09/2018)

Unraveling the functioning and mechanism of medium additives in CHO cell cultures. *ProcessNET 2018. Aachen, Germany.*

**Verhagen, N**, Teleki A, Takors, R (05/2019)

Medium Additives in CHO Cell Cultures: Potential to Enhance Cell Culture Performance. *DECHEMA Himmelfahrtstagung 2019. Hamburg, Germany.*





## **Declaration of Authorship**

I declare that the submitted work has been completed by me and that I have not used any other than permitted reference sources or materials. All references and other sources used by me have been appropriately acknowledged in the work.

Hiermit erkläre ich, dass ich die vorliegende Arbeit selbstständig angefertigt habe. Es wurden von mir nur die in der Arbeit ausdrücklich benannten Quellen und Hilfsmittel benutzt. Übernommenes Gedankengut wurde von mir als solches kenntlich gemacht.

Stuttgart, den

---

Natascha Verhagen

## List of Publications

### Manuscript 1

Verhagen N, Wijaya AW, Teleki A, et al. Comparison of L-tyrosine containing dipeptides reveals maximum ATP availability for L-prolyl-L-tyrosine in CHO cells. *Eng Life Sci.* 2020; 1-11.

N.V. is the main author who conceived the first version of the manuscript, designed and conducted the experimental part and data analysis

N.V. and A.T. designed and conducted metabolomic measurements

A.W.W. conducted FBA analysis

A.T. and A.W.W. co-authored the manuscript

R.T. supervised the studies and co-authored the manuscript

### Manuscript 2

Verhagen N, Teleki A, Heinrich C, Schilling M, Unsöld A, Takors R. S-adenosylmethionine and methylthioadenosine boost cellular productivities of antibody forming Chinese hamster ovary cells. *Biotechnology and Bioengineering.* 2020; 1–9.

N.V. is the main author who conceived the first version of the manuscript, designed and conducted the experimental part and data analysis

N.V. and A.T. developed and conducted extracellular MTA measurements

A.T. co-authored the manuscript

R.T. supervised the studies and co-authored the manuscript

### Manuscript 3

Verhagen N, Zieringer J and Takors R. Methylthioadenosine (MTA) boosts cell-specific productivities of Chinese hamster ovary cultures: dosage effects on proliferation, cell cycle and gene expression. *FEBS Open Bio.* 2020; 1-14

N.V. is the main author who conceived the first version of the manuscript, designed and conducted the experimental part and data analysis

J.Z. analyzed transcriptome data and co-authored the manuscript

N.V. and J.Z. interpreted transcriptome data

R.T. supervised the studies and co-authored the manuscript

#### **Manuscript 4**

The novel additive methylthioadenosine causes metabolic reprogramming, improving NADPH availability and boosting cell-specific productivity of CHO cells

*submitted in Metabolic Engineering in December 2020*

N.V., A.T. and R.T. designed the experiment

N.V. conducted the experiments and data analysis and is one of main authors who conceived the first version of the manuscript

N.V. and A.T. conducted metabolomic measurements

A.W.W. conducted MFA analysis and is one of main authors who conceived the first version of the manuscript

A.T. co-authored the manuscript

R.T. supervised the studies and co-authored the manuscript

# Table of Contents

Declaration of Authorship .....	I
List of Publications.....	II
Table of Contents .....	IV
List of Abbreviations.....	VI
List of Figures.....	XIV
List of Tables.....	XVII
Abstract .....	XIX
Zusammenfassung.....	XXIII
<b>1 Introduction and Motivation.....</b>	<b>1</b>
1.1 CHO Cells and Medium Optimization.....	1
1.2 L-Tyrosine Containing Dipeptides.....	2
1.3 S-Adenosylmethionine (SAM) and Methylthioadenosine (MTA) as Additives.....	3
<b>2 Theoretical Background .....</b>	<b>5</b>
2.1 Chinese Hamster Ovary (CHO) Cells and the Biopharmaceutical Market.....	5
2.2 CHO Cell Lines: History and State of the Art .....	5
2.3 Establishment of Recombinant Protein Production in a CHO Cell Clone .....	6
2.4 Cell Cultivation Phases, Processes and Modes.....	9
2.5 Process Development, Qualification, Verification and Control in CHO Cell Cultivations.....	11
2.6 Interaction of Cell Growth and Productivity .....	12
2.7 Antibody: Structure and Characteristics .....	13
2.8 Cell Cycle and Apoptosis.....	14
2.9 Genome and Transcriptome.....	17
2.10 Cytoskeleton and Protein Secretion.....	18
2.11 CHO Cell: Overview of Cell Organelles and Metabolism .....	19
2.12 Glycolysis, TCA and Amino Acids .....	19
2.13 Polyamines, S-Adenosylmethionine (SAM) and 5'-Deoxy-5'-(methylthio)adenosine (MTA): Synthesis, Characteristics and Functions .....	24
2.14 Metabolomics and <sup>13</sup> C Experiments.....	28
2.15 Medium Ingredients and Optimization .....	29
2.16 Additives in Chemical Defined Media .....	30
<b>3 Results: Original Publications .....</b>	<b>33</b>

## Table of Contents

---

3.1	Manuscript 1: Comparison of L-Tyrosine Containing Dipeptides Reveals Maximum ATP Availability for L-Prolyl-L-Tyrosine in CHO Cells.....	33
3.2	Manuscript 2: S-Adenosylmethionine and Methylthioadenosine Boost Cellular Productivities of Antibody Forming Chinese Hamster Ovary Cells. ....	55
3.3	Manuscript 3: Methylthioadenosine (MTA) Boosts Cell-Specific Productivities of Chinese Hamster Ovary Cultures: Dosage Effects on Proliferation, Cell Cycle and Gene Expression .....	71
3.4	Manuscript 4: The Novel Additive MTA (Methylthioadenosine) Causes Metabolic Reprogramming Improving NADPH Availability and Boosting Cell-Specific Productivity of CHO Cells.....	93
4	Discussion.....	127
4.1	L-Tyrosine Containing Dipeptides.....	127
4.2	SAM and Its Degradation Product MTA .....	130
4.3	Metabolomics After MTA Addition .....	136
4.4	Conclusion .....	137
5	References.....	139
6	Appendix.....	179
6.1	Supplementary Material: Manuscript 1 .....	179
6.2	Supplementary Material: Manuscript 3 .....	190
6.3	Supplementary Material: Manuscript 4 .....	195
6.4	Original Publications.....	207

## List of Abbreviations

Abbreviation	Description
\$	dollar
%	percent
(x) g	gravitational force equivalent
°C	degree celsius
μ	growth rate or micro ( $10^{-6}$ ) in combination with SI units
<sup>13</sup> C MFA	<sup>13</sup> C metabolic flux analysis
a	atto ( $10^{-18}$ ) in combination with SI units
aa	amino acid
ACO	aconitase
ADCC	antibody-dependent cell mediated cytotoxicity
ADP	adenosine diphosphate
AHCY	adenosylhomocysteinase
AIBA	α-aminoisobutyric acid
Ala	alanine
ALAT	alanine aminotransferase
AMD	S-adenosylmethionine decarboxylase
AMP	adenosine monophosphate
AMPK	AMP-activated protein kinase
ASAT	aspartate aminotransferase
Asn	asparagine
Asp	aspartate
ASRGL	asparaginase
ATP	adenosine triphosphate
AxP	AMP, ADP and ATP
AY	L-Ala-L-Tyr
Bak	Bcl-2 homologous antagonist killer
Bax	Bcl-2-associated X protein

## List of Abbreviations

---

<b>BHK</b>	baby hamster kidney
<b>BHMT</b>	betaine-homocysteine S-methyltransferase
<b>bp</b>	base pair
<b>C</b>	carbon
<b>CAC</b>	citric acid cycle
<b>cAMP</b>	cyclic adenosine monophosphate
<b>CD</b>	chemically defined
<b>CDK</b>	cyclin dependent kinase
<b>cDNA</b>	complementary DNA
<b>CHCl<sub>3</sub></b>	chloroform
<b>CHO</b>	Chinese hamster ovary
<b><i>cisAco</i></b>	<i>cis</i> -aconitate
<b>CO<sub>2</sub></b>	carbon dioxide
<b>CoA</b>	coenzyme A
<b>CS</b>	citrate synthase
<b>CSP</b>	cell-specific productivity
<b>d</b>	day
<b>D-</b>	dextrorotary
<b>Da</b>	dalton
<b>DCK</b>	deoxycytidine kinase
<b>DEG</b>	differential expressed gene
<b>DHFR / <i>dhfr</i></b>	dihydrofolate reductase
<b>DNA</b>	desoxyribonucleic acid
<b>DNMT</b>	DNA (cytosine-5)-methyltransferase
<b>DO</b>	dissolved oxygen
<b>DOE</b>	design of experiments
<b>e.g.</b>	for example
<b>ELISA</b>	enzyme-linked immunosorbent assay
<b>EMP</b>	Embden-Meyerhof Parnas

## List of Abbreviations

---

<b>ER</b>	endoplasmic reticulum
<b>ESI</b>	electrospray ion source
<b>f</b>	femto ( $10^{-15}$ ) in combination with SI units
<b>Fab</b>	antigen binding fragment
<b>FAD</b>	flavin adenine dinucleotide (oxidized)
<b>FADH<sub>2</sub></b>	flavin adenine dinucleotide (reduced)
<b>FAH</b>	fumarylacetoacetase
<b>FBA</b>	flux balance analysis
<b>FBS</b>	fetal bovine serum
<b>Fc</b>	crystallizable fragment
<b>FDA</b>	Food and Drug Administration
<b>FDR</b>	false discovery rate
<b>FH</b>	fumarase
<b>FMOC</b>	9-fluorenylmethyl chloroformate
<b>g</b>	gram
<b>G0-phase</b>	gap 0 phase
<b>G1-phase</b>	gap 1 phase
<b>G2-phase</b>	gap 2 phase
<b>G6P</b>	glucose 6-phosphate
<b>GABA</b>	$\gamma$ -aminobutyric acid
<b>GCCP</b>	good cell culture practice
<b>Glc</b>	glucose
<b>GLM</b>	generalized linear model
<b>Gln</b>	glutamine
<b>GLS</b>	glutaminase
<b>Glu</b>	glutamate
<b>GLUD</b>	glutamate dehydrogenase
<b>Gly</b>	glycine
<b>GMP</b>	good manufacturing practice



## List of Abbreviations

---

<b>GS</b>	glutamine synthase
<b>GSTZ</b>	maleyl-acetoacetate isomerase
<b>GTP</b>	Guanosine triphosphate
<b>GY</b>	Gly-L-Tyr
<b>h</b>	hour
<b>H<sup>+</sup></b>	hydron
<b>H<sub>2</sub>O</b>	water
<b>HC</b>	heavy chain
<b>HEK</b>	human embryo kidney
<b>HGD</b>	homogentisate oxidase
<b>HILIC</b>	hydrophilic interaction chromatography
<b>His</b>	histidine
<b>HPD</b>	4-hydroxyphenylpyruvate dioxygenase
<b>HPLC</b>	high performance liquid chromatography
<b>HSL</b>	L-homoserine lactone
<b>i.e.</b>	that is
<b>IDH</b>	isocitrate dehydrogenase
<b>IgG</b>	immunoglobulin G
<b>IL</b>	interleukin
<b>KDPG</b>	2-dehydro-3-deoxy-D-gluconate 6-phosphate
<b>L</b>	liter
<b>L-</b>	levorotary
<b>Lac</b>	lactate
<b>LC</b>	light chain
<b>LC</b>	liquid chromatography
<b>LDH</b>	lactate dehydrogenase
<b>Nva</b>	norvaline
<b>LSC</b>	succinyl-CoA synthetase
<b>Lys</b>	lysine

List of Abbreviations

---

<b>M-phase</b>	Mitosis phase
<b>m</b>	meter or milli ( $10^{-3}$ ) in combination with SI units
<b>M</b>	molarity per liter
<b>mAB</b>	monoclonal antibody
<b>MAS</b>	malate-aspartate shuttle
<b>MAT</b>	S-adenosylmethionine synthetase
<b>MDH</b>	malate dehydrogenase
<b>MeOH</b>	methanol
<b>Met</b>	methionine
<b>MFA</b>	metabolic flux analysis
<b>min</b>	minute
<b>mol</b>	molarity
<b>MRI</b>	methylthioribose-1-phosphate isomerase
<b>MRM</b>	multiple reaction monitoring
<b>mRNA</b>	messenger RNA
<b>MS</b>	mass spectrometer
<b>MSX</b>	methionine sulphoximine
<b>MTA</b>	5'-Deoxy-5'-(methylthio)adenosine
<b>MTAP</b>	5'-methylthioadenosine phosphorylase
<b>mTOR</b>	mammalian target of rapamycin
<b>MTR</b>	5-methyltetrahydrofolate-homocysteine methyltransferase
<b>MTX</b>	methotrexate
<b>N</b>	agitation
<b>n</b>	nano ( $10^{-9}$ ) in combination with SI units
<b>N<sub>2</sub></b>	nitrogen
<b>NaBu</b>	sodium butyrate
<b>NAD<sup>+</sup></b>	nicotinamide adenine dinucleotide (oxidized)
<b>NADH</b>	nicotinamide adenine dinucleotide (reduced)
<b>NADP<sup>+</sup></b>	nicotinamide adenine dinucleotide phosphate (oxidized)

List of Abbreviations

---

<b>NADPH</b>	nicotinamide adenine dinucleotide phosphate (reduced)
<b>NH<sub>4</sub><sup>+</sup></b>	ammonia
<b>N-linked</b>	nitrogen linked
<b>O<sub>2</sub></b>	oxygen
<b>OGDH</b>	α-ketoglutarate dehydrogenase complex
<b>O-linked</b>	oxygen linked
<b>OPA</b>	ortho-phthaldialdehyde
<b><i>ori</i></b>	origin of replication
<b>osmol</b>	osmolarity
<b>OXPHOS</b>	oxidative phosphorylation
<b>P</b>	phosphor
<b>p</b>	pico (10 <sup>-12</sup> ) in combination with SI units
<b>P/O ratio</b>	phosphate/oxygen ratio
<b>p21</b>	cyclin-dependent kinase inhibitor 1
<b>p27</b>	cyclin-dependent kinase inhibitor 1B
<b>p57</b>	cyclin-dependent kinase inhibitor 1C
<b>PBS</b>	phosphate buffered saline
<b>PC</b>	principal component
<b>PEP</b>	proton-dependent oligopeptide transporter
<b>PFK</b>	phosphofructokinase
<b>pH</b>	power / potential of hydrogen
<b>PNP</b>	purine-nucleoside phosphorylase
<b>poly(A)</b>	polyadenylation
<b>PPI</b>	inorganic pyrophosphate (P <sub>2</sub> O <sub>7</sub> <sup>4-</sup> )
<b>PPP</b>	pentose phosphate pathway
<b>Pro</b>	proline
<b>PRRP</b>	phosphoribosyl pyrophosphate
<b>PTM</b>	post translational modifications
<b>PY</b>	L-Pro-L-Tyr

List of Abbreviations

---

<b>qAB</b>	cell-specific productivity
<b>qmAB</b>	cell-specific monoclonal antibody productivity
<b>QQQ-MS/MS</b>	triple quadrupole tandem mass spectrometer
<b>REF</b>	reference
<b>RNA</b>	ribonucleic acid
<b>RPLC</b>	reversed phase liquid chromatography
<b>rpm</b>	rounds per minute
<b>S-phase</b>	synthesis phase
<b>SAH</b>	S-adenosyl-L-homocysteine
<b>SAM</b>	S-adenosyl-L-methionine
<b>SDH</b>	succinate dehydrogenase
<b>si</b>	small interfering
<b>SIM</b>	selected ion mode
<b>SMS</b>	spermine synthase
<b>SRM</b>	spermidine synthase
<b>STAT</b>	signal transducer and activator of transcription
<b>STR</b>	stirred tank reactor
<b>SV40</b>	simian vacuolating virus 40
<b>T</b>	temperature
<b>TAT</b>	tyrosine aminotransferase
<b>TCA</b>	tricarboxylic acid cycle
<b>Tyr</b>	tyrosine
<b>V</b>	volume
<b>Val</b>	valine
<b>VCD</b>	viable cell density
<b>Y</b>	Tyr
<b>YA</b>	L-Tyr-L-Ala
<b>YH</b>	L-Tyr-L-His
<b>YK</b>	L-Tyr-L-Lys

**YV** L-Tyr-L-Val

**ZIC-pHILIC** zwitterionic hydrophilic interaction chromatography

**$\alpha$ KG**  $\alpha$ -ketoglutarate

**$\alpha$ KV**  $\alpha$ -ketovaleric acid

## List of Figures

<b>Figure 1.</b> Schematic overview of the establishment of recombinant protein expression in a DHFR deficient CHO cell line. ....	7
<b>Figure 2.</b> Schematic growth curve of a batch process with CHO cells. ....	9
<b>Figure 3.</b> Schematic illustration of the different process modes: batch, fed-batch and perfusion mode. ....	10
<b>Figure 4.</b> Schematic illustration of an immunoglobulin G antibody. ....	13
<b>Figure 5.</b> Schematic overview of the cell cycle and underlying mechanisms. ....	15
<b>Figure 6.</b> Schematic overview of tricarboxylic acid (TCA) cycle and degradation of the amino acids L-asparagine, L-aspartate, L-tyrosine, L-valine, L-proline, L-glutamine, L-glutamate and glycine.....	21
<b>Figure 7.</b> Schematic overview of the SAM cycle with its connections to sulfuration, methylation and polyamine synthesis. ....	26
<b>Figure 8.</b> (A) Time courses of viable cell density [ $10^6$ cells $\text{mL}^{-1}$ ] and viability [%] and (B) time courses of extracellular D-glucose (black) and L-lactate (red) concentrations [mM] of dipeptide supplemented cells (GY $\Delta$ , PY $\square$ , YV $\diamond$ ) and reference (REF $\bullet$ ). ....	41
<b>Figure 9.</b> TYR uptake and release rates [ $\text{pmol cell}^{-1} \text{d}^{-1}$ ] via dipeptides addition compared to reference cultures (REF) after 48, 72, 96, and 120 h of cultivation.....	42
<b>Figure 10.</b> L-Glutamine consumption rates [ $\text{pmol cell}^{-1} \text{d}^{-1}$ ] (A) and intracellular pool sizes [ $\text{amol cell}^{-1}$ ] (B) of dipeptide-supplemented cells (GY $\Delta$ , PY $\square$ , YV $\diamond$ ) and reference cells (REF $\bullet$ )......	43
<b>Figure 11.</b> Intracellular pools of AMP (A), ADP (B), and ATP (C) [ $\text{fmol cell}^{-1}$ ] of dipeptide supplemented cells (GY $\Delta$ , PY $\square$ , YV $\diamond$ ) and reference cells (REF $\bullet$ ). ....	44
<b>Figure 12.</b> (A) Central carbon metabolism flux distribution during exponential growth phase as determined FBA. The boxplot indicates the flux of each reaction with samples arranged in the sequence REF-GY-PY-TY from left to right; (B) Cytosolic NADH production and consumption. Cytosolic NADH is produced predominantly by the EMP pathway. ....	46
<b>Figure 13.</b> ATP flow in reference and PY cultures. ....	47
<b>Figure 14.</b> The correlation of TYR-containing dipeptides uptake rates with the fraction of TYR metabolized.....	47
<b>Figure 15.</b> S1: Antibody concentrations (titer) [ $\text{mg L}^{-1}$ ] of dipeptide supplemented cells (GY $\Delta$ , PY $\square$ , YV $\diamond$ ) and the reference (REF $\bullet$ ) during the cultivation. ....	52
<b>Figure 16.</b> S2: Extracellular concentrations (digits) [mM] compared to intracellular pools (bars) [ $\text{amol cell}^{-1}$ ] of dipeptide supplemented cells ((A) GY $\Delta$ , (B) PY $\square$ , (C) YV $\diamond$ ). ....	52
<b>Figure 17.</b> S3: Three examples of essential amino acids (L-leucine, L-lysine and L-isoleucine) uptake rates and catabolism rates. ....	53
<b>Figure 18.</b> (a) Time courses of viable cell density ( $10^6/\text{ml}$ ) and viability (%) of S-(5'-adenosyl)- L-methionine (SAM) supplemented cells ( $\square$ ) and reference (REF, $\Delta$ ). SAM was added at 48 hr cultivation time. (b) Growth rate per hour ( $\text{hr}^{-1}$ ) regarding the time interval 48-120 hr. ....	61

- Figure 19.** (a) Time courses of the antibody titer (mg/L) of *S*-(5'-adenosyl)-L-methionine (SAM) supplemented cells ( $\square$ ) and reference (REF,  $\Delta$ ). SAM was added after 48 hr cultivation time. (b) Cell specific productivity (pg/day) for the time interval 0-120 hr..... 62
- Figure 20.** (a) Degradation rate ( $\mu\text{M/hr}$ ) of *S*-(5'-adenosyl)-L-methionine (SAM) in medium at 37 °C, 5 %  $\text{CO}_2$ , and 150 rpm with and without cells. (b) Time courses of 5'-(methylthio)adenosine (MTA) concentration ( $\mu\text{M}$ ) in the medium of SAM supplemented cells ( $\square$ ), reference (REF,  $\Delta$ ) and medium + SAM without cells (o). ..... 63
- Figure 21.** (a) Time courses of viable cell density ( $10^6/\text{ml}$ ) and viability (%) of *S*-(5'-adenosyl)-L-methionine (SAM,  $\square$ ), 5'-(methylthio) adenosine (MTA, o), and L-homoserine lactone hydrochloride (HSL,  $\diamond$ ) supplemented cells compared with the reference (REF,  $\Delta$ ). SAM, MTA, or HSL was added at 48 hr. (b) Growth rate ( $\text{hr}^{-1}$ ) regarding the time interval 60-120 hr. .... 64
- Figure 22.** (a) Time courses of antibody titers (mg/L) of *S*-(5'-adenosyl)-L-methionine (SAM,  $\square$ ), 5'-(methylthio)adenosine (MTA, o), and L-homoserine lactone hydrochloride (HSL,  $\diamond$ ) supplemented cells compared with the reference (REF,  $\Delta$ ). SAM, MTA, or HSL was added after 48 hr cultivation. (b) Cell specific productivity (pg/day) regarding the time interval 0-120 hr. .... 65
- Figure 23.** (a-c) Time courses of cell cycle phase distribution (%) and (d) average cell diameter ( $\mu\text{m}$ ) of *S*-(5'-adenosyl)-L-methionine (SAM,  $\square$ ), 5'-(methylthio)adenosine (MTA, o), and L-homoserine lactone hydrochloride (HSL) supplemented cells ( $\diamond$ ) compared with the reference (REF,  $\Delta$ ) and common preculture (crossed  $\square$ ). .... 66
- Figure 24.** (A) VCD [ $10^6$  cells  $\text{mL}^{-1}$ ] and viability [%] of MTA supplemented cells and reference (REF  $\blacktriangle$ ). MTA was added at 48 h in different concentrations: c1 150  $\mu\text{M}$ (o), c2 250  $\mu\text{M}$ ( $\bullet$ ), c3 350  $\mu\text{M}$ ( $\square$ ), c4 450  $\mu\text{M}$ ( $\diamond$ ). (B) Growth rate per day [ $\text{d}^{-1}$ ] regarding the time interval 48-120 h. (C) Maximum antibody titer [ $\text{mg L}^{-1}$ ]. (D) CSP [ $\text{pg cell}^{-1} \text{d}^{-1}$ ] regarding the time interval 48-144 h. (E) CSP [ $\text{pg cell}^{-1} \text{d}^{-1}$ ] between 48-144 h plotted against the MTA amount per cell [ $\text{pmol}$ ] at 48 h. .... 80
- Figure 25.** Cell cycle phase distribution (A–C) [%] and average cell size (D) [ $\mu\text{m}$ ] of MTA supplemented cells, reference (REF  $\blacktriangle$ ) and common preculture (-). MTA was added at 48 h in different concentrations: c1 150  $\mu\text{M}$ (o), c2 250  $\mu\text{M}$ ( $\bullet$ ), c3 350  $\mu\text{M}$ ( $\square$ ), c4 450  $\mu\text{M}$ ( $\diamond$ ). .... 81
- Figure 26.** (A) VCD [ $10^6$  cells  $\text{mL}^{-1}$ ] and viability [%] of MTA supplemented cells and reference (REF  $\blacktriangle$ ). MTA was added with 0.167  $\text{pmol}_{\text{MTA}}$  per cell at 48, 84 or 108 h: MTA t1 48 h ( $\bullet$ ), MTA t2 84 h ( $\square$ ), MTA t3 108 h ( $\diamond$ ). (B) Growth rate per hour [ $\text{d}^{-1}$ ] regarding the time interval 48-120 h. (C) Maximum antibody titer [ $\text{mg L}^{-1}$ ]. (D) CSP [ $\text{pg cell}^{-1} \text{d}^{-1}$ ] regarding the time interval 48-120 h. (E) Average cell size [ $\mu\text{m}$ ]. . 83
- Figure 27.** Cell cycle phase distribution (A-C) [%] of MTA supplemented cells, reference (REF  $\blacktriangle$ ) and common preculture (-). MTA was added with 0.167  $\text{pmol}_{\text{MTA}}$  per cell at 48, 84 or 108 h: MTA t1 48 h ( $\bullet$ ), MTA t2 84 h ( $\square$ ), MTA t3 108 h ( $\diamond$ ). .... 84
- Figure 28.** Principal component (PC) analysis of the transcriptome samples taken in the experiment. .... 85
- Figure 29.** (A) Analysis of differential expressed genes (DEGs) ( $\log_2$ -fold-change  $\geq |1|$  and  $P$ -value  $\leq 0.05$ ) throughout the experiment. MTA supplemented cells (MTA) were compared to REF. Grey bars indicate downregulated and black bars show upregulated genes at different sampling time points. (B) Venn diagram shows overlap of DEGs at 84 h-96 h-144 h. .... 86

<b>Figure 30.</b> a: Time course of viable cell density [ $\times 10^5$ cells mL <sup>-1</sup> ] (●), D-glucose (D-Glc) [ $\times 10$ mM] (●), L-asparagine (L-Asn) [mM] (●) and L-glutamine (L-Gln) [mM] (●) of the reference (REF). b: Time course of viable cell density [ $\times 10^5$ cells mL <sup>-1</sup> ] (■), D-glucose (D-Glc) [ $\times 10$ mM] (■), L-asparagine (L-Asn) [mM] (■), L-glutamine (L-Gln) [mM] (■) and 5'-deoxy-5'-methylthioadenosine (MTA) [ $\times 10^2$ $\mu$ M] (■) in MTA-supplemented cells. ....	106
<b>Figure 31.</b> a: Growth rate per day [d <sup>-1</sup> ] for the different cultivation phases. b: Cell-specific uptake/secretion rates [pmol cell <sup>-1</sup> d <sup>-1</sup> ] for L-Gln, L-Asn, L-Glu, and L-Ala in overflow metabolism before MTA addition (A). c: Cell-specific uptake/secretion rates [pmol cell <sup>-1</sup> d <sup>-1</sup> ] for L-Gln, L-Asn, L-Glu, and L-Ala in overflow metabolism after MTA addition (B / C.I). d: Cell-specific uptake/secretion rates [pmol cell <sup>-1</sup> d <sup>-1</sup> ] for D-Glc and L-Lac in overflow metabolism before MTA addition (A). e: Cell-specific uptake/secretion rates [pmol cell <sup>-1</sup> d <sup>-1</sup> ] for D-Glc and L-Lac in overflow metabolism after MTA addition (B / C.I).....	107
<b>Figure 32.</b> a: Time course of the cell volume [fL] of MTA-supplemented cells (MTA: grey) and reference cells (REF: black) in the different phases. Cell volume was calculated with the assumption of a spherical cell shape. b: Cell-cycle phase distribution [%] of MTA-supplemented cells (MTA) and reference cells (REF) at 84 h (I: Overflow) and 132 h (II: N-limitation).....	108
<b>Figure 33.</b> Cell-specific IgG productivity (CSP) [ $\mu$ g cell <sup>-1</sup> d <sup>-1</sup> ] and cell-volume-specific IgG productivity (CVP) [ $\mu$ g L <sup>-1</sup> d <sup>-1</sup> ] regarding the different cultivation phases. a: Differential CSPs over cultivation time. b: Differential CVPs over cultivation time. ....	109
<b>Figure 34.</b> a: Time course of the ATP concentrations in the subcellular (mitochondrial, index S) compartment of MTA-supplemented cells (MTA: grey) and reference (REF: black). b: Time course of the ATP concentrations in the cytosolic compartment (index C) of MTA-supplemented cells (MTA: grey) and reference cells (REF: black).....	110
<b>Figure 35.</b> a. Metabolic flux distribution of the reference and MTA-supplemented CHO-DP12 cells. Arrows indicate flux direction, and the thickness of the arrows indicate strength in pmol cell <sup>-1</sup> day <sup>-1</sup> ; b. Comparison of key fluxes using abbreviations as follows: phosphoglucose-isomerase (pgi), G6P dehydrogenase (G6Pdh), endogenous glycogen exchange (fGlyco), PEP carboxykinase (PEPck), alanine amino transferase (alt), malic enzyme (me), pyruvate carboxylase (pc), and aspartate amino transferase (ast); c. Comparison of mitochondrial carrier activities: pyruvate/H <sup>+</sup> symporter (MPC), aspartate/glutamate antiporter (AGC), citrate/malate antiporter (CIC), dicarboxylic acid carrier (DIC), glutamate carrier (GC), aKG/malate antiporter (OGC), putative alanine carrier (mAla), and putative asparagine carrier (mAsn). ....	112
<b>Figure 36.</b> Comparison of NADPH, NADH <sub>cyt</sub> , and NADH <sub>mit</sub> production in reference culture and MTA-treated culture. ....	115
<b>Figure 37.</b> S1. Mitochondrial transporters assumption in the metabolic model.....	125



## List of Tables

<b>Table 1.</b> Ranges of CHO cell culture parameters for temperature (T), osmolarity, dissolved oxygen (DO) and pH .....	12
<b>Table 2.</b> Selection of differential expressed genes. ....	86
<b>Table 3.</b> S1. List of chemicals.....	121
<b>Table 4.</b> S2. Full names of abbreviated metabolites .....	121
<b>Table 5.</b> S3. Correction factor for the validation of the differential fast-filtration method for whole-cell and subcellular metabolome analyses. ....	122
<b>Table 6.</b> S4. Cell-specific productivity (CSP) [ $\mu\text{g cell}^{-1} \text{d}^{-1}$ ] regarding the different cultivation phases: MTA supplemented cells compared to REF.....	122
<b>Table 7.</b> S5. Metabolic model and carbon atom transition model. ....	122
<b>Table 8.</b> S1. List of differential expressed genes .....	190



## Abstract

Chinese hamster ovary (CHO) cells are the most commonly used production hosts in the biopharmaceutical industry. The knowledge about CHO cells themselves and their appropriate process conditions grows steadily, resulting in a strong increase in performance since the first cultivations. However, this increase in performance is mainly achieved by increasing the maximum viable cell density and extending the process time. Such improvements are beneficial as long as an increase in process volume is possible. Larger reactors typically lead to heterogeneous process conditions that can negatively influence the expected increase in productivity. In this regard, cultivations in perfusion mode enable higher volumetric productivities by a strong increase of achievable viable cell densities. Nevertheless, overall process yields are primarily based on cell-specific productivities, especially for cell-number- or time-limited processes. Increased cell-specific productivities can be achieved by process, media or cell optimization. In media optimization, the focus is on balancing of components as macronutrients in clearly defined recipes. Balanced compositions properly maintain the cellular metabolic processes and avoid or minimize the formation of by-products. Besides basic components, media development in recent years has increasingly focused on small molecules such as dipeptides. However, many studies in this field solely focus on extracellular changes and/or include transcriptome analyses. The focus of this work is the optimization of CHO cell process media with dipeptides or other additives under production-related conditions using system biological methods. This includes the investigation of growth and production effects, the analyses of the cell cycles and transcriptome data, as well as the study of extra- and intracellular kinetics of the additives and other metabolites. The results provide information about the actual cellular phenotype and enable a further strain and process development to increase productivity.

In this work, two different types of additives were tested in CHO cell medium: L-Tyr-containing dipeptides and *S*-adenosylmethionine (SAM) and its degradation product methylthioadenosine (MTA). In addition to phenotypic and transcriptional studies, the effect of the additive on metabolism is analyzed to understand its effect on the overall cellular system.

Resulting data sets and examined mechanisms represent possible entry points to increase immunoglobulin G (IgG) cell-specific productivity.

The first investigated additive group contains different L-Tyr-containing dipeptides. The application of L-Tyr-containing additives to CHO cells demonstrates that the composition of the dipeptides is important for the effect on the cells. While the dipeptides L-Tyr-L-Val and Gly-L-Tyr had no significant effect on the cells, a growth reduction could be observed after the addition of L-Pro-L-Tyr. Furthermore, these cells showed an altered L-glutamine metabolism and increased intracellular ATP concentrations. Interestingly, this did not lead to an increase in cell-specific productivity. This means that, besides sufficient ATP availability, other factors are necessary to increase cell-specific productivity.

The second group of additives studied includes the effector molecules SAM and MTA. SAM is a global, cellular donor that is required for methylation and other cellular pathways. After a single addition of SAM, an increase in cell-specific productivity in CHO cells was observed. In addition, there was a growth reduction, cell enlargement, and changes in the cell cycle dynamics. Further investigations showed that not SAM itself, but its degradation product MTA affected the cells. The single addition of MTA led to the same phenotypic observations as after SAM addition. To better understand the reactions of the cell after MTA addition, concentration- and time-dependent experiments were performed. MTA addition is most effective at a concentration titer of 250-300  $\mu\text{M}$  during the exponential growth phase (48 h). Compared to reference cultivations, cell-specific productivities can be enhanced by over 90 % and cellular viabilities are extended. In this context, the strategy lead to lowered maximum cell numbers but comparable antibody titers. Analysis of the transcriptome data after MTA addition reveals, among other things, differentially expressed genes in the areas of cytoskeleton, growth, cell survival and transcription. This defines MTA as multiple cellular effector, besides his already known role as polyamine synthesis inhibitor. Furthermore, MTA strongly affects the subcellular metabolism and energy balance. The increase of cytosolic ATP concentrations after MTA addition influences glycolysis and other central pathways. Next,  $^{13}\text{C}$  Metabolic Flux Analyses (MFA) reveals that MTA addition lead to predominate regeneration of the reduction equivalent NADPH by increased pentose-phosphate pathway

fluxes. By contrast, under reference conditions NADPH regeneration takes place mainly by the cytosolic malate enzyme. The change in flux distribution of MTA-treated cells lead to an enhanced NADPH synthesis capacity and further modulations of the CHO metabolism and results in an increased cell-specific productivity. In sum, this work shows the potential of additives in media optimization in cultivation processes with CHO cells. The addition of additives can activate not yet exhausted cellular potentials and give hints to which modulations or regulations are important in increasing cell-specific productivity.



## Zusammenfassung

Chinesische Hamster Ovarien (CHO)-Zellen sind die am häufigsten verwendeten Produktionszellen in der biopharmazeutischen Industrie. Das Wissen über CHO-Zellen selbst und die für sie geeigneten Prozessbedingungen ist stetig gewachsen, was eine starke Leistungssteigerung seit den ersten Kultivierungen zur Folge hatte. Diese Leistungssteigerung erfolgt vor allem durch eine Steigerung der maximalen viablen Zelldichte und eine Verlängerung der Prozesszeit. Diese Verbesserungen sind von Vorteil, solange eine Volumensteigerung des Prozesses möglich ist. Größere Reaktoren führen typischerweise zu heterogenen Prozessbedingungen, welche die erwartete Produktivitätssteigerung negativ beeinflussen können. In dieser Hinsicht ermöglichen Kultivierungen im Perfusionsmodus höhere volumetrische Produktivitäten durch eine starke Erhöhung der erreichbaren viablen Zelldichten. Dennoch basieren die Gesamtprozessausbeuten vor allem bei zellzahl- oder zeitbegrenzten Prozessen in erster Linie auf der zellspezifischen Produktivität. Eine höhere zellspezifische Produktivität kann durch eine Prozess-, Medien- oder Zelloptimierung erreicht werden. Bei der Medienoptimierung liegt der Schwerpunkt auf der ausgewogenen Basiskomposition von Makronährstoffen in definierten Rezepturen. Ausgewogene Zusammensetzungen erhalten zelluläre Stoffwechselprozesse aufrecht und vermeiden oder minimieren die Bildung von Nebenprodukten. Neben den Basiskomponenten hat sich die Medienentwicklung in den letzten Jahren zunehmend auf kleine Moleküle wie Dipeptide konzentriert. Viele Studien auf diesem Gebiet konzentrieren sich jedoch ausschließlich auf extrazelluläre Veränderungen und/oder schließen Transkriptomanalysen ein. Im Mittelpunkt dieser Arbeiten steht die Optimierung von CHO-Zellprozessmedien mit Dipeptiden oder anderen Zusätzen unter produktionsnahen Bedingungen mit systembiologischen Methoden. Dazu gehören die Untersuchung von Wachstums- und Produktionseffekten, die Analyse der Zellzyklen und Transkriptomdaten sowie die Untersuchung der extra- und intrazellulären Kinetik der Additive und anderer Metabolite. Die Ergebnisse geben Aufschluss über den tatsächlichen zellulären Phänotyp und ermöglichen eine weitere Zell- und Prozessentwicklung zur Produktivitätssteigerung.

In dieser Arbeit wurden zwei verschiedene Arten von Additiven in CHO-Zellmedium untersucht: L-Tyr-haltige Dipeptide und S-Adenosylmethionin (SAM) und sein Abbauprodukt Methylthioadenosin (MTA). Zusätzlich zu den phänotypischen und transkriptionellen Studien wird die Wirkung des Zusatzstoffs auf den Metabolismus analysiert, um die Wirkung auf das gesamte Zellsystem zu verstehen. Die resultierenden Datensätze und untersuchten Mechanismen stellen mögliche Ansatzpunkte zur Erhöhung der zellspezifischen Produktivität von Immunglobulin G (IgG) dar.

Die erste untersuchte Zusatzstoffgruppe enthält verschiedene L-Tyr-haltige Dipeptide. Die Anwendung von L-Tyr-haltigen Additiven auf CHO-Zellen zeigte, dass die Zusammensetzung der Dipeptide wichtig für die Wirkung auf die Zellen ist. Während die Dipeptide L-Tyr-L-Val und Gly-L-Tyr keine signifikante Wirkung auf die Zellen hatten, konnte nach Zugabe von L-Pro-L-Tyr eine Wachstumsreduktion beobachtet werden. Darüber hinaus zeigten diese Zellen einen veränderten L-Glutamin-Stoffwechsel und erhöhte intrazelluläre ATP-Konzentrationen. Interessanterweise führte dies nicht zu einer Erhöhung der zellspezifischen Produktivität. Dies bedeutet, dass neben einer ausreichenden ATP-Verfügbarkeit auch andere Faktoren notwendig sind, um die zellspezifische Produktivität zu erhöhen.

Zur zweiten Gruppe der untersuchten Zusatzstoffe gehören die Effektormoleküle SAM und MTA. SAM ist ein globales, zelluläres Protein, das für die Methylierung und andere zelluläre Signalwege benötigt wird. Nach einmaliger Zugabe von SAM wurde eine Steigerung der zellspezifischen Produktivität in CHO-Zellen beobachtet. Darüber hinaus kam es zu einer Wachstumsreduktion, Zellvergrößerung und Veränderungen in der Dynamik des Zellzyklus. Weitere Untersuchungen zeigten, dass nicht SAM selbst, sondern sein Abbauprodukt MTA die Zellen beeinflusst. Die einmalige Zugabe von MTA führt zu den gleichen phänotypischen Beobachtungen wie nach der Zugabe von SAM. Um die Reaktionen der Zelle nach der MTA-Zugabe besser zu verstehen, wurden konzentrations- und zeitabhängige Experimente nach der MTA-Zugabe durchgeführt. Die MTA-Zugabe ist bei einem Konzentrationstiter von 250-300  $\mu$ M während der exponentiellen Wachstumsphase (48 h) am wirksamsten. Im Vergleich zu Referenzkultivierungen konnten die zellspezifischen Produktivitäten um über 90 % gesteigert und die zellulären Viabilitäten stabilisiert werden. In diesem Zusammenhang führt



die Strategie zu niedrigeren maximalen Zellzahlen bei vergleichbaren Antikörpertitern. Die Analyse der Transkriptomdaten nach MTA-Zugabe ergibt unter anderem unterschiedlich exprimierte Gene in den Bereichen Zytoskelett, Wachstum, Zellüberleben und Transkription. Das definiert MTA als multizellulären Effektor, neben seiner bereits bekannten Rolle als Polyaminsynthese-Inhibitor. Darüber hinaus beeinflusst MTA stark den subzellulären Metabolismus und den Energiehaushalt. Der Anstieg der zytosolischen ATP-Konzentrationen nach MTA-Zugabe beeinflusst die Glykolyse und andere zentrale Stoffwechselwege. <sup>13</sup>C-Stoffwechselfluss-Analysen (MFA) demonstrieren, dass nach MTA-Zugabe ein erhöhter Fluss durch den Pentose-Phosphat-Weg zu einer vermehrten Regeneration des Reduktionsäquivalenten NADPH führt. Im Gegensatz dazu findet unter Referenzbedingungen die NADPH-Regeneration hauptsächlich durch das zytosolische Malat-Enzym statt. Die Veränderung der Flussverteilung der MTA-behandelten Zellen führt zu einer erhöhten NADPH-Synthesekapazität und weiteren Modulationen des CHO-Stoffwechsels und resultiert in einer erhöhten zellspezifischen Produktivität. Zusammenfassend zeigt diese Arbeit das Potential von Additiven zur Medienoptimierung bei Kultivierungsprozessen mit CHO-Zellen. Die Zugabe von Additiven kann noch nicht ausgeschöpfte zelluläre Potentiale aktivieren und Hinweise geben, welche Modulationen oder Regulationen für die Steigerung der zellspezifischen Produktivität wichtig sind.



# 1 Introduction and Motivation

## 1.1 CHO Cells and Medium Optimization

Chinese hamster ovary (CHO) cells are the most used cell line in the growing biopharmaceutical market [1]. Intensive research is ongoing to improve existing processes and to expand the knowledge about CHO cells and this resulted in sharp performance increase especially in product titers since their first application. These improvements are mostly based on increased viable cell densities and/or process durations [2]. Anyhow, enhanced cell-specific productivity is of higher interest because it allows further improvements in intensified time- or viable cell density-limited cultivations, in particular when using perfusion processes [3].

CHO cells demonstrate several advantages for biopharmaceutical production [1,4]: Recombinant gene expression methods are established [5], glycosylation motifs are human compatible [6–9], they are prone to viral infections [10,11] and they grow in suspension even in high volumes [5,6,12–14]. CHO cell culture optimization is continuously performed and includes strain and media development. Media development focuses on optimal and improved media composition. A balanced composition of chemical defined media is required to enhance metabolic efficiency and to avoid by-product formation that hampers growth and productivity [15]. Next to basal components, other additives like dipeptides come in stronger focus for a rational media design. Up to date, mostly phenotypic characteristics were investigated after additive supplementation and deeper insights are rare especially for dipeptide addition. Dipeptides are dosage forms of amino acids that can demonstrate advantages as higher solubility or stability compared to single amino acids [16]. L-Glutamine (L-Gln) containing dipeptides are more stable in medium compared to L-Gln [17] and some dipeptide combinations influenced the overflow metabolism as a surplus [18]. L-Tyrosine (L-Tyr) containing dipeptides showed positive effects on production and cell density [19]. Next to dipeptides, other small molecules were investigated as medium additives: catechins [20], sodium butyrate [21], valproic acid [22,23], as well as AMP [24] in addition to others. They often improved cell-specific productivities and diminished cell growth. However, they were

often detrimental at high concentrations as they hampered viability or induced unintentionally apoptosis. Phenotypical behavior was investigated after effector addition, sometimes accompanied by e.g. protein quantification [23] or cell cycle analysis [20,24]. These studies allowed to unravel cellular mechanisms of additive supplementation and indicate causes of high production phenotypes. The data was helpful for process development, genetic engineering, and further optimization strategies.

The interaction of cell-specific productivity and cell growth was widely demonstrated [25–28]. Somehow this effect was not linked to a certain cell cycle phase [29–33]. Additionally, cell volume was linked to productivity as well [33–36]. Low overflow [37], high ATP supply [3], protein secretion [38,39] and cytoskeleton composition [40–42] affect cell-specific productivity on top. All these aspects demonstrate that overall productivity is influenced by various factors of the whole cellular system. These manifold interactions belong to the research field of systems biology. Systems biology research allows holistic insights into metabolism and its regulation and wants to understand underlying complex cellular mechanisms [43].

## 1.2 L-Tyrosine Containing Dipeptides

L-Tyr containing dipeptides were investigated within the research of this thesis [44]. They allowed to increase the total available L-Tyr amount for cells, as they demonstrated a higher solubility compared to L-Tyr without the necessity of pH alterations [16]. Earlier investigations about L-Tyr containing dipeptides demonstrated positive effects on viability and titer (L-Tyr-L-His, L-Tyr-L-Lys, L-Tyr-L-Ala and L-Tyr-L-Val). As a surplus, they influenced the metabolic profile. Addition led to lower L-Lac and  $\text{NH}_4^+$  production and resulted in a better pH maintenance of the cultivation. A higher availability of L-Tyr through dipeptides correlated with increased cell-specific productivity because they served as an energy source for the cells [19]. The L-Tyr containing dipeptides Gly-L-Tyr, L-Ala-L-Tyr and L-Pro-L-Tyr showed different uptake rates and different effects on cell growth and productivity. They were directly taken up as dipeptides and metabolized intracellular which was hypothesized previously [18]. Overall, dipeptide effector functions are dependent on the corresponding amino acid [45].

In this thesis, the effects of L-Tyr containing dipeptides are investigated further. Focus is laid on phenotypical observations e.g. overflow and cell growth and they were combined with intracellular measurements as central carbon metabolites or adenylate nucleotides. The data allows specifying the metabolic and regulatory effects of the different L-Tyr containing dipeptides in the cell.

### **1.3 S-Adenosylmethionine (SAM) and Methylthioadenosine (MTA) as Additives**

The cell system inherits diverse levels of metabolic regulation. Fast regulation includes direct enzyme regulation via substrate or product concentrations. Slow regulation covers transcriptional procedures as gene expression or epigenetics [46]. Epigenetic research investigates DNA modifications as acetylation and methylation. Methylation requires S-(5'-adenosyl)-L-methionine (SAM) as global methyl donor in cells. SAM is a cellular naturally occurring high energy molecule and its regulation and formation occurs in the SAM cycle [47]. The SAM cycle is a starting point for several important cellular pathways as trans-methylation (DNA and membrane), sulfuration pathway (glutathione synthesis, oxidative stress) and polyamine synthesis. Consequently, SAM is an important cellular regulator of membrane fluidity, gene expression and apoptosis [47–49]. Polyamines which require SAM for their formation are cellular molecules that demonstrated roles in growth, survival [50–52] and cytoskeleton maintenance [53]. Their depletion was accompanied by cell cycle arrest in S-phase [54–56] and they are important for DNA synthesis initiation [57]. The formation of polyamines results in the release of 5'-deoxy-5'-(methylthio)adenosine (MTA). MTA is rapidly degraded and further recycled to the SAM precursors L-methionine and ATP [58,59]. MTA itself displayed diverse effects on cells as the inhibition of cell proliferation mainly due to polyamine depletion [49,60–63]. Moreover, control of gene expression, cell proliferation, lymphocyte activation, tumor development and invasiveness, the regulation of apoptosis [49,58–60,64,65], interactions with signaling pathways [61,62,66] and methylation [60,65,66] were observed.

In this thesis, effects of SAM and MTA addition are analyzed because they have the capability to influence the productivity of the cellular system. The experiments covered phenotypic investigations such as basic uptake and degradation kinetics and the relevance of concentration and time of the addition. Furthermore, transcriptome analysis was performed to evaluate the effect of the additive on the transcriptomic level. On top, the effect on the metabolism after addition was investigated with  $^{13}\text{C}$ -labeled carbon sources. This allows to unravel changed flux conditions in important metabolic pathways. Summarized, the data of this thesis includes phenotypic observations, cell cycle, transcriptome and metabolic analysis.

The overall systematic investigation of additive supplementation is crucial for mechanistic understanding, creation and development of new ideas in cell culture optimization.

## 2 Theoretical Background

### 2.1 Chinese Hamster Ovary (CHO) Cells and the Biopharmaceutical Market

The most applied mammalian organisms to synthesize recombinant products in the biopharmaceutical industry are Chinese hamster ovary (CHO) cells [1,4–6]. 84 % of newly approved recombinant products between 2015 and 2018 are produced in mammalian cell expressing systems and 84 % of these products were produced in CHO cells. In addition to CHO cells, murine myeloma (NS0, SP2/0) cells, baby hamster kidney (BHK) cells and human embryo kidney (HEK293) cells are frequent used mammalian cell lines in the industrial biotechnology market [1]. Recombinant products include antibodies, clotting factors, thrombolytics, anticoagulants, growth factors, interferons, vaccines, enzymes and cytokines in addition to others [1,67]. Monoclonal antibodies (mABs) are the largest group with 53 % of all approvals from 2015 to July 2018 [1] and are predominantly produced in CHO cells. The first recombinant products produced in dihydrofolate reductase (DHFR) deficient CHO cells were interferon- $\gamma$ , interferon- $\beta$  [68–70], the small tumor antigen of SV40 [71] and tissue-type plasminogen activator [72]. The constant high relevance of CHO cell lines for biopharmaceutical production is a result of their proved safety and acquired experience over decades resulting in minor or no approval issues [6,73].

### 2.2 CHO Cell Lines: History and State of the Art

CHO cells were first isolated and cultivated *in vitro* as a cell line in 1958 [74]. Further modifications with this initial cell line created different deficient cell lines: a glycine-dependent (CHO-K1) and a L-proline-dependent variant (CHO-pro3-) [75]. In 1980 CHO-K1 was further mutagenized by Urlaub & Chasin to the CHO-DXB11/DUKX/DUK-XB11 cell line that lacks one dihydrofolate reductase gene (*dhfr*) by an introduced missense mutation [76]. CHO-pro3- was further mutagenized to CHO-DG44, a variant with two deleted *dhfr* genes [77]. The DHFR is crucial for tetrahydrofolate production and the formation of folate and dihydrofolate which are essential co-factors in cellular metabolism providing one-carbon groups for

reactions [46,78]. These original cell lines are the basis for most of the CHO cell lines used today.

CHO cells are the most popular cell line in biopharmaceutical industry because they demonstrate the ability to grow stable in suspension in chemically defined media in bioreactors up to 20,000 L [5,6,12–14]. In 1986, cell cultures were able to reach an average of  $2 \times 10^6$  cells  $\text{mL}^{-1}$  with a cell culture duration of seven days and demonstrated an average productivity of  $10 \text{ pg cell}^{-1} \text{ d}^{-1}$ . Nearly 20 years later in 2004, these key numbers leapt significantly. Maximum viable cell densities (VCD) reached over  $10 \times 10^6$  cells  $\text{mL}^{-1}$  with a duration up to 21 days and cell-specific productivity up to  $90 \text{ pg cell}^{-1} \text{ d}^{-1}$  [2]. Tabuchi & Sugiyama [79] even demonstrated cell-specific productivities over  $100 \text{ pg cell}^{-1} \text{ d}^{-1}$  which were the result of a double overexpression strategy in an engineered host cell (cooverexpression of alanine aminotransferase 1 and taurine transporter). These improvements were possible due to intensive research. Gene expression mechanism, transcriptomic and metabolic research allows a deeper insight in potential targets for process optimization including host cell engineering and media optimization.

## **2.3 Establishment of Recombinant Protein Production in a CHO Cell Clone**

CHO cells are suitable for gene integration [80]. Nevertheless, the establishment of recombinant protein expression is a long multi-phase process [4,5].



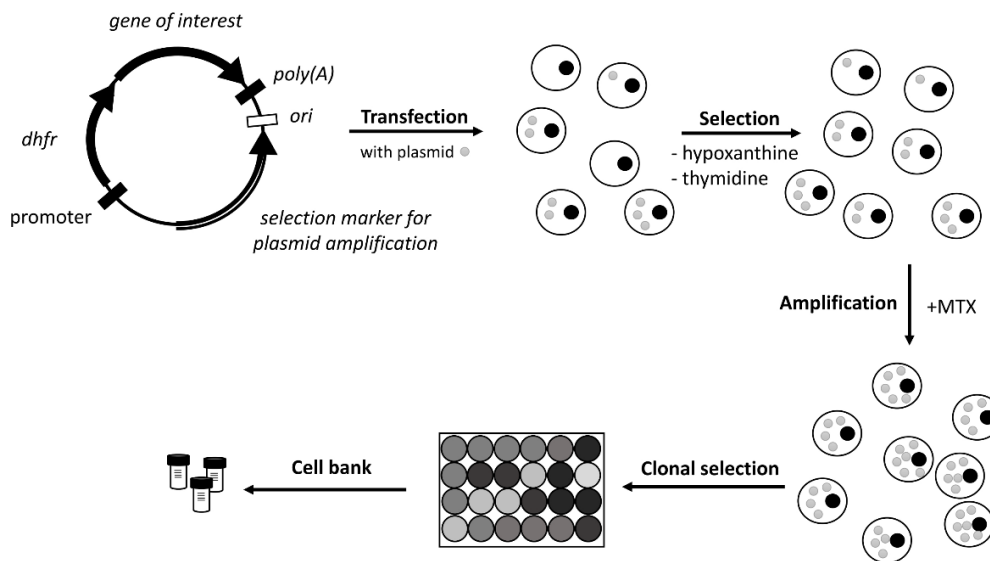


**Figure 1.** Schematic overview of the establishment of recombinant protein expression in a DHFR deficient CHO cell line. The process starts with the construction of a plasmid that contains the gene of interest (GOI), selection markers and promoter, *ori* and *poly(A)*. Transfection with the plasmid, selection with depleted medium (without hypoxanthine and thymidine), amplification (addition of MTX), clonal selection and creation of a cell bank are subsequent steps. Own schematic representation.

Construction of CHO cells for recombinant protein expression requires several steps (**Figure 1**). It starts with the transfection plasmid that contains the desired recombinant protein and selection gene next to regulatory and replication components (origin of replication (*ori*), *selection marker for plasmid amplification*, transgene, *dhfr*, DHFR). The DHFR expression system works best in CHO-DXB11 and CHO-DG44 cell lines that inherit a loss of one or both DHFR genes [76,77]. Several transfection methods are established for CHO [5] such as electroporation, nucleofection or lipofection. The integration locus is important for proper recombinant protein production. Nevertheless, an optimal integration locus is not an assurance for proper transgene expression. Gene copies can be lost, silenced, or activated through modifications of the DNA commonly summed up in the topic of epigenetics [81] and especially transgenes are prone to become rapidly silenced [82].

Transfection of cells is followed by selection due to selection marker genes on the transfected plasmid. Popular selection systems are genes encoding for DHFR [71,83–85] or glutamine synthetase (GS) [86,87]. Selection component depleted medium does not allow growth of

non-transfected cells and allows the separation of transfected cells. For the DHFR system a hypoxanthine and thymidine depleted medium is used whereas the selection with the GS system requires a L-glutamine (L-Gln) depleted medium. The next step, gene amplification, is conducted via the selection gene system as well [71,88]. High concentrations of the DHFR inhibitor methotrexate (MTX) allow the amplification of cells with high plasmid numbers. For amplification and enhanced selection pressure in the GS system the competitive GS inhibitor methionine sulphoximine (MSX) is used [86]. The amplification treatment can result in cells with up to hundred to thousand copies of the transfected gene by genetic rearrangement [5,71,85,89].

Random integration by transfection, selection and amplification results in high heterogeneity of the cells and necessitates further selection [6,71,90–92]. Cells that survived the selection and amplification are individually separated for clonal expansion. Clonal populations of single clones are screened for desired performance (e.g. growth, cell-specific productivity, product quality and expression stability) in scale-down processes [93]. This is mostly performed in multiwell plates with robotic methods, which is still very time consuming [2]. Furthermore, advanced screening tools have been developed to accelerate the clonal selection process [94–98]. Suitable cell clones with desired characteristics are selected to create cryo-cultures for a working cell bank [5].

## 2.4 Cell Cultivation Phases, Processes and Modes

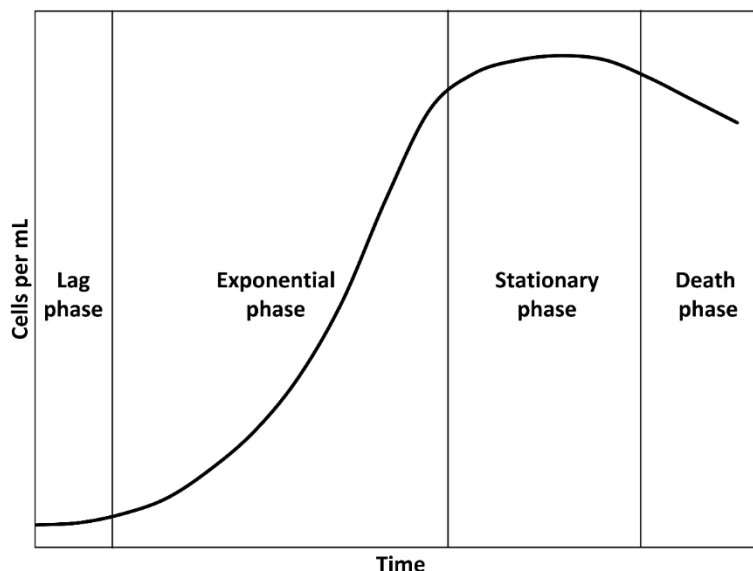


**Figure 2.** Schematic growth curve of a batch process with CHO cells. Cells per mL are displayed over time. The growth phase displays four phases: lag phase, exponential phase, stationary phase, and death phase. Own schematic representation.

Constant and reliable biopharmaceutical production relies on profound knowledge and accurate control of the biotechnological process, as minor variations can influence the final product. Cell culture processes in the biotechnological industry are generally divided in up- and downstream process. Upstream process includes cell line and medium development, process intensification, final process execution and harvest. Downstream process starts with the harvested product and focuses on isolation and purification [99].

The cell cultivation or process itself is part of the upstream process. It starts with the “seed train”. Cells are thawed from cryo-culture (cell bank) and expanded to the desired volume by multiple passaging steps [100]. Cell growth in batch mode normally demonstrates a lag phase followed by exponential, stationary and death phase (**Figure 2**). In the lag phase, the cells adjust to the new conditions by transcriptomic, proteomic and metabolomic adaptations before they initiate substantial growth. After growth starts, the growth rate increases to a maximum ( $\mu_{max}$ ) as the cells reach the exponential phase. When substrate or other limitations occur,

growth rate decreases and finally cells stop growing (stationary phase). When limitations finally impair cell maintenance, the death phase starts and cell numbers decline [101].

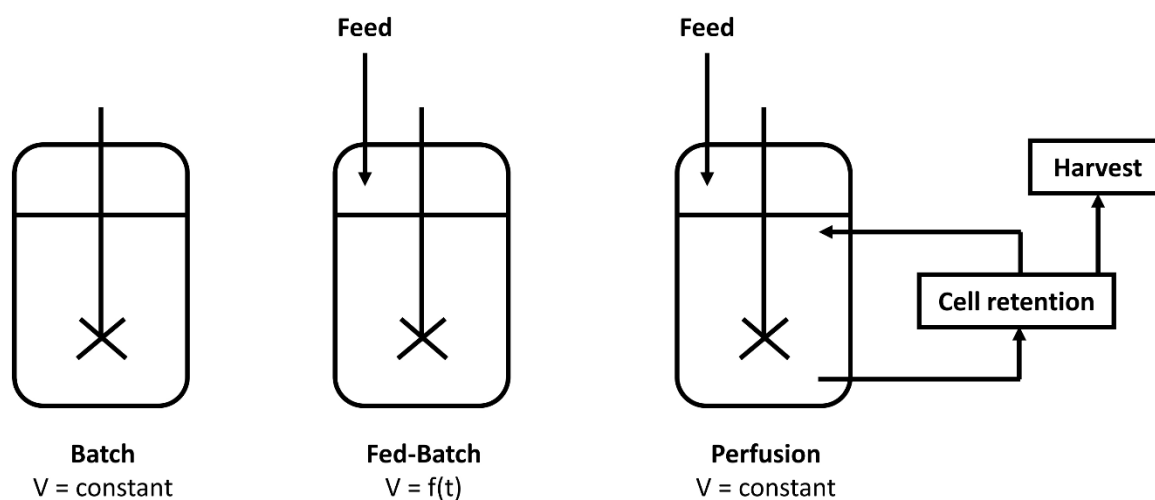


**Figure 3.** Schematic illustration of the different process modes: batch, fed-batch and perfusion mode.  $V$  = reactor volume. Own schematic representation.

Mammalian cell cultivations are performed in batch, fed-batch or perfusion mode (**Figure 3**). In batch mode, inoculated cells grow without any other addition or manipulation of the process. With increasing process time, cells face substrate deficiency mainly due to high viable cell densities (VCD) and protein production rates [101,102]. Batch processes demonstrate uncontrolled accumulation of by-products as L-lactate (L-Lac) or ammonia. This accumulation is enforced by high initial substrate concentrations that are required for sufficient growth. These by-products can hamper growth, product quality and productivity [103,104]. The accumulation of toxic by-products is a major concern in cell culture as e.g. L-Lac, L-Ala and ammonia can affect cell growth, product concentration and quality [103–108].

The fed-batch mode alleviates the accumulation and starvation problems of the batch mode. Cells are inoculated in media with moderate or low substrate concentrations and new substrates are fed demand-oriented during the cultivation in a concentrated solution [102]. This mode reduces by-product formation and substrate limitation and favors high VCDs and product titers. Optimal feeding is based on stoichiometric analysis of the cell culture

requirements and is accurately controlled to maintain proper concentrations. The fed-batch mode balances between limitation and excess [15,101].

In perfusion mode the volume added by feed is continuously withdrawn from the total cultivation volume with simultaneous cell retention, resulting in a constant cultivation working volume [109,110]. This strategy allows to further diminish by-product accumulation [101,111] and cultivations for long time periods and the synthesis of instable products [101].

## **2.5 Process Development, Qualification, Verification and Control in CHO Cell Cultivations**

Process development includes scale-up and final process design, whereas process qualification is needed to ensure a proper process design that allows a reproducible production. Continued process verification is the surveillance during routine production to ensure a constant and safe product [101]. The performance of cells depends on intrinsic (cellular) and extrinsic (environmental) factors including process mode, parameters, and media composition. Optimization and harmonization of all factors is required to allow a reproducible and stable high-quality process. The overall goal is to understand, control and avoid process variations.

In addition, scale-up characteristics must be taken into account as 5000 L bioreactors demonstrate a longer mixing time, lower oxygen transfer coefficient and lower dCO<sub>2</sub> removal rate [112]. In process development it is considered whether parameters are similar or easy scalable (e.g. volume of culture and feeding) or require adaption (e.g. agitation and aeration). Unfavorable aeration or agitation lead to accumulation of gases (e.g. CO<sub>2</sub>) or increased shear stress that hampers the process [113–115]. Process strategy screening and qualification starts with micro-scale stirred tank reactors (STR) that allow parallel testing and evaluation with design of experiment (DOE) strategies. Further testing occurs in bench top STRs and the final strategy is tested in pilot scale STRs to get a reliable process [2,100,116–118].

**Table 1.** Ranges of CHO cell culture parameters for temperature (T), osmolarity, dissolved oxygen (DO) and pH [13,101,119].

Parameter	Range
Temperature (T)	36 °C - 38 °C
Osmolarity	250 mOsmol kg <sup>-1</sup> - 400 mOsmol kg <sup>-1</sup>
Dissolved oxygen (DO)	25 % - 50 %
pH	6.7 – 7.4

Process mode and parameters are fine-tuned and process monitoring does at least include dissolved oxygen (DO), agitation (N), pH and temperature (T). Optimum process parameters and cultivation settings for CHO processes can significantly vary (**Table 1**). Cooling and heating devices allow temperature regulation. Osmolarity is initially adjusted in the media but can be influenced by subsequent feeds. DO depends on agitation and gas flow rate. Furthermore, the gas mixture is important and controlled by a device that mixes O<sub>2</sub>, air, CO<sub>2</sub> and N<sub>2</sub> according to the requirements [13,100]. Control of pH often occurs via base addition and CO<sub>2</sub> sparging (in bicarbonate buffered culture media). All parameters influence each other and are constantly monitored and adjusted.

## 2.6 Interaction of Cell Growth and Productivity

Cell cycle arrest boosts cell-specific productivity (CSP) [25–28], but productivity is not linked to a certain cell cycle phase [29–33]. Anyhow, it remains unclear if the arrest is the only reason for increased CSP as increased cell volume is linked to increased productivity in four CHO cell lines as well [33]. Cellular volume and cell cycle are connected, and increased productivity could be a result of both effects [34–36]. Overexpression of mTOR resulted in increased cell size, protein content, proliferation, CSPs and robustness [120]. Obviously, cell cycle arrest and reduced growth enables the cell to use remaining energy for other processes [121]. The observed interaction can be influenced by cell engineering of cytostatic genes [122] or medium additives as sodium butyrate (NaBu) [123]. Lowering the temperature is another approach that demonstrated decreased growth and increased protein productivity

[25,27,124]. An optimal balance between cell growth and productivity can maximize productivity.

## 2.7 Antibody: Structure and Characteristics

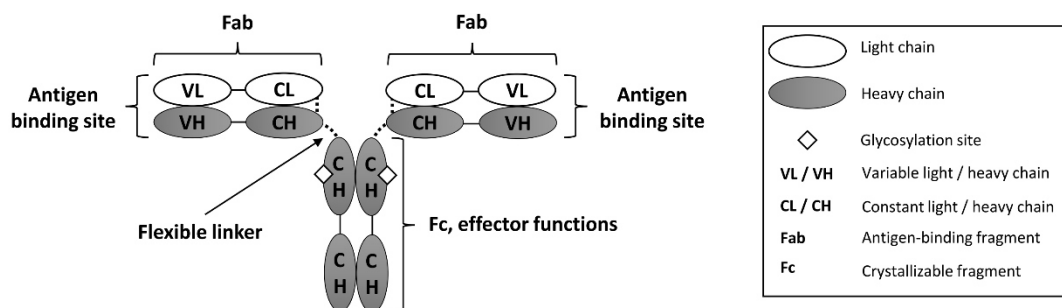


**Figure 4.** Schematic illustration of an immunoglobulin G antibody. The antibody consists of antigen-binding fragments (Fab) and the crystallizable fragment (Fc) that are made of light (L) and heavy (H) chains. The Fab and Fc parts are linked flexible. The antigen binding site is variable (V) whereas the remaining antibody is constant (C). The Fc has effector functions and inherits glycosylation sites. Own schematic representation according to [46,125,126].

Immunoglobulin G (IgG) is a class of antibodies that consists of two light and two heavy chains (**Figure 4**). The chains are associated covalently and non-covalently with each other and form three protein moieties that are linked in a flexible way. The antigen-binding fragment (Fab) consists of two identical protein moieties and is connected to the crystallizable fragment (Fc) that is a homodimer with a disulfide bridge. It forms interactions with ligands and inherits effector functions. The Fc region is composed of a part of the heavy chains, is naturally conserved, and has preserved sites for *N*-linked glycosylation. The light chains are crucial for the antibody recognition and binding as they contain a part of the antigen binding fragment [46,125,127,128]. The antigen binding site itself (epitope) is very variable and sometimes *N*-glycosylated (~15-20 %) [127,129]. Characteristics and classification of antibodies are dependent on their glycosylation pattern. These PTMs must be human-like which can be performed by mammalian cell systems [6–9]. Pharmacodynamic and -kinetic characteristics as bioactivity, distribution, solubility, stability, immunogenicity, and clearance rate depend on defined protein glycosylation patterns [125,130]. CHO cells demonstrate homologous genes

(over 99 %) of human glycosylation though 53 % are actually expressed [11]. Anyhow, CHO cells still differ: e.g. they express D-galactose- $\alpha$ -1,3-D-galactose ( $\alpha$ -gal) [131,132] and N-glycolylneuraminic acid (Neu5Gc) and lack  $\alpha$ -2,6-sialyltransferase [133] and  $\alpha$ -1,3-fucosyltransferases [134].

Post-translational modifications are highly diverse [127]. Anyhow, glycosylation and disulfide bridges are the most dominant group of post-expression adjustments in antibodies [135]. Disulfide bridge formation takes place in the ER with its non-reducing environment [136]. Glycosylation is O- or N-linked and occurs along the biosynthetic secretory pathway in Golgi and ER whereas N-linked glycosylation occurs exclusively in the ER [127,137].

The monitoring of the glycosylation pattern is highly important in biopharmaceutical production processes to produce reliable recombinant products. In this connection, glycosylation patterns are influenced by culture conditions, cultivation parameters or medium composition and are even directly engineered to improve antibody properties [137–139]. Engineering includes improvement of antibody-dependent cell mediated cytotoxicity (ADCC) [139–142] or reduction of non-human variants [143,144].

## 2.8 Cell Cycle and Apoptosis

The division process of one cell in two equal daughter cells is known as cell cycle. The cell cycle is highly regulated and conserved between species. It consists of the mitosis (M) phase and the interphase that is subdivided in gap 1 (G1), synthesis (S) and gap 2 (G2) phase (**Figure 5**). In G1-phase cell size increases and enhanced protein and organelle synthesis occurs. In the S-phase the semi-conservative chromosomal DNA replication took place. In the G2-phase the cell grows again. Finally, the cell divides during mitosis (M) phase [101,145,146]. In between the phases check points ensure proper execution of the mechanisms [147–149].



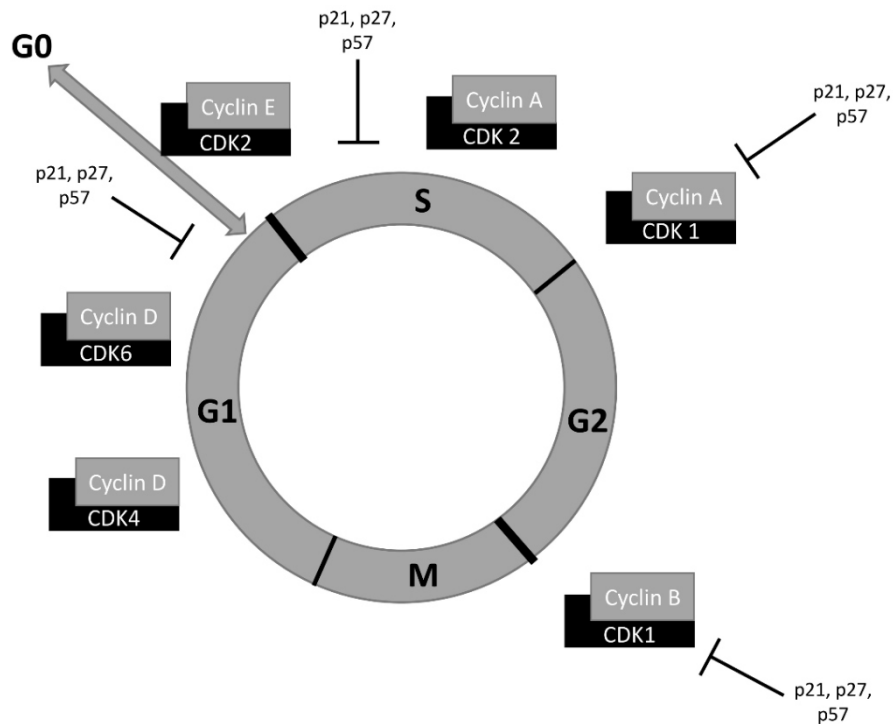


**Figure 5.** Schematic overview of the cell cycle and underlying mechanisms. G0: gap 0, G1: gap 1, S: synthesis, G2: gap 2, M: mitosis, CDK: cyclin dependent kinases. Black bars indicate cell cycle checkpoints with thicker bars indicating DNA damage checkpoints. Own schematic representation according to [145].

The cell cycle is tightly controlled by cyclin dependent kinases (CDK) and their controlling protein subunits, the cyclins (**Figure 5**). The binding of cyclins activates CDKs [145,150] and allows successive actions. During G1-phase CDK 2, 4 and 6 are important. Cyclin D protein amounts rise and bind to CDK 4 and 6. Transition of G1- to S-phase is marked by a rise of cyclin E that binds to CDK 2. The complexes of CDKs and cyclins phosphorylate and inactivate transcription factors, inhibitors and corepressors (signal transduction). These modifications allow to pass the current cell cycle checkpoints. If the progression is restricted, cells can enter G0-phase. In S-phase, cyclin A levels increase, bind to CDK 2 and replace cyclin E. At the end of S-phase, cyclin A binds to CDK 1 and initiates the transition of S- to G2-phase. G2-phase ends with binding of cyclin B to CDK 1 and the subsequent start of mitosis [145,151]. These mechanisms are further influenced by CDK inhibitors (CDKIs) as p21, p57 and others that are activated after DNA damage or other stressors and can enforce cell cycle checkpoints.

Proceeding is dependent on their deactivation or degradation [145]. DNA damage is a commonly occurring phenomenon that is induced by external and internal stimuli [147]. As above mentioned, checkpoints especially in G1- and G2-phase allow the cell to arrest the ongoing cycle and to repair damages [147,148,152,153]. If the damage is not repairable, apoptosis is induced. In M-phase the cell divides into daughter cells by equal chromosome and organelle separation with the help of the mitotic spindle. This process is regulated by kinases: the mitotic spindle is assembled, the nuclear envelope is broken down and the chromosomes are moved [148,152,154,155]. Finally, the cells divide.

Cell cycle mechanism are engineered as well. Engineering strategies focus on cyclin E [156] and demonstrated improved growth rate and VCD. Others focus on cell cycle arrest to improve productivity [121,122]. The overexpression of p27 demonstrated effects on metabolism that are probable based on increased consumption of oxygen, D-Glc and L-Gln and increased intracellular pools of AMP, ADP and ATP [157].

The aforementioned DNA damage and accumulation of misfolded proteins in the ER are the main reasons for apoptosis induction. Programmed cell death named apoptosis allows the cell to conduct its death after cellular damage without altering neighboring cells. For this purpose, the cells initiate a complex enzymatic program that starts its own degradation. Hallmarks are cell shrinkage, nuclear DNA fragmentation and membrane blebbing. By contrast, necrosis is cell death that occurs uncontrolled after cellular damage and is accompanied by swelling and bursting of the cell [145]. Apoptosis is initiated via extrinsic or intrinsic signaling pathway and conducted by caspases. The extrinsic pathway requires the binding of an extracellular ligand on death receptors whereas the intrinsic pathway is mitochondria mediated. Both pathways result in a caspase cascade initiation that includes executor caspases e.g. for DNA, nuclear matrix or cytoskeleton degradation. Anti-apoptotic factors hinder apoptosis initiation and are amplified by e.g. growth factors [145].

Apoptosis is the main reason for cell death in bioreactors. Its manipulation can prolong cell culture duration and therefore enhance protein production [12,158,159]. The main reason for apoptosis in bioreactors is nutrient depletion including oxygen, accumulation of by-products,

elevated osmolarity and mechanical shear stress. Apoptosis avoiding additives include insulin growth factor [160], suramin [161] and *N*-acetylcysteine [162,163]. Apoptotic mechanisms are important targets for genetic engineering. Permanent elimination of Bax and Bak genes [164] resulted in cells that were more resistant against apoptotic stimuli and demonstrated improved survival. The overexpression of Bcl-xL in CHO-DG44 cells improved recombinant protein expression [165].

## 2.9 Genome and Transcriptome

In 2011, the genomic sequence of CHO-K1 was completely elucidated. The data revealed 37.79 % transposable elements (mouse: 37 % and human: 46 %). Xu et al. predicted 24,383 genes that demonstrated 19,711 homologues in human, 20,612 in mouse and 21,229 in rat [11]. Genomic data of different CHO cell lines confirmed the chromosomal diversity. Becker et al. identified 24,576 possible genes in K1 cell line whereas Xu et al. identified 24,383 genes [11,166]. Earlier, prediction of genes was performed by plotting against reference genomes of *Homo sapiens*, *Mus musculus* and *Rattus norvegicus* [11,167]. This procedure was not applied anymore since CHO genome data is available. Nevertheless, additional mapping to human or other rodents can still increase mapping hits [168,169].

The transcriptome is the entirety of all transcribed RNAs at a certain time in the cell and represents the cell's adaption to its environment e.g. via histone proteins [170]. It does not cover the whole genome that contains coding and non-coding regions in eukaryotic cells. Transcriptomes and expression changes are analyzed with microarrays or RNA-Sequencing (RNA-Seq). In RNA-Seq, isolated cellular RNA is translated into complementary DNA (cDNA) that is finally sequenced using methods of next-generation sequencing. Transcriptomics research mainly focuses on adaptations and changes in the expression patterns due to extrinsic and intrinsic changes. In CHO cell cultivations, the broad range covers adaptations of expression patterns during lower temperature [171,172], cell cycle phases [173], polyamine starvation [174], osmotic stress [175], in fast- and slow-growing cells [176], in high- and low- [177] and in stable and unstable producers [178]. These studies try to unravel genes and expression patterns that are required for high VCDs, CSPs, viability and stability. Other studies focus on

effects that are the result of media additives such as NaBu, caffeine or 3-methyladenine [171,172,179]. The analyzed patterns demonstrate correlations to favorable behaviors and give hints for a targeted and optimized cell line engineering [172].

## 2.10 Cytoskeleton and Protein Secretion

The cytoplasm consists of cytosol, organelles, and cytoskeleton. The cytoskeleton is a composition of actin microfilaments, microtubules, and intermediate filaments. Microtubules define a structure that anchors organelles in the cell. Intermediate filaments are diverse and differ between cell types. Actin microfilaments are detrimental for e.g. movement, phagocytosis, and division [154]. They have functions in cell shape, protein synthesis [180], transport [181] and secretion [182,183]. The cytoskeleton is important for high producer cell lines as actin, tubulin and the actin-binding cofilin are important in protein transport [184]. Transcriptome analysis of high producers revealed higher gene expression of actin- and cytoskeleton-related proteins [41,42].

Protein secretion and post-translational mechanisms are potential bottlenecks in CHO cell line protein expression. In order to improve the protein secretion system, different genetic engineering approaches were investigated. An enhanced productivity was observed after engineering of SNAREs [38], overexpression of calnexin (CNX) and calreticulin (CRT) [185], engineering of vesicle traffic and organelles (ER and Golgi) [186]. High recombinant protein production and secretion can lead to unfolded and misfolded protein accumulation in the endoplasmic reticulum (ER) and subsequent to the induction of unfolded protein response (UPR). Knockdown of related factors as activating transcription factor 6 beta (ATF6 $\beta$ ) resulted in enhanced antibody titer by balancing UPR [187]. Interference with the ER-proteins ceramide synthase 2 (CerS2) and Rab1 GAP Tbc domain family member 20 (Tbc1D20) via *mitosRNA-1978* resulted in improved cell-specific productivity [39]. Modification and engineering of protein secretion is of high interest to improve CSPs.

## 2.11 CHO Cell: Overview of Cell Organelles and Metabolism

The cell has different organelles that are distributed in the cytosol. Mitochondria that demonstrate an important role in the cell are eukaryotic cellular compartments next to e.g. endoplasmic reticulum (ER), nucleus, Golgi apparatus or lysosomes. Mitochondria have an inner and an outer membrane. The outer membrane consists of lipids (around 50 %), enzymes and the transport protein porin. Open porins are permeable for ATP, NAD and coenzyme A. The inner membrane is folded which increases its surface massively. The folded structure defines the intercrisae space and the matrix space. The inner membrane has a high protein to lipid ratio (around 1:15) and many of the phospholipids are cardiolipins. Contraire to the outer membrane, the inner one is highly impermeable, and transporters are necessary [154,188]. At least 30 metabolite transporters with about 50 transport processes have been reported [188]. Mitochondria incorporate important parts of the metabolism and cellular regulation as tricarboxylic cycle, electron transport chain, oxidative phosphorylation, and apoptosis [46,154].

The metabolism of CHO consists mainly of several catabolic pathways as glycolysis, tricarboxylic cycle (TCA), pentose phosphate pathway (PPP), anaplerotic pathways, oxidative phosphorylation and  $\beta$ -oxidation. They provide important precursor metabolites that serve for nucleotide and amino acids synthesis next to others that are essential building blocks for the synthesis of macromolecules as proteins, DNA and RNA [46].

## 2.12 Glycolysis, TCA and Amino Acids

The growth of CHO cells is aerobic as they need mandatory oxygen for their metabolism. The main carbon (C)-source is D-glucose (D-Glc), but other sugars (as D-fructose and D-galactose) are potential C-sources as well. In glycolysis, imported D-Glc is rapidly converted into glucose 6-phosphate (G6P) via the enzyme hexokinase. In contrast to D-Glc, G6P cannot pass the membrane anymore and is conducted into the glycolysis pathway or the pentose phosphate pathway (PPP).

In the PPP, G6P is converted into ribulose 5-phosphate and two  $\text{NADP}^+$  are converted to NADPH,  $\text{CO}_2$  and two  $\text{H}^+$  are released which displays the oxidative part. In the nonoxidative part, epimerases, isomerases, trans-ketolases and -aldolases convert  $\text{C}_3$ ,  $\text{C}_4$ -,  $\text{C}_5$ -,  $\text{C}_6$ - and  $\text{C}_7$ -molecules into each other and leads PPP intermediates back to the glycolysis. The intermediate ribose 5-phosphate itself is a precursor for nucleotide synthesis, as it can be converted to its activated form phosphoribosyl pyrophosphate (PRRP) [46]. The synthesis of nucleotides e.g. adenine nucleotides can occur *de novo* or via salvage pathways. *De novo* synthesis is energy demanding and recycling is favored. One example is the adenine-phosphoribosyl transferase that catalyzes the conversion of adenine and phosphoribosyl pyrophosphate (PRRP) to adenosine monophosphate (AMP) (and  $\text{PPi}$ ) [46].

In the glycolysis G6P is subsequent converted into pyruvate over several reaction steps [46]. In CHO cells over 90 % of the carbon received from D-Glc is shuttled into glycolysis [189,190]. Summarized, in the glycolysis G6P is converted to two pyruvates and the overall energy output is two ATP and two NADH.

Pyruvate can be converted into L-lactate by oxidation/regeneration of NADH to  $\text{NAD}^+$ . This phenomenon is called Warburg effect [191] and allows the cell to rapidly consume high levels of D-Glc by regenerating essential reductive molecules without the slower oxidative phosphorylation. Nevertheless, a lot of the usable energy of D-Glc is wasted in this overflow scenario. However, some CHO cell lines demonstrate a switch to L-Lac re-uptake and recycle the remaining energy. The mechanism behind the L-Lac shift seems to be multifactorial and is intensively investigated [106,192–194]. The investigation of the L-Lac shift with flux balance analysis (FBA) demonstrated a higher energy efficiency of cells during L-Lac consumption [37] that may explain the endured cell culture duration with enhanced viability and improved productivity that is often seen in correlation with L-Lac shift. Transcriptomic and metabolic studies revealed that the L-Lac shift is a result of a low glycolytic flux and high extracellular L-Lac concentrations that may trigger signaling pathways [195]. Other research pointed out that media composition and mitochondrial oxidative potential affect the L-Lac shift/recycling [196]. The L-Lac shift is favorable for process performance as it allows the metabolization of

L-Lac to pyruvate that is subsequently used in the TCA. Anyhow, this mechanism is influenced by multiple factors and therefore is hardly to control.

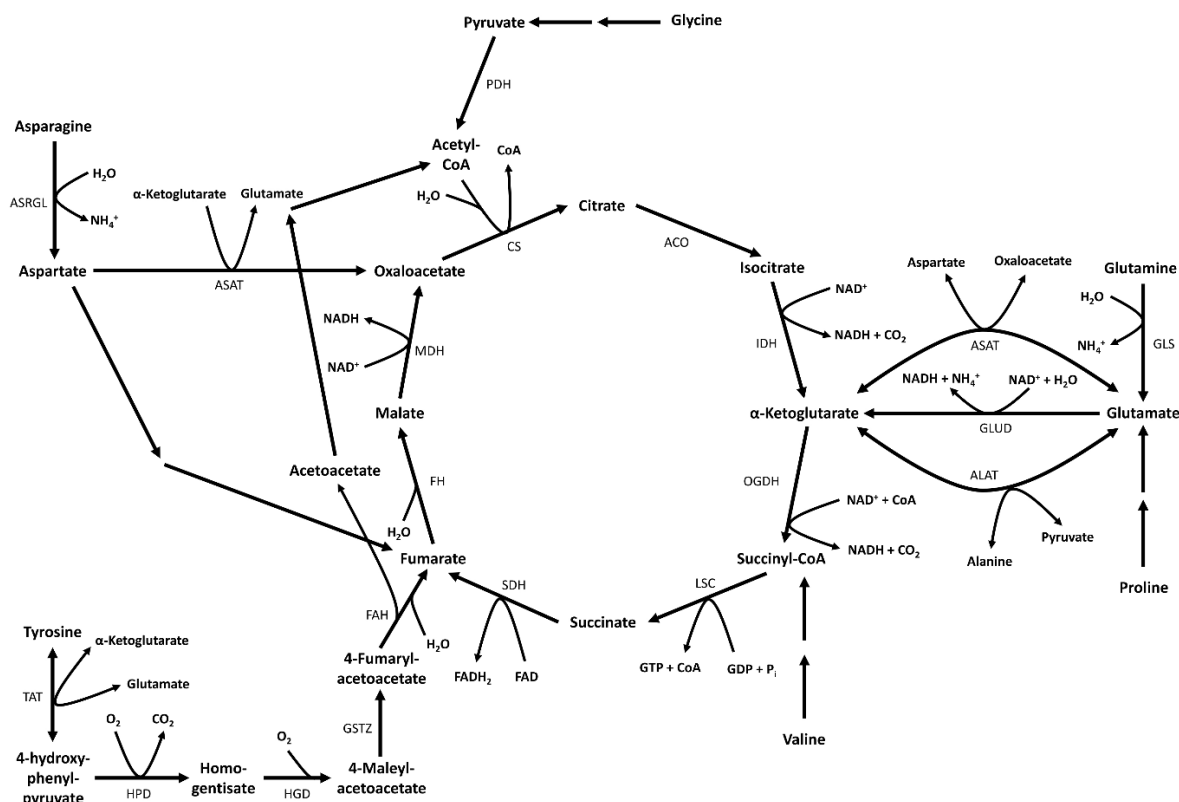


**Figure 6.** Schematic overview of tricarboxylic acid (TCA) cycle and degradation of the amino acids L-asparagine, L-aspartate, L-tyrosine, L-valine, L-proline, L-glutamine, L-glutamate and glycine. ACO (aconitase), ALAT (alanine aminotransferase), ASAT (aspartate aminotransferase), ASRGL (asparaginase), CS (citrate synthase), FAH (fumaryl-acetoacetase), FH (fumarase), GLS (glutaminase), GLUD (glutamate dehydrogenase), GSTZ (maleyl-acetoacetate isomerase), HGD (homogentisate oxidase), HPD (4-hydroxyphenylpyruvate dioxygenase), IDH (isocitrate dehydrogenase), LSC (succinyl-CoA synthetase), MDH (malate dehydrogenase), OGDH ( $\alpha$ -ketoglutarate dehydrogenase complex), PDH (pyruvate dehydrogenase), SDH (succinate dehydrogenase), TAT (tyrosine aminotransferase). Own schematic representation according to [46].

Instead of its conversion into L-Lac, pyruvate can be shuttled into mitochondria. Its conversion to acetyl-CoA (oxidative decarboxylation by pyruvate dehydrogenase) marks the starting point of tricarboxylic acid (TCA) cycle (**Figure 6**). Acetyl-CoA's linkage to oxaloacetate (citrate synthase) forms citrate that is subsequently isomerized to isocitrate (via cis-aconitase by aconitase). In a next step, isocitrate is converted (oxidative decarboxylation, isocitrate

dehydrogenase) into  $\alpha$ -ketoglutarate ( $\alpha$ KG) and then to succinyl-CoA ( $\alpha$ KG-dehydrogenase, oxidative decarboxylation). These two steps produce NADH and CO<sub>2</sub>. The conversion of succinyl-CoA to succinate via succinyl-CoA synthetase provides a GTP. The reduction of FAD to FADH<sub>2</sub> is the result of the oxidation of succinate to fumarate via succinate dehydrogenase. Fumarate is then hydrated to malate via fumarate hydratase. The final oxidation to oxaloacetate by malate dehydrogenase closes the circle and reduces NAD<sup>+</sup> to NADH. The overall energy balance of the TCA is 3 mol NADH, 1 mol FADH<sub>2</sub> and 1 mol GTP per 1 mol D-Glc [46].

L-Glutamine (L-Gln) and L-asparagine (L-Asn) are the essential main nitrogen(N)-sources in CHO cells. Connected to this, L-glutamate (L-Glu) is usually not converted to L-Gln. Incorporated L-Gln is initially deaminated to L-Glu that can be converted to  $\alpha$ KG by oxidative deamination via glutamate dehydrogenase, via alanine aminotransferase or transamination with oxaloacetate to  $\alpha$ KG and L-aspartate (L-Asp) via aspartate transaminase [46,197]. It was demonstrated that this pathway is an important source for ATP production in CHO cells [198]. The produced  $\alpha$ KG is converted to malate throughout the TCA and the former L-Gln molecule can be catabolized to CO<sub>2</sub> in several TCA rounds. This metabolization of L-Gln is one possible way of the so called “glutaminolysis” and inherits several other pathways that allow the usage of L-Gln as an energy source in cells [197]. In exponential growth phases, L-Gln contributes the major part to TCA activity due to the Warburg effect that leads to a conversion of pyruvate to L-Lac [199].

Incorporated L-asparagine (L-Asn) is converted to L-Asp that can be converted to fumarate (via urea cycle) or transaminated to oxaloacetate [46]. Aromatic amino acids as L-tyrosine (L-Tyr) are degraded with the help of oxygen. Finally, it is converted to fumarate and acetoacetate [46]. L-Proline faces several reactions in its conversion to L-Glu that can enter the TCA via  $\alpha$ KG. Glycine is converted to L-serine that is deaminated to pyruvate. L-Valine is degraded to propionyl-CoA that can enter TCA via succinyl-CoA. Summarized, amino acids and their degradation products can contribute substantial parts to TCA activity.



The oxidative phosphorylation (OXPHOS) takes place in the mitochondria [46]. The complex consists of NADH dehydrogenase (complex I), succinate dehydrogenase (complex II), cytochrome  $bc_1$  complex (complex III), cytochrome c oxidase (complex IV) and ATP synthase (complex V) in the inner mitochondrial membrane. Reduced cofactor equivalents (as NADH and  $FADH_2$ ) and direct reactants of the TCA (succinate to fumarate) are used to shuttle  $H^+$  contrary to a gradient into the intermembrane space (cytoplasm) of mitochondria. Complexes I, II and III pump transfer electrons and transfer  $H^+$  to the intermembrane space (cytoplasm). Complex IV, the cytochrome c oxidase, oxidizes cytochrome c and the released electrons are transferred to oxygen to form water and shuttle  $H^+$  in the intermembrane space (cytoplasm). The need of oxygen for this reaction defines cells as aerobic [46]. The accumulation of  $H^+$  in the cytoplasm induces an electrical and pH gradient whose potential energy is used by ATP synthase to produce ATP. This is called oxidative phosphorylation and this chemiosmotic mechanism was first published by Mitchell in 1961 [200]. Summarizing, an electric and chemical gradient is established by complex I to IV that pump  $H^+$  from the mitochondrial matrix to the cytoplasmic intermembrane space. Complex V, the mitochondrial ATP-synthase phosphorylates ADP to ATP based on the  $H^+$  reflux with the gradient through the rotating molecule [46].

The process is classified by the P/O ratio that defines the coupled efficiency of electron-transport chain and oxidative phosphorylation. It demonstrates the number of produced ATP per reduced oxygen [201]. Literature describes an average P/O ratio of 1.5 (0.88 - 2.2; theoretical ideal: 2.25) for succinate/ $FADH_2$  and 2.5 (0.7 - 3.5; theoretical ideal: 3.75) for NADH in CHO cells [201,202].

Apart from their energy role, adenine nucleotides work as regulators of the metabolism. The glycolytic enzyme phosphofructokinase (PFK) is allosterically inhibited by adenosine triphosphate (ATP). This inhibition is abolished by high levels of AMP. Pyruvate kinase is allosterically inhibited by ATP as well [46]. In addition, adenine nucleotides demonstrate roles in TCA regulation. The pyruvate dehydrogenase is the entrance enzyme of the TCA which is regulated in an allosteric way and via phosphorylation. ATP and adenosine diphosphate (ADP)

are important players in both mechanisms. High ADP levels stimulate pyruvate dehydrogenase activity and high ATP levels inhibit its action. The enzyme isocitrate dehydrogenase is activated allosterically by ADP whereas ATP acts as an inhibitor. The  $\alpha$ -ketoglutarate dehydrogenase is inhibited by high ATP concentrations as well [46]. Even more, the glutamate dehydrogenase is affected by ADP, ATP (and GTP). It is activated by ADP, whereas ATP demonstrated activation or inhibition dependent on its concentration [203,204]. The AMP-activated protein kinase (AMPK) is an important sensor of the cells' energetic status. AMPK acts under low energy conditions and regulates anabolic and catabolic pathways in order to increase ATP production and decrease ATP consumption [205]. It is activated by allosteric binding of AMP and subsequent phosphorylation [206] that is a result of a rising AMP:ATP ratio [207,208]. AMPK can phosphorylate parts of the mTOR complex and interacts with cell growth checkpoints [209]. AMPK can influence glycolysis because it phosphorylates related enzymes [210] and interacts with transcription [211,212]. In conclusion, adenine nucleotides are important energy molecules and regulators in cells.

In sum, the CHO cells produce energy molecules by multiple metabolic paths and mechanisms. Whereas the conversion of pyruvate to L-Lac results in a total theoretically energy yield of 2 mol ATP per 1 mol D-Glc, the complete metabolization of pyruvate through the TCA with followed oxidative phosphorylation results in theoretically 30-36 mol ATP per 1 mol D-Glc [46,213]. The complete oxidation of 1 mol L-Gln to CO<sub>2</sub> via TCA results in 24-27 mol ATP [197].

### **2.13 Polyamines, S-Adenosylmethionine (SAM) and 5'-Deoxy-5'-(methylthio)adenosine (MTA): Synthesis, Characteristics and Functions**

Growth and function of normal cells is dependent on polyamines (putrescine, spermidine and spermine) which are critical for cell survival [50]. They are cationic molecules that can interact with polyanionic molecules. Their formation is tightly connected to the SAM cycle (**Figure 7**). Putrescine is formed from ornithine via ornithine decarboxylase. Spermidine synthase forms spermidine from putrescine and spermine synthase forms finally spermine. Both reactions

need decarboxylated SAM and form MTA [214]. Polyamines are related to programmed cell death [51,52], as depletion of polyamine levels in different cell lines resulted in apoptosis activation and a disruption of mitochondrial membrane potential [215]. Moreover, they are associated with cell growth [52] and its homeostasis is important for genetic regulation [214], ion channels [52,214] and membrane functions [216]. Additionally, they are important to maintain the actin and microtubule network in CHO and a depletion leads to its destruction [53]. Polyamines prone the capacity for oxidation and the emerging products can induce mitochondrial dysfunction [51]. They are molecular interactors that influence the cell cycle, as polyamine levels demonstrate fluctuations during the cell cycle and are required to overcome cell cycle checkpoints [217]. Their depletion results in a stop of cell growth and an increase in size. Moreover, p21 is activated which leads to changes in gene expression and a loss of cellular proliferation capacity [218]. Polyamine depletion in CHO cells led to arrested cells in S- and G2-phase that cannot enter mitosis revealing an impact on DNA replication [54]. CHO cells treated with a S-adenosylmethionine decarboxylase inhibitor (formation of spermidine and spermine) demonstrated an increased length of S-phase [56]. Treatment of CHO cells with a spermine analog resulted in decreased cell proliferation that was the result of a delayed S-phase. Other phases were affected later as well [55]. The impact of polyamines on DNA is multi-factorial: They are important for DNA synthesis initiation [57] and they regulate a part of nucleosome conformation thus facilitating replication and transcription [219]. Polyamine and their relatives play an important role in mammalian cells and may serve as medium additives.

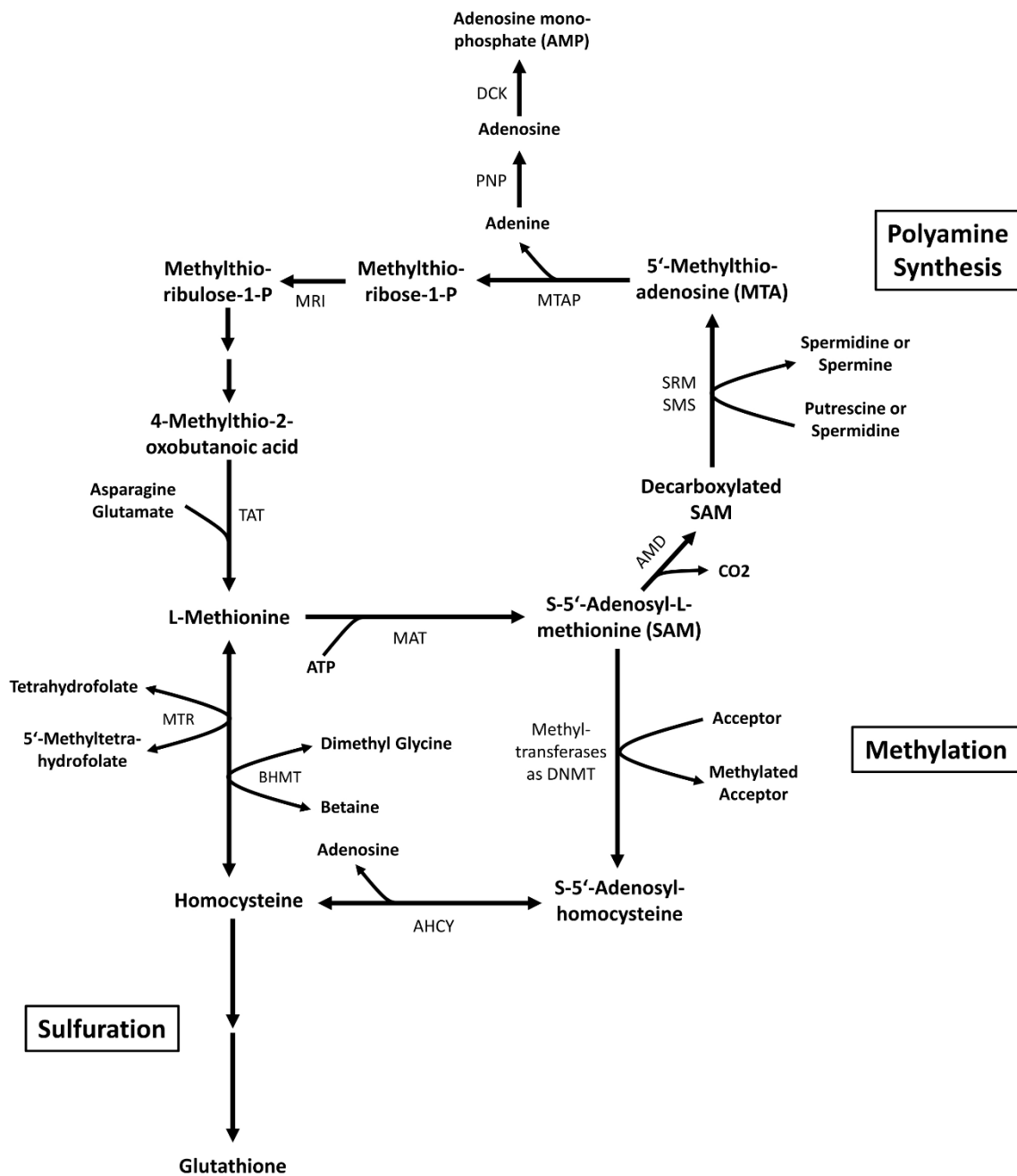


**Figure 7.** Schematic overview of the SAM cycle with its connections to sulfuration, methylation and polyamine synthesis. AHCY (adenosylhomocysteinase), AMD (*S*-adenosylmethionine decarboxylase), BHMT (betaine-homocysteine *S*-methyltransferase), DCK (deoxycytidine kinase), DNMT (DNA (cytosine-5)-methyltransferase), MAT (*S*-adenosylmethionine synthetase), MTAP (5'-methylthioadenosine phosphorylase), MTR (5-methyltetrahydrofolate-homocysteine methyltransferase), MRI (methylthioribose-1-phosphate isomerase), PNP (purine-nucleoside phosphorylase), SMS (spermine synthase), SRM (spermidine synthase), TAT (tyrosine aminotransferase). Own schematic representation according to [47,220,221].

As mentioned above, polyamine synthesis requires *S*-adenosylmethionine (SAM) and its conversion to 5'-deoxy-5'-(methylthio)adenosine (MTA). SAM is a naturally occurring cell component that was discovered by Cantoni in 1951 [222]. *S*-Adenosylmethionine synthetase (MAT) creates it from L-methionine (L-Met) and adenosine triphosphate (ATP). The SAM cycle displayed in **Figure 7** is a central point of its metabolism [47]. Transmethylation of SAM results in *S*-adenosyl-L-homocysteine (SAH) that is de-adenylated to homocysteine. Re-methylation of homocysteine results in L-Met and its adenylation finally forms SAM again [48,223]. SAM is involved in polyamine synthesis, trans-methylation and -sulfuration and is important for DNA and phospholipid methylation. These functions point out its crucial role in membrane fluidity and gene expression [48,223]. An example for methylation is *N*-methyltransferase that requires SAM for  $\epsilon$ -Lys methylation of histones. Additionally, the SAM cycle is important for the recycling of tetrahydrofolate, which is a cofactor of DNA and RNA synthesis [48]. The SAM cycle provides the precursor homocysteine for glutathione synthesis that is an antioxidant [224]. The importance of SAM as intracellular component is further confirmed by observations in liver disease as extracellular SAM is imported and affects the cellular glutathione level [48]. Moreover, SAM reduced the growth and development of liver cancer [225,226] and demonstrated an anti-apoptotic mechanism [49].

MTA is a naturally occurring molecule in mammalian tissues that consists of L-Met and ATP and is a side product in polyamine synthesis [58,227]. It occurs by spermidine and spermine synthesis and is rapidly metabolized by 5'-methylthioadenosine phosphorylase to adenine and *S*-methylthioribose 1-phosphate and finally to L-Met. The adenine is recycled in the nucleotide synthesis to form AMP, ADP or ATP. The MTA precursor SAM can be recovered by the reaction of L-Met and ATP [58,59]. As MTA is a potent inhibitor of spermidine and spermine synthase its fast degradation is crucial [64,227,228]. MTA can inhibit cell proliferation in different cell lines [49,60–62]. The observed arrest is mainly linked to the inhibition of polyamine synthesis [63] and DNA synthesis [64] as reduced polyamine intermediates arrested CHO cells in S-phase [229]. Other cellular mechanisms that are influenced by MTA are control of gene expression, cell proliferation, lymphocyte activation, tumor development and invasiveness, and the regulation of apoptosis [49,58–60,64,65]. Anyhow, the effect of MTA depends on the cell line.

Hepatocytes remained viable and prevented apoptosis whereas hepatocarcinoma cells suffered from apoptosis when they received MTA addition [49]. The interference of MTA with signaling pathways is diverse. MTA can inhibit the arginine methylation of the STAT1 transcription factor that finally influences gene transcription [66]. Furthermore, MTA can inhibit cAMP-phosphodiesterase [61,62]. The additional influence of MTA on methylation might be due to its close relation to the SAM cycle. It interacts with methyltransferases, inactivates *S*-adenosyl-L-homocysteine hydrolase [58] and is capable to inhibit protein methylation that demonstrates its role as post-translational modifier and accordingly as a regulator of gene expression and cellular signaling [60,65,66].

## 2.14 Metabolomics and <sup>13</sup>C Experiments

Metabolomics is an experimental field of systems biology that wants to identify and quantify metabolites of biochemical cellular networks. The metabolome contains all low molecular weight molecules (< 1500 Da) of a cell that are targets of enzymes. It displays a picture of the current physiological status of the cell [230,231] and allows the fundamental understanding of the intracellular phenotype and its interaction with the environment [232].

Metabolic flux analysis (MFA) is a tool to unravel interactions between metabolism and multiple cellular levels and helps to understand the fate of different medium contents as amino acids or peptides. Nyberg et al., 1998 demonstrated with the help of metabolomics that significant peptide uptake must be taken in account to adequately fit their model [233]. Use of labeled molecules improves MFA further and allows to determine metabolic fluxes with higher validity [234]. Fluxomics (<sup>13</sup>C-metabolic flux analysis – <sup>13</sup>C-MFA) is a scientific field that allows the determination of fluxes and the observation of biochemical pathways with the help of isotopic labeled substances [230,231,235]. It integrates *in vivo* measurements of metabolic pools into stoichiometric *in silico* network models [236]. To deepen the understanding of a CHO fed-batch a combination of metabolomics and *in silico* modeling was applied and revealed mechanisms that are related to growth [237]. The analysis of extracellular cell culture media with a metabolomic-based approach allowed to develop enhanced feeding strategies or discovered potential metabolic engineering aims [238]. Metabolomics is used to identify

important parameters that influence cell survival and productivity, revealing the importance of functional mitochondria and pointing out potential metabolic engineering targets [239]. In metabolomics, sample preparation is crucial as it can strongly influence the transient data. The selection of an optimal sampling, quenching and extraction method is highly important to guarantee the quantitative recovery of chemical stable metabolites [240]. Relative and absolute quantification of pool concentrations is often performed by gas or liquid chromatography coupled with mass spectrometry [241]. Metabolomics are an experimental field of highest interest, as it allows elucidating the actual cellular state.

## **2.15 Medium Ingredients and Optimization**

The medium basis contains water, carbon, nitrogen, phosphate, amino acids, fatty acids, vitamins, trace elements and salts [242]. One of the first synthetic media was developed by Eagle and colleagues in the 1950ies named Eagle's minimum essential medium (MEM) [243–245]. Their investigations about media compositions revealed that the need of 13 amino acids occurs due to a loss of biosynthetic mechanisms, lack of precursors or cofactors and a limited biosynthesis capacity [243–245]. Cells require vitamins as biotin, folic acid, nicotinamide, pantothenate, pyridoxal, riboflavin, and thiamine [244]. Especially L-Gln that is not essential in mammals demonstrates necessity in cultured cells [246]. Furthermore, L-Tyr is essential because L-phenylalanine conversion is often not sufficient in cultured cells [243].

Medium optimization is an ongoing process since decades. First mammalian cell cultures required fetal bovine serum (FBS) for growth and constant high viability. Serum was a frequently used medium supplement that consists of nutrients, hormones, growth factors, carrier proteins, and metabolites [247]. Production state-of-the-art uses serum-free chemically defined media because serum displays disadvantages. It has ethical considerations (unborn calf), as a natural product, it underlies lot-to-lot variations and harbors the risk of virus contaminations. Consequently, the use of chemically defined medium is favorable as it allows an increased definition of the process [248]. Additionally, it is appreciated in the sense of good manufacturing practice (GMP) and good cell culture practice (GCCP). Murakami et al. investigated serum and revealed that insulin, transferrin, ethanolamine, and selenium are

some of the essential components for cellular growth [249]. In 1958, Pumper adapted a mouse lung cell tissue cell line to serum-free medium for the first time [250]. Later, serum-free cultivation succeeded with a rat neuroblastoma and rat pituitary cell line [251,252]. In 1959, Ham succeeded to cultivate CHO cells in a synthetic medium, anyhow this did not allow high VCDs [253]. The serum-free [254] and protein-free [255] cultivation and antibody production of a CHO cell line was demonstrated in 1995.

Medium optimization is a multidimensional approach that includes component titration, media blending, spent media analysis and automated screening [256]. The development of a model to use the stoichiometric nutritional demands of the cells for medium development [257] and medium contents is carefully balanced to avoid the production of (toxic) side-products [15]. Statistical approaches as Plackett-Burman can be used for media design and process optimization [258]. There is not the one and only chemically defined media solution, every mammalian cell line has other needs and even CHO clones may differ [12]. Benchmarking of eight different commercial media with a CHO DG44 cell line and further evaluation of commercially available feed media points out that balanced D-Glc and amino acids concentrations fitting the cell lines needs are important to avoid overflow metabolism [259]. An optimal media is chemically defined, contains critical nutrients and growth factors for survival, growth, and production. It avoids accumulation of unwanted products as inhibitory and toxic metabolites.

## **2.16 Additives in Chemical Defined Media**

Amino acids are crucial for cell culture growth and survival as 13 amino acids are essential in synthetic cell culture medium [243–245]. Some amino acids display disadvantages regarding their stability (L-Gln) or solubility (L-Tyr). Consequently, dipeptides and longer peptides were investigated as medium additives as they often demonstrate an enhanced stability or solubility [16]. Furthermore, the investigation of hydrolysate spiked medium with a LC-MS/MS platform revealed potential contributors to cell culture productivity. A small number of dipeptides was identified including L-tyrosyl-L-leucine, L-phenylalanyl-L-valine and LL-cyclo(leucylprolyl). However, single addition of the dipeptides did not imitate observed



enhancing conditions [260]. Minamoto et al. created a serum-free medium with L-Gln containing dipeptides that demonstrated enhanced stability. The L-Gln in the dipeptide form was available and usable for the cells. The use of L-alanyl-L-glutamine (L-Ala-L-Gln) and glycyl-L-glutamine (Gly-L-Gln) instead of L-Gln is possible and showed that dipeptides can serve as L-Gln source and furthermore influence the metabolism [17]. The use of Gly-L-Gln influenced specific consumption rates and decreased accumulation rates of by-products [18]. Replacement parameters must be carefully investigated to optimize dipeptide usage in respect to reduced side-product formation [6,261] and balanced use can reduce apoptosis rates in cultures [262]. In experiments with L-Tyr-containing dipeptides, productivity and culture viability were enhanced in antibody producing cells. Moreover, a reduced by-product formation and better pH maintenance were observed [19]. L-Lys-containing peptides (3-5 aa) promoted cell cycle S-phase, consequently altered cell cycle distribution and demonstrated that product formation is not linked to a specific cell cycle phase [263]. This experiment demonstrated that peptides are more than additional nutrients. They may act as signaling molecules as seen in amino acids that were able to prevent apoptosis [264,265].

Addition of dipeptides was investigated by Christe and Butler as well as Kang et al. [18,19]. Both suggested a rather fast uptake of the dipeptides instead of extracellular hydrolysis. This hypothesis was further clarified by Sánchez-Kopper et al. who measured dipeptides intracellular. Furthermore, they observed different uptake velocities dependent on the dipeptide composition [45]. Nevertheless, transport of oligopeptides remains unclear in CHO cells. Mammalian cells have a proton-dependent oligopeptide transporter (PEP) that needs a membrane potential for transport. Moreover, the sequence of the concerning amino acids is crucial for transport and affinity [45,266].

Apart from short peptides, various small molecules were investigated. These chemicals can influence cell cycle, cell metabolism, redox regulation and other cellular mechanisms. Two examples are sodium butyrate (NaBu) and valproic acid. Both molecules negatively affect the maximum VCD and increase protein production. They demonstrate that the observed effect is dependent on its concentration and the cell line. Both are known histone deacetylase

inhibitors, whereas sodium butyrate demonstrated interaction with DNA accessibility as well [21,22]. Valproic acid is hypothesized to increase mRNA levels of the recombinant protein [21,23]. Noteworthy, both molecules have the potential to induce apoptosis that reduces overall productivity [21,22]. Other investigated molecules are catechins that demonstrate effects on growth and trapped cells in S-phase [20]. AMP addition trapped cells concentration dependent in S-phase as well and subsequent they demonstrated increased productivity [24]. Molecules with sulfate groups as suramin, dextran sulfate (DS) or polyvinyl sulfate can enhance cell viability and prevent apoptosis [161,267–269]. The interaction with autophagy mechanisms by 3-methyladenine (3-MA) led to an increased CSP when concentrations were within an ideal range [270,271]. Inhibition of cell growth can enhance productivity and is realized with valeric acid, rapamycin and CDK interactors [272–274] whereas cell growth was increased by addition of pyrimidine nucleosides [275].

Even more molecules were investigated as potential medium additives and were reviewed [276]. They can modulate protein synthesis, post-translational modifications and cell growth and are of high interest for medium optimization in process intensification.

### **3 Results: Original Publications**

The following manuscripts were partly adapted as figures were shifted to the results part to allow comfortable reading.

#### **3.1 Manuscript 1: Comparison of L-Tyrosine Containing Dipeptides Reveals Maximum ATP Availability for L-Prolyl-L-Tyrosine in CHO Cells**

The following manuscript was published in Engineering in Life Sciences in 2020 and reproduced with permission of the authors (copyright holders).

Verhagen N, Wijaya AW, Teleki A, et al. Comparison of L-tyrosine containing dipeptides reveals maximum ATP availability for L-prolyl-L-tyrosine in CHO cells. Eng Life Sci. 2020; 1-11.

Research Article

**Comparison of L-tyrosine containing dipeptides reveals maximum ATP availability for L-prolyl-L-tyrosine in CHO cells**

Natascha Verhagen<sup>1</sup>, Andy Wiranata Wijaya<sup>1</sup>, Attila Teleki<sup>1</sup>, Muhammad Fadhlullah<sup>1</sup>, Andreas Unsöld<sup>2</sup>, Martin Schilling<sup>3</sup>, Christoph Heinrich<sup>4</sup>, Ralf Takors<sup>1\*</sup>

<sup>1</sup>Institute of Biochemical Engineering, University of Stuttgart, Stuttgart, Germany

<sup>2</sup>Boehringer Ingelheim Pharma GmbH & Co. KG, Biberach, Germany

<sup>3</sup>Evonik Nutrition and Care GmbH, Darmstadt, Germany

<sup>4</sup>Xell AG, Bielefeld, Germany

**Correspondence**

Prof. Dr.-Ing Ralf Takors, University of Stuttgart, Institute of Biochemical Engineering, Allmandring 31, 70563 Stuttgart, Germany.

Email: ralf.takors@ibvt.uni-stuttgart.de

**Funding information**

Bundesministerium für Bildung und Forschung (BMBF), Grant/Award Number: 031L0077A

### **Keywords**

dipeptides, flux balance analysis, CHO, media optimization, monoclonal antibody

### **Abbreviations**

CAC, citric acid cycle; CHO, Chinese hamster ovary; EMP, Embden-Meyerhof Parnas; FBA, flux balance analysis; GY, glycyL-L-tyrosine; mAB, monoclonal antibody; MAS, malate-aspartate shuttle; NADH, nicotinamide adenine dinucleotide; PY, L-prolyl-L-tyrosine; REF, reference; TYR, L-tyrosine; VCD, viable cell density; YV, L-tyrosyl-L-valine

### **Practical application**

L-Tyrosine (TYR) is an essential amino acid for mammalian cells and shows poor solubility in cell culture media at neutral pH. Accordingly, TYR-containing dipeptides are commonly used that offer improved cellular supply. Here, we investigate the application of three L-tyrosine containing dipeptides showcasing the production of IgG1 with Chinese hamster ovary (CHO) cells. L-Prolyl-L-tyrosine (PY) caused the highest intracellular ATP availability that is an important property for all experimentalists in this field.

### **Abstract**

Increasing markets for biopharmaceuticals, including monoclonal antibodies, have triggered a permanent need for bioprocess optimization. Biochemical engineering approaches often include the optimization of basal and feed media to improve productivities of Chinese hamster ovary (CHO) cell cultures. Often, L-tyrosine is added as dipeptide to deal with its poor solubility at neutral pH. Showcasing IgG1 production with CHO cells, we investigated the supplementation of three L-tyrosine (TYR, Y) containing dipeptides: glycyL-L-tyrosine (GY), L-tyrosyl-L-valine (YV), and L-prolyl-L-tyrosine (PY). While GY and YV led to almost no phenotypic and metabolic differences compared to reference samples, PY significantly amplified TYR uptake thus maximizing related catabolic activity. Consequently, ATP formation was roughly four times higher upon PY application than in reference samples.

## 1 Introduction

Chinese hamster ovary (CHO) cells are important hosts for recombinant protein production and are the preferred system for monoclonal antibody production [14]. Early bioprocesses relied on the use of animal-derived sera like FBS to meet the growth and productivity needs of those cells [247]. However, the use of such sera is no longer favored because of the inherent risk of viral contamination [277] and typically high lot-to-lot variations, potentially affecting bioprocess performance and product quality [19,248].

Chemically defined (CD) media were introduced about five decades ago and predominately consisted of essential L-amino acids (Eagle's media [278]; F12 media [253]). At a concentration of about 2 mg/mL in water at room temperature and neutral pH, L-tyrosine (TYR) has the lowest solubility of all essential amino acids. Accordingly, only small amounts of TYR can be added to basal and feed media to avoid unwanted media precipitation, thereby trying to ensure process stability [19]. Non-wanted TYR insolubility could be prevented by feeding TYR with high pH because the latter greatly increases TYR solubility. However, pH control, salt concentration, and precipitation in the bioreactor are potential problems that can occur with such an approach. A safer and more robust approach is the replacement of single TYR by TYR-containing, chemically defined dipeptides, which can increase solubility up to 250-fold at neutral pH [16].

The industrial performance of CHO cells using specific TYR dipeptides was examined by Kang et al. [19], who demonstrated that substituting free amino acids with L-tyrosyl-L-lysine (YK), L-tyrosyl-L-histidine (YH), L-tyrosyl-L-alanine (YA), and L-tyrosyl-L-valine (YV) decreased secretion of L-lactate and ammonium by-products. Sánchez-Kopper et al. (2016) [45] showed that dipeptides such as L-alanyl-L-tyrosine (AY), glycyl-L-tyrosine (GY), and L-prolyl-L-tyrosine (PY) are taken up by CHO cells and cleaved intracellularly before entering catabolic and anabolic pathways. Furthermore, recent patents [279] demonstrate industrial interest in protecting the use of TYR-containing dipeptides in feed media.

In this study, we focus on the use of TYR-dipeptides as additional feeding compounds. We investigated the impact of related dipeptides on cellular metabolism. While the potential of

TYR-containing dipeptides has been shown by the above studies, little is known about the metabolic consequences resulting from their consumption. Showcasing IgG1 production with CHO cells, our investigation focused on the metabolic impact of dipeptide bolus feeding. We chose GY, YV, and PY as our model dipeptides. Phenotypic tests were complemented by quantitative metabolomics and flux analysis to decipher differences caused by dipeptides compared to cells lacking dipeptides in their feed. Whereas GY and YV did not significantly alter metabolism, PY increased the ATP supply, which represents a promising optimization target for future studies.

## **2 Materials and Methods**

### **2.1 Seed train, shake flask cultivation, and addition of dipeptides**

The following dipeptides containing TYR were supplied by Evonik Nutrition and Care GmbH (Darmstadt, Germany): glycyl-L-tyrosine (GY), L-prolyl-L-tyrosine (PY), and L-tyrosyl-L-valine (YV). The IgG1-producing CHO suspension cell line BIBH1 (provided by Boehringer Ingelheim Pharma GmbH & Co. KG, Biberach, Germany) was grown in chemically defined TC-42 medium (Xell AG, Bielefeld, Germany) supplemented with 4 mM L-glutamine (Carl Roth GmbH & Co. KG, Karlsruhe, Germany), 200 nM methotrexate (Sigma-Aldrich, Steinheim, Germany), and 0.1 g/L geneticin (Fisher-Scientific, Schwerte, Germany). Seed train and experiments were performed in pre-sterilized disposable shake flasks (Corning Inc., New York, USA) in a humidified and incubated rotary shaker (Infors HT Minitron, Infors GmbH, Einsbach, Germany) at 37°C, 150 rpm with 50 mm displacement, and 5% CO<sub>2</sub>. Stock solutions of TYR-based dipeptides were solved at neutral pH and introduced at the beginning of cultivation (0.05 mM). Furthermore, daily additions (0.05 mmol) of dipeptides were performed from 48 to 120 h of cultivation. In reference cell cultures, sterilized water was used to mimic the additional liquid volume in experimental cultures. Cultivation was performed with biological duplicates in two independent experiments.

## 2.2 Extracellular analysis

Samples were taken at least once a day during cultivation. Viable cell density and viability were determined using trypan blue staining and a Cedex XS cell counter (Innovatis AG, Bielefeld, Germany). The extracellular concentrations of D-glucose (D-Glc) and L-lactate (L-Lac) were determined using a Labotrace automatic analyzer (Trace Analytics GmbH, Braunschweig, Germany). The concentration of produced IgG was determined with an ELISA [28]. All sampling and measurement procedures were performed with three technical replicates. The extracellular concentrations of all proteinogenic amino acids with the exception of L-cysteine were quantified using reversed-phase chromatography (Agilent 1200 Series, Agilent Technologies, Waldbronn, Germany) with a precolumn fluorometric derivatization step using ortho-phthaldialdehyde (OPA)/9-fluorenylmethyl chloroformate (FMOC) [280,281]. The internal standard  $\gamma$ -aminobutyric acid (GABA) was added to all standard based external calibration levels and the analyzed samples.

## 2.3 Intracellular analysis

For each intracellular sample,  $1.6 \times 10^7$  cells were harvested, gently centrifuged (10 min,  $300 \times g$ ,  $4^\circ\text{C}$ ), washed, and quenched in liquid nitrogen. Washing steps were performed three times using ice-cold isotonic PBS solution to remove all extracellular compounds attached to the cells. Samples were taken after 60, 72, 76, 84, 96, 108, and 120 h of cultivation. Pre-processed cell pellets were stored at  $-70^\circ\text{C}$ . The intracellular metabolome was extracted from defined pellets using an adapted cold methanol/chloroform extraction method [45]. An ice-cold 1:2  $\text{CHCl}_3$ :MeOH solution was added to cells followed by ice-cold  $\text{CHCl}_3$  solution and finally by ice-cold water, with 5 min of vortexing after each addition. Resulting suspensions were incubated for 1 h at  $4^\circ\text{C}$  in a rotary overhead-shaker. Phase separation was afterward achieved by centrifugation for 10 min at  $3200 \times g$  and  $0^\circ\text{C}$ . The upper aqueous phase was separated and stored at  $-70^\circ\text{C}$  for further analysis. Dipeptide, amino acid, and central metabolite concentrations were determined on an HPLC system (Agilent 1200 Series) coupled with an Agilent 6410B triple quadrupole tandem mass spectrometer (QQQ-MS/MS, Agilent Technologies, Waldbronn, Germany). The LC-MS method was based on a bicratic (two-phase)



zwitterionic hydrophilic interaction chromatography (ZIC-pHILIC) under alkaline mobile phase conditions without any derivatization [282,283]. Targeted metabolites were detected with high selectivity with pre-optimized precursor-to product ion transitions and associated MS/MS settings in multiple reaction monitoring (MRM) mode. Absolute quantifications were performed by adapted standard based external calibrations with constant addition of global internal standards (50  $\mu$ M L-norvaline and GABA). Data were analyzed using MassHunter B.06.00 Analysis software.

Intracellular pools of AxP nucleotides were determined using an ion-pair-reversed-phase chromatography method with a HPLC system (Agilent 1200 Series) [284]. Underivatized samples were detected via UV light (diode array detector). Quantifications were performed by external standard calibration and selected samples were spiked with AMP, ADP, and ATP (internal calibration) to evaluate the influence of the sample matrix.

## 2.4 Cell-specific rate estimations

Cell-specific rates of changes in extracellular metabolites were used as constraints when performing flux balance analysis (FBA). Cell-specific exo-metabolic rates were estimated from extracellular metabolite concentrations and viable cell density over time. Using Equations 1 and 2 and linear regression, growth rate and specific exo-metabolome uptake and secretion rates were estimated.

$$\frac{dC_x}{dt} = \mu C_x \Rightarrow \ln(C_x) = \mu(t - t_0) + \ln(C_0) \quad [1]$$

$$\frac{dC_i}{dt} = q_i C_x \Rightarrow C_i = \left(\frac{q_i}{\mu}\right) C_x - C_{i,0} \quad [2]$$

## 2.5 Flux balance analysis

The metabolic model used in this study is a simplified genome-based model derived from the following sources: KEGG [285], CHOMINE [286], and *Mus musculus* GeM [287]. The detailed metabolic model is presented in 6.1. This model includes the central carbon metabolic pathway (consisting of the Embden- Meyerhof Parnas [EMP; glycolysis], pentose phosphate pathway [PPP], citric acid cycle [CAC], and anaplerotic reactions), the biosynthesis of essential

biomass precursors (fatty acids, steroids, glycogen, and nucleotides), and amino acid catabolism. The biomass composition required to model cell growth uses values reported by Sheikh et al. [288], whereas antibody composition is based on Martens [289]. Dipeptide cleavage occurs intracellularly following findings reported by Sanchez-Kopper et al. [45].

FBA was used to predict the fate of intracellular dipeptides and determine their role in CHO metabolism. FBA was performed using Insilico Discovery (Insilico Biotechnology, Stuttgart, Germany). FBA was carried out during the exponential growth phase, when the highest amount of dipeptide consumption occurs. Multiple assumptions were made for FBA. First, FBA was performed under a metabolic steady state with a constant growth rate and specific rates of change in D-glucose, L-lactate, L-glutamine, and L-asparagine levels. Additionally, the P/O ratio of nicotinamide adenine dinucleotide (NADH) and flavin adenine dinucleotide (FADH<sub>2</sub>) oxidation was assumed to be 1.5 and 1.2 mol ATP per mol of the nucleotide, respectively. FBA was performed using growth rate and extracellular metabolome uptake/secretion rates as constraints. The objective function of FBA was to maximize the model-predicted growth rate.

Three simulations were performed for experimental and control cultures (REF, GY, PY, and YV) to obtain the maximum, minimum, and median rate predictions. Maximum (best-case scenario) and minimum predictions were simulated using the maximum or minimum uptake and secretion rates, respectively. For median estimation, maximum and minimum settings were applied as constraints. Upper and lower confidence intervals were calculated using twice the standard error of the predictions (i.e., 95 % confidence level).

### **3 Results**

#### **3.1 The addition of L-prolyl-L-tyrosine alters cell growth and metabolism**

Initially, TYR-containing dipeptides were added to a final concentration of 0.5 mM to cell culture medium used to cultivate CHO BIBH1 cells for IgG1-antibody production. Fresh additions of TYR-containing dipeptides (0.05 mmol) took place after 48, 72, 96, and 120 h of cultivation (indicated by arrows in **Figure 8**). The addition of L-prolyl-L-tyrosine (PY) significantly reduced viable cell density (VCD), unlike the addition of glycyl-L-tyrosine (GY) and

L-tyrosyl-L-valine (YV). Cells receiving regular additions of PY only reached a maximum viable cell density of  $(4.030 \pm 0.153) \times 10^6$  cells/mL, which was approximately two-thirds of the viable cell densities of GY, YV, and reference (REF) cultures.

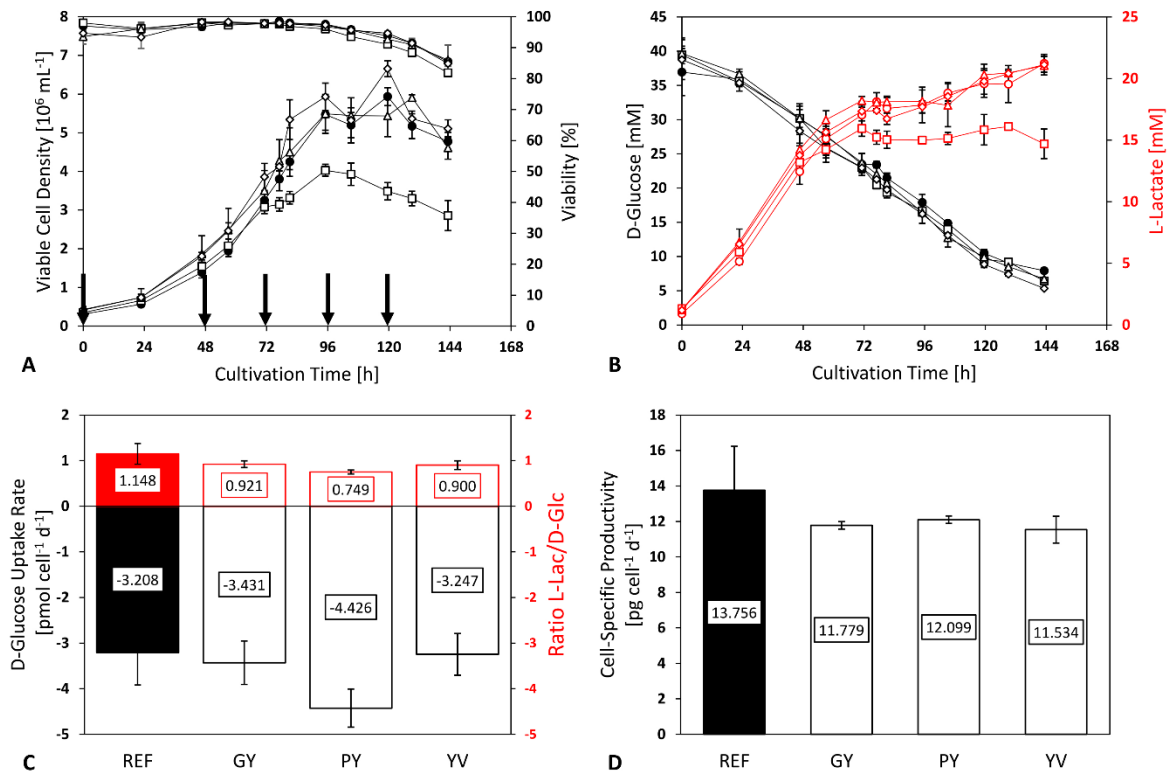


**Figure 8.** (A) Time courses of viable cell density [ $10^6$  cells mL<sup>-1</sup>] and viability [%] and (B) time courses of extracellular D-glucose (black) and L-lactate (red) concentrations [mM] of dipeptide supplemented cells (GY  $\Delta$ , PY  $\square$ , YV  $\diamond$ ) and reference (REF  $\bullet$ ). Arrows indicate time points at which dipeptides or water were added. (C) Cell-specific rates of the exponential phase are calculated in [ $\mu\text{mol cell}^{-1} \text{d}^{-1}$ ] for D-glucose consumption (black) and D-glucose-to-L-lactate-ratio (red). (D) Cell-specific productivity [ $\mu\text{g cell}^{-1} \text{d}^{-1}$ ] of dipeptide supplemented cells (GY, PY, YV) and the reference (REF) in the exponential phase. Error bars show standard deviations of biological duplicates.

PY addition affected antibody titer (**Figure 15**) whereas cell-specific antibody productivity was similar for all experimental conditions. Specific D-glucose consumption rates were highest after PY addition during the exponential phase. Furthermore, cells that grew in medium with PY showed reduced L-lactate formation reflected in the low ratio of D-glucose consumption to L-lactate secretion (PY:  $0.749 \pm 0.030$  mol<sub>D-Glucose</sub>/mol<sub>L-Lactate</sub>; REF:  $1.148 \pm 0.161$  mol<sub>D-Glucose</sub>/mol<sub>L-Lactate</sub>; **Figure 8**).

### 3.2 Dipeptide uptake depends on composition and causes metabolic changes

Uptake dynamics of TYR at different cultivation time points (48, 72, 96, and 120 h) are displayed in **Figure 9**. PY addition led to the largest total TYR uptake rates (indicated by the entire columns) and the largest fractions of TYR that remained intracellular (white columns) after 48, 72, and 96 h of cultivation. Remarkably, each addition of a TYR-containing dipeptide increased TYR uptake compared to reference cultures. However, some TYR from the decomposed dipeptide was always secreted (indicated by the red bar).

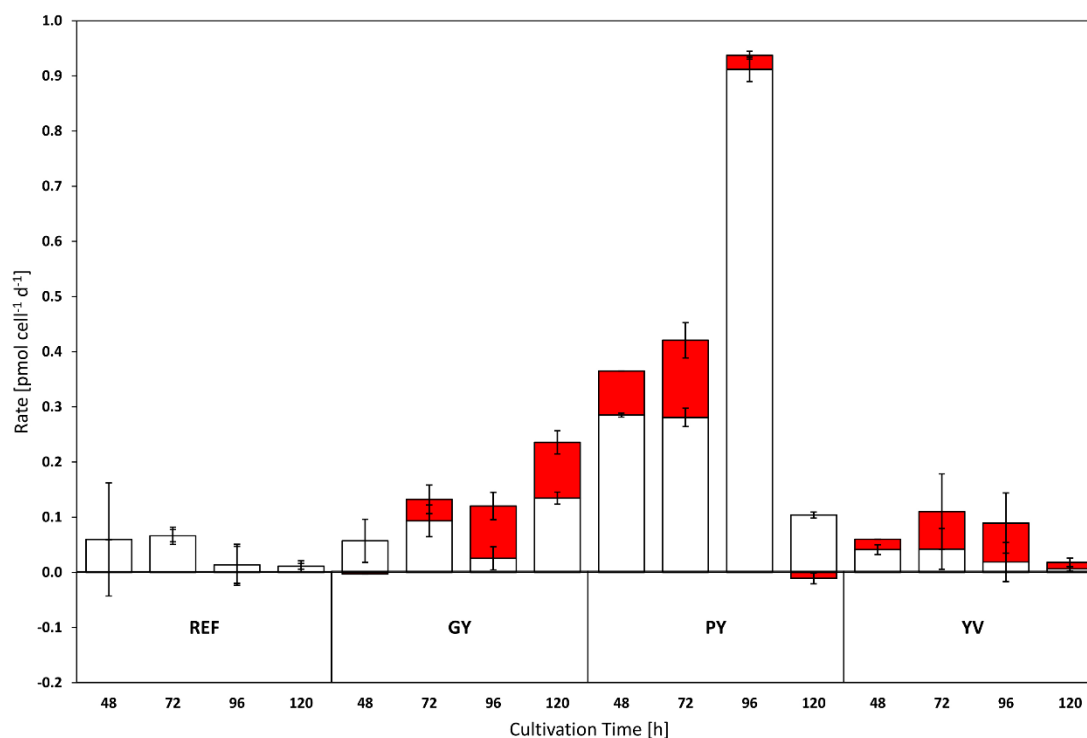


**Figure 9.** TYR uptake and release rates [pmol cell<sup>-1</sup> d<sup>-1</sup>] via dipeptides addition compared to reference cultures (REF) after 48, 72, 96, and 120 h of cultivation. Columns indicate the total levels of dipeptide uptake consisting of retained (white) and released (red) parts of TYR. Error bars show standard deviations of biological duplicates.

Small intracellular pools of dipeptides measured in intracellular extracts indicate the uptake of all dipeptides by cells. Intracellular fluctuations reflect extracellular bolus feeding. Repeated dipeptide addition to the medium (48, 72, 96, and 120 h) increased extracellular concentrations and consequently increased intracellular pool sizes of the intact dipeptides

thereafter. Besides GY and YV, extracellular PY is depleted at 72 and 96 h demonstrating the faster uptake of PY (**Figure 16**).

Uptake rates of the essential amino acid L-glutamine were similar in PY ( $-1.297 \pm 0.047$  pmol cell<sup>-1</sup> d<sup>-1</sup>), GY ( $-1.243 \pm 0.170$  pmol cell<sup>-1</sup> d<sup>-1</sup>), and REF ( $-1.373 \pm 0.042$  pmol cell<sup>-1</sup> d<sup>-1</sup>) conditions but differed under YV conditions ( $-1.028 \pm 0.038$  pmol cell<sup>-1</sup> d<sup>-1</sup>). In contrast, sizes of intracellular L-glutamine pools differed. Compared to REF cultures, YV addition increased the L-glutamine pool while GY addition diminished the L-glutamine pool and PY addition nearly depleted the L-glutamine pool (**Figure 10**).

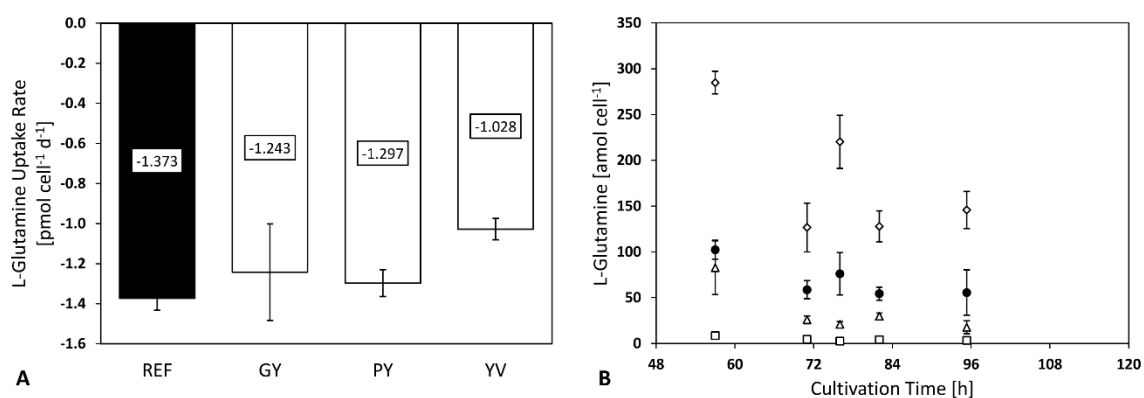


**Figure 10.** L-Glutamine consumption rates [pmol cell<sup>-1</sup> d<sup>-1</sup>] (A) and intracellular pool sizes [amol cell<sup>-1</sup>] (B) of dipeptide-supplemented cells (GY Δ, PY □, YV ◇) and reference cells (REF ●). Negative values indicate an uptake. Error bars show standard deviations of biological duplicates.

As outlined in **Figure 9**, cells always consumed the surplus of TYR provided by dipeptide addition and retained different fractions of that TYR. The additional TYR provided by PY affected the energetic status of the cells and increased ATP pool sizes beginning from 72 h after cultivation (**Figure 11**). Simultaneously, AMP pool sizes decreased after dipeptide addition.

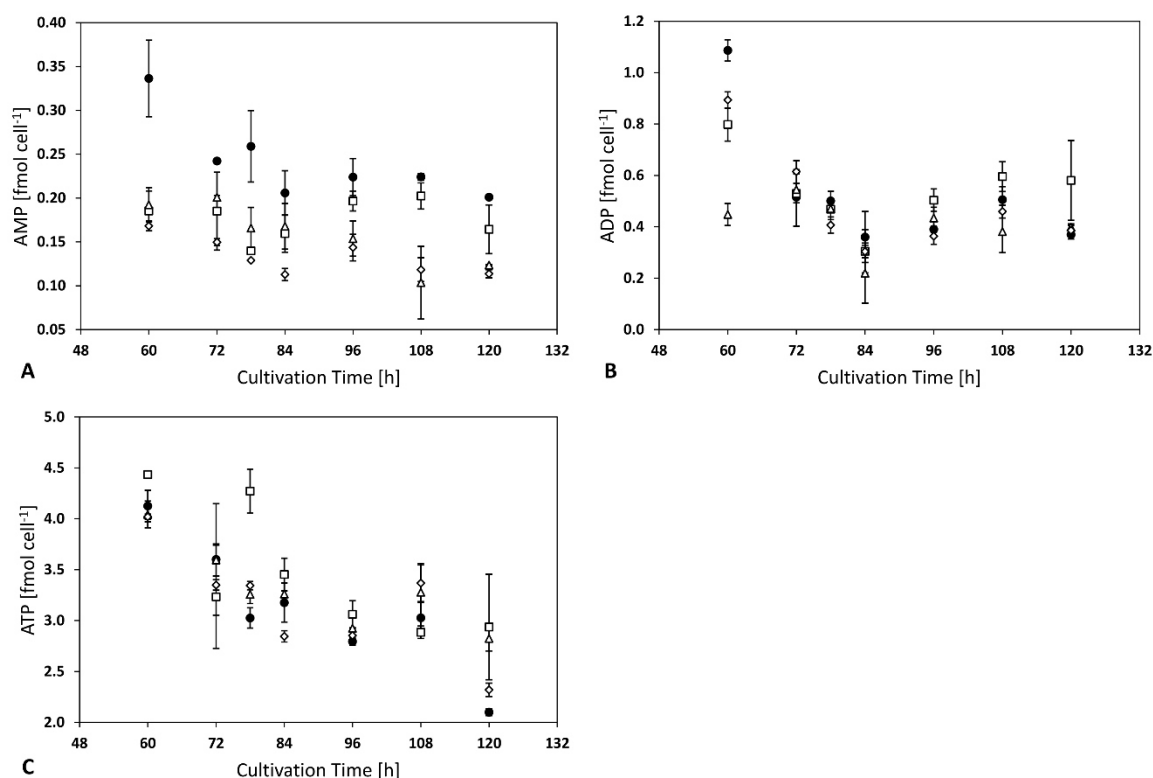
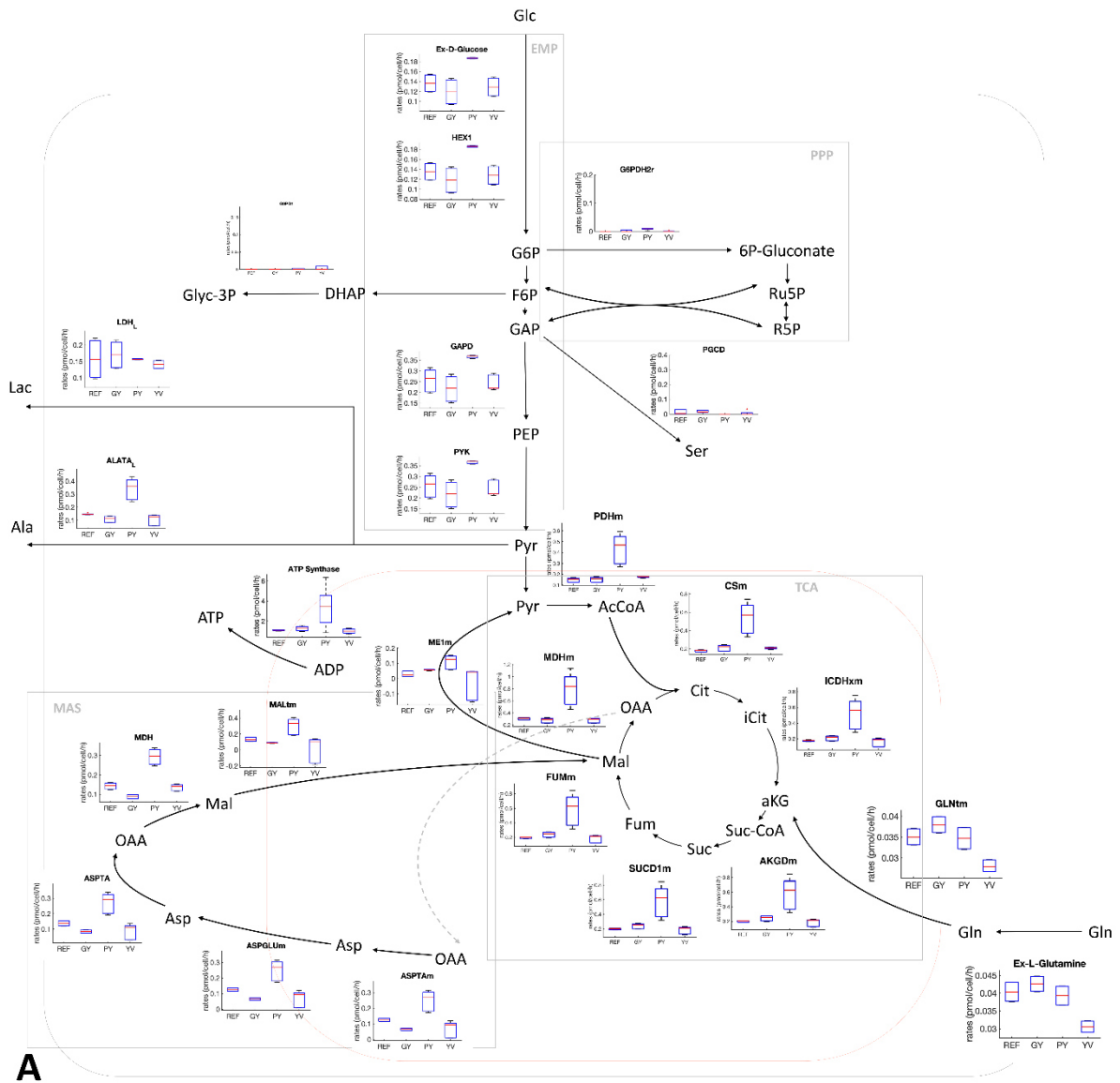


**Figure 11.** Intracellular pools of AMP (A), ADP (B), and ATP (C) [ $\text{fmol cell}^{-1}$ ] of dipeptide supplemented cells (GY  $\Delta$ , PY  $\square$ , YV  $\diamond$ ) and reference cells (REF  $\bullet$ ). Error bars show standard deviations of biological duplicates.

### 3.3 *In silico* analysis of the effects of TYR-containing dipeptides on metabolic activities of CHO cells

**Figure 12** shows the flux distributions obtained using FBA. FBA was performed during the exponential growth phase (0-96 h of cultivation) where the TYR-containing dipeptides were supplemented to the cultures. Due to the higher D-glucose uptake rate and similar L-lactate secretion rate in PY cultures, it is expected that more glycolytic carbon was channeled to mitochondria in PY cultures compared to other cultures. The fraction of carbon diverted to the PPP, L-serine biosynthesis, and glycerophospholipid biosynthesis is negligible since cellular requirements for purine and glycerophospholipids are low. Moreover, L-serine was also available in the cultivation media.

Accordingly, the estimated citric acid cycle (CAC) flux of PY cultures was about three times higher than in the other cultures.



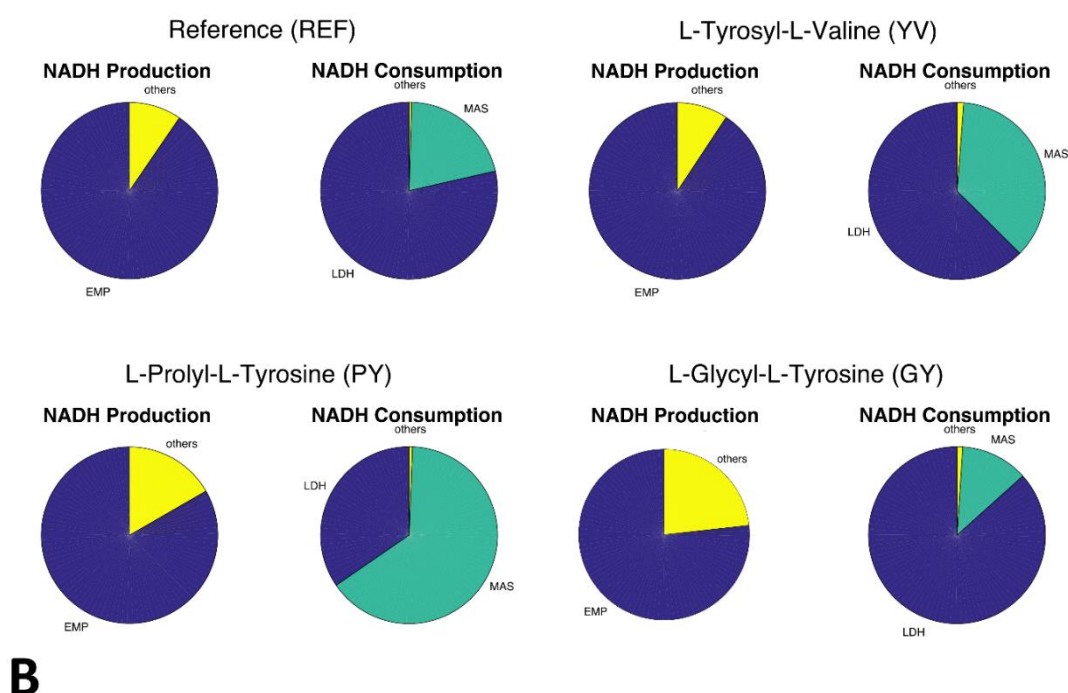


**Figure 12.** (A) Central carbon metabolism flux distribution during exponential growth phase as determined FBA. The boxplot indicates the flux of each reaction with samples arranged in the sequence REF-GY-PY-TY from left to right; (B) Cytosolic NADH production and consumption. Cytosolic NADH is produced predominantly by the EMP pathway. Additionally, NADH/NAD conversion can occur via lactate dehydrogenase (LDH) and/or the malate-aspartate shuttle (MAS). The pie chart indicates fractional amounts, not absolute amounts.

Higher glycolytic flux in PY cultures increased production of cytosolic nicotinamide adenine dinucleotide (NADH). Since the activity of NADH-consuming lactate dehydrogenase was low, NADH was transferred to mitochondria to fuel oxidative phosphorylation. NADH enters mitochondria via the malate-aspartate shuttle (MAS). In our *in silico* analysis (**Figure 12**) MAS activity in the PY cultures was  $0.29 \text{ pmol}_{\text{NADH}} \text{ cell}^{-1} \text{ h}^{-1}$  and responsible for 65 % of cytosolic NADH while MAS activity in REF, YV, and GY cultures yielded 21 %, 36 %, and 13 % cytosolic NADH, respectively. Additionally, FBA predictions revealed that incoming carbon from L-glutamine catabolism did not significantly affect the total CAC flux.



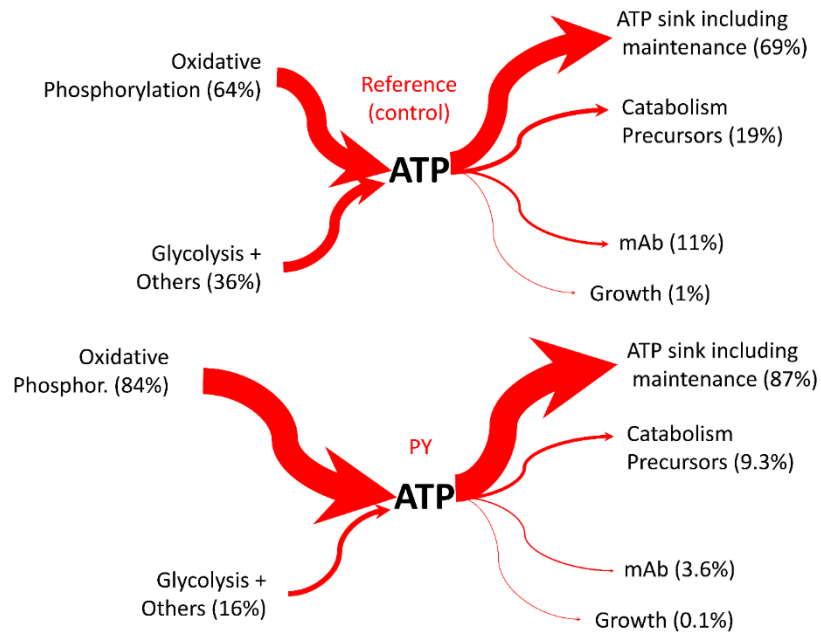


**Figure 13.** ATP flow in reference and PY cultures. The percentage indicates the portion produced or consumed by cellular metabolism.

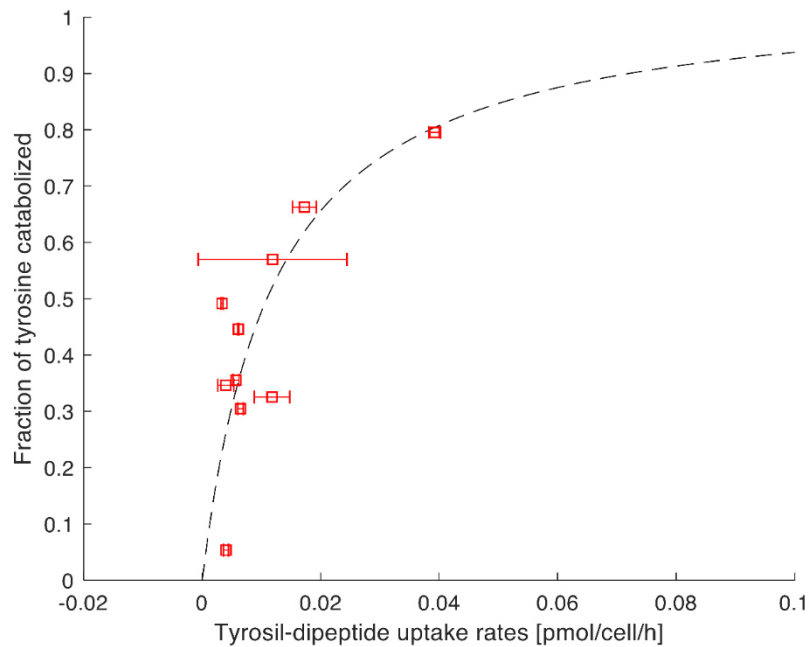


**Figure 14.** The correlation of TYR-containing dipeptides uptake rates with the fraction of TYR metabolized. This correlation forms saturating kinetics indicating that there is a maximal TYR metabolism.

In addition to alleviated D-glucose uptake rates, PY cultures also showed elevated essential amino acid consumption (**Figure 17**). Considering that cells grew at equal rates in all cultures, the increased amino acid uptake of PY cells is predicted to provide additional ATP. Different dipeptide uptake rates were observed in cultures leading to different fractions of catabolized TYR in FBA calculations (**Figure 13**). **Figure 14** displays the correlation between TYR-containing dipeptide uptake and TYR fraction metabolism in cells. Additionally, a saturating uptake kinetic is observed, hinting at a maximum internal TYR metabolism.

#### 4 Discussion

Dipeptides are promising supplements for cell culture media in order to compensate for low solubility and stability of individual amino acids. Previous studies have demonstrated that peptide addition may have diverse effects on cellular performance, motivating further tests to elucidate the underlying mechanisms [19,45]. The initial goal of this study was to identify TYR-containing dipeptides that can increase the maximum supply of TYR to cells through cell culture medium. Our experimental findings support the hypothesis that the metabolic effects of TYR depend on the molecular structure of the TYR-containing dipeptide. More specifically, L-prolyl-L-tyrosine (PY) alters cellular metabolism, unlike glycyl-L-tyrosine (GY) and L-tyrosyl-L-valine (YV).

The data support the potential for different uptake mechanisms and kinetics of TYR-containing dipeptides [45]. Moreover, the investigation of intracellular dipeptide pools showed that PY, GY, and YV were taken up as intact dipeptides (**Figure 16**). Once they entered the cell, the dipeptides were either rapidly degraded, metabolized, or exported. Based on recent CHO genome sequencing and annotation studies, the importers PepT1 and PepT2 may be responsible for dipeptide uptake [286], however, such identification does not yet explain the dipeptide type-dependent differences. PY showed the strongest impact of all tested dipeptides on CHO metabolism and caused decreased growth, increased D-glucose uptake, and reduced overflow metabolism (**Figure 8**). Moreover, PY supplementation also altered CAC activity, intracellular ATP pools (**Figure 11** and **Figure 12**) and depleted the L-glutamine pool (**Figure 10**).

The dipeptide PY possibly works as a signal molecule (demonstrated for amino acids by Franek and Sramkova) inducing a reprogramming of the cellular metabolism [264]. An altered intracellular pH ( $\text{pH}_i$ ) may contribute especially to reduced VCD and modified enzyme activities. In this experiment, our data did not encourage a changed  $\text{pH}_i$  as we observed enhanced D-Glc uptake [290]. Additionally, the data set is not sufficient to reveal this effect as intracellular data of L-Lac,  $\text{NH}_4^+$ , and  $\text{pH}_i$  were not applicable in this setting and were not within the scope of this study. Nevertheless, addition of PY possibly triggers signaling pathway that contribute to decreased VCD and enhanced ATP formation.

Our FBA results suggest that CAC activity was increased in PY-treated cultures based on relatively low L-lactate formation relative to the D-glucose consumed. Moreover, D-glucose uptake rates of PY-treated cultures were approximately 30 % higher compared to other cultures and mitochondrial malate-aspartate shuttle (MAS) activity was tripled in PY cultures compared to the reference (REF) culture. Such phenomenon can be interpreted as cellular responses to increased NADH supply in the cytosol while MAS activity reflects increases in glycolytic activity and reductions in L-lactate formation. MAS, a known indirect transporter of NADH from the cytosol to mitochondria, shuffles excess cytosolic NADH into the mitochondrion to fuel respiration and ATP formation. These metabolic changes resulted in an approximately four times higher ATP formation in PY culture compared to the others.

For our FBA model, only three TYR sinks are possible: (i) TYR utilization for building macromolecules like cellular proteins or mAB, (ii) TYR export, and (iii) TYR catabolism. Interestingly enough, we identified sink (iii) as the dominant fate of TYR, thus TYR was predominately used for ATP formation, beginning with its deamination using  $\alpha$ -ketoglutarate ( $\alpha$ KG) as amino acceptor. Next, the remaining carbon backbone is converted into fumarate and acetyl-CoA in mitochondria, thus fueling the CAC and supporting respiration. To generate sufficient  $\alpha$ KG supply for such scenarios, one of two routes may be engaged, either through quick deamination of L-glutamate, the product of  $\alpha$ KG amination, to create a steady-state cycle or the replenishment of  $\alpha$ KG by the sequential deamination of L-glutamine. The observation of diminishing levels of intracellular  $\alpha$ KG and extracellular L-glutamine pools

favors the second scenario. Notably, GY and YV consumption did not result in similar trends of intracellular  $\alpha$ KG and extracellular L-glutamine levels compared to PY consumption. Instead, upon GY or YV consumption, L-glutamine pools remained steady or were even elevated and  $\alpha$ KG levels showed no decrease.

Becker et al. [3] demonstrated that the cell-specific mAB productivity  $q_{\text{mAB}}$  rises in D-glucose-limited perfusion cultures when ATP formation via respiration is increased [3]. However, those results are not strictly applicable to our study as our cells were analyzed under D-glucose-saturated conditions. Accordingly, our observations should be compared to those of Bulte et al. [291] who observed increased CAC activity without rising  $q_{\text{mAB}}$  [291]. Apparently, ATP supply does not limit mAB production under D-glucose-saturating conditions.

Mammalian cells are well known for their high ATP requirements to meet maintenance demands. Kilburn et al. [292] estimated this ATP requirement to be larger than 65 % of total ATP [292]. Consequently, D-glucose-limited cells, including those in perfusion cultures, may be in an ATP-limited condition such that an additional ATP supply fuels maintenance demands, establishes ion gradients [293] and boosts anabolic mAB formation. In contrast, D-glucose-saturated cells are likely to satisfy ATP maintenance demands, allowing for the use of excess ATP for the formation of recombinant proteins like mAB production. However, such demands are fairly low, only requiring about 11 % of total ATP in the reference cultures (**Figure 13**). As indicated, ATP demands in reference cultures were estimated as 69 % of total ATP, in line with the findings of Killburn et al. [292].

## 5 Concluding remarks

In conclusion, we demonstrated that TYR-containing dipeptides influence CHO cell metabolism in different ways depending on their specific amino acid combination. While the dipeptides glycyl-L-tyrosine (GY) and L-tyrosyl-L-valine (YV) showed minimal impact on cellular metabolism, L-prolyl-L-tyrosine (PY) increased L-glutamine usage and increased ATP availability in the cells. Strictly speaking, the FBA approach cannot distinguish between rising ATP demands for maintenance or improved ATP availability beyond what is required for maintenance. Additional  $^{13}\text{C}$  flux studies may help to decipher the maintenance versus excess

question experimentally. Our evidence of increased ATP pools in PY cultures favors the presence of improved ATP supply with unchanged maintenance demands. As next step, this exploitation potential could be used to transfer the additional energy into improved product formation. Input parameters like proper D-glucose limitation in combination with different PY feed scenarios should be tested to further optimize production performance.

### **Nomenclature**

$C_i$	[mmol/L]	Extracellular concentration of metabolite $i$
$C_x$	[cell/L]	Viable Cell Density (VCD)
$q_i$	[pmol/cell/h]	Extracellular production/consumption rate of $i$
$\mu$	[h <sup>-1</sup> ]	cell-specific growth rate

### **Acknowledgments**

The authors gratefully acknowledge the funding by the Bundesministerium für Bildung und Forschung (BMBF), (Funding Number 031L0077A).

### **Conflict of interest**

The authors have declared no conflict of interest.

### **6 References**

see 5 References, p.139

## Supplementary Material 2

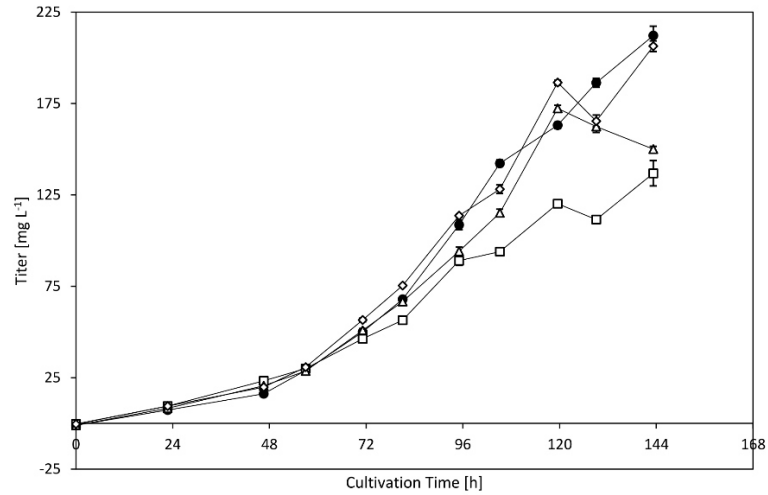


**Figure 15.** S1: Antibody concentrations (titer) [ $\text{mg L}^{-1}$ ] of dipeptide supplemented cells (GY  $\Delta$ , PY  $\square$ , YV  $\diamond$ ) and the reference (REF  $\bullet$ ) during the cultivation. Error bars show standard deviations of biological duplicates and technical replicates.

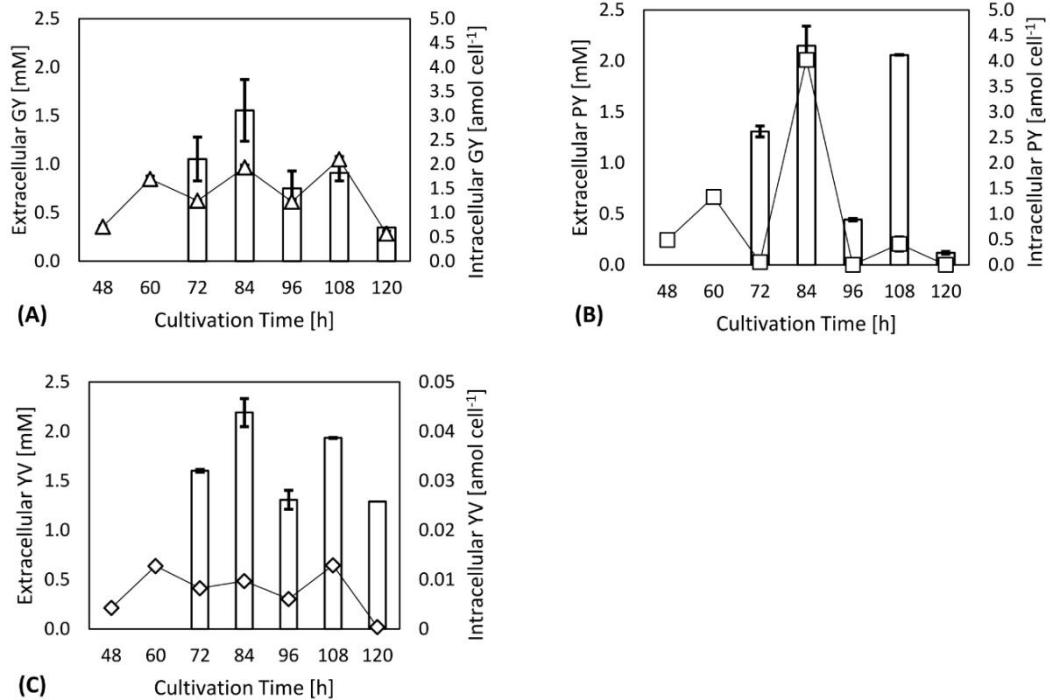


**Figure 16.** S2: Extracellular concentrations (digits) [mM] compared to intracellular pools (bars) [ $\text{amol cell}^{-1}$ ] of dipeptide supplemented cells ((A) GY  $\Delta$ , (B) PY  $\square$ , (C) YV  $\diamond$ ). Error bars show standard deviations of biological duplicates.

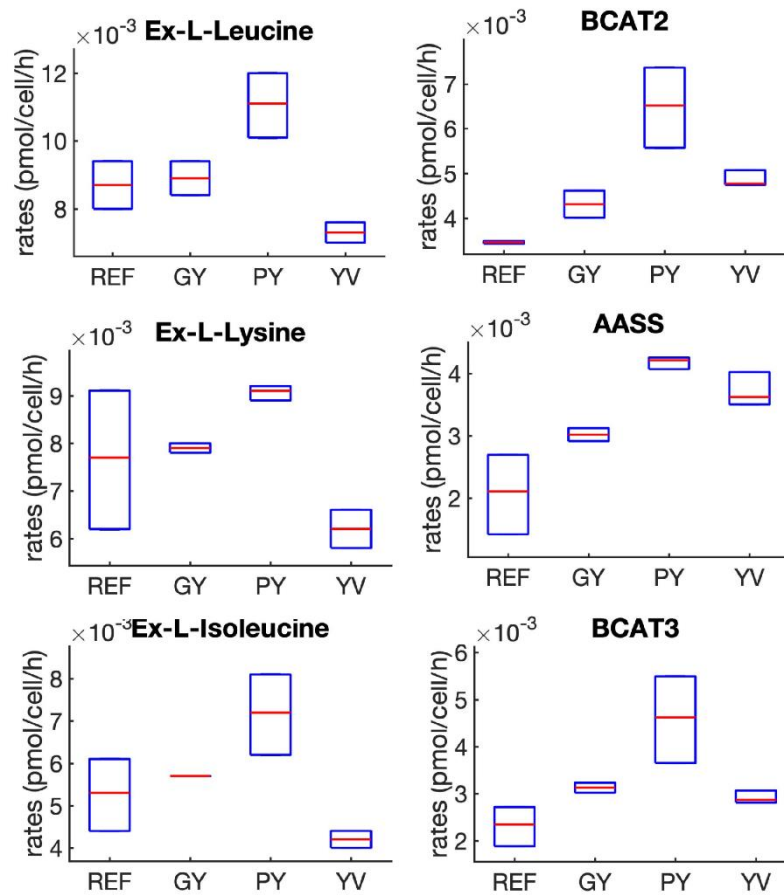


**Figure 17.** S3: Three examples of essential amino acids (L-leucine, L-lysine and L-isoleucine) uptake rates and catabolism rates. The uptake rates are presented in the first column (left hand side) while the catabolism rates of the respective amino acids are displayed in the second column (right hand side). The uptake rates were quantified from extracellular concentrations, while the catabolism rates were estimated from FBA.

### Supplementary Material 1

see 6.1 Supplementary Material: Manuscript 1, p.179





### **3.2 Manuscript 2: S-Adenosylmethionine and Methylthioadenosine Boost Cellular Productivities of Antibody Forming Chinese Hamster Ovary Cells.**

The following manuscript was published in Biotechnology and Bioengineering in 2020 and reproduced with permission of the authors (copyright holders).

Verhagen N, Teleki A, Heinrich C, Schilling M, Unsöld A, Takors R. S-adenosylmethionine and methylthioadenosine boost cellular productivities of antibody forming Chinese hamster ovary cells. Biotechnology and Bioengineering. 2020; 1-9.

Article

**S-adenosylmethionine and methylthioadenosine boost cellular productivities of antibody forming Chinese hamster ovary cells**

Natascha Verhagen<sup>1</sup>, Attila Teleki<sup>1</sup>, Christoph Heinrich<sup>2</sup>, Martin Schilling<sup>3</sup>, Andreas Unsöld<sup>4</sup> and Ralf Takors<sup>1\*</sup>

<sup>1</sup>University of Stuttgart, Institute of Biochemical Engineering, Allmandring 31, Stuttgart, 70569, Germany

<sup>2</sup>Xell AG, Bielefeld, 33689, Germany

<sup>3</sup>Evonik Nutrition & Care GmbH, Darmstadt, 64293, Germany

<sup>4</sup>Boehringer Ingelheim Pharma GmbH & Co. KG, Biberach, 88400, Germany

**Correspondence**

Ralf Takors, Institute of Biochemical Engineering, University of Stuttgart, Allmandring 31, 70569 Stuttgart, Germany.

Email: ralf.takors@ibvt.uni-stuttgart.de

**Funding information**

Bundesministerium für Bildung und Forschung, Grant/Award Number: 031L0077A

### **Abstract**

The improvement of cell specific productivities for the formation of therapeutic proteins is an important step towards intensified production processes. Among others, the induction of the desired production phenotype via proper media additives is a feasible solution provided that said compounds adequately trigger metabolic and regulatory programs inside the cells. In this study, *S*-(5'-adenosyl)-L-methionine (SAM) and 5'-deoxy-5'-(methylthio)adenosine (MTA) were found to stimulate cell specific productivities up to approx. 50 % while keeping viable cell densities transiently high and partially arresting the cell cycle in an anti-IL-8-producing CHO-DP12 cell line. Noteworthy, MTA turned out to be the chemical degradation product of the methyl group donor SAM and is consumed by the cells.

### **Keywords**

5'-deoxy-5'-(methylthio)adenosine (MTA), cell cycle arrest, cell specific productivity, Chinese hamster ovary (CHO) cell, medium optimization, *S*-(5'-adenosyl)-L-methionine (SAM)

## 1 Introduction

Therapeutic proteins such as monoclonal antibodies (mAB) dominate the global market for biopharmaceuticals and are mostly produced in Chinese hamster ovary (CHO) cells [1]. The last decades of biomanufacturing witnessed a steady rise of product titers in conventional fed-batch modes reaching 5-8 g/L in 12-14 days process time [2,259,294]. However, those volumetric productivity improvements predominately mirror elevated viable cell densities rather than the equal rise of cell specific productivities (CSPs). The latter however, is of outstanding importance when the next generation of intensified bioprocesses should be realized, in particular when using perfusion processes [3,295,296].

Consequently, novel approaches are needed that boost CSPs for pharmaceutical proteins. As a prerequisite, detailed understanding of the roles of interacting partners in the complex regulatory patterns of CHO metabolism is necessary. As a result of this, novel switches to enhance CSPs may be derived. Promising studies focused on metabolism [297–299], transcription [300,301], and on epigenetics. Epigenetic adaption mechanisms that is histone modification via acetylation and DNA methylation are basic features of CHO cell adaption. Nematpour et al. (2017) showed that stabilized acetylation by inhibition of histone deacetylases with medium additives enhanced mAB productivity in CHO cells [302]. Furthermore, DNA methylation which links genetics with transcriptomics [303] was revealed to be the main reason for particular downregulation and upregulation patterns found in high-producer cell lines [304,305]. Recent studies of Dhiman et al. (2019) demonstrated that more than half of the analyzed nuclear genes are susceptible to methylation [306]. Consequently, the addition of molecules interacting with epigenetic regulation mechanisms offers the intrinsic potential to improve CSPs. In this context, the cosubstrate S-(5'-adenosyl)-L-methionine (SAM) was chosen as a medium additive whose structure was discovered in the early 1950s [222]. SAM may be involved in aminopropylation (polyamine synthesis), trans-methylation and -sulfuration underlining its crucial role for cellular growth and regulation. Accordingly, SAM limitation may affect gene expression, membrane fluidity, and glutathione availability reflecting its roles in DNA methylation, methylation of phospholipids, and trans-

sulfuration, respectively [47,48]. Metabolically, the methyl group donor SAM is created by methionine adenosyltransferase (MAT) using adenosine triphosphate (ATP) and L-methionine as substrates. In CHO, the latter needs to be supplemented in the medium. In methylation reactions, SAM is de-methylated to S-(5'-adenosyl)-L-homocysteine (SAH) further de-adenylated to homocysteine, re-methylated to methionine, and finally re-adenosylated to SAM again (SAM cycle; [47,48]). Accordingly, the cycle not only regenerates the key methyl donor SAM, it also provides important precursors: Homocysteine serves as a precursor for glutathione synthesis [224] which is an important antioxidant in cells. By analogy, SAM enters the polyamine synthesis [47]. Investigations on liver disease demonstrated that extracellular SAM influences the cellular glutathione level. Likely, SAM is taken up by the cells [48] which may explain why SAM-treated liver cells showed decreased growth rate, prevented the development of liver cancer [225,226] and disclosed antiapoptotic mechanisms [49].

Summarizing, SAM is a crucial cosubstrate that serves as a key methyl donor thereby linking metabolism with cellular regulation and epigenetics. Consequently, it offers the intrinsic potential to function as an additive that boosts CSPs in CHO cells.

## **2 Materials and Methods**

### **2.1 Seed train, shake flask cultivation, and addition of SAM, 5'-deoxy-5'-(methylthio)adenosine (MTA), and L-homoserine lactone hydrochloride (HSL)**

The following additives are products of Sigma-Aldrich (Steinheim, Germany): SAM, MTA, and HSL. The anti-IL-8-producing CHO-DP12 cell line (ATCC® CRL 12445™) adapted to grow in suspension was cultivated in chemically defined TC-42 medium (Xell AG, Bielefeld, Germany) supplemented with 4 mM L-glutamine (Carl Roth GmbH & Co. KG, Karlsruhe, Germany) and 200 nM methotrexate (Sigma-Aldrich, Steinheim, Germany). Seed train and experiments were performed in presterilized disposable shake flasks (Corning Inc., NY) in a humidified rotary shaker (Infors HT Minitron, Infors GmbH, Einsbach, Germany) at 37 °C, 150 rpm with 50 mm displacement, and 5 % CO<sub>2</sub>. The additives SAM, MTA, and HSL were introduced after 48 hr of cultivation. In reference cell cultures, sterilized water was used to mimic the additional liquid

volume in experimental cultures. Cultivation was performed with biological duplicates or quadruplicates.

## **2.2 Extracellular analysis**

Samples were taken at least once a day. Viable cell density, viability, and average cell diameter were determined using trypan blue staining using a Cedex XS cell counter (Innovatis AG, Bielefeld, Germany) for read out. The extracellular concentrations of D-glucose and L-lactate were determined using a Labotrace automatic analyzer (Trace Analytics GmbH, Braunschweig, Germany). The product concentration of immunoglobulin G (IgG) was determined applying enzyme-linked immunosorbent assay (ELISA; [28]). Each sampling and measurement procedure was performed in replicates.

## **2.3 SAM and MTA determination**

The amount of SAM and MTA was quantified on an Agilent 1200 Series HPLC system coupled with an Agilent 6410B triple quadrupole tandem mass spectrometer (QQQ-MS/MS; Agilent Technologies, Waldbronn, Germany). The LC-MS/MS method was based on a bicratic zwitterionic hydrophilic interaction chromatography (ZIC-pHILIC) under alkaline mobile phase conditions (10 mM ammonium acetate, pH 9.2) without prior derivatization [282,283]. Targeted analytes were detected with high selectivity in multiple reaction monitoring (MRM) mode using pre-optimized precursor-to-product ion transitions and MS/MS parameters. Absolute quantification was performed by adapted standard-based external calibration with constant addition of global internal standards (L-norvaline and  $\gamma$ -aminobutyric acid) in diluted samples (1:8). Data were analyzed using MassHunter B.06.00 Analysis software.

## **2.4 Cell cycle analysis**

Cell cycle analysis was performed with an adapted method [307].  $10 \times 10^6$  cells were harvested and washed with ice-cold phosphate-buffered saline (PBS). After washing, the cells were immediately fixed with ice-cold fixation buffer (70 % EtOH, 30 % PBS [vol/vol]) and stored at -20 °C until further analysis. The staining procedure started with gently thawing and resuspending of the cells. Then, cells were washed twice with PBS, resuspended in staining

solution (propidium iodide and RNase A in PBS) and incubated for 10 min at 37 °C in the dark. Samples stayed on ice until cell cycle analysis. The BD Accuri™ C6 Plus flow cytometer was used with 610/20 nm filter and detected 50,000 events per sample. Data were analyzed with BD Csampl software.

## 2.5 Statistical methods

Error bars show standard deviations that were calculated based on four or two biological replicates (considering the technical replicates). Unpaired one-sided Student's t test was performed to investigate the data for statistical significance ( $***p = .001$ ,  $**p = .01$ ,  $*p = .05$ ).

## 3 Results

### 3.1 SAM addition boosted CSP while repressing growth

After 48 hr cultivation time, SAM was added reaching a concentration of 250  $\mu\text{M}$ . Notably, REF received the equivalent volume of water to prevent any bias due to medium dilution. The SAM-treated cultures reduced maximum viable cell density (VCD) and growth rate (between 48 and 120 hr) by 10 % and 18 % compared with REF, respectively (**Figure 18**). However, high cell viabilities remained.

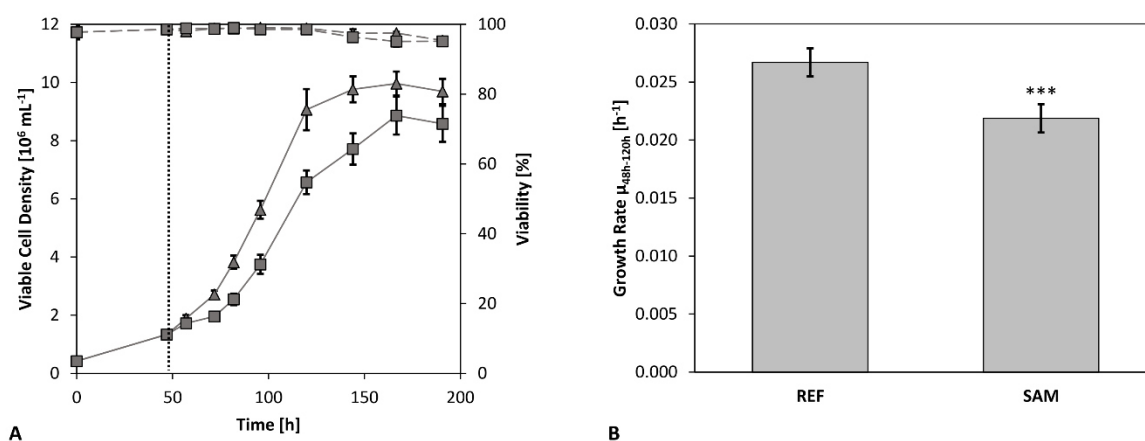


**Figure 18.** (a) Time courses of viable cell density ( $10^6/\text{ml}$ ) and viability (%) of S-(5'-adenosyl)-L-methionine (SAM) supplemented cells ( $\square$ ) and reference (REF,  $\Delta$ ). SAM was added at 48 hr cultivation time. (b) Growth rate per hour ( $\text{hr}^{-1}$ ) regarding the time interval 48-120 hr. Error bars show standard deviations of biological quadruplicates and technical replicates. Significance was tested with one-sided t-test.  $***p = .001$

Although, SAM supplemented cells showed lower VCD than REF they reached more than 50 % higher antibody titer (SAM:  $192.73 \pm 18.24$  mg/L and REF:  $123.39 \pm 12.63$  mg/L). The increased titer (>48 hr) transformed to increased CSP between 0 and 120 hr: SAM supplemented cells produced  $9.81 \pm 0.89$  pg/day whereas the reference only showed  $6.24 \pm 0.51$  pg/day. This corresponds to a 57 % increase in CSP (**Figure 19**) after SAM addition.

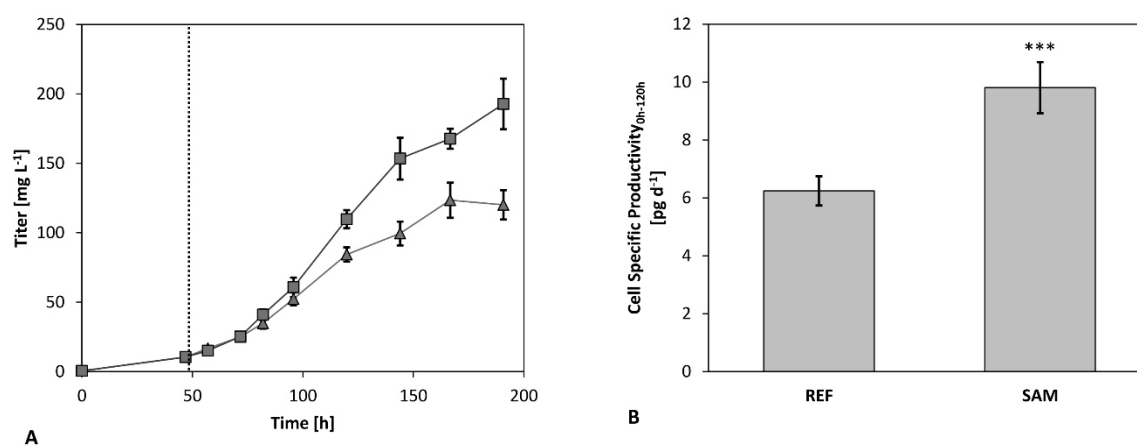


**Figure 19.** (a) Time courses of the antibody titer (mg/L) of *S*-(5'-adenosyl)-L-methionine (SAM) supplemented cells ( $\square$ ) and reference (REF,  $\Delta$ ). SAM was added after 48 hr cultivation time. (b) Cell specific productivity (pg/day) for the time interval 0-120 hr. Error bars show standard deviations of biological quadruplicates and technical replicates. Significance was tested with one-sided t-test. \*\*\* $p = .001$

### 3.2 SAM degradation was not affected by the presence of cells

To investigate the effects of SAM addition and uptake extracellular SAM concentrations were monitored in the medium. The anticipated SAM “uptake” coincided with equally fast degradation rates observed in cell-free cultivation medium under similar conditions (medium + SAM + cells,  $11.54 \pm 0.32$   $\mu\text{M/hr}$ ; medium + SAM,  $10.95 \pm 0.30$   $\mu\text{M/hr}$ ). Consequently, the direct cellular uptake of SAM seemed unlikely. To better understand SAM degradation, MTA as literature described degradation product was measured in the medium [308,309]. Indeed, MTA was detectable in medium with and without cells but not in the reference (water addition). MTA concentration increased over time in medium without cells. In contrast, cell culture studies only showed high MTA levels at the beginning which decreased during the cultivation (**Figure 20**).



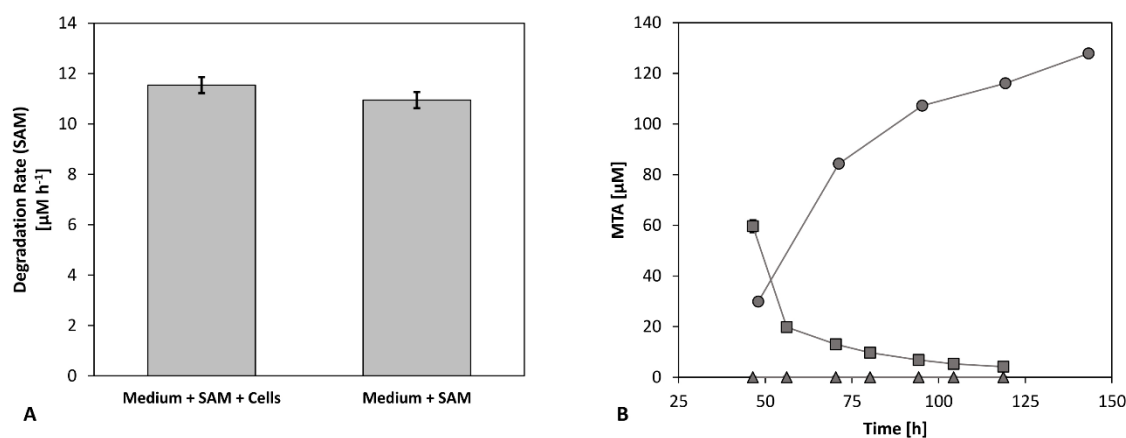


**Figure 20.** (a) Degradation rate ( $\mu\text{M}/\text{hr}$ ) of *S*-(5'-adenosyl)-L-methionine (SAM) in medium at 37 °C, 5 %  $\text{CO}_2$ , and 150 rpm with and without cells. (b) Time courses of 5'-(methylthio)adenosine (MTA) concentration ( $\mu\text{M}$ ) in the medium of SAM supplemented cells ( $\square$ ), reference (REF,  $\Delta$ ) and medium + SAM without cells ( $\circ$ ). Error bars show standard deviations of biological duplicates.

### 3.3 SAM and its degradation products MTA and HSL

To check whether MTA is the inducer of the growth and IL-8 production phenotype, SAM and the degradation products MTA and HSL were studied in supplementation tests. The addition of substrates occurred after 48 hr of cultivation with a final concentration of 250  $\mu\text{M}$  (REF was supplied with the same volume of water). The addition resulted in maximum VCDs ( $10^6$  cells/ml) of SAM  $7.085 \pm 0.326$ , MTA  $5.512 \pm 0.203$ , HSL  $8.216 \pm 0.780$ , and REF  $8.961 \pm 0.576$ . As indicated in **Figure 21**, SAM and MTA supplementation caused reduced growth during 60-120 hr leading to a growth rate of  $0.022 \pm 0.002 \text{ hr}^{-1}$  and  $0.017 \pm 0.001 \text{ hr}^{-1}$ , respectively. However, there was no effect on the growth phenotype after HSL addition ( $0.028 \pm 0.002 \text{ hr}^{-1}$ ) compared with the reference ( $0.028 \pm 0.001 \text{ hr}^{-1}$ ).

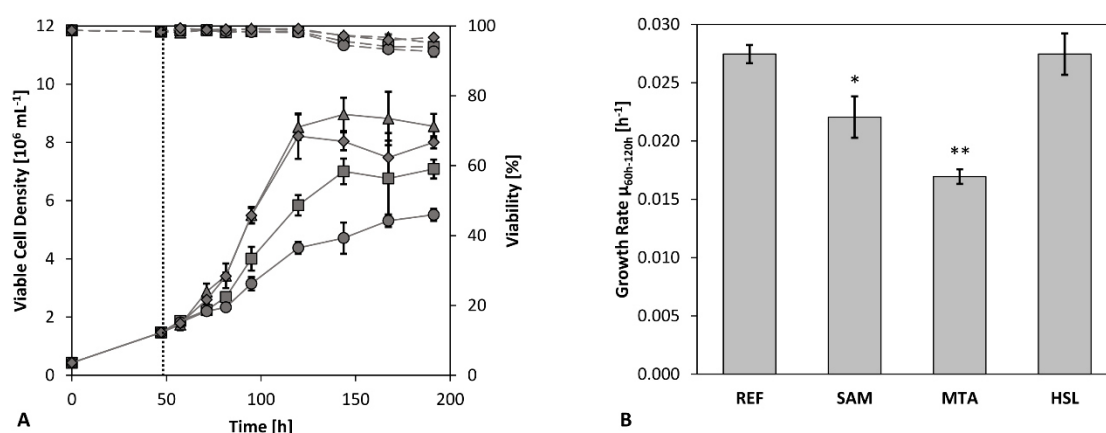


**Figure 21.** (a) Time courses of viable cell density (10<sup>6</sup>/ml) and viability (%) of *S*-(5'-adenosyl)-L-methionine (SAM, □), 5'-(methylthio) adenosine (MTA, ○), and L-homoserine lactone hydrochloride (HSL, ◇) supplemented cells compared with the reference (REF, Δ). SAM, MTA, or HSL was added at 48 hr. (b) Growth rate (hr<sup>-1</sup>) regarding the time interval 60-120 hr. Error bars show standard deviations of biological duplicates and technical replicates. Significance was tested with one-sided t-test. \*\**p* = .01, \**p* = .05

Antibody titers were differently affected by the supplemented additives. Cultivations with SAM or MTA addition showed increased titers (SAM: 165.17 ± 7.53 mg/L and MTA: 167.72 ± 15.77 mg/L) whereas experiments with HSL (HSL: 125.94 ± 23.30 mg/L) and the reference (REF: 132.11 ± 9.61 mg/L) showed no improvements. Accordingly, CSPs (**Figure 22**) of the first 120 hr revealed increased CSPs after the addition of SAM or MTA (SAM: 11.02 ± 1.70 pg/day and MTA: 8.73 ± 0.20 pg/day). These values corresponded to a 27-60 % surplus of production. For comparison, HSL addition did not have an influence compared with the reference (HSL: 7.15 ± 0.64 pg/day and REF 6.87 ± 0.43 pg/day).

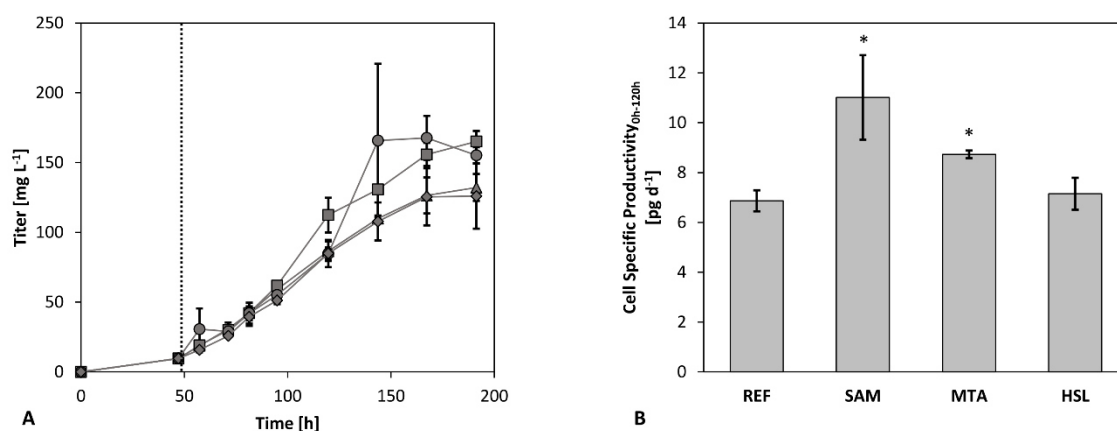


**Figure 22.** (a) Time courses of antibody titers (mg/L) of *S*-(5'-adenosyl)-L-methionine (SAM, □), 5'-(methylthio)adenosine (MTA, ○), and L-homoserine lactone hydrochloride (HSL, ◇) supplemented cells compared with the reference (REF, Δ). SAM, MTA, or HSL was added after 48 hr cultivation. (b) Cell specific productivity (pg/day) regarding the time interval 0-120 hr. Error bars show standard deviations of biological duplicates and technical replicates. Significance was tested with one-sided t-test. \* $p = .05$

### 3.4 SAM and MTA interact with the cell cycle

Propidium iodide staining revealed differences in the cell cycle phase distribution (**Figure 23**). All cells started from a common preculture that was split after 48 hr cultivation before adding SAM, MTA, HSL, or water (REF) as described above. About 12 hr after addition (60 hr cultivation time) SAM supplemented cells accumulated in G2-phase whereas MTA supplemented cells showed an increase in S-phase compared with the reference. Noteworthy, both cultures reduced the fraction of cells in G1-phase. Cells supplemented with HSL behaved like the reference. 12 hr later (72 hr cultivation time), the scenario of SAM-treated cultures had changed. Now, the fraction of cells in G1-phase was even higher than that in G2-phase compared with the reference. Still, MTA-treated cultures revealed alleviated numbers of cells in S-phase and less in G1-phase. After additional 12 hr (84 hr cultivation time) S-phase differences leveled out. Cells that were supplemented with SAM or MTA had more cells in G1-phase but less in G2-phase than the reference.

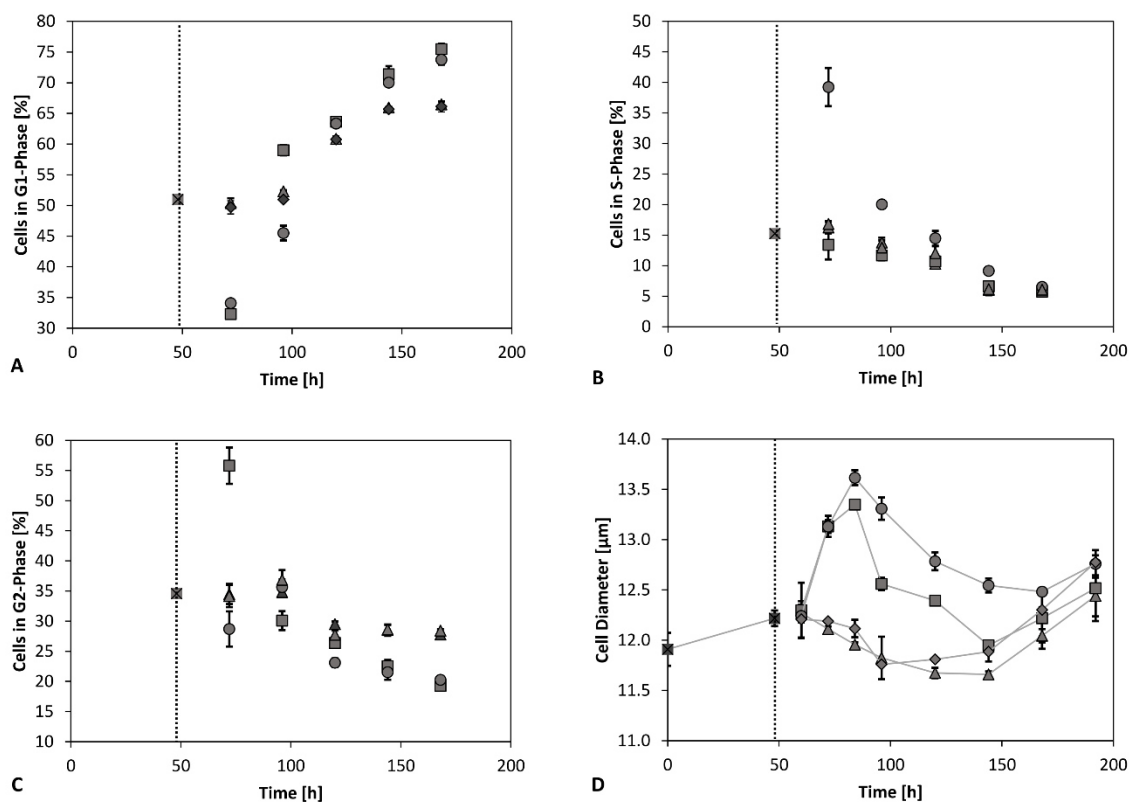


**Figure 23.** (a-c) Time courses of cell cycle phase distribution (%) and (d) average cell diameter ( $\mu\text{m}$ ) of *S*-(5'-adenosyl)-L-methionine (SAM,  $\square$ ), 5'-(methylthio)adenosine (MTA,  $\circ$ ), and L-homoserine lactone hydrochloride (HSL) supplemented cells ( $\diamond$ ) compared with the reference (REF,  $\Delta$ ) and common preculture (crossed  $\square$ ). Error bars show standard deviations of biological duplicates and technical replicates.

Additionally, the average cell diameter of all cultures was monitored. Cells supplemented with SAM or MTA revealed a rising average cell diameter of about 10 % (SAM + 11.66 %; MTA + 13.90 %) 36 hr after addition. However, cell size was reduced to the size of the reference culture in the later phase of the cultivation.

#### 4 Discussion

We added SAM to the medium of CHO cells to interact with the cellular metabolism and with SAM mediated regulation [47,48]. Clearly, SAM addition decreased the growth rate (**Figure 18**) which is in agreement with previous findings in liver cells [225,226]. It may be anticipated that changes in the DNA methylation pattern caused the growth phenotype [304].

Unfortunately, the identification of methylation differences with and without SAM addition was not manageable within the scope of the study.

Significantly increased CSP was found in CHO-DP12 cells after SAM addition (**Figure 19**), although growth rates were reduced. Metabolically, this phenomenon may be understood by assuming that SAM enters the cell boosting the precursor supply of the SAM cycle and/or alleviating the ATP dependent recycling. Mato et al. (1997) anticipated that liver cells take up extracellular SAM. The hypothesis was deduced from rising intracellular glutathione levels [48]. However, **Figure 20** reveals that decreasing extracellular SAM levels were observed irrespective of whether cells were present or not. Consequently, the cellular uptake of SAM is unlikely.

A computational study demonstrated that SAM degrades to MTA and HSL in water [310]. Consequently, we investigated the addition of these degradation products to the media. Whereas HSL did not create any particular phenotype, MTA caused effects very similar to the SAM addition (**Figure 21**). Noteworthy, MTA natively occurs in mammalian cells as part of the polyamine biosynthesis [58,227]. There, SAM is decarboxylated to MTA to access spermidine and spermine. Because high MTA levels inhibit polyamine synthesis MTA is rapidly degraded by 5'-methylthioadenosine phosphorylase. MTA was shown to permeate the cellular membrane. Furthermore, MTA was found to induce particular gene expression patterns, to regulate apoptosis, and to inhibit cell proliferation in hepatocytes, leukemia cells, fibroblasts, and lymphoma cells [49,60–62]. The latter reflects the inhibition of polyamine synthesis by high MTA levels which reduces cell cycle progression in turn [63]. Experiments with hepatic cells revealed inhibited DNA synthesis after MTA addition [64]. The reduction of polyamine pathway intermediates such as spermidine after the addition of metabolic inhibitors induced arrest in the cell cycle's S-phase of CHO cells [229].

In agreement with this, we observed the accumulation of cells in S-phase after MTA addition concomitantly with a diminishing number in G1-phase compared with the REF (**Figure 23**). We hypothesize that MTA inhibited polyamine synthesis finally creating the observed cytostatic effect [311].

Both, SAM and MTA additions increased CSPs of CHO-DP12 cells (**Figure 22**). One explanation could be that cell cycle arrest particularly boosted cellular production rates [25–28]. However, those improvements are neither necessarily nor exclusively linked to a single cell cycle phase. Instead, they may benefit from multiple phases [29–33]. Accordingly, one may argue whether the improvement of CSP mirrors the benefits of arresting the cell cycle alone. Lloyd et al. (2000) observed CSPs proportional to the cell volume investigating four different CHO cell lines [33]. As cell volume and cell cycle status are linked too, unequivocal conclusions are hard to get. As a result, they concluded that rather cells in S- and G2/M-phase show improved cellular productivity than those in G1-phase. However, this statement somewhat contradicts the findings of other groups [25–28]. In our studies, cell diameters rose after MTA and SAM addition (**Figure 23**) which agrees with the findings of Lloyd et al. (2000) [33]. Strictly speaking, the observation does not exclude potential beneficial effects resulting from cell cycle arrest. In general, cell cycle arrest allows cells to use more energy for recombinant antibody production because biomass formation is hampered [121].

Besides the consequences of MTA and SAM on cell cycle and diameter, MTA may interact with a lot of other cell mechanisms [49,60–62]. For instance, MTA inactivates SAH hydrolase [58] leading to increased SAH levels finally resulting in reduced DNA methylation [49]. As methylation is a crucial part of epigenetic regulation [304] affecting transcription too [303] further transcriptional regulation programs are likely to be activated as well. Consequently, the substrate MTA will be further investigated, and its balanced addition is expected to intensify its boosting capability and avoid potential negative effects.

## 5 Conclusion

The study was motivated by the idea to identify novel, nonconventional media components as promising additives to boost CSPs showcasing IgG-1 formation with CHO-DP12 cells. Testing the methyl group donor SAM, a multilevel effector was selected that may interact with different hierarchy levels of cellular regulation concomitantly. SAM addition improved CSPs by approx. 50 % arresting the cell cycle and reducing cellular growth at the same time. A

similar phenotype occurred when MTA was added which turned out to be the real effector resulting from SAM degradation and can transfer the cellular membrane.

The underlying mechanisms why CSPs are improved are not fully elucidated yet. However, the observations of cell cycle arrest and rising cell volumes support current state-of-the-art understanding but do not disclose key benefits in detail. Further metabolic and transcriptional studies are needed that are beyond the scope of this contribution. Nevertheless, the identification of SAM and MTA as promising media additives to boost CSPs may open the door for the search of other beneficial compounds that trigger cellular performance on multiple levels of metabolism and control.

### **Acknowledgments**

The authors gratefully acknowledge the funding by the Bundesministerium für Bildung und Forschung (BMBF, Funding Number 031L0077A). Open access funding enabled and organized by Projekt DEAL.

### **Conflict of interests**

The authors declare that there are no conflict of interests.

### **6 References**

see 5 References, p.139





### **3.3 Manuscript 3: Methylthioadenosine (MTA) Boosts Cell-Specific Productivities of Chinese Hamster Ovary Cultures: Dosage Effects on Proliferation, Cell Cycle and Gene Expression**

The following manuscript was published in FEBS Open Bio in 2020 and reproduced with permission of the authors (copyright holders).

Verhagen N, Zieringer J, Takors R. Methylthioadenosine (MTA) boosts cell-specific productivities of Chinese hamster ovary cultures: dosage effects on proliferation, cell cycle and gene expression. FEBS Open Bio. 2020; 1-14.

Research Article

**Methylthioadenosine (MTA) boosts cell-specific productivities of Chinese hamster ovary cultures: dosage effects on proliferation, cell cycle and gene expression**

Natascha Verhagen<sup>1</sup>

Julia Zieringer<sup>1</sup>

Ralf Takors<sup>1</sup>

<sup>1</sup> Institute of Biochemical Engineering, University of Stuttgart, Stuttgart, Germany

**Correspondence:** R. Takors, Institute of Biochemical Engineering, University of Stuttgart, Allmandring 31, 70569 Stuttgart, Germany

E-mail: ralf.takors@ibvt.uni-stuttgart.de

**Keywords:** cell cycle arrest, cell-specific productivity, Chinese hamster ovary cell, medium optimization, methylthioadenosine, transcriptome analysis

Abbreviations: CHO, Chinese hamster ovary; CSP, cell-specific productivity; DEG, differential expressed gene; MTA, 5'-deoxy-5'-(methylthio)adenosine; PC, principal component; REF, reference; SAM, S-(5'-adenosyl)-L-methionine; VCD, viable cell density

## **Abstract**

A major goal for process and cell engineering in the biopharmaceutical industry is enhancing production through increasing volumetric and cell-specific productivities (CSP). Here, we present 5'-deoxy-5'-(methylthio)adenosine (MTA), the degradation product of *S*-(5'-adenosyl)-L-methionine (SAM), as a highly attractive native additive which can boost CSP by 79 % when added to exponentially growing cells at a concentration of 250-300  $\mu$ M. Notably, cell viability and cell size remain higher than in non-treated cultures. In addition, cell cycle arrests first in *S*-, then in G2-phase before levelling out compared to non-treated cultivations. Intensive differential gene analysis reveals that expression of genes for cytoskeleton mediated proteins and vesicle transport is amplified by treatment. Furthermore, the interaction of MTA with cell proliferation additionally stimulated recombinant protein formation. The results may serve as a promising starting point for further developments in process and cell engineering to boost productivity.

## **Running Heading**

The effector MTA boosts productivity in CHO cells.

## Introduction

Biopharmaceutical markets are dominated by therapeutic proteins, particularly monoclonal antibodies (mAB) which are predominantly produced by CHO cells [1]. In the last decades, significant increase of maximum viable cell density (VCD) improved volumetric productivity and reached titers up to 5-8 g L<sup>-1</sup> in fed-batch processes [2,259,294]. Process intensifications are performed to raise production performance. As a prerequisite, increasing CSPs are needed for the next step of process development [3,296].

5'-Deoxy-5'-(methylthio)adenosine (MTA) consists of L-methionine (L-Met) and adenosine triphosphate (ATP) and is a naturally occurring molecule in mammalian tissues [58,227]. It is produced from S-(5'-adenosyl)-L-methionine (SAM) in the polyamine synthesis [58] in cells. Production of spermidine and spermine needs the decarboxylation of SAM to MTA that is rapidly metabolized by 5'-methylthioadenosine phosphorylase to adenine and S-methyl-5-thio-D-ribose 1-phosphate and finally to L-Met. The adenine can be used to replenish adenosine monophosphate (AMP), adenosine diphosphate (ADP) and ATP pools. Final recovery of SAM from ATP and L-Met closes the SAM cycle [58,59]. Rapid degradation of MTA is crucial because it inhibits spermine synthase, spermidine synthase and ornithine decarboxylase [64,227].

MTA inhibited cell proliferation in hepatocytes, leukemia cells, fibroblasts and lymphoma cells [49,60–62] that is mainly the consequence of its polyamine synthesis inhibition [63]. A reduction of polyamine intermediates arrested CHO cells in their S-phase [229]. Furthermore, MTA addition inhibited DNA synthesis in hepatic cells [64] but it remained unclear whether MTA or a downstream metabolite is the effector [311].

Beside its interaction with polyamine synthesis, MTA demonstrated importance for expression control of genes, cell proliferation inhibition, lymphocyte activation, tumor development and invasiveness, and the regulation of apoptosis [49,58–60,64,65]. MTA addition induced apoptosis in hepatocarcinoma cells, whereas hepatocytes remained viable and were protected against programmed cell death [49]. Additionally, MTA demonstrated beneficial effects in immune response [312].

Several groups [61,62] observed the inhibition of growth factor-induced protein tyrosine phosphorylation and the increase of intracellular cyclic AMP (cAMP) levels through the inhibition of cAMP-phosphodiesterase by MTA pointing out the interaction with signaling pathways. Furthermore, increased MTA levels inhibited arginine methylation of the STAT1 transcription factor, finally impairing gene transcription [66].

Due to the relation to the SAM cycle, MTA revealed capabilities to inhibit protein methylation pinpointing to its role as post-translational modifier and accordingly as a regulator of cellular signaling and gene expression [60,65,66]. Evidences are given by its direct interaction with methyltransferases and via the indirect inactivation of S-(5'-adenosyl)-L-homocysteine hydrolase [58].

Single MTA addition to the medium increases CSP in CHO cells. Furthermore, cells demonstrated cell cycle arrest and increased cell size [313]. Growth arrest induction is a common strategy to increase CSP [314]. Protein production was increased by effector-induced cell cycle arrest in G1- and S-phase [26,315]. However, cell size controls transitions between cell cycle phases which underlines its importance for proper cell cycling and proliferation [34–36] that correlated with protein production in different cell lines [33]. The complex interactions between cell size, cell growth, and protein production are not fully elucidated, yet. Additionally, genes involved in post-translational steps, secretion and cytoskeleton were reported to enhance CSP [38,316,317].

Strategies to induce growth arrest for enhancing protein production comprise (a) hypothermia and (b) the addition of effector molecules, e.g. to increase hyperosmolality. Regarding (a), the mechanism of hypothermia is not understood but certainly linked to G1-phase arrest [27] and accompanied by an increased cell size [171,318]. With respect to (b) additives were investigated to modulate cell growth, product stabilization, and to reduce chemical modifications. Examples are sodium butyrate [21], zinc [319], valeric acid [320], glycine betaine [321], valproic acid [22] and sodium chloride [300] among others.

Own studies have already revealed that MTA addition diminished growth, increased CSP, altered cell cycle phases and cell size [313]. Consequently, MTA should be considered as a

multi-layer regulator of cell growth, cell cycle, and protein formation that is a highly promising additive for boosting CSP. Accordingly, we conducted experiments with anti-IL-8-producing CHO cells analyzing different levels and intervals of MTA addition and the effect of MTA on transcriptomic level.

## **Materials and Methods**

### **Different MTA concentrations and addition time points: Seed train, shake flask cultivation and MTA addition**

MTA was a product of Sigma-Aldrich (Steinheim, Germany). The anti-IL-8-producing CHO DP-12 cell line (ATCC® CRL 12445™) adapted to suspension was grown in chemically defined TC-42 medium (Xell AG, Bielefeld, Germany) supplemented with 4 mM L-glutamine (Carl Roth GmbH & Co. KG, Karlsruhe, Germany) and 200 nM methotrexate (Sigma-Aldrich). Seed train and experiments were performed in pre-sterilized disposable shake flasks (Corning Inc., US) in a humidified and incubated rotary shaker (Infors HT Minitron, Infors GmbH, Germany) at 37 °C, 150 rpm with 50 mm displacement and 5 % CO<sub>2</sub>. In the experiment with different concentrations, MTA was introduced after 48 h of cultivation in different concentrations (125, 250, 350 and 450 μM). In reference (REF) cell cultures, sterilized water was used to mimic the additional liquid volume in experimental cultures (volume corresponding to the 450 μM addition). In the experiment with different addition time points, MTA was introduced after 48, 84 and 108 h of cultivation in a concentration of 150 pmol cell<sup>-1</sup>. At every addition time point, all other settings received sterilized water to mimic the additional liquid volume in experimental cultures. Cultivation was performed with biological duplicates.

### **Extracellular and cell cycle analysis**

Samples were taken at least once a day. Viable cell density (VCD), viability and average cell size were determined using trypan blue staining and a Cedex XS cell counter (Innovatis AG, Bielefeld, Germany). The extracellular concentrations of D-glucose (D-Glc) and L-lactate (L-Lac) were determined using a LaboTRACE automatic analyzer (Trace Analytics GmbH, Braunschweig, Germany). The concentration of secreted antibody was determined with an

enzyme-linked immunosorbent assay (ELISA) [28]. All sampling and measurement procedures were performed with three technical replicates. The determination of cell cycle distribution was performed as described before [313]. All sampling and measurement procedures were performed with two technical replicates.

### **Transcriptome analysis**

Experimental equipment and settings were used as described above (MTA at 48 h: 250  $\mu$ M) in biological triplicates. The isolated RNA was processed by c.ATG. Analysis of raw data was performed on the Galaxy-Server [322], and data were analyzed using the free statistical computing environment R.

### **Experiment and sampling for transcriptome analysis and ribonucleic acid (RNA) sequence analysis**

Experimental equipment and settings were described in the manuscript. Sampling for transcriptome analysis occurred on 48-h, 60-h, 72-h, 84-h, 96-h and 144-h cultivation time and followed an adapted protocol [300]. A total number of  $2 \times 10^6$  cells were harvested and centrifuged, and supernatant was discarded. Cells were resuspended in RNeasy Protect Cell Reagent (Qiagen, Hilden, Germany), quickly frozen in liquid nitrogen and stored at  $-70$  °C. The RNA was isolated with the RNeasy Kit (Qiagen) and RNeasy Rytel (Qiagen). An extra procedure of clean-up to get rid of DNA (Turbo DNase<sup>TM</sup> and Turbo DNase<sup>TM</sup> Buffer, Ambion (Life Technologies, Carlsbad, CA, USA)) and increase the RNA concentration (RNA Clean & Concentrator<sup>TM</sup>, Zymo Research, Irvine, CA, USA) was added. The kits were used as indicated by the manuals. Sequencing of the transcriptome was performed by c.ATG (Tübingen, Germany). Preparation of high-quality mRNA-Seq data was performed using the Illumina TruSeq RNA Sample Preparation Kit. Quality was assessed by an Agilent Fragment Analyzer. Samples with high RNA integrity number (RIN > 8) were selected for library construction using the NEBNext Ultra II Directional RNA Library Prep Kit. Libraries were sequenced as paired-end (50 bp read length) at a depth of 30-40 million reads each.

### **Read mapping and gene counting**

Read mapping and gene counting was performed on the Galaxy-Server. Sequencing statistics including the quality per base and adapter content assessment of resulting transcriptome sequencing data were checked by FastQC reports. Genes were aligned to the CHO-K1 reference genome (RefSeq: GCF\_000223135.1) (downloaded from <http://www.chogenome.org/>, 07/08/2019) using the RNA sequencing aligner BOWTIE2 v. 2.3.2.2 [323]. On average, the mapping of the reads covers 94.3 %. Aligned reads were counted for each gene based on the corresponding annotation available from the CHOgenome webpage for the chosen reference sequence applying HTSEQ-COUNT v. 0.6.1 [324] in the union mode. On average, 71.0 % of the sequenced reads could be assigned uniquely to annotated genes. Sequencing depth was around 33 million reads per sample on average.

### **Transcriptome data analysis**

Differential gene expression analysis was performed with the R-package DESEQ2 v. 1.26.0 [325] available from Bioconductor [326] (<http://www.bioconductor.org>). Prior to statistical analysis, a non-specific filter was applied to remove low coverage genes with less than one count per million (33 reads on average) in two out of three replicates per condition. Samples were grouped by replicates, and an experimental design was chosen that used sample time and treatment (CPC, REF, MTA) as a combined environmental factor. To normalize the read counts for comparison purposes on sequencing depth and RNA composition, DESeq2 uses the median of ratios method to derive a scaling factor. Dividing the original read counts by the scaling factor normalized count values are generated. To model count-based expression data, DESeq2 uses a negative binomial model as a distribution assumption and fits the expression data for each gene to a generalized linear model (GLM). No outliers were observed in the three biological replicates using Pearson correlation. Resulting *P*-values were adjusted for multiple testing according to [327] to control the false discovery rate (FDR). Genes were identified as significantly differentially expressed by applying FDR adjusted *P*-values < 0.05 and a log<sub>2</sub>-fold-change ≥ |1|. A principal component analysis was used to display the sample to sample distances calculated within the DESeq2 package using the function plotPCA.san available on



Github (<https://gist.github.com/sansense/3399064897f1252d31b23ea5178c033c>). Raw counts and processed data can be found in the supplementary information. Data analysis was performed using the free statistical computing environment R v. 3.6.2.

## Results

### The effect of MTA addition depends on its concentration

MTA was added in different concentrations (c1: 150  $\mu\text{M}$ , c2: 250  $\mu\text{M}$ , c3: 350  $\mu\text{M}$ , c4: 450  $\mu\text{M}$ ) to the cells after 48-h cultivation time. All MTA treated cultures showed reduced VCD and growth rate (regarding 48-120 h) dependent on the concentration (**Figure 24**). Higher MTA amounts reduced VCD and growth rate stronger than low additions. The lowest concentration c1 led to 30 % reduction of growth rate whereas the two highest concentrations c3 and c4 halved it. c2 reduced growth rate by 44 %. However, maximum inhibition trends were observed for c3 and c4: The reduction of growth rate plateaued. Addition of MTA with c1, c2 and c3 demonstrated a higher viability in the last cultivation phase compared to REF. By trend, analysis of maximum product titers unraveled slightly elevated amounts of antibodies for all MTA additions except c3 (**Figure 24**). Calculating cell-specific productivities revealed boosted CSPs for all MTA additions between 48-144 h. Concentration c2 showed the best performance (+79.7 %) and c1 the lowest (+43.9 %). Fitting the CSPs to a 2<sup>nd</sup> order polynomial function reveals optimum MTA addition of 0.167  $\text{pmol}^{\text{MTA}} \text{cell}^{-1}$  at 48 h (**Figure 24**). The equivalent medium concentration of 295.59  $\mu\text{M}$  is close to the tested level of c2 with the highest CSP in the experimental series.

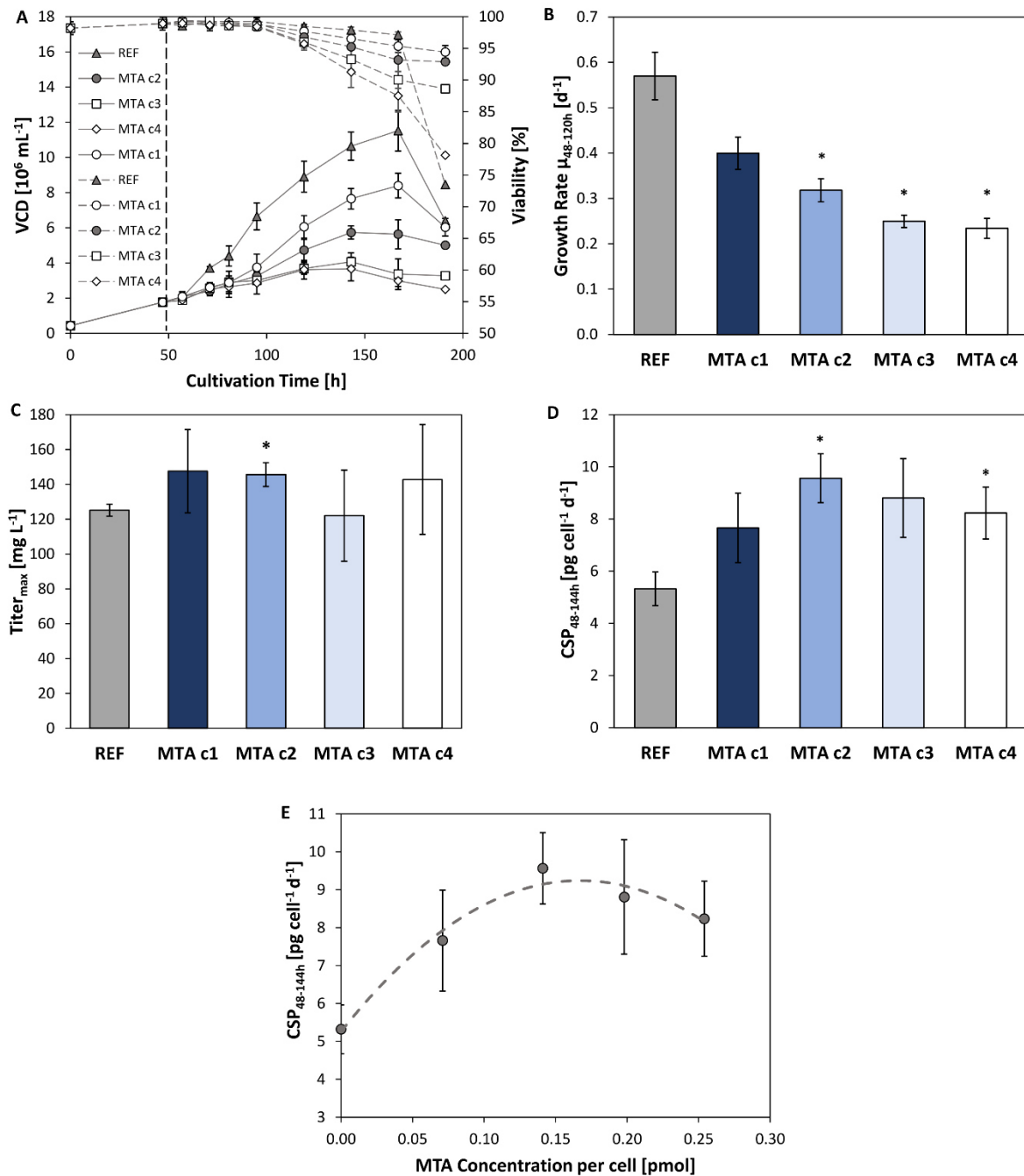


**Figure 24.** (A) VCD [ $10^6$  cells  $\text{mL}^{-1}$ ] and viability [%] of MTA supplemented cells and reference (REF  $\blacktriangle$ ). MTA was added at 48 h in different concentrations: c1 150  $\mu\text{M}$ (o), c2 250  $\mu\text{M}$ ( $\bullet$ ), c3 350  $\mu\text{M}$ ( $\square$ ), c4 450  $\mu\text{M}$ ( $\diamond$ ). (B) Growth rate per day [ $\text{d}^{-1}$ ] regarding the time interval 48-120 h. (C) Maximum antibody titer [ $\text{mg L}^{-1}$ ]. (D) CSP [ $\text{pg cell}^{-1} \text{d}^{-1}$ ] regarding the time interval 48-144 h. (E) CSP [ $\text{pg cell}^{-1} \text{d}^{-1}$ ] between 48-144 h plotted against the MTA amount per cell [pmol] at 48 h. Error bars show standard deviations of biological duplicates. Significance (to REF) was tested with a t-test; \* < 0.05.

Cell cycle phase distribution revealed the concentration-dependent effect of MTA (**Figure 25**). A common preculture split right before MTA (48 h) served as a starting point. Half a day after MTA addition, cells accumulated in G1-phase. 12 h later, i.e. one day after addition, the number of cells in S-phase increased for the sake of those in G1-phase. At 84 h (36 h after addition) cells in G2-phase dominated and the number of cells in G1-phase kept dropping. Two days after addition the ratios started to normalize. Cultures with c3 and c4 approached REF conditions whereas c1 and c2 kept an elevated fraction of cells in G1-phase. The different MTA concentrations caused diverse effects on cell size. In general, cell size was smallest in REF and largest after c3 and c4 addition. By trend, all MTA treated cells kept enlarged cell size on different levels compared to REF.

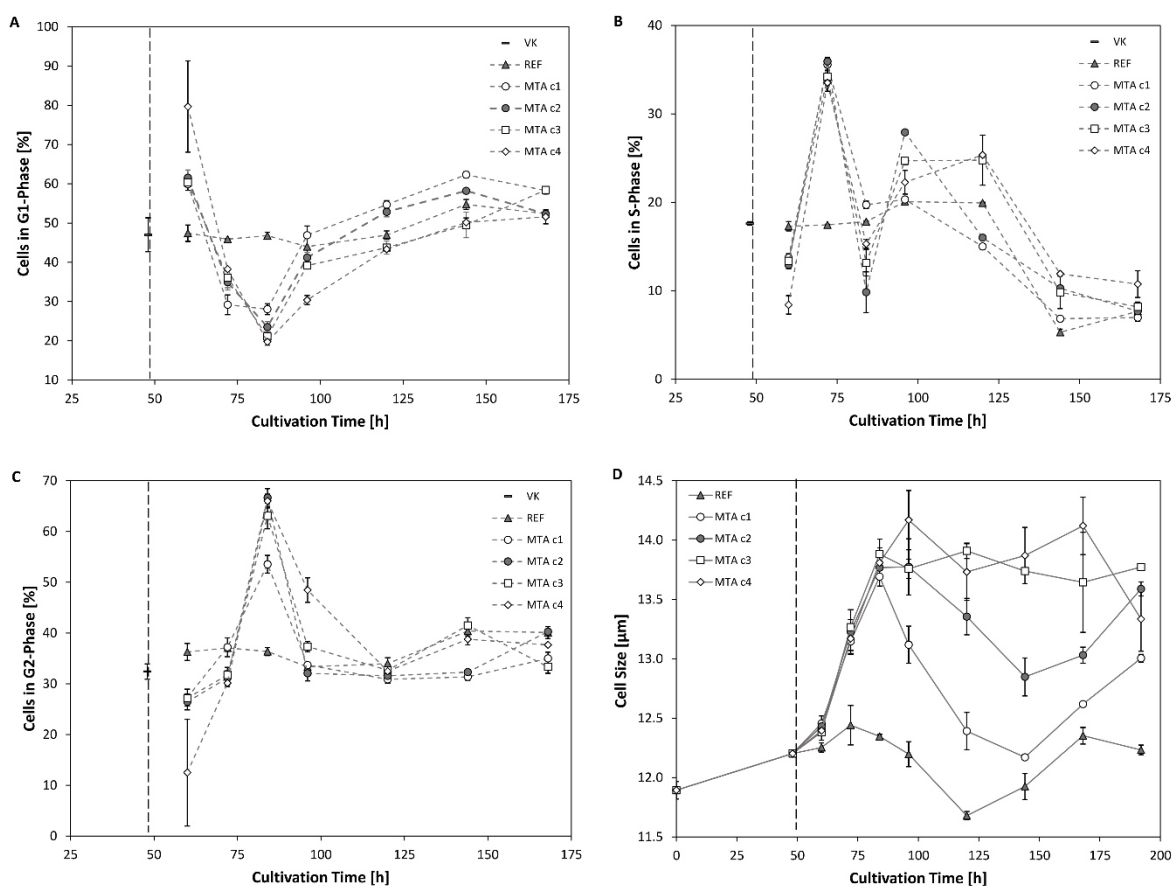


**Figure 25.** Cell cycle phase distribution (A–C) [%] and average cell size (D) [ $\mu\text{m}$ ] of MTA supplemented cells, reference (REF▲) and common preculture (-). MTA was added at 48 h in different concentrations: c1 150  $\mu\text{M}$ (○), c2 250  $\mu\text{M}$ (●), c3 350  $\mu\text{M}$ (□), c4 450  $\mu\text{M}$ (◇). Error bars show standard deviations of biological duplicates.

### **The effect of MTA is time-dependent**

In another experimental series, cells received  $0.167 \text{ pmol}_{\text{MTA}} \text{ cell}^{-1}$  after 48, 84 and 108 h (**Figure 26**). The rise of VCD slowed down after each MTA addition. Growth reduction was more pronounced the earlier MTA was added with the 48-h-shot showing the slowest post-MTA growth rate. However, the viability of the treated cells remained even higher than the performance of REF. Regarding growth rate the 48-h-addition caused 44.7 % reduction whereas the 84-h-addition only reduced growth by 19.6 %. Late addition (108 h) did not cause any growth difference compared to REF. Maximum antibody titers [ $\text{mg L}^{-1}$ ] did not increase after MTA additions at 84 and 108 h (**Figure 26**) but rose after 48 h. The trend is even more pronounced with respect to CSPs. The 48-h-supplementation almost doubled CSP (+97.4 %) compared to REF whereas later MTA treatments showed no effects. By analogy, cell size raises the most when MTA was added at 48 h.

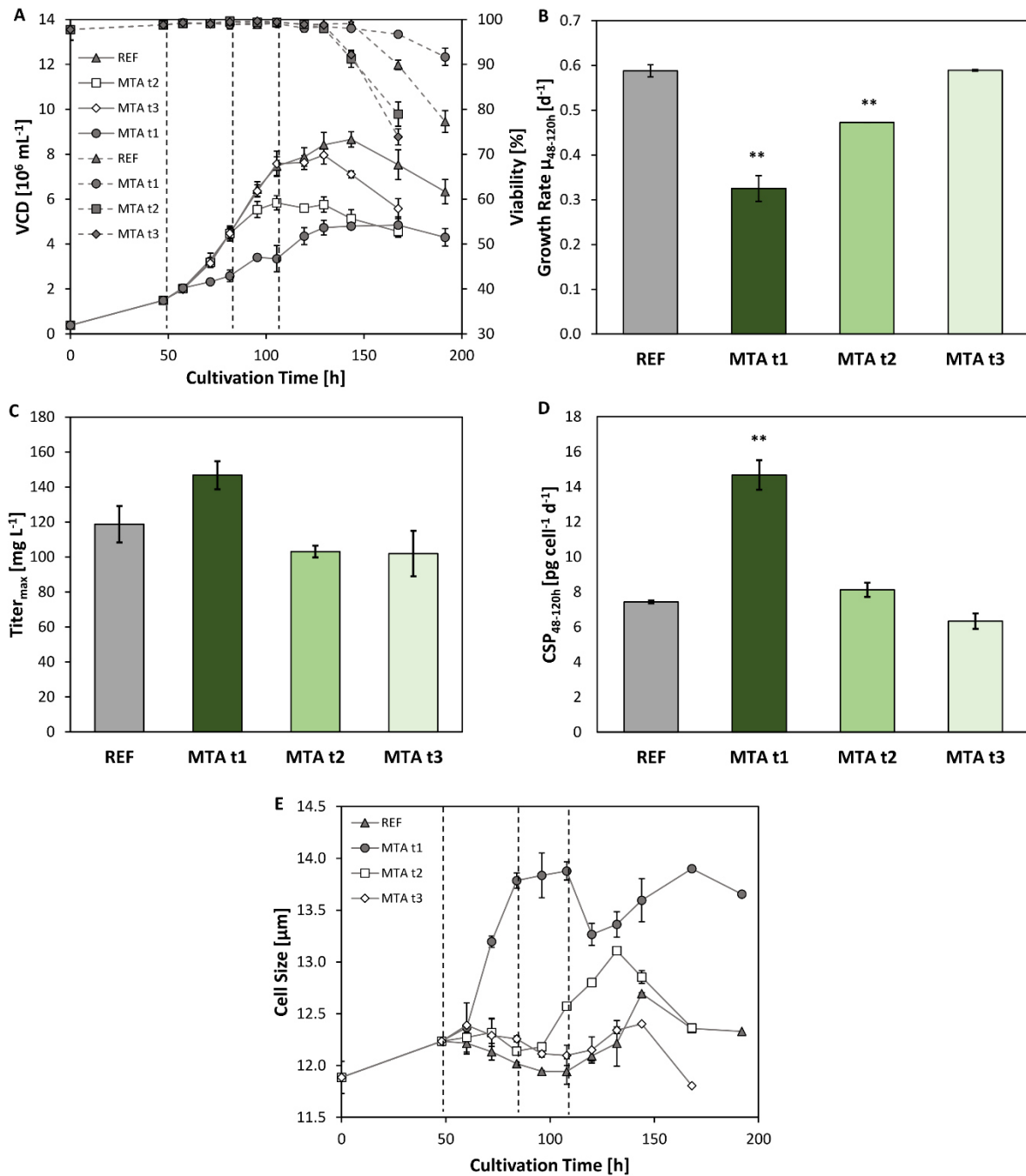


**Figure 26.** (A) VCD [ $10^6 \text{ cells mL}^{-1}$ ] and viability [%] of MTA supplemented cells and reference (REF ▲). MTA was added with  $0.167 \text{ pmol}_{\text{MTA}}$  per cell at 48, 84 or 108 h: MTA t1 48 h (●), MTA t2 84 h (□), MTA t3 108 h (◇). (B) Growth rate per hour [ $\text{d}^{-1}$ ] regarding the time interval 48-120 h. (C) Maximum antibody titer [ $\text{mg L}^{-1}$ ]. (D) CSP [ $\text{pg cell}^{-1} \text{ d}^{-1}$ ] regarding the time interval 48-120 h. (E) Average cell size [ $\mu\text{m}$ ]. Error bars show standard deviations of biological duplicates. Significance (to REF) was tested with a t-test; \*\* < 0.01.

Cell cycle phase distributions and cell sizes are displayed in **Figure 27**. Again, highest impact was found for 48-h-cultures whereas later MTA addition did not reveal strong differences compared to REF. Early supplementation caused increasing cell fractions in S-phase and decreasing percentages in G1- and G2-phase 36 h after addition. 60 h after addition, the partition of cells in G2-phase increased and there were still less cells in G1-phase.

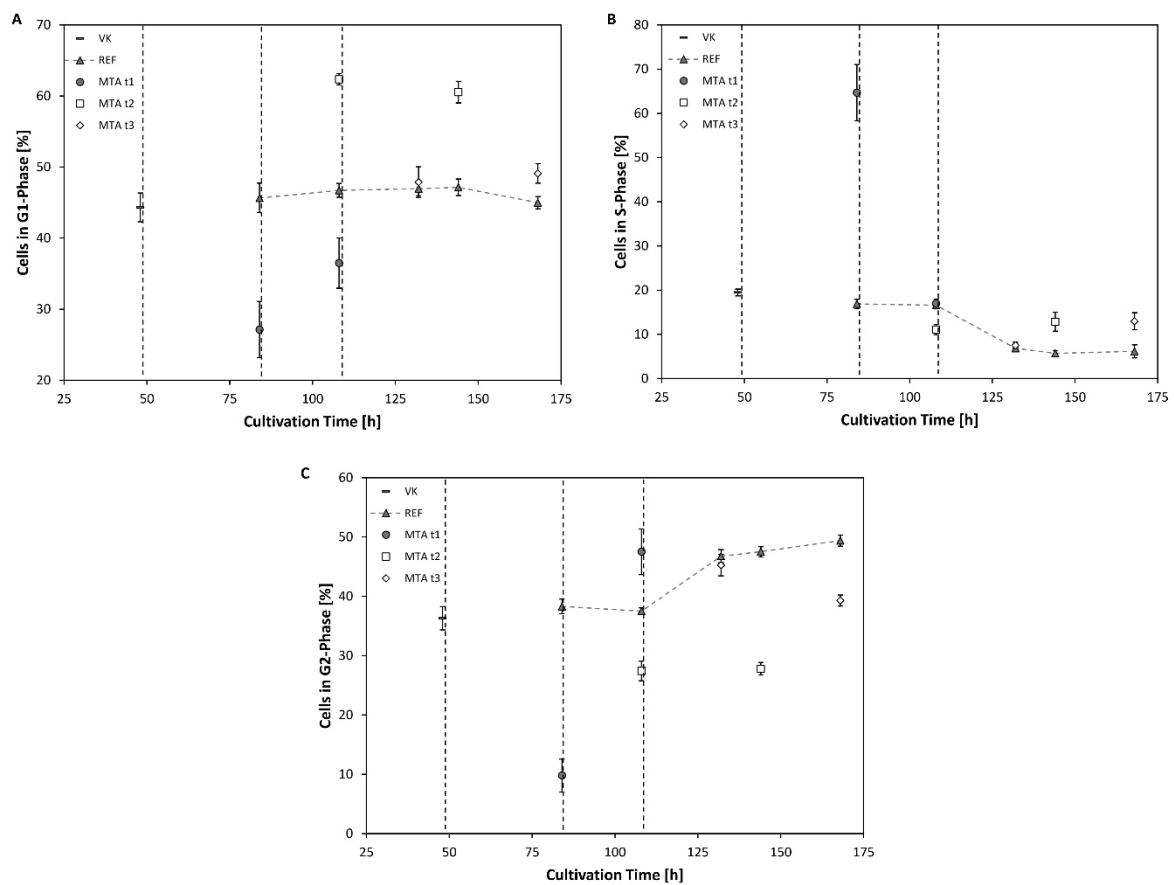


**Figure 27.** Cell cycle phase distribution (A-C) [%] of MTA supplemented cells, reference (REF ▲) and common preculture (-). MTA was added with  $0.167 \text{ pmol}_{\text{MTA}}$  per cell at 48, 84 or 108 h: MTA t1 48 h (●), MTA t2 84 h (□), MTA t3 108 h (◇). Error bars show standard deviations of biological duplicates.

### Monitoring transcriptional responses after MTA addition

The impact of MTA on the transcriptome was evaluated via differential gene expression (DEG) analysis based on RNA sequencing. mRNAs of biological triplicates supplemented with MTA were compared at different time points (60, 72, 84, 96, 144 h) to REF. Around 91 % of total variance is covered by two principal components (PC) clearly grouping biological triplicates of

equal sampling points. Apparently, cultivation time is represented by PC1 and MTA addition by PC2 (**Figure 28**). In total, 122 DEGs were identified according to the constraints  $\log_2$ -fold-change  $\geq |1|$  and adjusted  $P$ -value  $\leq 0.05$ . Downregulation of genes occurred mostly 12-36 h after addition (60 h: 1, 72 h: 8, 84 h: 12, 96 h: 3, 144 h: 1) (**Figure 29**). Later, i.e. 84 h process time, upregulation of genes dominated DEGs by far (60 h: 0, 72 h: 4, 84 h: 30, 96 h: 85, 144 h: 40). The Venn diagram comprising DEGs at 84 h-96 h-144 h reveals 6 commonly upregulated genes compared to REF. All DEGs that were significantly up- or downregulated at more than one sampling time point are listed in **Table 2**.

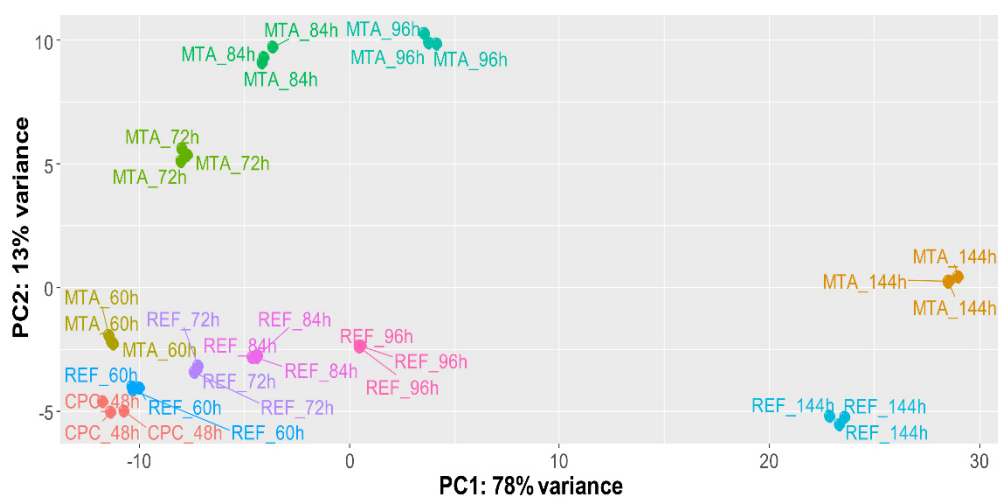


**Figure 28.** Principal component (PC) analysis of the transcriptome samples taken in the experiment. The two main principal components are cultivation time (PC1) and condition (MTA treatment, PC2). Samples were taken in the common preculture (CPC) at 48-h cultivation time and after MTA addition (final concentration: 250  $\mu$ M) at the cultivation time points 60, 72, 84, 96 and 144 h. Reference (REF) cultures received the equal volume of water to avoid dilution effects.

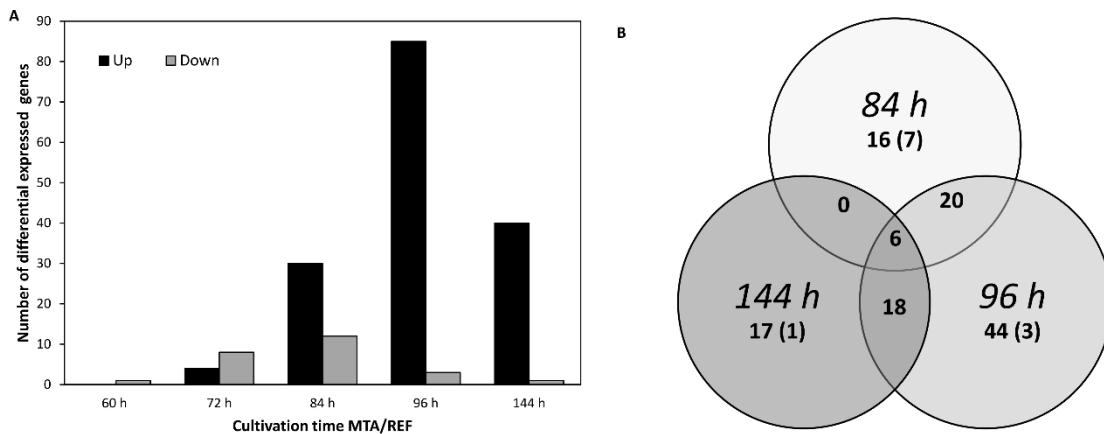


**Figure 29.** (A) Analysis of differential expressed genes (DEGs) ( $\log_2$ -fold-change  $\geq |1|$  and  $P$ -value  $\leq 0.05$ ) throughout the experiment. MTA supplemented cells (MTA) were compared to REF. Grey bars indicate downregulated and black bars show upregulated genes at different sampling time points. (B) Venn diagram shows overlap of DEGs at 84 h-96 h-144 h. Numbers display all DEGs with the number of downregulated genes in brackets.

Four genes of the six DEGs observed at 84 h-96 h-144 h are annotated: *Aqp1*, *Lcp1*, *Plau* and *St14* whereas two are unknown loci. Aquaporin 1 (*Aqp1*) is a commonly amplified water channel. *Lcp1* codes for plastin, an actin-binding cellular component. Plasminogen activator (*Plau*) and matriptase (*St14*) are serine proteases.

**Table 2.** Selection of differential expressed genes. Downregulated genes are highlighted in grey.

Cultivation time	Gene name	Encoded protein
84 h-96 h-144 h	<i>Plau</i>	Urokinase-type plasminogen activator
	<i>Aqp1</i>	Aquaporin-1
	<i>Lcp1</i>	Plastin-2
	<i>St14</i>	Suppressor of tumorigenicity 14 protein homolog
72 h-84 h	<i>Apc2</i>	Adenomatous polyposis coli protein 2
	<i>Il11</i>	Interleukin-11
84 h-96 h	<i>Rassf6</i>	Ras association domain-containing protein 6
	<i>Abhd6</i>	monoacylglycerol lipase ABHD6
	<i>Hr</i>	Lysine-specific demethylase hairless
	<i>Dnase1l3</i>	Deoxyribonuclease gamma
	<i>Il17f</i>	Interleukin-17F
	<i>Lpin3</i>	Phosphatidate phosphatase LPIN3
	<i>Arnt2</i>	Aryl hydrocarbon receptor nuclear translocator 2
	<i>Sh2d1b</i>	SH2 domain-containing protein 1B
	<i>Fam110c</i>	Protein FAM110C
<i>Cd53</i>	Leukocyte surface antigen CD53	



	<i>Oasl</i>	2'-5'-oligoadenylate synthase-like protein 2
	<i>Egfr</i>	Epidermal growth factor receptor
	<i>St8sia6</i>	Alpha-2,8-sialyltransferase 8F
96 h-144 h	<i>Add2</i>	beta-adducin
	<i>Loxl2</i>	Lysyl oxidase homolog 2
	<i>Il7r</i>	Interleukin-7 receptor subunit alpha
	<i>Tmprss11f</i>	Transmembrane protease serine 11F
	<i>Adgrd1</i>	Adhesion G-protein coupled receptor D1
	<i>Sema4d</i>	Semaphorin-4D
	<i>Akr1d1</i>	Aldo-keto reductase family 1 member D1
	<i>Mpeg1</i>	Macrophage-expressed gene 1 protein
	<i>Pglyrp2</i>	N-acetylmuramoyl-L-alanine amidase

A lot of genes are differentially expressed at two time points after MTA addition. 12 and 24 h after MTA addition (72 h-84 h) two annotated genes are differentially expressed: Adenomatous polyposis coli protein 2 (*APC2*), a gene transcription regulator is downregulated whereas *Il11* (interleukin-11) is upregulated. 24 and 36 h after MTA addition (84 h-96 h) 13 additional upregulated DEGs were observed: (a) the small G-protein (ras) associated domain-containing protein 6 (*Rassf6*) which is associated with cellular apoptosis, (b) the epidermal growth factor receptor (*Egfr*) involved in proliferation, (c) interleukin-17F (*Il17f*), a pro-inflammatory cytokine, (d) the lysine-specific demethylase hairless (*Hr*), a histone demethylase, (e) deoxyribonuclease gamma (*Dnase1l3*), an enzyme with hydrolytic DNA activity. Nucleus associated upregulated transcripts are: (f) *Arnt2* coding for Aryl hydrocarbon receptor nuclear translocator 2, a transcription factor and (g) the protein FAM110C (*Fam110c*) known for interactions with microtubules and nucleus. Other upregulations are (h) phosphatidate phosphatase LPIN3 (*Lpin3*) involved in lipid synthesis, (i) monoacylglycerol lipase ABHD6 (*Abhd6*) forming intraluminal vesicles and (j) the glycosylating protein alpha-2,8-sialyltransferase 8F (*St8sia6*). Genes linked to immune functions are upregulated, including (k) the signaling factor SH2 domain-containing protein 1B (*Sh2d1b*), (l) the tetraspanin leukocyte surface antigen CD53 (*CD53*), and (m) the viral response component 2'-5'-oligoadenylate synthase-like protein 2 (*Oasl*).

## Discussion

### **Optimum MTA addition levels during growth are 250-300 $\mu$ M and stimulate cell cycle arrest, increase cell size and ensure high viability**

We investigated concentration and time dependency of MTA addition in CHO cell cultures to elucidate the impact of these factors on the CSPs. Different effector levels at 48-h cultivation time (**Figure 24** and **Figure 25**) revealed clear concentration dependency. Effects on growth, cell cycle and cell size were affected by different concentrations plateauing  $> 350 \mu\text{M}$ . CSP maxed out at about 250-300  $\mu\text{M}$ . Furthermore, the two highest concentrations c3 and c4 even disclosed negative effects as decreasing viability and CSP. Noteworthy, effector levels  $< 350 \mu\text{M}$  ensured higher viabilities and higher CSPs than REF.

Similar dependencies of effector levels on CHO growth were observed for catechins trapping cells in S-phase [20]. By analogy, treatment of cells with AMP is concentration-dependent and resulted in S-phase accumulation. As a consequence, CSP increased [24].

Further investigations on optimum MTA additions showed that supplementation during exponential growth is most beneficial (**Figure 26**). Coinciding growth-dependent cell size increase may further support the effect. Apparently, the combination of cell cycle arrest, high viability, and increasing cell size defines a key scenario for boosting CSP.

Many studies outlined the boosting effect of temporary cell cycle arrest on CSP although independent of a specific cell cycle phase [26–28,30,31,33]. In several CHO cell lines, CSP and cell size correlated [33]. However, cell size increase is linked to cell cycle [34–36] which makes the independent study of each impact hardly possible. Consequently, the combinatorial benefit of cell cycle arrest with increased cell size, still ensuring high cell viability, should be concluded as beneficial for high CSP. Moreover, impaired cell growth yields less biomass formation and allows to use redundant energy and metabolic precursors for protein production [121]. Apparently, MTA initiates the beneficial combination when an optimum effector level of 250-300  $\mu\text{M}$  is installed during exponential growth in the medium.

### **Fundamental cell engineering strategies**

Cell engineering for improved CSPs focus on engineering apoptosis, metabolism, cell cycle and protein secretion [328]. Transcript studies of low and high producers revealed that high recombinant protein formation negatively correlates with gene expression of cell cycle, metabolic RNA and protein processes [301]. Enhanced gene expression was observed in protein folding, cell survival, cell growth, vesicular trafficking and cytoskeleton organization [42]. As the map of functional gene annotations is still fragmented for CHO, identification of promising novel gene functions is necessary.

### **The role of the cytoskeleton part actin for CSP after MTA addition**

The water importer aquaporin 1 (encoded by *Aqp1*) was upregulated 84 h-96 h-144 h after MTA addition (**Table 2**) coinciding with increased cell size (**Figure 25** and **Figure 26**). This observation was seen in stress situations [329,330] (e.g. hyperosmolarity) that caused increased intracellular protein content and CSP [331,332]. In this experiment, the increased need of membrane molecules as glycerolipids could be satisfied by the upregulated phosphatidase phosphatase LPIN3 (*Lpin3*) at 84 h-96 h. Co-upregulation of *Lcp1* and *St14* occurred (84 h-96 h-144 h) coding for the actin-associated enzyme plastin and matriptase [333,334]. Noteworthy, actin microfilaments, microtubules and intermediate filaments compose the cytoskeleton which takes over crucial functions for cell shape, protein synthesis [180], transport [181] and secretion [182,183]. Dinnis et al., [184] observed that actin, tubulin, or the actin-binding cofilin demonstrated an important role in protein transport and secretion of high producers. Selection procedures for high producers revealed according to data with enhanced gene expression of actin-related proteins [41]. Recently, Berger et al., [42] identified DEGs involved in cytoskeleton organization and vesicular trafficking as *Rassf9* that is linked to endosome recycling and is a trafficking regulator [335] in high producers. Our studies revealed upregulated genes (84 h-96 h) associated with intraluminal vesicles (monoacylglycerol lipase ABHD6 (*Abhd6*)) and protein processing (glycosylation) (alpha-2,8-sialyltransferase 8F (*St8sia6*)) in the Golgi (**Table 2**). Actin cooperates with polymerases via pre-initiation complex influencing gene expression [336,337] and is involved in cellular response to DNA damaging

agents and toxins in CHO cells [338]. Next to the abovementioned actin-related genes, *Add2* (beta-adducin) at 96 h-144 h [339] and *Fscn1* (fascin) at 96 h [340] were upregulated in our data. Right after MTA addition (72 h-84 h) adenomatous polyposis coli protein 2 (*APC 2*), a transcription factor linked with actin [341] is downregulated. It is associated with microtubules and interphase [342] as protein FAM110C (*Fam110c*, upregulated at 84 h-96 h) that impairs cell cycle progression [343].

Several gene expressions related to cytoskeleton parts either for transport and secretion or cell growth are differentially regulated in our data highlighting their importance in the CSP enhancing mechanism of MTA.

### **Genes encoding for cellular survival, transcriptional regulation and immune system**

Plasminogen activator (*Plau*) upregulated at 84 h-96 h-144 h is a growth factor, mitogen and apoptotic reducer [344,345]. Another upregulated gene (84 h-96 h) associated with cell growth, survival and transcription is the tumor-suppressor ras association domain-containing protein 6 (*Rassf6*) an important regulator of cell cycle arrest and apoptosis and whose upregulated family members were observed in high producers [42,170]. The transcription factor aryl hydrocarbon receptor nuclear translocator 2 (*Arnt2*) correlated with cell proliferation [346] was downregulated at 72 h-84 h. At 84 h-96 h *Dnase1l3* and *Egfr* were upregulated encoding deoxyribonuclease gamma (*Dnase1l3*) and epidermal growth factor receptor (EGFR), respectively. *Dnase1l3* is a apoptosis-related factor [347] whereas EGFR is associated with DNA synthesis and proliferation [348]. *Atf5* (cyclic AMP-dependent transcription factor ATF-5) was upregulated at 84 h which agrees with studies searching for transcription and protein production regulators in CHO cells [349].

Next to growth and cellular survival factors, DEGs for histone proteins influenced transcription and replication [170]. Upregulation occurred for lysine-specific demethylase hairless (*Hr*), a histone demethylase (84 h-96 h), that interacts with cell cycle regulation [350]. Additionally at 96 h-144 h, lysyl oxidase homolog 2 (*Loxl2*) and chromodomain-helicase-DNA-binding protein 5 (*Chd5*), both histone modifying enzymes are upregulated [351,352].

Genes involved in immune functions as SH2 domain-containing protein 1B (*Sh2d1b*), CD53 (*CD53*), viral response component 2'-5'-oligoadenylate synthase-like protein 2 (*Oasl*), interleukin-17F (*Il17f*) (84 h-96 h) and interleukin-11 (*Il11*) (72 h-84 h) were upregulated after MTA addition demonstrating a connection to the immune system and its connected signaling pathways [312].

DEGs regarding growth, survival and transcription including DNA modification point out the multi-level effects of MTA that enhanced viability and CSP.

### **Concluding Remarks**

MTA, the degradation product of SAM, boosts CSPs in an anti-IL-8-producing CHO-DP12, presumed that optimum MTA levels of 250-300  $\mu$ M are installed for exponentially growing cells. Indeed, the rise of VCDs slowed down but CSPs increased up to +97 %, even ensuring cell viabilities better than REF. Moreover, titers were comparable to REF in the best MTA addition case. These improvements coincided with cell cycle modulations, i.e. accumulations in S-phase followed by elevated cell numbers in G2-phase which both levelled out during cultivation. DEGs clearly showed upregulations of cytoskeleton, growth, survival and transcription-associated genes as predominant regulation patterns. Although those DEGs may be qualified as a particular response on MTA next to its function as polyamine synthesis inhibitor that correlate with findings of other independent studies outlining that actin-interacting proteins, cell proliferation and histone proteins are promising candidates for further cell engineering.

With MTA, a native compound is identified that clearly boosts CSPs after 'simple' medium addition. It is the key degradation product of SAM whose price will reduce with its microbial production [353]. MTA initiates regulation programs that deserve further investigations, not only because they may offer even further improvements but also because major findings may be translated to other production cell lines. Apparently, MTA addition positively stimulates cell cycle arrest, cytoskeleton and cell survival genes concomitantly, thereby addressing key topics of current cell line engineering. These findings should be considered for process intensification studies, especially for perfusion processes where improvements of CSPs are an important goal of optimization.

### **Acknowledgment**

The authors gratefully acknowledge the funding by the Bundesministerium für Bildung und Forschung (BMBF, Funding Number 031L0077A). The authors would like to thank the group of Computational Biology at the Institute of Biochemical Engineering for the use of the Galaxy-Server. Open access funding enabled and organized by ProjektDEAL.

### **Conflict of Interest**

The authors declare no conflict of interest.

### **Author Contributions**

NV and RT designed the experiment. NV conducted the experiments and data analysis. JZ analyzed transcriptome data. NV and JZ interpreted transcriptome data. NV, JZ and RT wrote the manuscript.

### **Data Accessibility**

Processed transcriptome data is accessible in the supplemental part. Further data will be available from the corresponding author upon reasonable request.

### **References**

see 5 References, p.139

### **Supporting Information**

see 6.2 Supplementary Material: Manuscript 3, p.190

Additional supporting information may be found online in the Supporting Information section at the end of the article.

Table S1. List of differential expressed genes (FDR adjusted  $p$ -values  $\leq 0.05$  and a  $\log_2$ -fold-change  $\geq |1|$ ) between MTA treated cells and REF at different sampling points.

Appendix S1. Transcriptome analysis. Sample description, mapping statistics and counts.

### **3.4 Manuscript 4: The Novel Additive MTA (Methylthioadenosine) Causes Metabolic Reprogramming Improving NADPH Availability and Boosting Cell-Specific Productivity of CHO Cells**

The following manuscript was submitted in Metabolic Engineering in December 2020.

**The novel additive methylthioadenosine causes metabolic reprogramming, improving NADPH availability and boosting cell-specific productivity of CHO cells**

Andy Wiranata Wijaya<sup>a1</sup>, Natascha Verhagen<sup>a1</sup>, Attila Teleki<sup>a</sup>, and Ralf Takors<sup>a\*</sup>

<sup>a</sup>Institute of Biochemical Engineering, University of Stuttgart, Allmandring 31, 70569 Stuttgart, Germany

<sup>1</sup>Equal first authors/Co-first author

\*Corresponding author

**Correspondence**

Prof. Dr-Ing. Ralf Takors

Institute of Biochemical Engineering

University of Stuttgart

Allmandring 31, 70569 Stuttgart, Germany

Tel: +49 (0)711 685-64535

Fax: +49 (0)711 685-55164

Email: ralf.takors@ibvt.uni-stuttgart.de



## Highlights

- The novel additive MTA (5'-deoxy-5'-(methylthio)adenosine) boosts cell-specific productivities (CSPs) of monoclonal antibody formation in CHO cells by 50 %.
- CSP enhancement is accompanied by cell cycle arrest, increasing cell volume, and fundamental metabolic reprogramming.
- Compartment-specific  $^{13}\text{C}$  flux analysis reveals 3-fold increased NADPH supply by massive detouring carbon flux through oxidative pentose-phosphate pathway (PPP).
- The importance of cytosolic malic enzyme as key NADPH supplier shifts to predominant NADPH formation via oxidative PPP.
- Mitochondrial shuttles adapt activities (e.g., glutamate carrier GC) or even reverse fluxes (e.g., OGC transporter) to support the fundamental flux changes in central metabolism.
- Elevated cytosolic ATP levels are anticipated to mediate the metabolic reprogramming by inhibiting phosphofructokinase.

**Abstract**

Increasing cell-specific productivities (CSPs) for the production of heterologous proteins in Chinese hamster ovary (CHO) cells is an omnipresent need in the biopharmaceutical industry. The novel additive 5'-deoxy-5'-(methylthio)adenosine (MTA), a chemical degradation product of *S*-(5'-adenosyl)-L-methionine (SAM) and intermediate of polyamine biosynthesis, boosts the CSP of IgG1-producing CHO cells by 50 %. Compartment-specific <sup>13</sup>C flux analysis revealed a fundamental reprogramming of the central metabolism after MTA addition accompanied by cell-cycle arrest and increased cell volumes. Carbon fluxes into the pentose-phosphate pathway increased 22 fold in MTA-treated cells compared to that in non-MTA-treated reference cells. Most likely, cytosolic ATP inhibition of phosphofructokinase mediated the carbon detour. Mitochondrial shuttle activity of the  $\alpha$ -ketoglutarate/malate antiporter (OGC) was reversed, reducing cytosolic malate transport. In summary, NADPH supply in MTA-treated cells improved 3 fold compared to that in non-MTA-treated cells, which can be regarded as a major factor for explaining the boosted CSPs.

**Keywords**

Chinese hamster ovary (CHO) cell; cell-specific productivity, <sup>13</sup>C metabolic flux analysis (<sup>13</sup>C MFA), 5'-deoxy-5'-(methylthio)adenosine (MTA), metabolism, nicotinamide adenine dinucleotide phosphate (NADPH)

**Abbreviations**

Chinese Hamster ovary (CHO) cell; cell-specific productivity (CSP), <sup>13</sup>C metabolic flux analysis (<sup>13</sup>C MFA), 5'-deoxy-5'-(methylthio)adenosine (MTA), viable cell density (VCD)

## Introduction

Biopharmaceutical markets are steadily increasing worldwide; monoclonal antibody production in Chinese hamster ovary (CHO) cells continue to possess the largest share [1]. Product titers improved 100-fold during the last few decades [2,259,294]; however, cell-specific productivities (CSPs) have increased only 3-8 fold. Optimization of CSP is a striking demand, envisaging the current need for intensifying bioprocesses and considering continuous production in perfusion processes [3,295,296].

However, optimization of CSP requires a detailed understanding of intracellular regulation, which typically requires the concerted application of omics technologies [354] comprising genome analysis [11,355], genome-scale modeling [286], transcript analysis [300,301], epigenetics [304,305], metabolomics [297], and fluxomics [295,298,356].

Efforts have been undertaken for enhancing CSP through initiating growth arrest [314]. In addition to osmolarity and temperature shifts [25–28], studies have focused on the addition of effectors such as sodium butyrate [21], valeric acid [320], glycine betaine [321], and catechin [20]. As a common observation, alterations in cell-cycle phases coincided with increase in cell size. Both were anticipated to improve CSP [34,35,315,357,358]. However, the underlying mechanisms that explain the phenotype remain fragmented. Recently, Verhagen et al. [313,359] demonstrated that cell-cycle arrest could be achieved by exposing CHO cells to the effector 5'-deoxy-5'-(methylthio)adenosine (MTA), which increased CSP by 50 %.

MTA is a degradation product of the crucial methyl group donor *S*-adenosyl-methionine (SAM) and a by-product of polyamine synthesis [58,227]. MTA is an anticipated effector of the polyamine pathway, DNA synthesis, gene expression control, cell proliferation, lymphocyte activation, tumor development, invasiveness, apoptosis, and signaling pathways [49,58–62,64,65]. Furthermore, MTA is rapidly metabolized and the end products can be used to replenish adenosine-based nucleotide pools [58,59]. Recently, Verhagen et al. [313,359] revealed that MTA addition influenced cell size, cell cycle, and transcript levels, ultimately enhancing the IgG1 CSP of CHO-DP12 cells. Consequently, this study was performed to identify

the metabolic processes underlying the improvement of the CSP phenotype after MTA addition.

Compartment-specific  $^{13}\text{C}$  metabolic flux analysis ( $^{13}\text{C}$  MFA) was applied to assess the flux changes in the CHO-DP12 culture with and without MTA supplementation. We observed that the cells underwent significant metabolic reprogramming after MTA exposure. The maximization of NADPH formation was identified as a crucial target, which resulted in optimization of CSP. This result opens the door for follow-up studies on optimizing bioprocesses and engineering hosts to install analogous metabolic rewiring through genetic alterations.

## **Material and Methods**

### **Cell culture conditions and effector and isotopic tracer studies**

An IgG1 antibody (anti-IL-8)-producing CHO DP12 cell line (ATCC<sup>®</sup> CRL-1445<sup>™</sup>) was adapted to suspension and grown in chemically defined TC-42 medium (Xell AG, Germany). Media were supplemented with 4 mM L-glutamine (L-Gln) and 200 nM methotrexate. Precultures were scaled up in shaking flasks (Corning, USA) at 37 °C and 150 rpm (50 mm displacement) and under 5 % CO<sub>2</sub> with initial cell densities of  $0.5 \times 10^6$  cells mL<sup>-1</sup> in a humidified incubator (Infors HT, Switzerland).

Bioreactor cultivations in batch mode were performed in a 4-fold DASGIP parallel bioreactor system DS1500ODSS (Eppendorf, Germany) with a starting volume of 1.2 L supplemented with 20 mM non-labeled [U- $^{12}\text{C}_6$ ] D-glucose (D-Glc) and an initial cell density of  $0.4 \times 10^6$  cells mL<sup>-1</sup>. The temperature was set to 37 °C, and the pH was maintained at 7.1 with 1 M Na<sub>2</sub>CO<sub>3</sub> and CO<sub>2</sub> gassing, which was monitored using a conventional pH probe (Mettler-Toledo, USA). The agitation speed was fixed at 150 rpm, and dissolved oxygen (DO) was controlled at 40 % using an amperometric electrode (Mettler-Toledo, USA). After 48 h, effector studies (EFF) were performed as biological duplicates (n = 2) by the addition of 250 μM MTA. Two reactors (n = 2) served as a reference (REF), and an equal volume of sterilized water was added to mimic dilution effects. After 60 h, isotopic tracer studies were performed through addition of

<sup>13</sup>C-labeled D-Glc, resulting in an extracellular ratio of 25 % [U-<sup>12</sup>C]-, 30 % [1-<sup>13</sup>C<sub>1</sub>]-, and 45 % [U-<sup>13</sup>C]-D-Glc in all reactors.

### **Quantification of viable cell density and extracellular metabolites**

Viable cell density (VCD) and viability were determined using an automated cell counting system (Cedex XS, Roche Innovatis, Germany) using trypan blue staining. Extracellular concentrations of D-Glc and L-lactate (L-Lac) were monitored using an amperometric biosensor system (LaboTRACE, Trace Analytics, Germany). Extracellular antibody concentrations (anti-IL-8 IgG1) were determined using an enzyme-linked immunosorbent assay (ELISA), as described previously [28].

Extracellular amino acid concentrations were measured using an Agilent 1200 HPLC system based on a bicratic reversed phase liquid chromatography (RPLC) method (Agilent Zorbax Eclipse Plus C18 column 250 × 4.6 mm, 5 μm) equipped with an Agilent Zorbax Eclipse Plus C18 guard column 12.5 × 4.6 mm, 5 μm) with automated pre-column derivatization and fluorometric detection [281]. We performed absolute quantification using a standard-based external calibration and adapted sample dilutions (1 to 8) with γ-aminobutyric acid (GABA) as an internal standard.

### **Fast filtration sampling and extraction for metabolomics**

Samples for subcellular metabolome analyses were collected at 48, 60, 61, 72, 84, 108, 132, and 168 h of cultivation time in technical duplicates from each reactor, according to a modified differential fast filtration protocol [298,360]. Filtered and quenched cells ( $3 \times 10^7$  cells per sample) were extracted directly (whole cell) or after selective permeabilization with digitonin (subcellular fractions), following addition of 5 mL ice-cold 70 % (v/v) methanol (MeOH) to the filters. Additionally, we used L-norvaline (L-Nva) and 2-dehydro-3-deoxy-D-gluconate 6-phosphate (KDPG) as internal standards to monitor the stability of the filtration, extraction, and measurement. Filters with captured cells were incubated in sample cups at -20 °C for 90 min, and the extraction solutions were subsequently separated using a vacuum pump (MZ 2, Vacuubrand, Germany). The filters and sample cups were rinsed with 2 mL of ice-cold 50 %

(v/v) MeOH, and the collected extraction solutions were mixed with 500  $\mu$ L of ice-cold chloroform and vortexed for 20 s. The emulsion was centrifuged at  $3200 \times g$  for 11 min at 4 °C (Megafuge 1.0, Heraeus, Germany). The upper aqueous phase was aliquoted into microcentrifuge tubes (4  $\times$  1 mL), evaporated for 95 min at < 20 °C (RVC 2.33 IR, Christ), and stored at -70 °C. During the entire process, the weights of the sample cups, filters, and microcentrifuge tubes were tracked to calculate the final extraction volumes.

### **Subcellular metabolomics by LC-MS/MS and HPLC-UV**

Subcellular adenosine monophosphate (AMP), adenosine diphosphate (ADP), and adenosine triphosphate (ATP) concentrations in metabolic extracts were determined using an Agilent 1200 HPLC system based on a bicratic ion-pair RPLC method (Hypersil™ BDS C18 column 15 cm  $\times$  4.6 mm, 3  $\mu$ m equipped with a Hypersil™ BDS C18 guard column 10  $\times$  4 mm, 5  $\mu$ m) and UV light (diode array detector) detection without derivatization [284]. We performed absolute quantification using a standard-based external calibration and selected spikes of reference standard mixes to evaluate the influence of the sample matrices.

Subcellular metabolome studies were performed using an Agilent 1200 HPLC system coupled with an Agilent 6410B triple quadrupole mass spectrometer (MS-QQQ) with an electrospray ion source (ESI). System control, acquisition, and analysis of data were performed using the commercial Mass Hunter B.06.00 software. Endogenous metabolites were separated under alkaline mobile phase conditions (pH 9.2) using bicratic hydrophilic interaction chromatography (HILIC), according to a previously described method [282] with modifications. GABA and  $\alpha$ -aminoisobutyric acid (AIBA) were previously added (50  $\mu$ M) as internal standards and considered for monitoring instrumental fluctuations. Targeted <sup>13</sup>C tracer analysis of isotopically labeled metabolite pools was performed in selected ion monitoring (SIM) mode using pre-optimized precursor ion transitions (0.3 u) with adapted MS parameters and ESI conditions [283]. Subcellular metabolite pools were absolutely quantified through a three-fold addition of defined amounts of non-labeled reference standards (internal calibration). Applied multicomponent standard mixtures were adjusted according to the linear dynamic range of the targeted metabolites and previously estimated concentration levels [361].

$^{13}\text{C}$  mass isotopomer detection of highly reactive  $\alpha$ -keto acid pools ( $\alpha\text{KG}$ , Pyr, Gxy) was performed using a previously established LC-MS protocol [298] using the abovementioned platform. Previously derivatized (phenylhydrazine) metabolite isotopologue pools [362] using  $\alpha$ -ketovaleric acid ( $\alpha\text{KV}$ ) were separated under acidic conditions (pH 3) using an RPLC method and were detected in SIM mode with pre-optimized settings. Determination of absolute pool concentrations was performed analogous to the abovementioned strategy.

### **Isotopic-non-stationary $^{13}\text{C}$ metabolic flux analysis**

For CHO cells, previous studies already outlined the advantages of using isotopically non-stationary  $^{13}\text{C}$  MFA for intracellular flux estimation [190,298,356]. Fluxes were estimated through analyzing the time series of isotopically transient  $^{13}\text{C}$  labeling profiles in compartment-specific metabolite pools using MATLAB version 2018a (The MathWorks, Inc., Natick, Massachusetts, USA).

### ***Compartment-specific metabolic model***

The metabolic network model consisted of two compartments: the cytosol and the mitochondrion, each comprising a stoichiometric and a carbon atom transition model with 36 metabolites and 62 metabolic reactions (**Table 7**). A cell density of  $122 \text{ pg cell}^{-1}$  was assumed. Several sink reactions for amino acids and central carbon metabolites were considered to mimic anabolic demands for the *de novo* synthesis of carbohydrates, proteins, nucleic acids, and lipids, according to Sheikh et al. [288].

***Growth, nutrient uptake and product formation rates***

The cell-specific growth rate was estimated using the weighted linear regression of VCDs with related standard deviations based on Equation [1].

$$\frac{dc_X}{dt} = \mu c_X \quad [1]$$

By analogy, cell-specific nutrient uptake and product formation rates were calculated:

$$\frac{dc_i}{dt} = q_i c_X \quad [2]$$

Linear regressions were performed in MATLAB and Curve Fitting Toolbox Release 2018a (The MathWorks, Inc., Natick, Massachusetts, USA).

***Metabolite and isotopomer balancing***

The balancing of metabolite  $i$  is described in Equation [3], assuming a (pseudo) steady state for the observation window:

$$\frac{dc_i}{dt} = N \cdot v, \quad [3]$$

where  $\mathbf{c}_i$  is the concentration vector containing all intracellular metabolites;  $N$  is the metabolic network stoichiometry matrix, containing the number of  $i$  metabolites and  $j$  reactions; and  $\mathbf{v}$  is the vector containing all fluxes.

Bidirectional fluxes were defined for each of the reversible reactions according to Schaub et al. [363] and Maier et al. [364], as described by Equation [4].

$$\begin{aligned} \bar{v}_j &= \beta_j v_j^{net} \\ \hat{v}_j &= \bar{v}_j - v_j^{net} \end{aligned} \quad [4]$$

where  $\beta_j$  is the reversibility factor of reaction  $j$  ( $\beta_j \geq 1$ ).



To model transient  $^{13}\text{C}$  enrichments, the isotopomers of each metabolite  $i$  were balanced by Equation [5].

$$\frac{d(\mathbf{C}_i \mathbf{l}_i)}{dt} = \sum_{j=1}^N \left[ \alpha \left( \begin{array}{c} 0 \\ \otimes \left( \sum_{m=1}^{v_{ij}} \mathbf{IMM}_{k \rightarrow m} \right) \mathbf{l}_k \end{array} \right) r_j + (1 - \alpha)(v_{ij} r_j \mathbf{l}_i) \right] \quad [5]$$

with

$$\alpha = \begin{cases} 1, & \text{if } v_{ij} > 0 \\ 0, & \text{else} \end{cases}$$

where  $\mathbf{c}_i$ ,  $\mathbf{l}_i$ , and  $\mathbf{l}_k$  denote vectors of intracellular concentrations of metabolites  $i$  and isotopomer distribution vectors, containing molar ratios that correspond to the fractional amounts of the individual isotopologues for metabolites  $i$  and  $k$ , respectively. The isotopomer mapping matrix  $\mathbf{IMM}_{k \rightarrow m}$  describes the isotopomer transition from reactant  $k$  to product  $m$  [365].  $v_{ij}$  equals the stoichiometric coefficient of metabolite  $i$  in reaction  $j$ , whose molar rate is  $r_j$ . The operator  $\otimes$  denotes element-by-element vector multiplication.

Furthermore, isotopomer balancing was considered for extracellular metabolites that were heavily exchanged with intracellular pools (L-Lac, L-Ala, L-Glu, and L-Asp), according to Nicolae et al. [366]. Equation [6]:

$$\frac{d(\mathbf{I}_{i,ex})}{dt} = \frac{1}{\mathbf{C}_{i,ex}} \left[ \overline{\mathbf{C}}_X \left( \overrightarrow{\mathbf{q}}_{i,ex} \cdot \mathbf{I}_{i,in} - \overleftarrow{\mathbf{q}}_{i,ex} \cdot \mathbf{I}_{i,ex} \right) - \frac{d\mathbf{C}_{i,ex}}{dt} \mathbf{I}_{i,ex} \right]$$

with

$$\begin{aligned} \overrightarrow{\mathbf{q}}_{i,ex} &= \beta_i \cdot \mathbf{q}_{i,ex}^{net} \\ \overleftarrow{\mathbf{q}}_{i,ex} &= \overrightarrow{\mathbf{q}}_{i,ex} - \mathbf{q}_{i,ex}^{net} \end{aligned} \quad [6]$$

### **Simulation of $^{13}\text{C}$ labeling experiment**

The total set of ordinary differential equations (ODEs), comprising 972 equations, were solved using MATLAB 2018a based on *ode15s* solver (The MathWorks, Inc., Natick, Massachusetts, USA).

**Parameter estimation and uncertainty**

Simulated isotopologue distributions,  $\mathbf{x}$ , were obtained through minimizing the weighted least square sum, subtracting the measured isotopologue values,  $\mathbf{x}_m$ , as indicated in Equation [7]. In total, ODEs contain 43 parameters: 8 intracellular fluxes and 35 reversibility constants. Parameter fitting was performed using MATLAB 2018a with *fmincon* and *GlobalSearch* (The MathWorks, Inc., Natick, Massachusetts, USA) and was repeated at least 100 times starting with randomized initiation settings.

$$\min_{\mathbf{p}} \Phi = \sum \frac{(\mathbf{x} - \mathbf{x}_m)^2}{\sigma_x^2}, \quad [7]$$

where  $\mathbf{x}$  denotes vectors for the isotopologue fractions.  $\sigma$  denotes the standard deviation of each measured value.

The goodness of fit of the obtained flux distribution was assessed using the chi-square test to determine whether the model accurately reflects the *in vivo* data. Statistical acceptance was assigned on the 95 % confidence level ( $\alpha = 0.05$ ). Additional details are presented in 6.3 Supplementary Material: Manuscript 4.

The measured extracellular rates,  $\mathbf{q}_m$ , and estimated intracellular rates (optimized parameter,  $\mathbf{p}$ ) were used to constrain the flux distribution,  $\mathbf{v}$ , as described in Equation [8].

$$\mathbf{v} = \begin{pmatrix} \mathbf{S} \\ \mathbf{M} \end{pmatrix}^{-1} \begin{pmatrix} 0 \\ [\mathbf{q}_m \quad \mathbf{p}] \end{pmatrix} \quad [8]$$

where  $\mathbf{M}$  is the measurement matrix containing all stoichiometric coefficients of  $\mathbf{q}_m$  (measured rates [pmol cell<sup>-1</sup> h<sup>-1</sup>]) and  $\mathbf{p}$  (estimated parameter using mass-isotopomer data; as intracellular fluxes [pmol cell<sup>-1</sup> h<sup>-1</sup>]).

Parameter uncertainty was assessed using the non-linear algorithm from Antoniewicz et al. [367]. The method assumes that the sum of squared residual is  $\chi^2$  distributed. Thus, the uncertainty of parameter  $\theta$  was determined when optimizing the said systems with one degree of freedom ( $\chi^2$  distributed).

## Results

### (I) MTA effector and $^{13}\text{C}$ tracer studies in CHO cells

Previous MTA supplementation studies by Verhagen et al. [313,359] revealed the phenotype of significant growth reduction and improved CSP after MTA addition. Considering that cells undergo an interim phase of dynamic adaptation, we performed  $^{13}\text{C}$  labeling tests to investigate cellular metabolism following MTA addition and dynamic adaptation. Accordingly,  $^{13}\text{C}$ -isotope D-Glc was added during phase (C) (> 60 h), following the dynamic adaptation period (B) (48-60 h), and the growth phase (A) (0-48 h). Notably, the latter was the same in all replicates. (B) implied the addition of 250  $\mu\text{M}$  MTA and sterilized water in duplicated MTA and REF runs, respectively. The extracellular glucose composition of 25 % [U- $^{12}\text{C}$ ]-, 30 % [1- $^{13}\text{C}_1$ ]-, and 45 % [U- $^{13}\text{C}$ ]-D-Glc was equal in all quadruplicates during phase (C). The labeled substrate composition enabled quantification of flux distribution in the central metabolism comprising the Embden-Meyerhof-Parnas pathway (EMP), pentose-phosphate pathway (PPP), citric acid cycle (CAC), anaplerotic reactions, and amino acids. In particular, the [1- $^{13}\text{C}_1$ ]-D-Glc fraction significantly improved the PPP flux resolution [368].

Daily and 12 h samplings were performed for subcellular metabolomics with technical duplicates from each bioreactor, beginning with  $t_0$  immediately after labeling was initiated. Sample processing enabled the assignment of metabolite pools to cytosolic and mitochondrial compartments. Cytosolic depletion and mitochondrial integrity were evaluated using glucose 6-phosphate (G6P), fructose 6-phosphate (F6P), and *cis*-aconitate (*cisAco*) concentrations (Table 5).

### (II) MTA reduced cellular growth rate while increasing cell volume

During phase A (0-48 h) cells grew under ample nutrient supply with a maximal specific growth rate of  $0.705 \pm 0.021 \text{ d}^{-1}$  while consuming D-Glc, L-Asn, L-Gln, and other essential amino acids (Figure 31). Metabolic overflow products, such as L-Lac, L-alanine (L-Ala), L-asparagine (L-Asp), and L-glutamate (L-Glu) were excreted. After MTA addition during phase B, cellular growth slowed to  $0.322 \pm 0.003 \text{ d}^{-1}$  and recovered after > 60 h. During the first part of phase C, C.I

(60-108 h), glucose was steadily consumed. By analogy, MTA was taken up by  $0.177 \pm 0.037 \text{ pmol cell}^{-1} \text{ d}^{-1}$  before depletion (approximately 96 h). In accordance, the cytosolic and mitochondrial MTA levels rose, exceeding REF pool sizes by 170 and 800 times, respectively. Coincidentally, the supplemented cells showed increased L-Ala and L-Glu secretion compared to the initial phase A. D-Glc, L-Asn, and L-Gln were still consumed, whereas L-Lac was secreted. In contrast, reference cultures (without MTA addition) grew with an unaffected high growth rate ( $0.677 \pm 0.031 \text{ d}^{-1}$ ) (**Figure 31**). After 108 h, L-Asn was depleted in all cultures. Similarly, L-Gln depletion occurred in REF, whereas low levels were maintained in MTA-supplemented cells. Accordingly, phase C was divided into C.I (60-108 h) with sufficient L-Asn and L-Gln supply, phase C.II with nitrogen limitation (108-144 h), and C. III as strict starvation ( $> 144 \text{ h}$ ). In REF, the growth reduced to  $0.258 \pm 0.039 \text{ d}^{-1}$ , reflecting L-Gln and L-Asn limitation during C.II. Similar growth trends were observed during phase C.II for MTA-treated cultures, with a growth rate of  $0.203 \pm 0.012 \text{ d}^{-1}$  (**Figure 30**). Both cultures experienced strict starvation during C.III (144-168 h) with maximum VCDs of  $(110.55 \pm 9.82) \times 10^5 \text{ cells mL}^{-1}$  for REF and  $(69.92 \pm 6.77) \times 10^5$  for MTA-supplemented cells (**Figure 30**).

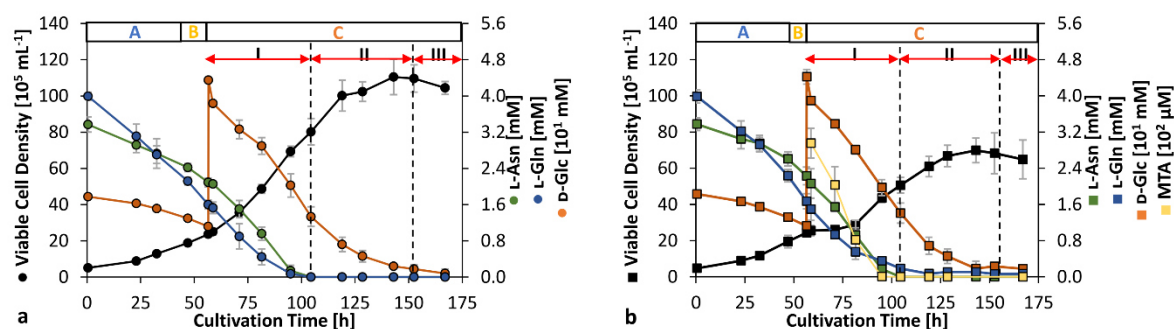


**Figure 30.** a: Time course of viable cell density [ $\times 10^5 \text{ cells mL}^{-1}$ ] ( $\bullet$ ), D-glucose (D-Glc) [ $\times 10 \text{ mM}$ ] ( $\bullet$ ), L-asparagine (L-Asn) [mM] ( $\bullet$ ) and L-glutamine (L-Gln) [mM] ( $\bullet$ ) of the reference (REF). b: Time course of viable cell density [ $\times 10^5 \text{ cells mL}^{-1}$ ] ( $\blacksquare$ ), D-glucose (D-Glc) [ $\times 10 \text{ mM}$ ] ( $\blacksquare$ ), L-asparagine (L-Asn) [mM] ( $\blacksquare$ ), L-glutamine (L-Gln) [mM] ( $\blacksquare$ ) and 5'-deoxy-5'-methylthioadenosine (MTA) [ $\times 10^2 \text{ }\mu\text{M}$ ] ( $\blacksquare$ ) in MTA-supplemented cells. MTA was added after phase A (0-48 h), at a final MTA concentration of 250  $\mu\text{M}$ . Glucose labeling was initiated after phase B (48-60 h). Phase C (60-168 h) is divided into I: overflow; II: N-Limitation; and III: starvation. Error bars indicate the standard deviations for biological duplicates and technical replicates.

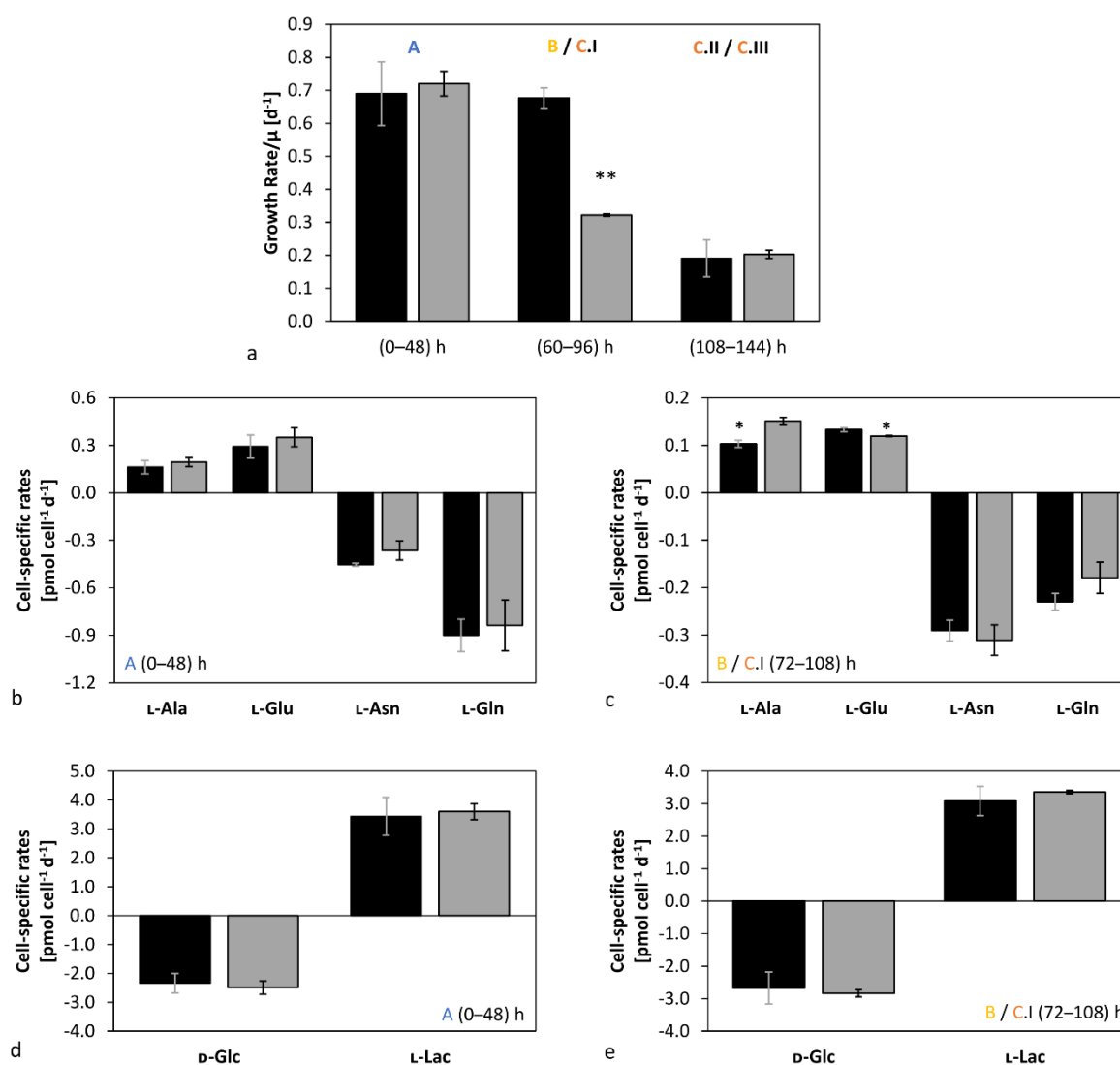
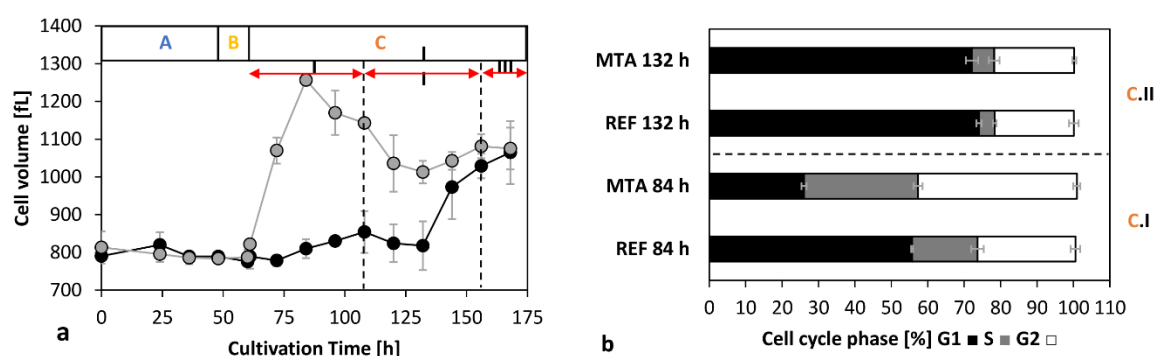


**Figure 31.** a: Growth rate per day [d<sup>-1</sup>] for the different cultivation phases. b: Cell-specific uptake/secretion rates [pmol cell<sup>-1</sup> d<sup>-1</sup>] for L-Gln, L-Asn, L-Glu, and L-Ala in overflow metabolism before MTA addition (A). c: Cell-specific uptake/secretion rates [pmol cell<sup>-1</sup> d<sup>-1</sup>] for L-Gln, L-Asn, L-Glu, and L-Ala in overflow metabolism after MTA addition (B / C.I). d: Cell-specific uptake/secretion rates [pmol cell<sup>-1</sup> d<sup>-1</sup>] for D-Glc and L-Lac in overflow metabolism before MTA addition (A). e: Cell-specific uptake/secretion rates [pmol cell<sup>-1</sup> d<sup>-1</sup>] for D-Glc and L-Lac in overflow metabolism after MTA addition (B / C.I). MTA-supplemented cells (grey) compared to REF (black). MTA was added after phase A (0-48 h) at a final MTA concentration of 250  $\mu$ M. Glucose labeling was initiated after phase B (48-60 h). Phase C (60-168 h) is divided into I: overflow; II: N-limitation; and III: starvation. Error bars indicate the standard deviations for biological duplicates and technical replicates. Significance was tested using one-sided t-test. \*\* p < 0.01 \* p < 0.05.

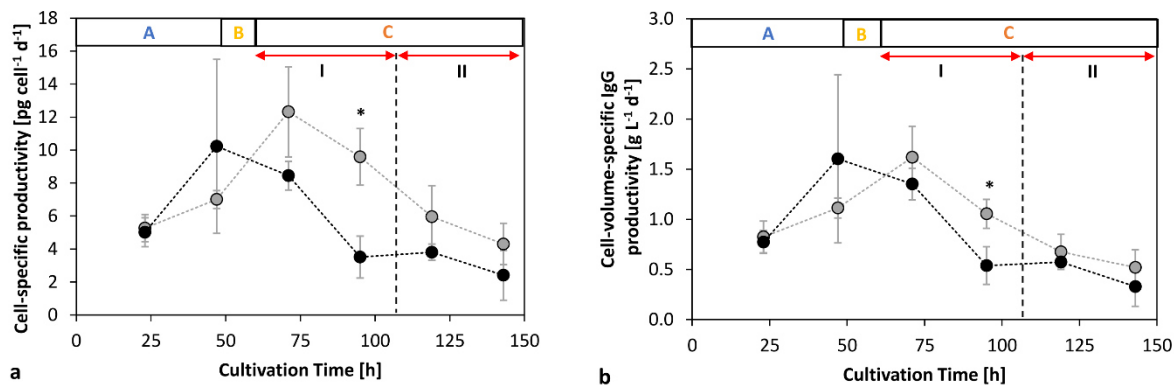
In addition to the diminished growth rate, MTA addition led to temporary increases in cell volumes. On the basis of the measured cell diameters, the volume of supplemented cells

increased by 55 % (84 h) and shrank by 31 % during phase C.II. In contrast, the cell size of the reference cultures was stable until the end of the cultivation phase C.II. Upon initiating carbon starvation (phase C.III), the cell volumes rose, and the differences leveled out (**Figure 32 a**).

The increase in cellular volumes coincided with a change in the cell-cycle distribution after MTA addition (**Figure 32 b**). At 84 h, the supplemented cells showed a lower G1-fraction (MTA:  $26.02 \pm 0.70$  %; REF:  $55.70 \pm 0.26$  %) and higher S-fraction (MTA:  $31.32 \pm 1.23$  %; REF:  $17.98 \pm 1.71$  %) and G2-fraction (MTA:  $43.60 \pm 0.95$  %; REF:  $26.88 \pm 1.26$  %). Cells subjected to nitrogen limitation in phase C.II (132 h) exhibited equalization of the cell-cycle phase distribution compared to the reference cultures.



**Figure 32.** a: Time course of the cell volume [fL] of MTA-supplemented cells (MTA: grey) and reference cells (REF: black) in the different phases. Cell volume was calculated with the assumption of a spherical cell shape. b: Cell-cycle phase distribution [%] of MTA-supplemented cells (MTA) and reference cells (REF) at 84 h (I: Overflow) and 132 h (II: N-limitation). MTA was added after phase A (0-48 h) at a final MTA concentration of  $250 \mu\text{M}$ . Glucose labeling was initiated after phase B (48-60 h). Phase C (60-168 h) is divided into I: overflow; II: N-limitation; and III: starvation. Error bars indicate standard deviations for biological duplicates and technical replicates.

**(III) MTA addition enhanced cell-specific productivity and ATP availability**

**Figure 33.** Cell-specific IgG productivity (CSP) [ $\text{pg cell}^{-1} \text{d}^{-1}$ ] and cell-volume-specific IgG productivity (CVP) [ $\text{g L}^{-1} \text{d}^{-1}$ ] regarding the different cultivation phases. a: Differential CSPs over cultivation time. b: Differential CVPs over cultivation time. MTA-supplemented cells (grey) compared to REF cells (black). MTA was added after phase A (0-48 h) at a final MTA concentration of  $250 \mu\text{M}$ . Glucose labeling was initiated after phase B (48-60 h). Phase C (60-168 h) is divided into I: overflow; II: N-limitation; and III: starvation. Error bars indicate standard deviations for biological duplicates and technical replicates. Significance was tested using one-sided t-test. \*  $p < 0.05$ .

**Figure 33 a** depicts cell-specific (CSP) and cell-volume-specific (CVP) IgG productivities during the exponential growth phase A with abundant nutrient supply. The CSP exhibited no significant difference before MTA supplementation (e.g., differential CSP at 24 h): REF,  $5.01 \pm 0.88 \text{ pg cell}^{-1} \text{d}^{-1}$ ; MTA,  $5.26 \pm 0.83 \text{ pg cell}^{-1} \text{d}^{-1}$ . Similarly, the CVP was not significantly different before supplementation (**Figure 33 b**). Interestingly, the CSP following MTA supplementation was 170 % higher ( $9.59 \pm 1.72 \text{ pg cell}^{-1} \text{d}^{-1}$ ) than that in REF ( $3.51 \pm 1.27 \text{ pg cell}^{-1} \text{d}^{-1}$ ) during C.I after transient phase B. The subsequent phases C.II and C.III show reduced CSPs for all cultures, which indicates the dominating impact of limited nutrient supply in accordance with observations of Junghans et al. [298] (**Table 6**). The CVPs only increased by roughly 95 % (MTA:  $1.05 \pm 0.14 \text{ g L}^{-1}$ ; REF:  $0.54 \pm 0.19 \text{ g L}^{-1}$ ), whereas the CSPs rose by 170 %. Thus, CSP improvements mirror the combinatorial effects of elevated cell volumes and metabolic changes. The latter will be investigated through  $^{13}\text{C}$  metabolic flux analysis.

The cellular energy status was studied based on the basis of the ATP concentrations in the cytosolic and mitochondrial compartments (**Figure 34**).

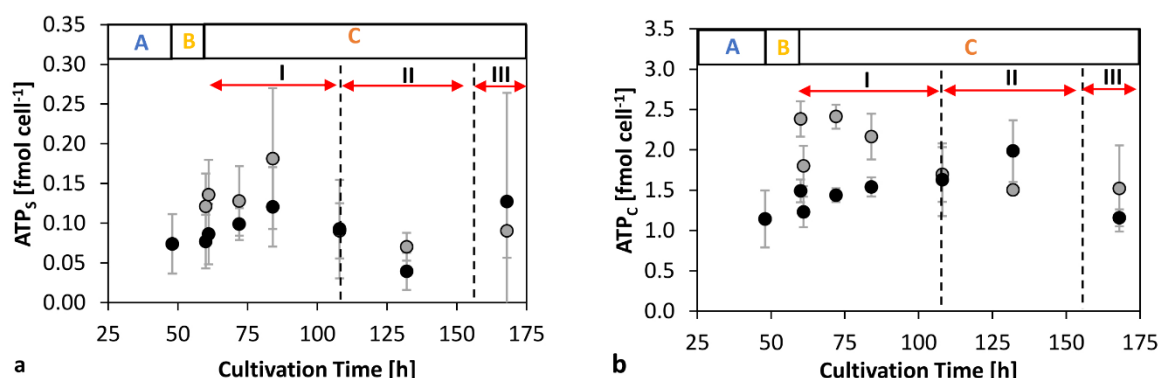


**Figure 34.** a: Time course of the ATP concentrations in the subcellular (mitochondrial, index S) compartment of MTA-supplemented cells (MTA: grey) and reference (REF: black). b: Time course of the ATP concentrations in the cytosolic compartment (index C) of MTA-supplemented cells (MTA: grey) and reference cells (REF: black). MTA was added after phase A (0-48 h) at a final MTA concentration of 250  $\mu$ M. Glucose labeling was initiated after phase B (48-60 h). Phase C (60-168 h) is divided into I: overflow; II: N-limitation; and III: starvation. Error bars represent the standard deviations for biological duplicates and technical replicates.

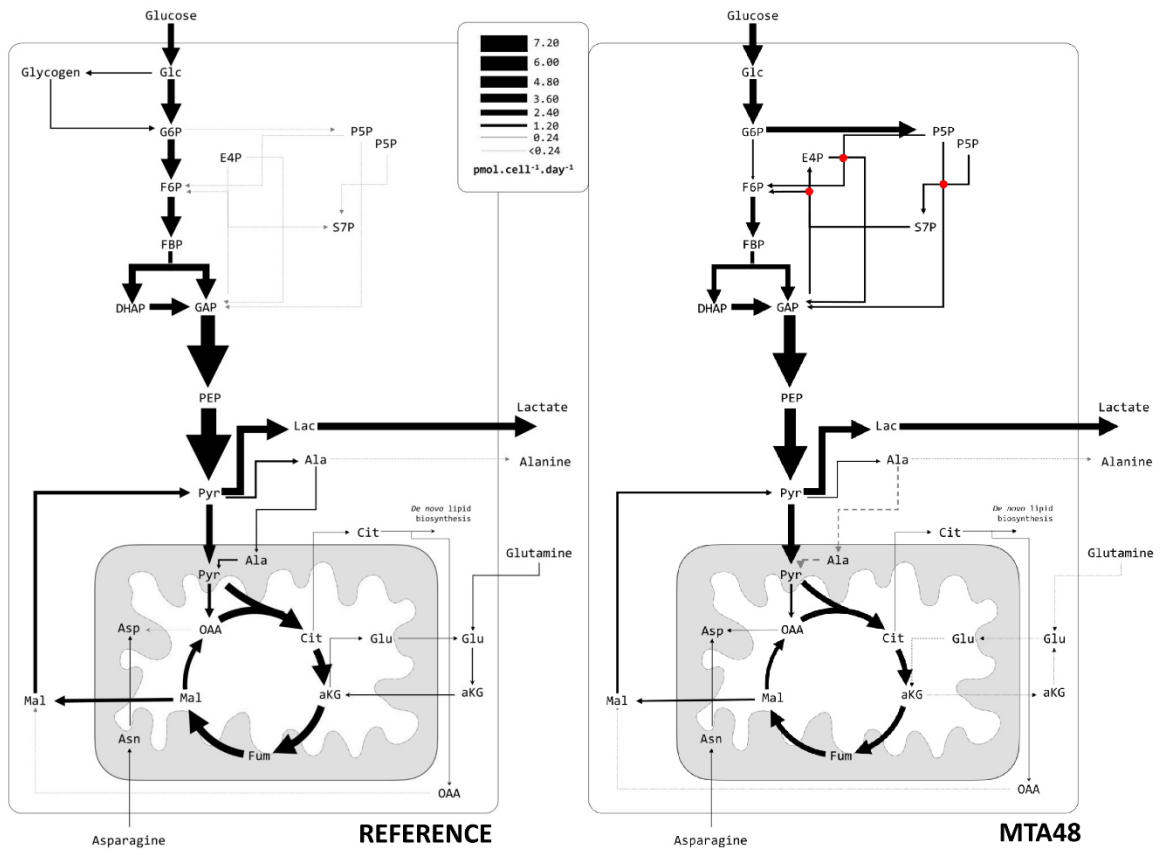
Considering the error bars in **Figure 34 a**, MTA addition did not change the ATP levels in the mitochondria but increased the ATP content in the cytosol. The latter peaked 12 h after MTA addition before approaching the corresponding levels in REF at the end of C.I (**Figure 34 b**). Notably, the cytosolic ATP trend is in accordance with the CSP profile (**Figure 33 a**).

#### (IV) MTA-treated cells detour carbon into PPP

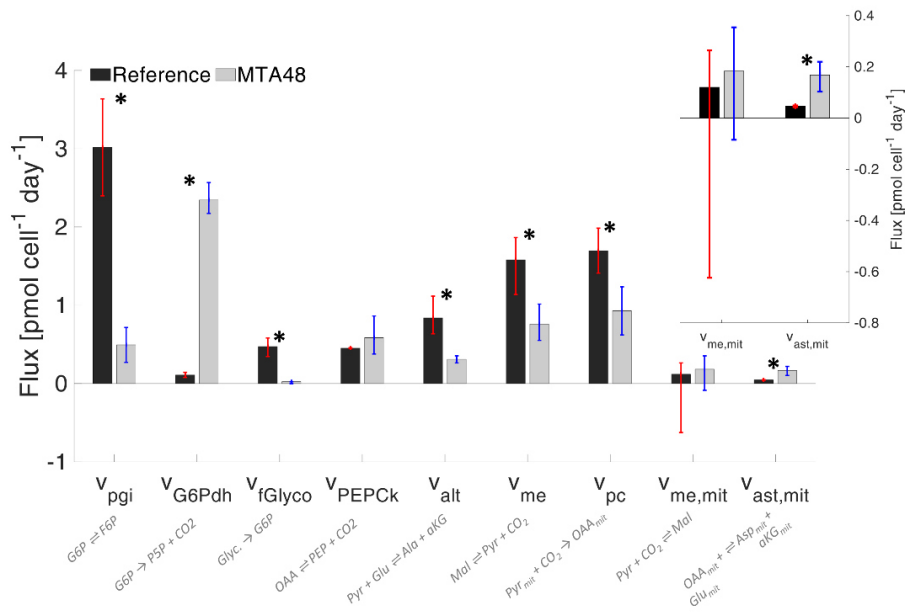
Isotopically transient  $^{13}\text{C}$  MFA was performed to elucidate the impact of MTA addition on central metabolism under ample nutrient supply coinciding with the highest CSPs observed in phase C.I.

**Figure 35 a** depicts the cytosolic and mitochondrial carbon flux distributions of MTA-supplemented and reference cultures during the exponential growth in phase C.I.

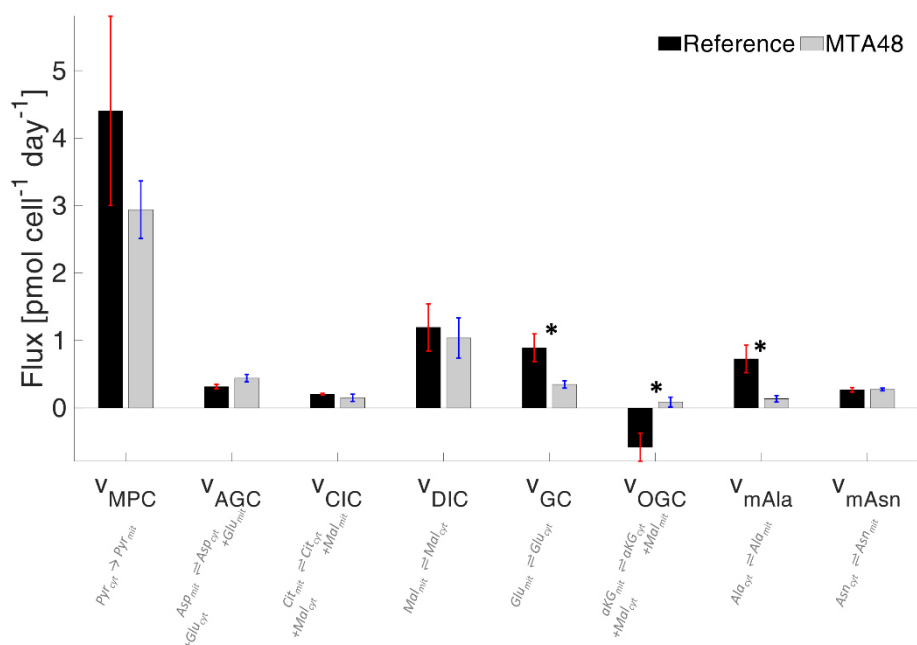




(a)



(b)



(c)

**Figure 35.** a. Metabolic flux distribution of the reference and MTA-supplemented CHO-DP12 cells. Arrows indicate flux direction, and the thickness of the arrows indicate strength in pmol cell<sup>-1</sup> day<sup>-1</sup>; b. Comparison of key fluxes using abbreviations as follows: phosphoglucose-isomerase (pgi), G6P dehydrogenase (G6Pdh), endogenous glycogen exchange (fGlyco), PEP carboxykinase (PEPCK), alanine amino transferase (alt), malic enzyme (me), pyruvate carboxylase (pc), and aspartate amino transferase (ast); c. Comparison of mitochondrial carrier activities: pyruvate/H<sup>+</sup> symporter (MPC), aspartate/glutamate antiporter (AGC), citrate/malate antiporter (CIC), dicarboxylic acid carrier (DIC), glutamate carrier (GC), aKG/malate antiporter (OGC), putative alanine carrier (mAla), and putative asparagine carrier (mAsn). \* indicates  $p < 0.05$ .

Focusing on the upper glycolysis, the CHO-DP12 REF cultures (**Figure 35 a**) showed a metabolic phenotype comparable to that reported by Junghans et al. [298]. Under abundant nutrient supply, approximately 18 % of total D-Glc was continuously exchanged with non-labeled endogenous carbon storage ( $v_{fGlyco}$ :  $0.474 \pm 0.109$  pmol cell<sup>-1</sup> d<sup>-1</sup>). At the same time, a remarkably low fraction of consumed D-Glc (about 4 %) was channeled into the oxidative PPP ( $v_{G6Pdh}$ :  $0.110 \pm 0.032$  pmol cell<sup>-1</sup> d<sup>-1</sup>), which corresponds to the earlier findings of Ahn and Antoniewicz [356] and Templeton et al. [190].

In contrast, MTA-supplemented cells exhibited a considerably different flux distribution (**Figure 35 b**). The labeling kinetics of G6P indicate significantly reduced carbon exchange with

endogenous carbon storage compounds such as glycogen ( $v_{fGlyco}$ :  $0.024 \pm 0.024$  pmol cell<sup>-1</sup> d<sup>-1</sup>). Instead, approximately 83 % of consumed glucose was diverted into the oxidative PPP ( $v_{G6Pdh}$ :  $2.346 \pm 0.171$  pmol cell<sup>-1</sup> d<sup>-1</sup>). This corresponds to a remarkable rise of 21 fold in the G6Pdh flux in the MTA-supplemented cells compared to that in the G6Pdh flux in the reference culture.

The PPP influx of MTA-supplemented culture exceeded the anabolic ribose 5-phosphate (R5P) requirements, i.e., precursor needs for nucleotide biosynthesis, by a factor of 166. Consequently, approximately 81 % of the carbon re-entered glycolysis via fructose 6-phosphate (F6P) and glyceraldehyde 3-phosphate (GAP). Interestingly, lower glycolysis (represented by GAP dehydrogenase) showed statistically similar fluxes in MTA-supplemented ( $v_{GAPdh}$ :  $4.867 \pm 0.289$  pmol cell<sup>-1</sup> d<sup>-1</sup>) and REF culture cells ( $v_{GAPdh}$ :  $6.176 \pm 1.237$  pmol cell<sup>-1</sup> d<sup>-1</sup>).

#### **(V) MTA supplementation reduced the net malate export from mitochondria**

The compartment-specific <sup>13</sup>C MFA revealed the *in vivo* activity of the mitochondrial pyruvate carrier, MPC, and the other solute carriers belonging to the family 2A (SLC25A; **Figure 37**). In the REF culture, the highest mitochondrial carrier activity was observed for the MPC ( $v_{MPC}$ :  $4.404 \pm 1.405$  pmol cell<sup>-1</sup> d<sup>-1</sup>), supporting the observations of Junghans et al. [298]. The dicarboxylic acid carrier (DIC) and the glutamate carrier (GC) showed the second strongest rates of 0.89 to 1.19 pmol cell<sup>-1</sup> d<sup>-1</sup>.

Shuttling activities for malate well described the cellular status [298]. Previous analysis of malate shuttling revealed that DIC is the key malate carrier in CHO cells. With approximately 1 pmol cell<sup>-1</sup> day<sup>-1</sup>, malate export from the mitochondria via DIC was approximately 6-fold higher than malate export via CIC. OGC further supports the export of mitochondrial malate by importing cytosolic  $\alpha$ KG. In total, net malate export occurs from the mitochondria to the cytosol at  $1.573 \pm 0.407$  pmol cell<sup>-1</sup> d<sup>-1</sup>, which implies malate-mediated NADPH production in the cytosol [298].

MTA supplementation fundamentally altered the shuttling activities of GC, OGC, and putative alanine carrier (mAla). Remarkably, OGC transport was reverted, resulting in the export of  $\alpha$ KG to the cytosol and import of malate into the mitochondria. Accordingly, the net malate export to the cytosol was reduced to  $0.800 \pm 0.311$  pmol cell<sup>-1</sup> d<sup>-1</sup> due to the MTA supplementation. Additionally, cells exposed to MTA exhibited a reduction in  $v_{GC}$  and  $v_{mAla}$  to  $0.348 \pm 0.055$  and  $0.135 \pm 0.048$  pmol cell<sup>-1</sup> d<sup>-1</sup>, respectively.

#### **(VI) Reprogramming of NADPH production strategies while maintaining a similar NADH supply**

NADPH is a vital cofactor and crucial redox partner in various cellular reactions, typically anabolic reactions [369]. In CHO-DP12, NADPH is produced via oxidative PPP and the cytosolic malic enzyme ( $me_{cyt}$ ). The latter requires sufficient malate shuttling activity from the mitochondria via the concerted activities of MPC, CIC, and DIC in the citrate-pyruvate shuttle systems. This study identified a relatively high cytosolic malic enzyme flux ( $v_{me_{cyt}}$ :  $1.580 \pm 0.284$  pmol cell<sup>-1</sup> d<sup>-1</sup>) in the REF culture, which is in accordance with Junghans et al. [298]. Notably, fluxes via  $me_{cyt}$  were entirely fueled by malate exported from the mitochondria.

In the MTA-supplemented cultures,  $me_{cyt}$  activity ( $0.761 \pm 0.209$  pmol cell<sup>-1</sup> d<sup>-1</sup>) was reduced by 43 %, mirroring the reduction of shuttling activities. Consequently, the NADPH supply fundamentally differed between the REF and MTA-treated cells (**Figure 36**). In the REF culture, NADPH supply via cytosolic malic enzyme ( $me_{cyt}$ ) comprises 88 % of the total production compared to 14 % in the culture treated with MTA. Despite severe reduction *in*  $me_{cyt}$  activity, the MTA-treated culture produced approximately 3-fold more NADPH than REF through amplification of the NADPH formation via PPP. Notably, PPP-mediated NADPH formation was approximately  $4.692 \pm 0.343$  pmol cell<sup>-1</sup> d<sup>-1</sup>, reflecting a 21-fold increase compared to REF. Regarding NADH supply, no statistically significant differences were observed between the REF and MTA-treated cells (**Figure 36**).

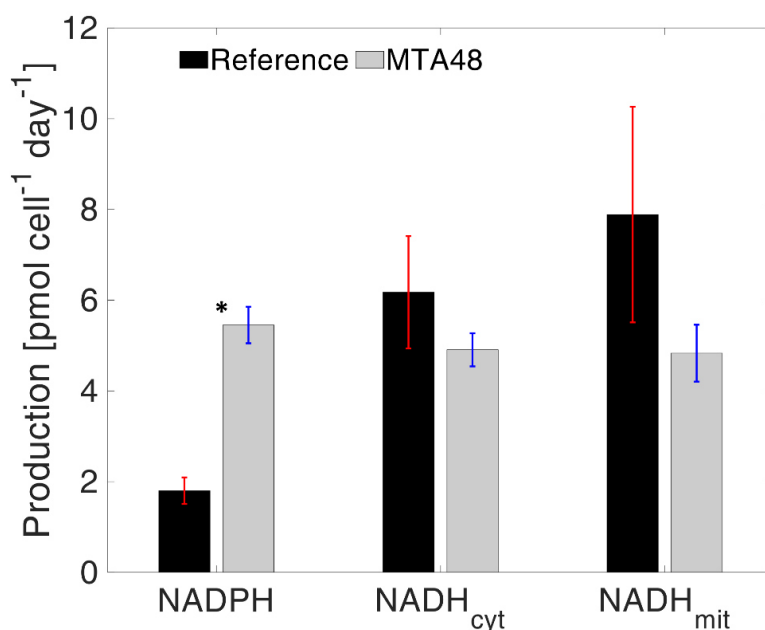


**Figure 36.** Comparison of NADPH, NADH<sub>cyt</sub>, and NADH<sub>mit</sub> production in reference culture and MTA-treated culture. \* indicates a significant difference ( $p < 0.05$ ).

### (VII) Glutamine and alanine metabolism

L-Gln uptake rate was reduced in the MTA-treated cells ( $0.156 \pm 0.027$  pmol cell<sup>-1</sup> day<sup>-1</sup>) compared to the REF culture ( $0.222 \pm 0.012$  pmol cell<sup>-1</sup> day<sup>-1</sup>). Nevertheless, L-Gln catabolic rates remained similar in both cultures (REF:  $0.168 \pm 0.012$  pmol cell<sup>-1</sup> day<sup>-1</sup>; MTA treated:  $0.136 \pm 0.028$  pmol cell<sup>-1</sup> day<sup>-1</sup>). In REF, L-Gln was taken up and initially catabolized in the cytosol via glutaminase (**Figure 35 a**). Next, the intermediate product (L-glutamate) was deaminated via cytosolic amino-transferases yielding  $\alpha$ KG, which fueled into the CAC via the Mal/ $\alpha$ KG symporter (OGC). This observation is consistent with the observations of Junghans et al. [298]. Interestingly, cultures treated with MTA showed a variation: cytosolic glutamate was imported directly into the mitochondria via AGC, and it did not require further cytosolic deamination to  $\alpha$ KG.

Cellular secretion of L-alanine (L-Ala) was significantly higher in the MTA-supplemented cells than in REF (**Figure 31**). In contrast, intracellular L-Ala formation mirrors cytosolic alanine-

aminotransferase ( $alt_{cyt}$ ) activities  $v_{alt_{cyt}}$ , which were lower in the MTA-treated cells ( $0.310 \pm 0.045 \text{ pmol cell}^{-1} \text{ day}^{-1}$ ) than in REF ( $0.840 \pm 0.204 \text{ pmol cell}^{-1} \text{ day}^{-1}$ ).

## Discussion

The addition of MTA and its boosting effect on the CSP in CHO-DP12 cells was studied by Verhagen et al. [313,359]. MTA plays an essential role in mammalian cell metabolism, especially in polyamine synthesis [58,227]. In this pathway, MTA serves as an intermediate decarboxylation product of SAM to produce spermidine and spermine. High MTA levels are anticipated to inhibit polyamine biosynthesis, finally inducing cell-cycle arrest [63]. Besides, MTA is known to impact gene expression patterns, including apoptosis, cell proliferation in hepatocytes, leukemia cells, fibroblasts, and lymphoma cells [49,60–62]. In summary, MTA serves as a multi-level regulatory compound that exerts genetic, epigenetic, and metabolic control.

The reduction in spermidine and spermine synthesis after MTA addition is known to induce S-phase arrest in CHO cells [229]. This study confirmed the cytostatic effect, as displayed in **Figure 30**. MTA addition significantly reduced the maximum VCD and cell-specific growth rate (**Figure 31 a**). Concomitantly, cellular volume increased (**Figure 32 a**), cell-cycle distribution changed (**Figure 32 b**), and CSP ( $q_{mAb}$ ) (**Figure 33** and **Table 6**) increased following MTA addition. Cellular fractions in the S- and G2-phases were temporarily increased 36 h after MTA addition, while the number of cells in G1-phase decreased (**Figure 32 b**). The increase in  $q_{mAb}$  (**Figure 33**) 48 h after MTA addition might be attributed to cell-cycle arrest, as previously reported by independent studies [25–28]. Notably, CSP raise is not limited to a distinct cell-cycle phase.

Moreover, increase in cell volumes [358,370] have been reported to enhance CSP. Although rising cell volumes were observed in our study (**Figure 32 a**), comparably low CVPs suggested that post-MTA CSP improvements were not caused by rising cell volumes alone (**Figure 33**). Indeed, the CVPs of MTA-treated cells remained relatively high until the end when the REF cells showed declining values (**Figure 33, Table 6**). However, fundamental reorganization of metabolism in arrested cells is supposed to be the key factor explaining rising CSPs [121].

Metabolic rearrangements were studied via  $^{13}\text{C}$  labeling analysis. Thus, the approach complements earlier studies by Verhagen et al. [313,359], which focused on the SAM/MTA interplay and transcriptional responses after MTA feeding. Particularly, compartment-specific flux analysis was applied according to a previously reported protocol [298] for determining the putative impact of NADPH supply. Moreover, compartment-specific metabolomics essentially enabled flux tracking inside cellular compartments to unravel the putative impact of trans-compartment shuttling activities. Both data are qualified as important information *per se*.

MTA addition apparently influences the energetic status of the cells, which is reflected by an increase in cytosolic ATP pools (**Figure 34**). The temporal rise in ATP levels likely inhibits phosphofructokinase (PFK) activity, considering the equally high ATP inhibition constants [371–373]. This metabolic inhibition may explain why fluxes through PFK are lower following MTA addition than in the absence of MTA addition in REF (**Figure 35**).

Moreover, Moreadith and Lehninger [374] showed that malic enzyme activity is inhibited by high ATP levels. Consequently, enhanced flux into the oxidative PPP is likely to reflect ATP-mediated metabolic inhibition of PFK and malic enzyme. The latter caused a reduction in NADPH formation, which was counterbalanced by an increase in PPP fluxes, ultimately achieving elevated NADPH production (**Figure 36**). The coincidence of metabolic rearrangement and cell-cycle arrest following MTA addition is consistent with the findings of Vizán et al. [375]. The authors additionally observed a relatively high oxidative PPP activity during the late G1- and S-phases, suggesting that more precursors for nucleotide biosynthesis are needed during the S-phase in the cell cycle.

In addition, compartment-specific flux analysis revealed that OGC flux was reversed in MTA-supplemented cultures compared to REF. Whereas OGC exported malate into the cytosol in REF, OGC imported cytosolic malate in MTA-treated cultures. Nevertheless, malate net export into the cytosol continued to be realized via DIC.  $v_{\text{DIC}}$  was comparable with that of REF; however, lack of OGC contribution reduced the net malate export into the cytosol following MTA addition. Consequently, cytosolic malate was adapted to the decrease in cytosolic malic

enzyme activity. Notably, the reversion of OGC reverted the flux of the counter ion  $\alpha$ KG. Specifically, instead of importing  $\alpha$ KG in the REF culture,  $\alpha$ KG was exported into the cytosol in the MTA-treated cultures.

In REF, L-Gln was deaminated via cytosolic glutaminase and glutamate dehydrogenase before importing  $\alpha$ KG into the mitochondria. Because OGC shuttling is reversed, the MTA-treated cells require an alternative pathway to fuel the L-Gln intermediate into CAC. Nevertheless, L-Gln was deaminated via cytosolic glutaminase. Next, L-Glu was imported into the mitochondrion via the amplified activities of the shuttle AGC. Subsequent deamination to  $\alpha$ KG occurred in the mitochondrion. Interestingly, the potential export of mitochondrial L-Glu via GC slowed down to ensure sufficient L-Glu supply inside the mitochondrion.

The compartment-specific  $^{13}\text{C}$  MFA additionally revealed that alanine amino-transferase ( $alt_{mit}$  and  $alt_{cyt}$ ) activities were reduced in the MTA-treated culture. As L-Glu was net imported into the mitochondria, the formation of L-Ala as the amino receptor from L-Glu in the cytosol was significantly reduced (**Figure 35**). Consequently, less L-Ala was imported into the mitochondria (reduced  $m_{ala}$ ). Furthermore, the substrate  $\alpha$ KG of  $alt_{mit}$  was shuttled out of the mitochondria in exchange with malate and  $v_{alt,mit}$  was finally reduced. In essence, the activity of intracellular L-Ala metabolism was lowered, which led to increased L-Ala secretion into the medium.

Both scenarios reflect the changes in L-Gln metabolism; they are essentially consequences of the rearrangement of glycolytic fluxes following MTA addition. Specifically, the temporal ATP rise was likely to inhibit PFK and cytosolic malic enzyme activities, which resulted in strongly amplified PPP fluxes for improving NADPH formation. Cytosolic malic enzyme lost its dominant role as a key NADPH supplier, which resulted in reduced mitochondrial malate exports and L-Gln metabolic rearrangements, as described above.

### **Improving NADPH supply**

Junghans et al. [298] previously outlined the high sensitivity and positive correlation between NADPH supply and CSP for monoclonal antibody formation in CHO cells. Their compartment-specific metabolome analysis revealed cytosolic malic enzyme as the key NADPH provider in



growing cells. Previously, the crucial role of malic enzyme as the major NADPH source was anticipated by Ahn and Antoniewicz [356] and Templeton et al. [190]. Sengupta et al. [376] analyzed fluxes in late-stage non-growing CHO and disclosed increasing fluxes into the PPP, apparently for NADPH formation. Furthermore, Tuttle et al. [377] observed a 200-fold increase in G6PDH activity under oxidative stress conditions.

The key reason for the occurrence of fundamental metabolic reprogramming in arrested cells remains open and deserves future studies. However, a beneficial link to heterologous protein formation exists. Flux balance analysis using the simplified metabolic model published by Verhagen et al. [44] considered that the maximum NADPH supply should be supported by high cytosolic malic enzyme flux and high oxidative PPP activity (6.3 Supplementary Material: Manuscript 4). Interestingly, MTA treatment provides an optimal flux distribution to maximize the NADPH supply. This observation opens the door for bioprocess optimization, including investigation of the impact of serial MTA bolus shots to extend the phase of high-level CSPs.

Alternately, metabolic engineering strategies may focus on redirecting fluxes for the highest NADPH supply. Balsa et al. [378] evaluated deletions of *G6PDH*, *ME1*, and *IDH1* to foster PPP fluxes and NADPH formation. However, *G6PDH* deletion resulted in higher oxidative stress, slowed down growth, and even led to cell death. This finding is in accordance with the observations of Tuttle et al. [377]. Till date, deletions of *ME1* or *IDH1* have not been reported to induce anticipated NADPH improvements.

## **Conclusion**

The current study merges recent approaches of compartment-specific metabolomics and non-stationary  $^{13}\text{C}$  flux analysis to investigate the impact of MTA addition on monoclonal antibody-producing CHO cells. Complementing the studies of Verhagen et al. [313,359], improvement in CSPs was determined to be tightly linked with cellular arrest and reprogramming of metabolism. MTA addition initiates a cascade of regulatory responses comprising cell proliferation, transcription, and metabolic control. Most likely, the first is the consequence of MTA-mediated feedback inhibition in polyamine biosynthesis. The resulting accumulation of ATP impairs glycolytic and malic enzyme fluxes, finally enabling significantly enhanced NADPH

supply via boosting PPP activity. This knowledge should be exploited via future bioprocess development and metabolic engineering studies for improving the CSP for next-generation CHO hosts. Besides, it may illustrate the close network of cellular responses ranging from cell proliferation to reverting mitochondrial shuttle activities because of MTA addition to a CHO culture.

### **Acknowledgements**

The authors gratefully acknowledge funding from the Bundesministerium für Bildung und Forschung (BMBF, DiImpact Project, Funding Number 031L0077A). We thank DiImpact project partners supporting this study: Andreas Unsöld (Boehringer Ingelheim Pharma GmbH & Co. KG), Martin Schilling (Evonik Nutrition and Care GmbH), and Christoph Heinrich (Xell AG). Furthermore, we thank the research group of Prof. Dr. Noll for providing CHO-DP12 cells.

### **Author Contributions**

Andy Wiranata Wijaya – Software, Formal analysis, Data Curation, Writing-Original Draft, Writing-Review & Editing, Visualization

Natascha Verhagen – Conceptualization, Investigation, Validation, Formal analysis, Writing-Original Draft, Writing-Review & Editing, Visualization

Attila Teleki – Conceptualization, Validation, Investigation, Writing-Original Draft, Writing-Review & Editing

Ralf Takors – Conceptualization, Writing-Review & Editing, Supervision, Project administration, Funding acquisition

### **Declaration of Interests**

The authors declare no competing interests.

### **References**

see 5 References, p.139

**Supplemental Material 1****Table 3.** S1. List of chemicals

Chemical	Supplier
L-glutamine	Carl Roth GmbH & Co. KG, Germany
methotrexate	Sigma-Aldrich, Germany
D-glucose [U- <sup>12</sup> C]	Carl Roth GmbH & Co. KG, Germany
D-glucose [U- <sup>13</sup> C]	Cambridge Isotope Laboratories, Inc, US
D-glucose [1- <sup>13</sup> C <sub>1</sub> ]	Sigma-Aldrich, Germany

**Table 4.** S2. Full names of abbreviated metabolites.

1	1,3-BPG	1,3-bisphosphoglycerate	27	Gly	glycine
2	2/3-PG	2/3-phosphoglycerate	28	Glyco	glycogen
3	AcCoA	acetyl coenzyme A	29	Gxy	glyoxylate
4	ADP	adenosine diphosphate	30	IsoCit	isocitrate
5	aKG	α-ketoglutarate	31	Isoleu	isoleucine
6	aKV	α-ketovalerate	32	KDPG	2-keto-3-deoxy-6-phosphogluconate
7	Ala	alanine	33	Lac	lactate
8	AMP	adenosine monophosphate	34	Leu	leucine
9	Arg	arginine	35	Mal	malate
10	Asn	asparagine	36	Met	methionine
11	Asp	aspartate	37	MMA	mono-methyl-adipate
12	ATP	adenosine triphosphate	38	NAD	ox nicotinamide adenine dinucleotide
13	cisAco	cis-aconitate	39	NADH	red nicotinamide adenine dinucleotide
14	Cit	citrate	40	NADP	ox nicotinamide adenine dinucleotide phosphate
15	CoA	Coenzyme A	41	NADPH	red nicotinamide adenine dinucleotide phosphate
16	DHAP	dihydroxyacetone phosphate	42	Nva	norvaline
17	F16bp	fructose 1,6-bisphosphate	43	OAA	oxaloacetate
18	F6P	fructose 6-phosphate	44	PEP	phosphoenolpyruvate
19	FAD	flavin adenine dinucleotide	45	Pro	proline
20	FADH <sub>2</sub>	FAD (hydroquinone form)	46	Pyr	pyruvate
21	Fum	fumarate	47	R(u)5p	rib(ul)ose 5-phosphate
22	G6P	glucose 6-phosphate	48	Ser	serine
23	GAP	glyceraldehyde 3-phosphate	49	Suc	succinate
24	Glc	glucose	50	Thr	threonine
25	Gln	glutamine	51	Tyr	tyrosine
26	Glu	glutamate	52	Val	valine

**Table 5.** S3. Correction factor for the validation of the differential fast-filtration method for whole-cell and subcellular metabolome analyses. The compartment-specific internal standards G6P, F6P (cytosol) and cisAco (mitochondria) were used to evaluate mitochondrial integrity and cytosol depletion. The correction factor was separately calculated for REF and MTA supplemented cells as in Junghans et al. [298]. Standard deviation of all intracellular samples. Significance was tested with a one-sided t-test.

	Correction Factor [%]		Comment
	MV	SD	
<b>REF</b>	79.75	6.47	
<b>MTA</b>	80.51	7.00	insignificant

**Table 6.** S4. Cell-specific productivity (CSP) [ $\mu\text{g cell}^{-1} \text{d}^{-1}$ ] regarding the different cultivation phases: MTA supplemented cells compared to REF. MTA was added after phase A (0–48 h) installing at a final MTA concentration of 250  $\mu\text{M}$ . Glucose labelling started after phase B (48–60 h). Phase C (60–168 h) is divided in I: Overflow. II: N-Limitation. III: starvation. Error bars show standard deviations of biological duplicates and technical replicates. Significance was tested with one-sided t-test. \*  $p < 0.05$ .

[ $\mu\text{g cell}^{-1} \text{d}^{-1}$ ]	A (0 - 48) h			B / C.I (72 - 108) h			C.II / C.III (120 - 156) h		
	MV	SD	Comment	MV	SD	Comment	MV	SD	Comment
<b>REF</b>	8.72	3.74	insignificant	3.82	0.06	significant, *	1.22	0.25	insignificant
<b>MTA</b>	6.64	0.06		9.73	2.26		3.07	3.52	

**Table 7.** S5. Metabolic model and carbon atom transition model.

ID	Enzyme name	Reaction and carbon atom transition
tGln	Glutamine importer	Gln_ex[(1,2,3,4,5)] => Gln[(1,2,3,4,5)]
gs	Glutaminase	Gln[(1,2,3,4,5)] => Glu[(1,2,3,4,5)]
tGlu	Glutamate transporter	Glu[(1,2,3,4,5)] = Glu_ex[(1,2,3,4,5)]
gdh	Glutamate dehydrogenase	aKG_m[(1,2,3,4,5)] = Glu_m[(1,2,3,4,5)]
tGlc	Glucose importer	Glc_ex[(1,2,3,4,5,6)] => G6P[(1,2,3,4,5,6)]
fGlyco	Carbon storage (glycogen) degradation	Glyco_ex[(1,2,3,4,5,6)] => G6P[(1,2,3,4,5,6)]
pgi	Phospho-glucose-isomerase	G6P[(1,2,3,4,5,6)] = F6P[(1,2,3,4,5,6)]
pfk	Phosphofructokinase + fructose-1,6-bisphosphatase	F6P[(1,2,3,4,5,6)] = FBP[(1,2,3,4,5,6)]

Results: Original Publications

fbpa	Fructose-bisphosphate aldolase	$FBP[(1,2,3,4,5,6)] = DHAP[(3,2,1)] + GAP[(4,5,6)]$
tpi	Triphosphate isomerase	$DHAP[(1,2,3)] = GAP[(1,2,3)]$
gapdh	GAP dehydrogenase + biphosphoglycerate mutase	$GAP[(1,2,3)] = 3PG[(1,2,3)]$
eno	Phosphoglycerate hydratase	$3PG[(1,2,3)] = PEP[(1,2,3)]$
pkm	Pyruvate kinase	$PEP[(1,2,3)] \Rightarrow Pyr[(1,2,3)]$
ldh	Lactate dehydrogenase	$Pyr[(1,2,3)] = Lac[(1,2,3)]$
tLac	Lactate transporter	$Lac[(1,2,3)] \Rightarrow Lac\_ex[(1,2,3)]$
G6Pdh	Glucose-6-phosphate dehydrogenase	$G6P[(1,2,3,4,5,6)] \Rightarrow Ru5P [(2,3,4,5,6)] + CO2[(1)]$
rpi	Ribulose-5-phosphate isomerase	$Ru5P[(1,2,3,4,5)] = R5P[(1,2,3,4,5)]$
tkt1	Transketolase	$R5P[(1,2,3,4,5)(6,7,8,9,10)] = S7P[(6,7,1,2,3,4,5)] + GAP[(8,9,10)]$
tald	Transaldolase	$E4P[(1,2,3,4)] + R5P[(5,6,7,8,9)] = F6P[(5,6,1,2,3,4)] + GAP[(7,8,9)]$
tkt2	Transketolase	$S7P[(1,2,3,4,5,6,7)] + GAP[(8,9,10)] = E4P[(4,5,6,7)] + F6P[(1,2,3,8,9,10)]$
tCO2	CO <sub>2</sub> evolution	$CO2[(1)] \Rightarrow CO2\_ex[(1)]$
MPC1	Pyruvate/H <sup>+</sup> symporter	$Pyr[(1,2,3)] \Rightarrow Pyr\_m[(1,2,3)]$
CIC	Citrate/Malate antiporter	$Cit\_m[(1,2,3,4,5,6)] + Mal[(7,8,9,10)] \Rightarrow Cit[(1,2,3,4,5,6)] + Mal\_m[(7,8,9,10)]$
DIC	PO <sub>3</sub> <sup>4-</sup> /Malate antiporter	$Mal\_m[(1,2,3,4)] = Mal[(1,2,3,4)]$
GC1	Glutamate/H <sup>+</sup> symporter	$Glu\_m[(1,2,3,4,5)] = Glu[(1,2,3,4,5)]$
OGC	Malate/aKG antiporter	$Mal[(1,2,3,4)] + aKG\_m[(5,6,7,8,9)] = Mal\_m[(1,2,3,4)] + aKG[(5,6,7,8,9)]$
AGC1	Aspartate/glutamate antiporter	$Glu[(1,2,3,4,5)] + Asp\_m[(6,7,8,9)] \Rightarrow Glu\_m[(1,2,3,4,5)] + Asp[(6,7,8,9)]$
mAla	Unknown alanine transporter	$Ala[(1,2,3)] = Ala\_m[(1,2,3)]$
mAsn	Unknown asparagine transporter	$Asn[(1,2,3,4)] = Asn\_m[(1,2,3,4)]$
pdh	Pyruvate dehydrogenase	$Pyr\_m[(1,2,3)] \Rightarrow AcCoA\_m[(2,3)] + CO2[(1)]$

Results: Original Publications

cs	Citrate synthase	$OAA\_m[(1,2,3,4)] + AcCoA\_m[(5,6)] \Rightarrow Cit\_m[(4,3,2,6,5,1)]$
idh	Iso-citrate dehydrogenase	$Cit\_m[(1,2,3,4,5,6)] = aKG\_m[(1,2,3,4,5)] + CO2[(6)]$
adh	aKG dehydrogenase + succinyl-CoA ligase + succinate dehydrogenase +	$aKG\_m[(1,2,3,4,5)(6,7,8,9,10)] = Fum\_m[(2,3,4,5)(10,9,8,7)] + CO2[(1)(6)]$
fus	fumarase	$Fum\_m[(1,2,3,4)(5,6,7,8)] = Mal\_m[(1,2,3,4)(8,7,6,5)]$
mdh	Malate dehydrogenase	$Mal\_m[(1,2,3,4)(5,6,7,8)] = OAA\_m[(1,2,3,4)(8,7,6,5)]$
pepck	Phosphoenolpyruvate carboxykinase	$OAA[(1,2,3,4)] = PEP[(1,2,3)] + CO2[(4)]$
me_c	Cytosolic malic enzyme	$Mal[(1,2,3,4)] = Pyr[(1,2,3)] + CO2[(4)]$
me_m	Mitochondrial malic enzyme	$Mal\_m[(1,2,3,4)] = Pyr\_m[(1,2,3)] + CO2[(4)]$
pc	Pyruvate carboxylase	$Pyr\_m[(1,2,3)] + CO2[(4)] = OAA\_m[(1,2,3,4)]$
mdh_c	Cytosolic malate dehydrogenase	$OAA[(1,2,3,4)(5,6,7,8)] = Mal[(1,2,3,4)(8,7,6,5)]$
tSer	Serine importer	$Ser\_ex[(1,2,3)] \Rightarrow Ser[(1,2,3)]$
phdgh	Phosphoglycerate dehydrogenase + phosphoserine phosphatase	$3PG[(1,2,3)] \Rightarrow Ser[(1,2,3)]$
sds	Serine dehydratase	$Ser[(1,2,3)] \Rightarrow Pyr[(1,2,3)]$
tAla	Alanine transporter	$Ala[(1,2,3)] = Ala\_ex[(1,2,3)]$
alt_c	Cytosolic alanine aminotransferase	$Pyr[(1,2,3)] + Glu[(4,5,6,7,8)] = Ala[(1,2,3)] + aKG[(4,5,6,7,8)]$
alt_m	Mitochondrial alanine aminotransferase	$Ala\_m[(1,2,3)] + aKG\_m[(4,5,6,7,8)] = Pyr\_m[(1,2,3)] + Glu\_m[(4,5,6,7,8)]$
tAsp	Aspartate transporter	$Asp\_ex[(1,2,3,4)] = Asp[(1,2,3,4)]$
tAsn	Asparagine importer	$Asn\_ex[(1,2,3,4)] \Rightarrow Asn[(1,2,3,4)]$
ast_c	Cytosolic aspartate aminotransferase	$Asp[(1,2,3,4)] + aKG[(5,6,7,8,9)] = OAA[(1,2,3,4)] + Glu[(5,6,7,8,9)]$
ast_m	Mitochondrial aspartate aminotransferase	$Asp\_m[(1,2,3,4)] + aKG\_m[(5,6,7,8,9)] = OAA\_m[(1,2,3,4)] + Glu\_m[(5,6,7,8,9)]$
asns	Asparaginase	$Asn\_m[(1,2,3,4)] = Asp\_m[(1,2,3,4)]$
muG6P	Biomass formation from G6P	$G6P[(1,2,3,4,5,6)] \Rightarrow G6P\_X\_ex[(1,2,3,4,5,6)]$

muGAP	Biomass formation from GAP	$GAP[(1,2,3)] \Rightarrow GAP\_X\_ex[(1,2,3)]$
muRu5P	Biomass formation from Ru5P	$R5P[(1,2,3,4,5)] \Rightarrow R5P\_X\_ex[(1,2,3,4,5)]$
acl	Acetyl-CoA lyase	$Cit[(1,2,3,4,5,6)] \Rightarrow OAA[(6,3,2,1)] + AcCoA[(5,4)]$
muAcCoA	Biomass formation from AcCoA	$AcCoA[(1,2)] \Rightarrow AcCoA\_X\_ex[(1,2)]$
muSer	Biomass formation from serine	$Ser[(1,2,3)] \Rightarrow Ser\_X\_ex[(1,2,3)]$
muAla	Biomass formation from alanine	$Ala[(1,2,3)] \Rightarrow Ala\_X\_ex[(1,2,3)]$
muAsp	Biomass formation from aspartate	$Asp[(1,2,3,4)] \Rightarrow Asp\_X\_ex[(1,2,3,4)]$
muAsn	Biomass formation from asparagine	$Asn[(1,2,3,4)] \Rightarrow Asn\_X\_ex[(1,2,3,4)]$
muGln	Biomass formation from glutamine	$Gln[(1,2,3,4,5)] \Rightarrow Gln\_X\_ex[(1,2,3,4,5)]$
muGlu	Biomass formation from glutamate	$Glu[(1,2,3,4,5)] \Rightarrow Glu\_X\_ex[(1,2,3,4,5)]$

Indices: c: cytosolic, m: mitochondrial, ex: extracellular

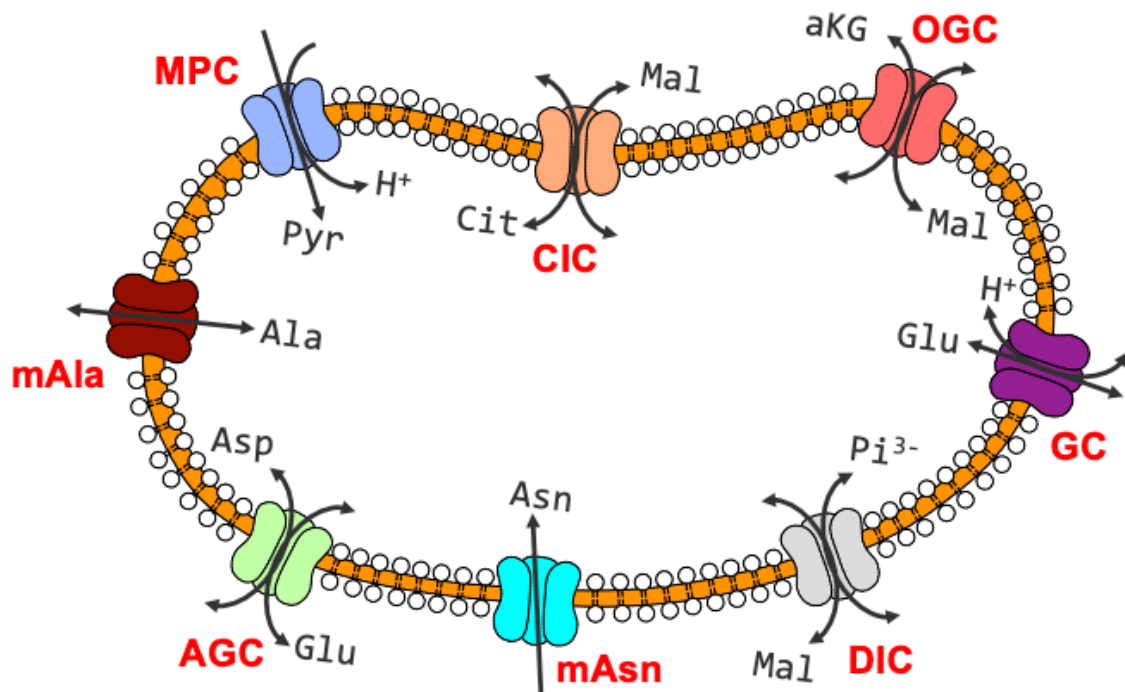


Figure 37. S1. Mitochondrial transporters assumption in the metabolic model

**Supplementary Material**

See 6.3 Supplementary Material: Manuscript 4, p.195



## 4 Discussion

To satisfy the growing biopharmaceutical market, cell-specific productivities (CSPs) of therapeutic proteins must increase. Process improvements typically focus on cell engineering and medium optimization. Discovery and modification of cellular regulatory switches that trigger increased productivity are required. Systems biological studies to uncover these mechanisms use metabolomics [298,299,379], transcriptomics [300,301] or epigenetics [302–305]. These investigations include medium components that demonstrate functions as energy supply and/or in cellular signaling. Traditional medium compositions contain undefined complex components such as sera or hydrolysates. Both consist of many components making it hard to understand single mechanisms or synergistic effects. Many essential medium components are already known as water, carbon, nitrogen, phosphate, amino acids, fatty acids, vitamins, trace elements and salts. Anyhow, identification of more stimulating and boosting components with regulatory impact is required to explore the full potential of cellular performance.

### 4.1 L-Tyrosine Containing Dipeptides

The application of peptides as medium supplements is of high interest as amino acids are required for cell cultivation [244] but some demonstrate disadvantages as low stability or solubility of single components. By contrast, synthetic dipeptides show increased solubility (up to 35 times) and stability during sterilization procedures [16]. Previous studies with dipeptides demonstrated diverse outcomes and focused on phenotypical effects. Especially L-Gln based dipeptides were investigated. The use of the L-Gln containing dipeptides Gly-L-Gln and L-Ala-L-Gln allowed to generate a heat-sterilizable serum-free medium [17]. The application of such dipeptides demonstrated comparable monoclonal antibody production and moreover the use of Gly-L-Gln changed cellular metabolism [18,261,262]. Next to L-Gln containing dipeptides, L-Tyr containing dipeptides were phenotypically investigated [19]. Anyhow, metabolic effects of such dipeptides are not investigated in detail yet.

A part of this thesis focuses on L-Tyr containing dipeptides which allow to increase the maximum L-Tyr supply without the necessity of pH alterations. The three different dipeptides L-Pro-L-Tyr (PY), L-Tyr-L-Val (YV) and Gly-L-Tyr (GY) were added to defined medium. The relevance of the corresponding amino acid for the dipeptide's mechanism, uptake, or effector function is supported by the experimental observations (**Figure 8** and **Figure 9**; [45,266]). All three dipeptides were taken up intact (**Figure 16**) and subsequently degraded, metabolized or re-exported. These investigations additionally clarified that dipeptides are intracellularly cleaved and metabolized [18,45]. Dipeptides are likely taken up via PEPT1/2 with H<sup>+</sup> symport in CHO cells, mouse and human [266,286].

The consumption of dipeptides in cells was investigated and revealed different uptake rates dependent on its amino acid composition (**Figure 9**). PY demonstrated the highest uptake rate and demonstrated a strong impact on CHO cells compared to GY and YV. It caused decreased growth, increased D-Glc uptake and reduced overflow mechanism (**Figure 8**). Contradictory, a study focusing on L-Tyr containing dipeptides indicated positive effects on cellular viability and product titer. Anyhow, cultures supplemented with dipeptides had changed metabolic profiles that include lower L-Lac and NH<sub>4</sub><sup>+</sup> secretion [19]. This is comparable to the reduced overflow metabolism after PY addition (**Figure 8**). L-Gln containing dipeptides showed metabolic effects as well [18]. The optimized use of L-Ala-L-Gln instead of L-Gln strongly reduced ammonia formation and demonstrated the additional role of dipeptides as metabolic effectors [261]. The applicability of L-Ala-L-Gln in CHO cell culture revealed increased product titers and reduced ammonia formation [262]. However, these experiments did not provide data about further metabolic changes.

An influence on intracellular ATP (**Figure 11**) and L-Gln concentrations (**Figure 10**) occurred after PY addition. On top, the overall uptake and incorporation of L-Tyr was higher with GY and PY compared to YV addition. PY addition enabled the highest L-Tyr incorporation revealing the importance of amino acid composition within the dipeptide (**Figure 9**). As demonstrated in previous publications, the different L-Tyr containing dipeptides showed different uptake rates and effects on the cellular phenotype [45]. Another study investigated effects of

dipeptides and longer oligopeptides containing glycine, L-alanine, L-serine, L-threonine, L-lysine, and L-histidine on a phenotypic level. Concomitantly, the study pointed out that the composition of peptides is highly important since the investigated peptides demonstrated totally diverse effects e.g. on cell growth. Furthermore, the study showed anti-apoptotic activities of the dipeptides [265]. All investigated L-Lys containing dipeptides and peptides interfered with the cell cycle and predominantly stopped it in the S-phase. Additionally, their capability of production increase was correlated with their growth inhibiting features [263].

The data presented in this thesis demonstrate diverse effects of L-Tyr containing dipeptide addition for CHO medium. For in depth analysis of dipeptide usage in CHO cells, intracellular profile data was extended with flux balance analysis (FBA). FBA (conducted by AW Wiranata) further confirmed phenotypical observations after PY addition (**Figure 12**): It implies higher D-Glc uptake and lower L-Lac formation which resulted in reduced overflow. This is in line with the phenotypic data. Consequently, TCA activity increased. Additionally, the mitochondrial malate-aspartate shuttle (MAS) activity was enhanced compared to the other dipeptide supplementations. MAS is typically an indirect mitochondrial NADH transporter. The altered mechanism might be an adaption of the cells to an increased supply of cytosolic NADH from a higher glycolytic flux. The higher flux does not result in a higher L-Lac production but may be managed by a higher MAS activity that allows the usage of increased NADH levels in OXPHOS for ATP formation (**Figure 12**). The FBA model provides three possible L-Tyr sinks: the building of macromolecules as mAB, export and anaplerotic catabolism. The FBA model predicts the catabolism of L-Tyr as predominated scenario after all dipeptide additions. L-Tyr is catabolized into fumarate and acetyl-CoA that fuel the TCA and subsequent enhance ATP formation. The degradation of L-Tyr requires  $\alpha$ KG [46] whose demand is increased under PY conditions as PY allows the cell to inherent more L-Tyr compared to the other dipeptides (**Figure 9**). Consequently, intracellular L-Gln pools are depleted under PY conditions. L-Gln concentrations after GY addition were in between L-Gln concentrations of PY and YV (**Figure 10**). This underlines the increased metabolization of L-Tyr after GY addition compared to YV addition that demonstrated the lowest usable L-Tyr availability. However, the addition of YV still enabled higher available L-Tyr concentrations compared to the reference cultivation

**(Figure 9).** Despite increased ATP availability after PY supplementation, CSP was not increased. This is contradictory to Becker et al., [3], who demonstrated increased CSP due to higher ATP formation via respiration in D-Glc limited perfusion mode CHO cell culture. Anyhow, enhanced TCA activity without increased CSP in a D-Glc excess scenario was previously examined by Bulté et al., [291]. Moreover, CHO cells are known for their high maintenance demand that is estimated to be higher than 65 % of the total ATP supply [292]. As a result, high production accompanied by low substrate availability can compete with challenging maintenance demands and this results in lower overall performance of the cells. PY as additive allows the cells to improve its glycolysis, reduce its overflow metabolism, enhance its TCA activity, and generate more ATP. However, this did not result in a higher CSP in this cell line pointing out that other bottlenecks as the vesicular protein secretion pathway may additionally hinder a higher production/excretion rate. Summarizing, our data indicate that ATP is not the only limiting factor of antibody production under D-Glc excess conditions in the used CHO cell line. By implication, other cell lines may increase their CSP after PY addition.

Whereas the enhanced TCA activity is partially a result of the higher L-Tyr degradation the impact on glycolysis and overflow metabolism can hardly be explained by merely metabolic fueling. This indicates an action of PY as signal molecule that reprograms the cells' metabolic regulation. Signal molecule activity was still observed for selected amino acids and dipeptides [264,265]. This work demonstrated that the amino acid composition in dipeptides is important as well for its cellular availability and activity pointing out the necessity of careful investigation and evaluation of dipeptide addition in cell culture medium.

## **4.2 SAM and Its Degradation Product MTA**

Different small molecules are investigated as they influence and interact with cellular signaling pathways. More than half of analyzed nuclear genes are prone for methylation [306] and therefore interesting for epigenetic research and modification. This points out the relevance of additive supplementation that can interact with epigenetic mechanisms. S-(5'-Adenosyl)-L-methionine (SAM) is a cellular molecule that is global a methyl donor in mammalian cell systems. In addition to trans-methylation, it interacts with gene expression, polyamine

synthesis, trans-sulfuration, membrane fluidity, and glutathione availability [47,48] indicating its prominent features in cellular regulation. For these reasons, SAM addition to the medium of CHO cells was further investigated in this thesis.

SAM addition decreased the growth rate (**Figure 18**) comparable to previous observations in liver cells [225,226]. Despite SAM uptake was assumed as consequence of rising glutathione levels [48], the experimental work in this thesis demonstrated that extracellular SAM levels also decreased in the cells' absence at cultivation conditions (**Figure 20**) and indicate rather chemical degradation than uptake. The chemical degradation of SAM in water was investigated computationally and revealed 5'-deoxy-5'-(methylthio)adenosine (MTA) and L-homoserine lactone (HSL) as degradation products of SAM at pH 7 or lower [310]. Consequently, addition of both molecules to the medium was investigated. Whereas HSL demonstrated no effect on cell culture, MTA addition resulted in a comparable effect to SAM addition. This led to the conclusion that MTA, the degradation product of SAM is the actual effector (**Figure 21** and **Figure 22**). Hydrophobic MTA can permeate the membrane [49,60,61] whereby intracellular pools are formed from decarboxylated SAM as by-product of polyamine synthesis [58,227]. Degradation of MTA occurs rapidly by 5'methylthioadenosine phosphorylase as high MTA concentrations hamper polyamine synthesis. It is involved in gene expression induction, apoptosis regulation and cell proliferation [49,60–62]. The impact of MTA on the cell cycle arises from its interaction with polyamine [63,229,311] and DNA synthesis [64]. Anyhow, next to polyamine synthesis, other acting sites as cellular nucleotide concentrations or cell membranes must be considered [380] as inhibition of polyamine synthesis was not reversed by spermidine addition in mouse fibroblasts [381]. The data in this thesis demonstrate parallels, such as interactions of MTA with cell cycle, especially a pronounced S-phase arrest of the cells (**Figure 23**).

SAM and MTA increased CSP whilst they inhibited cell growth (**Figure 21** and **Figure 22**). Enhanced CSP is often accompanied by cell cycle arrest [25–28] but this is not exclusively linked to a certain cell cycle phase since the increase of cell productivity occurs in different phases [29–33]. As cell cycle and volume are tightly connected [34–36] it is not surprising that

other research groups linked increased CSP with increased cell volume [33]. In the presented data, SAM and MTA addition resulted in an increase of cell volume in addition to cell cycle arrest (**Figure 23**). Consequently, an interaction of both mechanisms to increase CSP is likely. The growth arrest allows the cell to use remaining energy for productivity [121]. Anyhow, MTA interacts with several other cell mechanisms and regulations [49,60,61]. For this reason, additional mechanisms for the increased productivity are probable.

The addition of small molecules is often concentration and time dependent. The dose and/ or time dependency of MTA was demonstrated in leukemia U391 cells [60] and fibroblasts [61]. The positive effect of MTA on CSP is concentration dependent in CHO cells as well (**Figure 24** and **Figure 25**). Different additive concentrations (150, 250, 350 and 450  $\mu\text{M}$ ) showed that effects on growth, cell size and cell cycle occur with all concentrations but remained constant over additions of 350  $\mu\text{M}$ . The highest increase of CSP occurred after 250  $\mu\text{M}$  MTA addition. Moreover, higher concentrations (350 and 450  $\mu\text{M}$ ) demonstrated negative effects on viability and CSP whereas lower concentrations (150 and 250  $\mu\text{M}$ ) ensured high viabilities and increased CSP levels. As demonstrated before, cells were temporary trapped in S-phase. Other small molecule additions as catechins or AMP resulted in a S-phase blockade and CSP increase dependent on their applied concentration in CHO cells as well [20,24]. To evaluate if the addition time is relevant for MTA as effector, MTA was added at different growth phases of the cultivation (**Figure 26** and **Figure 27**). MTA addition is most effective in exponential growth phase. Later addition resulted in less or no effect of MTA. Summarizing, CSP increase is predominantly the result of cell size increase, cell cycle arrest and high viability. MTA works most efficient when concentrations between 250 and 300  $\mu\text{M}$  ( $0.167 \text{ pmol}_{\text{MTA}} \text{ cell}^{-1}$ ) were applied in the cell's medium in the exponential growth phase (48 h).

MTA interacts with gene expression induction, apoptosis and cell proliferation [62]. As a result, an effect of MTA on the transcriptome is probable. Transcriptome analysis reveals genetic modifications and mechanisms of cells to adapt to new challenges or environment. The gained information can be used for cell engineering. Examples are transcriptomic studies of low and high producer cell lines which demonstrated that high recombinant protein

secretion is negatively correlated to the cell's gene expression, metabolic RNA and protein processes [301]. Another study demonstrated that enhanced gene expression related to protein folding, cell survival, cell growth, vesicular trafficking and cytoskeleton organization is typically for high producers [42]. As a result, fine tuning of cellular mechanism is highly required to gain an overall process improvement.

Cytoskeleton compartments and their regulation are related to CSP. The cytoskeleton consists of actin microfilaments, microtubules and intermediate filaments and is important for cell shape, protein synthesis [180], transport [181] and secretion [182,183]. These important functions of the cytoskeleton reveal its importance in the recombinant protein formation. The transcriptomic changes after MTA addition showed several genes that are related to the cytoskeleton. The water importer aquaporin 1 (*Aqp1*) was upregulated 84 h-96 h-144 h after MTA addition (**Table 2**) which occurred parallel to cell size increase (**Figure 25** and **Figure 26**). Similar observations were examined under stress conditions, e.g. hyperosmolarity accompanied by higher intracellular protein content and CSP [124,329,330,332]. Cell size increase resulted in a higher need of membrane molecules e.g. glycerolipids, that may be the reason for an upregulated phosphatide phosphatase LPIN3 (*Lpin3*) at 84 h-96 h (**Table 2**). The two actin-associated enzymes plastin and matriptase [333,334] were upregulated at 84 h-96 h-144 h (*Lcp1* and *St14*) (**Table 2**). Protein transport and secretion in high producers is dependent on actin, tubulin, or the actin-binding cofilin [184] pointing out the importance of the highly dynamic system. This observation was intensified by transcriptome studies of a high producer that demonstrated enhanced gene expression of actin related proteins [41]. Another research group identified cytoskeleton and vesicular trafficking related genes in high producers. One is Rassf9 that is linked to vesicular trafficking regulation and especially to endosome recycling [42]. Differential upregulated genes (DEGs) at 84 h and 96 h associated with vesicular trafficking were revealed after MTA addition including intraluminal vesicles (monoacylglycerol lipase ABHD6 (*Abhd6*)) and protein processing (glycosylation) ( $\alpha$ -2,8-sialyltransferase 8F (*St8sia6*)) in the Golgi apparatus (**Table 2**). Next to cytoskeleton functions, actin interacts with polymerases via pre-initiation complex and influences gene expression [336,337]. The importance of actin and its regulation is displayed by additional DEGs such as

Add2 ( $\beta$ -adducin) at 96 h-144 h [339] and Fscn1 (fascin) at 96 h [340] that are actin related (**Table 2**). Another microtubule and actin related gene, adenomatous polyposis coli protein 2 (*APC 2*) is a transcription factor and was upregulated right after MTA addition at 72 h and 84 h [341,342] (**Table 2**). It is important for interphase as it interacts with microtubules [342]. Additionally, the interphase related protein FAM110C (*Fam110c*) was upregulated at 84 h and 96 h (**Table 2**). It impairs cell cycle progression [343]. In another cell line, MTA was demonstrated to hamper the assembly of the nuclear envelope. MTA could inhibit the carboxymethylation of the nuclear envelope part lamin B and induced apoptosis in leukemia U391 cells [60]. By contrast, MTA addition did not lead to increased apoptosis rates in CHO cells and even enhanced cellular viability. Summarizing, MTA addition must be carefully optimized to achieve desired cellular effects (**Figure 24** and **Figure 26**).

Genes involved in cell growth or protein formation e.g. transport and secretion are important for high producers. The transcriptomic data after MTA addition demonstrated that several genes associated with these features were differentially regulated and might contribute to the increased CSP and other observed phenotypes after MTA addition. Moreover, another phenotypic observation after MTA addition was decreased cell growth, cell cycle arrest and prolonged high viability. This indicates significant changes in transcriptional regulations. Several differentially expressed genes that are related to cellular survival and transcriptional regulation were observed after MTA addition (**Table 2**). This included plasminogen activator (*Plau*) a growth factor with mitogenic and apoptotic reduction capabilities that was upregulated at 84 h-96 h-144 h [344,345]. Associations with cell growth, survival and transcription were demonstrated for the tumor-suppressor ras association domain-containing protein 6 (*Rassf6*) that was upregulated at 84 h and 96 h. It regulates cell cycle arrest and apoptosis and its family members were upregulated in high producers [42,170]. Differential expressed genes related to cell proliferation are the transcription factor aryl hydrocarbon receptor nuclear translocator 2 (*Arnt2*) at 72 h and 84 h [346] and the epidermal growth factor receptor (*EGFR*) [348] at 84 h and 96 h that is additionally associated with DNA synthesis (**Table 2**). Deoxyribonuclease  $\gamma$  (*Dnase1l3*, *Dnase1l3*) was upregulated at 84 h and 96 h and is related to apoptosis [347] (**Table 2**). In liver cells, the concentration dependent addition of



SAM or MTA interacts with the apoptotic mechanism as well. Whereas primary liver cells were protected from apoptosis, the addition of SAM or MTA was pro-apoptotic for hepatoma cells. SAM or MTA addition prevented the release of cytochrome c from mitochondria and was not linked to its function in GSH system. Direct MTA addition bypasses the conversion of SAM and as a result lower amounts were required [49]. MTA addition to CHO cells resulted in prolonged viability (**Figure 24** and **Figure 26**) which is an indication for decreased apoptosis rates during cultivation. Another transcription factor that was differentially upregulated at 84 h was the cyclic AMP-dependent transcription factor ATF-5 (*Atf5*) that was determined as a regulator in transcription and protein production in CHO cells [349] (**Table 2**). Another possibility for transcriptional modification is epigenetics including acetylation and methylation. Genes of histone proteins are important for transcription and replication [170]. In the MTA transcriptome data three genes related to histone modifications were upregulated: lysine-specific demethylase hairless (*Hr*), lysyl oxidase homolog 2 (*Lox12*) and chromodomain-helicase-DNA-binding protein 5 (*Chd5*) (**Table 2**). Lysine-specific demethylase hairless upregulated at 84 h and 96 h is a histone demethylase that interacts with cell cycle regulation [350]. Lysyl oxidase homolog 2 and chromodomain-helicase-DNA-binding protein 5 are both histone modifying enzymes and were upregulated in the later cultivation phase at 96 h and 144 h [351,352].

Another group of DEGs linked to immunogenic functions were detected. This includes upregulation of SH2 domain-containing protein 1B (*Sh2d1b*), CD53 (*CD53*), viral response component 2'-5'-oligoadenylate synthase-like protein 2 (*Oasl*), interleukin-17F (*Il17f*) (84 h-96 h) and interleukin-11 (*Il11*) (72 h-84 h). These upregulations mirror a general connection between MTA addition and signaling pathways of the cells that were additionally linked to immunogenic mechanisms [312].

Phenotypic observations as decreased cell growth and prolonged high viability are supported by observed DEGs after MTA addition. Anyhow, published data is complex and diverse and does not always support the data in this thesis. This underlines that the function of the MTA effector is concentration and time dependent. High concentrations can result in negative

effects (**Figure 24**) and correct addition time points are required to intensify positive effects (**Figure 26**) even in the same cell line. As consequence, diverse outcomes between different cell lines are not surprising and demonstrate the requirement for careful evaluation of the MTA addition in each cell line or process.

### 4.3 Metabolomics After MTA Addition

Compartment-specific  $^{13}\text{C}$  metabolic flux analysis (in cooperation with AW Wiranata) was applied to determine flux changes in CHO cells after MTA addition. MFA analysis revealed that MTA addition resulted in a changed cellular flux pattern. The cytosolic malic enzyme ( $\text{me}_{\text{cyt}}$ ) activity and flux through glycolysis were reduced. Consequently, glucose 6-phosphate (G6P) was predominantly shuttled into the PPP resulting in an increased NADPH production. Phenotypic process data was comparable to shaking flask experiments such as decreased growth, increased cell volume, altered cell cycle and increased CSP (**Figure 30**, **Figure 32** and **Figure 33**). Intracellular data demonstrated that MTA addition influences the energetic status of the cell. ATP concentrations in the cytosol increased (**Figure 34**). Especially ADP and ATP are important regulators for cellular metabolism. Two enzymes of glycolysis, phosphofruktokinase and pyruvate kinase are inhibited by ATP. The observed ATP increase is within the inhibition range of phosphofruktokinase [371–373]. The inhibition of phosphofruktokinase by ATP might be the reason for reduced glycolytic flux after MTA addition. Consequently, G6P is directed into PPP (**Figure 35**). On top, malic enzyme is inhibited by ATP [374] that could enforce the necessity of the cells to enhance PPP fluxes for sufficient NADPH production (**Figure 35** and **Figure 36**). Different from cytosolic concentrations, mitochondrial ATP concentrations were comparable between REF and MTA. In consequence, no influence on TCA was detectable. Nevertheless, the increased cytosolic ATP concentration might be a direct result of degraded MTA and its effect on several enzymes resulted in metabolic reprogramming of the cells.

The reduced  $\text{me}_{\text{cyt}}$  activity led to further metabolic changes in the cell. As malate export to the cytosol was not favorable anymore, the flux direction of the malate/ $\alpha\text{KG}$  antiporter (*OGC*) was reversed. Consequently,  $\alpha\text{KG}$  was shuttled to the cytosol after MTA addition. This changed

direction altered the L-Gln metabolism. In REF, L-Gln was converted to L-Glu and subsequent to  $\alpha$ KG that was shuttled to the mitochondria. As  $\alpha$ KG was hampered by reversed flux directions, the cells imported L-Glu directly into the mitochondria by exchanging it with L-Asp (Asp/Glu antiporter (*AGC1/2*)). Additionally, cells reduced L-Glu export from mitochondria (*GC1/2*). This reprogramming allowed the cells to establish an alternative L-Gln use in TCA. The cellular strategy was enforced by changed L-Asn metabolism. L-Asn was relatively faster metabolized as L-Gln in MTA supplemented cells (**Figure 30**). The incorporated L-Asn was shuttled into mitochondria, converted to L-Asp and exchanged with cytosolic L-Glu. The imported L-Glu was converted to  $\alpha$ KG, that was required to shuttle malate into mitochondria. This was enforced by increased enzymatic activities of  $ast_{mit}$  and  $ast_{cyt}$  which favored  $\alpha$ KG formation in mitochondria and L-Glu formation in the cytosol.

The changed fluxes hampered the L-Ala metabolism as well. The activity of the alanine aminotransferases ( $alt_{mit}$  and  $alt_{cyt}$ ) were reduced after MTA addition. L-Ala formation in the cytosol requires L-Glu which was less available because it was predominantly shuttled into mitochondria. In mitochondria L-Ala was less converted as its reaction partner  $\alpha$ KG was predominantly exchanged with malate. Overall, the L-Ala metabolism was reduced in MTA treated cells. Consequently, mitochondrial L-Ala import ( $m_{ala}$ ) was reduced and remaining L-Ala was mainly exported.

In sum, the increased NADPH production was a result of increased flux through PPP. It demonstrated the potential of CHO cells to intensify this route of NADPH production despite previous studies pointed out that non-affected cells predominantly produce NADPH via malic enzyme and not PPP [298].

#### 4.4 Conclusion

Medium additives can significantly improve cell culture performance. The effect of L-Tyr containing dipeptides is dependent on their composition. PY addition (in contrast to GY and YV) led to an intracellular ATP increase, a reduced overflow metabolism and reduced growth rates in CHO cells. Anyhow, it did not affect CSP pointing out that increased CSP is not only a result of higher ATP availability. Next to L-Tyr containing dipeptides, the small effector

molecules SAM and MTA were investigated. Both are molecules of the cellular metabolism that have multiple roles in gene expression, growth, methylation and signaling. SAM addition led to increased CSP levels but further investigations revealed that MTA, its degradation product is the actual effector. The observed cell growth stop, cell cycle alteration and increased cell volume are linked to increased CSP levels. Further studies revealed that MTA is most effective in increasing CSPs with a concentration around 250  $\mu\text{M}$  provided that its addition occurred in the early exponential growth phase (48 h). Nevertheless, investigations to reveal key benefits of the MTA addition were conducted. These included transcriptomic and metabolic studies. Transcriptomic studies revealed DEGs predominantly linked to cytoskeleton, growth, survival and transcription associated genes. These include histone related proteins that were upregulated after MTA addition. These key groups demonstrated links to high producer phenotypes. As a consequence, the upregulated genes are promising engineering targets in CHO cells.

The addition of MTA resulted in several metabolic changes that influenced the cells metabolism. The fluxes into the PPP increased whereas flux through the malic enzyme was diminished. Overall, the cells were able to increase and balance their NADPH production with this strategy. The manipulation of cells with MTA revealed unknown potential of CHO cells. These metabolic changes allowed the cells to maintain a high productivity despite diminished cell growth.

Further investigation on MTA addition is required as quantification of apoptotic and epigenetic effects. Additionally, the effect of MTA on the cytoskeleton should be further investigated to understand important features of the cytoskeleton that promote high CSP.

## 5 References

- 1 Walsh G (2018) Biopharmaceutical benchmarks 2018. *Nat Biotechnol* **36**, 1136–1145.
- 2 Wurm FM (2004) Production of recombinant protein therapeutics in cultivated mammalian cells. *Nat Biotechnol* **22**, 1393–1398.
- 3 Becker M, Junghans L, Teleki A, Bechmann J & Takors R (2019) Perfusion cultures require optimum respiratory ATP supply to maximize cell-specific and volumetric productivities. *Biotechnol Bioeng* **116**, 951–960.
- 4 Lai T, Yang Y & Ng SK (2013) Advances in Mammalian cell line development technologies for recombinant protein production. *Pharmaceuticals (Basel)* **6**, 579–603.
- 5 Jayapal KP, Wlaschin KF, Hu WS & Yap MGS (2007) Recombinant protein therapeutics from CHO Cells - 20 years and counting. *Chem Eng Prog* **103**, 40–47.
- 6 Kim JY, Kim Y-G & Lee GM (2012) CHO cells in biotechnology for production of recombinant proteins: current state and further potential. *Appl Microbiol Biotechnol* **93**, 917–30.
- 7 Brooks SA (2004) Appropriate Glycosylation of Recombinant Proteins for Human Use: Implications of Choice of Expression System. *Mol Biotechnol* **28**, 241–256.
- 8 Durocher Y & Butler M (2009) Expression systems for therapeutic glycoprotein production. *Curr Opin Biotechnol* **20**, 700–707.
- 9 Ghaderi D, Zhang M, Hurtado-Ziola N & Varki A (2012) Production platforms for biotherapeutic glycoproteins. Occurrence, impact, and challenges of non-human sialylation. *Biotechnol Genet Eng Rev* **28**, 147–176.
- 10 Berting A, Farcet MR & Kreil TR (2010) Virus susceptibility of Chinese hamster ovary (CHO) cells and detection of viral contaminations by adventitious agent testing. *Biotechnol Bioeng* **106**, 598–607.
- 11 Xu X, Nagarajan H, Lewis NE, Pan S, Cai Z, Liu X, Chen W, Xie M, Wang W, Hammond S, Andersen MR, Neff N, Passarelli B, Koh W, Fan HC, Wang J, Gui Y, Lee KH, Betenbaugh

- MJ, Quake SR, Famili I, Palsson BO & Wang J (2011) The genomic sequence of the Chinese hamster ovary (CHO)-K1 cell line. *Nat Biotechnol* **29**, 735–741.
- 12 Butler M (2005) Animal cell cultures: recent achievements and perspectives in the production of biopharmaceuticals. *Appl Microbiol Biotechnol* **68**, 283–291.
- 13 Zhang J (2014) Mammalian Cell Culture for Biopharmaceutical Production. In *Manual of Industrial Microbiology and Biotechnology* pp. 157–178. ASM Press, Washington, DC, USA.
- 14 Birch JR & Racher AJ (2006) Antibody production. *Adv Drug Deliv Rev* **58**, 671–685.
- 15 Xie L & Wang DI (1996) Material balance studies on animal cell metabolism using a stoichiometrically based reaction network. *Biotechnol Bioeng* **52**, 579–90.
- 16 Fürst P (1998) Old and New Substrates in Clinical Nutrition. *J Nutr* **128**, 789–796.
- 17 Minamoto Y, Ogawa K, Abe H, Iochi Y & Mitsugi K (1991) Development of a serum-free and heat-sterilizable medium and continuous high-density cell culture. *Cytotechnology* **5**, 35–51.
- 18 Christie A & Butler M (1994) Glutamine-based dipeptides are utilized in mammalian cell culture by extracellular hydrolysis catalyzed by a specific peptidase. *J Biotechnol* **37**, 277–290.
- 19 Kang S, Mullen J, Miranda LP & Deshpande R (2012) Utilization of tyrosine- and histidine-containing dipeptides to enhance productivity and culture viability. *Biotechnol Bioeng* **109**, 2286–2294.
- 20 Toronjo-Urquiza L, Acosta-Martin AE, James DC, Nagy T & Falconer RJ (2020) The use of catechins in Chinese hamster ovary cell media for the improvement of monoclonal antibody yields and a reduction of acidic species. *Biotechnol Prog* **36**.
- 21 Jiang Z & Sharfstein ST (2008) Sodium butyrate stimulates monoclonal antibody over-expression in CHO cells by improving gene accessibility. *Biotechnol Bioeng* **100**, 189–

194.

- 22 Yang WC, Lu J, Nguyen NB, Zhang A, Healy N V., Kshirsagar R, Ryll T & Huang Y-M (2014) Addition of Valproic Acid to CHO Cell Fed-Batch Cultures Improves Monoclonal Antibody Titers. *Mol Biotechnol* **56**, 421–428.
- 23 Wulhfard S, Baldi L, Hacker DL & Wurm F (2010) Valproic acid enhances recombinant mRNA and protein levels in transiently transfected Chinese hamster ovary cells. *J Biotechnol* **148**, 128–132.
- 24 Zou W, Browne SM & Al-Rubeai M (2019) Physiological alterations of GS-CHO cells in response to adenosine monophosphate treatment. *J Biotechnol* **294**, 49–57.
- 25 Fox SR, Patel UA, Yap MGS & Wang DIC (2004) Maximizing interferon-gamma production by Chinese hamster ovary cells through temperature shift optimization: experimental and modeling. *Biotechnol Bioeng* **85**, 177–84.
- 26 Hendrick V, Winnepeninckx P, Abdelkafi C, Vandeputte O, Cherlet M, Marique T, Renemann G, Loa A, Kretzmer G & Werenne J (2001) Increased productivity of recombinant tissular plasminogen activator (t-PA) by butyrate and shift of temperature: a cell cycle phases analysis. *Cytotechnology* **36**, 71–83.
- 27 Kaufmann H, Mazur X, Fussenegger M & Bailey JE (1999) Influence of low temperature on productivity, proteome and protein phosphorylation of CHO cells. *Biotechnol Bioeng* **63**, 573–82.
- 28 Pfizenmaier J, Matuszczyk J-C & Takors R (2015) Changes in intracellular ATP-content of CHO cells as response to hyperosmolality. *Biotechnol Prog* **31**, 1212–1216.
- 29 Aggeler J, Kapp LN, Tseng SC & Werb Z (1982) Regulation of protein secretion in Chinese hamster ovary cells by cell cycle position and cell density. Plasminogen activator, procollagen fibronectin. *Exp Cell Res* **139**, 275–83.
- 30 Al-Rubeai M & Emery AN (1990) Mechanisms and kinetics of monoclonal antibody synthesis and secretion in synchronous and asynchronous hybridoma cell cultures. *J*

- Biotechnol* **16**, 67–85.
- 31 Kim WH, Kim YJ & Lee GM (2014) Gadd45-induced cell cycle G2/M arrest for improved transient gene expression in Chinese hamster ovary cells. *Biotechnol Bioprocess Eng* **19**, 386–393.
- 32 Kubbies M & Stockinger H (1990) Cell cycle-dependent DHFR and t-PA production in cotransfected, MTX-amplified CHO cells revealed by dual-laser flow cytometry. *Exp Cell Res* **188**, 267–271.
- 33 Lloyd DR, Holmes P, Jackson LP, Emery AN & Al-Rubeai M (2000) Relationship between cell size, cell cycle and specific recombinant protein productivity. *Cytotechnology* **34**, 59–70.
- 34 Ginzberg MB, Kafri R & Kirschner M (2015) On being the right (cell) size. *Science (80- )* **348**, 1245075–1245075.
- 35 Jorgensen P & Tyers M (2004) How Cells Coordinate Growth and Division. *Curr Biol* **14**, R1014–R1027.
- 36 Tzur A, Kafri R, LeBleu VS, Lahav G & Kirschner MW (2009) Cell Growth and Size Homeostasis in Proliferating Animal Cells. *Science (80- )* **325**, 167–171.
- 37 Martínez VS, Dietmair S, Quek L-E, Hodson MP, Gray P & Nielsen LK (2013) Flux balance analysis of CHO cells before and after a metabolic switch from lactate production to consumption. *Biotechnol Bioeng* **110**, 660–666.
- 38 Peng R-W, Abellan E & Fussenegger M (2011) Differential effect of exocytic SNAREs on the production of recombinant proteins in mammalian cells. *Biotechnol Bioeng* **108**, 611–620.
- 39 Pieper LA, Strotbek M, Wenger T, Gamer M, Olayioye MA & Hausser A (2017) Secretory pathway optimization of CHO producer cells by co-engineering of the mitoSNA-1978 target genes CerS2 and Tbc1D20. *Metab Eng* **40**, 69–79.



- 40 Dinnis DM & James DC (2005) Engineering mammalian cell factories for improved recombinant monoclonal antibody production: lessons from nature? *Biotechnol Bioeng* **91**, 180–189.
- 41 Pourcel L, Buron F, Arib G, Le Fourn V, Regamey A, Bodenmann I, Girod P & Mermoud N (2020) Influence of cytoskeleton organization on recombinant protein expression by CHO cells. *Biotechnol Bioeng* **117**, 1117–1126.
- 42 Berger A, Le Fourn V, Masternak J, Regamey A, Bodenmann I, Girod P & Mermoud N (2020) Overexpression of transcription factor Foxa1 and target genes remediate therapeutic protein production bottlenecks in Chinese hamster ovary cells. *Biotechnol Bioeng* **117**, 1101–1116.
- 43 Campbell K, Xia J & Nielsen J (2017) The Impact of Systems Biology on Bioprocessing. *Trends Biotechnol* **35**, 1156–1168.
- 44 Verhagen N, Wijaya AW, Teleki A, Fadhlullah M, Unsöld A, Schilling M, Heinrich C & Takors R (2020) Comparison of l-tyrosine containing dipeptides reveals maximum ATP availability for l-prolyl-l-tyrosine in CHO cells. *Eng Life Sci* **20**, 384–394.
- 45 Sánchez-Kopper A, Becker M, Pfizenmaier J, Kessler C, Karau A & Takors R (2016) Tracking dipeptides at work-uptake and intracellular fate in CHO culture. *AMB Express* **6**, 48.
- 46 Berg JM, Tymoczko JL & Stryer L (2013) *Stryer Biochemie*, 7th ed. Springer Berlin Heidelberg, Berlin, Heidelberg.
- 47 Finkelstein JD (1990) Methionine metabolism in mammals. *J Nutr Biochem* **1**, 228–37.
- 48 Mato JM, Alvarez L, Ortiz P & Pajares MA (1997) S-adenosylmethionine synthesis: molecular mechanisms and clinical implications. *Pharmacol Ther* **73**, 265–80.
- 49 Ansorena E, García-Trevijano ER, Martínez-Chantar ML, Huang Z-Z, Chen L, Mato JM, Iraburu M, Lu SC & Avila MA (2002) S-adenosylmethionine and methylthioadenosine are antiapoptotic in cultured rat hepatocytes but proapoptotic in human hepatoma cells. *Hepatology* **35**, 274–280.

- 50 Wallace HM, Fraser A V & Hughes A (2003) A perspective of polyamine metabolism. *Biochem J* **376**, 1–14.
- 51 Moschou PN & Roubelakis-Angelakis KA (2014) Polyamines and programmed cell death. *J Exp Bot* **65**, 1285–1296.
- 52 Pegg AE (2016) Functions of Polyamines in Mammals. *J Biol Chem* **291**, 14904–14912.
- 53 Pohjanpelto P, Virtanen I & Hölttä E (1981) Polyamine starvation causes disappearance of actin filaments and microtubules in polyamine-auxotrophic CHO cells. *Nature* **293**, 475–477.
- 54 Anehus S, Pohjanpelto P, Baldetorp B, Långström E & Heby O (1984) Polyamine starvation prolongs the S and G2 phases of polyamine-dependent (arginase-deficient) CHO cells. *Mol Cell Biol* **4**, 915–922.
- 55 Alm K, Berntsson PSH, Kramer DL, Porter CW & Oredsson SM (2000) Treatment of cells with the polyamine analog N 1 , N 11 -diethylnorspermine retards S phase progression within one cell cycle. *Eur J Biochem* **267**, 4157–4164.
- 56 Fredlund JO & Oredsson SM (1997) Ordered Cell Cycle Phase Perturbations in Chinese Hamster Ovary Cells Treated with an S-Adenosylmethionine Decarboxylase Inhibitor. *Eur J Biochem* **249**, 232–238.
- 57 Boynton AL, Whitfield JF & Isaacs RJ (1976) A possible involvement of polyamines in the initiation of DNA synthesis by human WI-38 and mouse BALB/3T3 cells. *J Cell Physiol* **89**, 481–488.
- 58 Williams-Ashman HG, Seidenfeld J & Galletti P (1982) Trends in the biochemical pharmacology of 5'-deoxy-5'-methylthioadenosine. *Biochem Pharmacol* **31**, 277–288.
- 59 Martínez-Chantar ML, Latasa MU, Varela-Rey M, Lu SC, García-Trevijano ER, Mato JM & Avila MA (2003) L-methionine availability regulates expression of the methionine adenosyltransferase 2A gene in human hepatocarcinoma cells. Role of S-adenosylmethionine. *J Biol Chem* **278**, 19885–19890.

- 60 Lee SH & Cho YD (1998) Induction of Apoptosis in Leukemia U937 Cells by 5'-Deoxy-5'-methylthioadenosine, a Potent Inhibitor of Protein Carboxymethyltransferase. *Exp Cell Res* **240**, 282–292.
- 61 Maher PA (1993) Inhibition of the tyrosine kinase activity of the fibroblast growth factor receptor by the methyltransferase inhibitor 5'-methylthioadenosine. *J Biol Chem* **268**, 4244–9.
- 62 Riscoe MK, Tower PA & Ferro AJ (1984) Mechanism of action of 5'-methylthioadenosine in S49 cells. *Biochem Pharmacol* **33**, 3639–3643.
- 63 Oredsson SM (2003) Polyamine dependence of normal cell-cycle progression. *Biochem Soc Trans* **31**, 366–70.
- 64 Pascale RM, Simile MM, De Miglio MR & Feo F (2002) Chemoprevention of hepatocarcinogenesis. *Alcohol* **27**, 193–198.
- 65 Law RE, Stimmel JB, Damore MA, Carter C, Clarke S & Wall R (1992) Lipopolysaccharide-induced NF-kappa B activation in mouse 70Z/3 pre-B lymphocytes is inhibited by mevinolin and 5'-methylthioadenosine: roles of protein isoprenylation and carboxyl methylation reactions. *Mol Cell Biol* **12**, 103–111.
- 66 Mowen KA, Tang J, Zhu W, Schurter BT, Shuai K, Herschman HR & David M (2001) Arginine methylation of STAT1 modulates IFNalpha/beta-induced transcription. *Cell* **104**, 731–41.
- 67 (Rob) Aggarwal S (2014) What's fueling the biotech engine—2012 to 2013. *Nat Biotechnol* **32**, 32–39.
- 68 Scahill SJ, Devos R, Van der Heyden J & Fiers W (1983) Expression and characterization of the product of a human immune interferon cDNA gene in Chinese hamster ovary cells. *Proc Natl Acad Sci* **80**, 4654–4658.
- 69 McCormick F, Trahey M, Innis M, Dieckmann B & Ringold G (1984) Inducible expression of amplified human beta interferon genes in CHO cells. *Mol Cell Biol* **4**, 166–172.

- 70 Haynes J & Weissman C (1983) Constitutive, long-term production of human interferons by hamster cells containing multiple copies of a cloned interferon gene. *Nucleic Acids Res* **11**, 687–706.
- 71 Kaufman RJ & Sharp PA (1982) Amplification and expression of sequences cotransfected with a modular dihydrofolate reductase complementary DNA gene. *J Mol Biol* **159**, 601–621.
- 72 Kaufman RJ, Wasley LC, Spiliotes AJ, Gossels SD, Latt SA, Larsen GR & Kay RM (1985) Coamplification and coexpression of human tissue-type plasminogen activator and murine dihydrofolate reductase sequences in Chinese hamster ovary cells. *Mol Cell Biol* **5**, 1750–9.
- 73 Butler M & Spearman M (2014) The choice of mammalian cell host and possibilities for glycosylation engineering. *Curr Opin Biotechnol* **30**, 107–112.
- 74 Tjio JH & Puck TT (1958) Genetics of somatic mammalian cells. II. Chromosomal constitution of cells in tissue culture. *J Exp Med* **108**, 259–68.
- 75 Kao FT & Puck TT (1968) Genetics of somatic mammalian cells, VII. Induction and isolation of nutritional mutants in Chinese hamster cells. *Proc Natl Acad Sci* **60**, 1275–1281.
- 76 Urlaub G & Chasin LA (1980) Isolation of Chinese hamster cell mutants deficient in dihydrofolate reductase activity. *Proc Natl Acad Sci U S A* **77**, 4216–20.
- 77 Urlaub G, Käs E, Carothers AM & Chasin LA (1983) Deletion of the diploid dihydrofolate reductase locus from cultured mammalian cells. *Cell* **33**, 405–12.
- 78 Hamlin JL & Ma C (1990) The mammalian dihydrofolate reductase locus. *Biochim Biophys Acta - Gene Struct Expr* **1087**, 107–125.
- 79 Tabuchi H & Sugiyama T (2013) Cooverexpression of alanine aminotransferase 1 in Chinese hamster ovary cells overexpressing taurine transporter further stimulates metabolism and enhances product yield. *Biotechnol Bioeng* **110**, 2208–2215.

- 80 Jordan M, Schallhorn A & Wurm FM (1996) Transfecting mammalian cells: optimization of critical parameters affecting calcium-phosphate precipitate formation. *Nucleic Acids Res* **24**, 596–601.
- 81 Richards EJ & Elgin SCR (2002) Epigenetic Codes for Heterochromatin Formation and Silencing. *Cell* **108**, 489–500.
- 82 Mutskov V & Felsenfeld G (2004) Silencing of transgene transcription precedes methylation of promoter DNA and histone H3 lysine 9. *EMBO J* **23**, 138–149.
- 83 Wigler M, Perucho M, Kurtz D, Dana S, Pellicer A, Axel R & Silverstein S (1980) Transformation of mammalian cells with an amplifiable dominant-acting gene. *Proc Natl Acad Sci* **77**, 3567–3570.
- 84 Gandor C, Leist C, Fiechter A & Asselbergs FAM (1995) Amplification and expression of recombinant genes in serum-independent Chinese hamster ovary cells. *FEBS Lett* **377**, 290–294.
- 85 Wurm FM, Gwinn KA & Kingston RE (1986) Inducible overproduction of the mouse c-myc protein in mammalian cells. *Proc Natl Acad Sci U S A* **83**, 5414–8.
- 86 Cockett MI, Bebbington CR & Yarranton GT (1990) High Level Expression of Tissue Inhibitor of Metalloproteinases in Chinese Hamster Ovary Cells Using Glutamine Synthetase Gene Amplification. *Nat Biotechnol* **8**, 662–667.
- 87 Bebbington CR, Renner G, Thomson S, King D, Abrams D & Yarranton GT (1992) High-Level Expression of a Recombinant Antibody from Myeloma Cells Using a Glutamine Synthetase Gene as an Amplifiable Selectable Marker. *Nat Biotechnol* **10**, 169–175.
- 88 Kaufman RJ & Schimke RT (1981) Amplification and loss of dihydrofolate reductase genes in a Chinese hamster ovary cell line. *Mol Cell Biol* **1**, 1069–76.
- 89 Kaufman RJ, Sharp PA & Latt SA (1983) Evolution of chromosomal regions containing transfected and amplified dihydrofolate reductase sequences. *Mol Cell Biol* **3**, 699–711.

- 90 Davies SL, Lovelady CS, Grainger RK, Racher AJ, Young RJ & James DC (2013) Functional heterogeneity and heritability in CHO cell populations. *Biotechnol Bioeng* **110**, 260–274.
- 91 Pilbrough W, Munro TP & Gray P (2009) Intraclonal Protein Expression Heterogeneity in Recombinant CHO Cells. *PLoS One* **4**, e8432.
- 92 Vcelar S, Melcher M, Auer N, Hrdina A, Puklowski A, Leisch F, Jadhav V, Wenger T, Baumann M & Borth N (2018) Changes in Chromosome Counts and Patterns in CHO Cell Lines upon Generation of Recombinant Cell Lines and Subcloning. *Biotechnol J* **13**, e1700495.
- 93 Kim NS, Kim SJ & Lee GM (1998) Clonal variability within dihydrofolate reductase-mediated gene amplified Chinese hamster ovary cells: Stability in the absence of selective pressure. *Biotechnol Bioeng* **60**, 679–688.
- 94 Gray F, Kenney JS & Dunne JF (1995) Secretion capture and report web: use of affinity derivatized agarose microdroplets for the selection of hybridoma cells. *J Immunol Methods* **182**, 155–163.
- 95 Powell KT & Weaver JC (1990) Gel Microdroplets and Flow Cytometry: Rapid Determination of Antibody Secretion by Individual Cells Within a Cell Population. *Nat Biotechnol* **8**, 333–337.
- 96 Manz R, Assenmacher M, Pfluger E, Miltenyi S & Radbruch A (1995) Analysis and sorting of live cells according to secreted molecules, relocated to a cell-surface affinity matrix. *Proc Natl Acad Sci* **92**, 1921–1925.
- 97 Holmes P & Al-Rubeai M (1999) Improved cell line development by a high throughput affinity capture surface display technique to select for high secretors. *J Immunol Methods* **230**, 141–147.
- 98 Brezinsky SC., Chiang G., Szilvasi A, Mohan S, Shapiro R., MacLean A, Sisk W & Thill G (2003) A simple method for enriching populations of transfected CHO cells for cells of higher specific productivity. *J Immunol Methods* **277**, 141–155.

- 99 Butler M & Meneses-Acosta A (2012) Recent advances in technology supporting biopharmaceutical production from mammalian cells. *Appl Microbiol Biotechnol* **96**, 885–894.
- 100 Li F, Vijayasankaran N, Shen AY, Kiss R & Amanullah A (2010) Cell culture processes for monoclonal antibody production. *MAbs* **2**, 466–79.
- 101 Chmiel H (ed.) (2011) *Bioprozesstechnik* Spektrum Akademischer Verlag, Heidelberg.
- 102 Wlaschin KF & Hu W-S (2007) Engineering cell metabolism for high-density cell culture via manipulation of sugar transport. *J Biotechnol* **131**, 168–176.
- 103 Lao M-S & Toth D (1997) Effects of Ammonium and Lactate on Growth and Metabolism of a Recombinant Chinese Hamster Ovary Cell Culture. *Biotechnol Prog* **13**, 688–691.
- 104 Yang M & Butler M (2000) Effects of ammonia on CHO cell growth, erythropoietin production, and glycosylation. *Biotechnol Bioeng* **68**, 370–380.
- 105 Pereira S, Kildegaard HF & Andersen MR (2018) Impact of CHO Metabolism on Cell Growth and Protein Production: An Overview of Toxic and Inhibiting Metabolites and Nutrients. *Biotechnol J* **13**, e1700499.
- 106 Ma N, Ellet J, Okediadi C, Hermes P, McCormick E & Casnocha S (2009) A single nutrient feed supports both chemically defined NS0 and CHO fed-batch processes: Improved productivity and lactate metabolism. *Biotechnol Prog* **25**, 1353–1363.
- 107 Le H, Kabbur S, Pollastrini L, Sun Z, Mills K, Johnson K, Karypis G & Hu W-S (2012) Multivariate analysis of cell culture bioprocess data—Lactate consumption as process indicator. *J Biotechnol* **162**, 210–223.
- 108 Chen P & Harcum SW (2006) Effects of elevated ammonium on glycosylation gene expression in CHO cells. *Metab Eng* **8**, 123–32.
- 109 Schmid G, Wilke CR & Blanch HW (1992) Continuous hybridoma suspension cultures with and without cell retention: kinetics of growth, metabolism and product formation.

- J Biotechnol* **26**, 343.
- 110 Butler M, Imamura T, Thomas J & Thilly WG (1983) High yields from microcarrier cultures by medium perfusion. *J Cell Sci* **61**, 351–63.
- 111 Hiller GW, Clark DS & Blanch HW (1993) Cell retention-chemostat studies of hybridoma cells-analysis of hybridoma growth and metabolism in continuous suspension culture in serum-free medium. *Biotechnol Bioeng* **42**, 185–95.
- 112 Xing Z, Kenty BM, Li ZJ & Lee SS (2009) Scale-up analysis for a CHO cell culture process in large-scale bioreactors. *Biotechnol Bioeng* **103**, 733–746.
- 113 Kimura R & Miller WM (1996) Effects of elevated pCO<sub>2</sub> and/or osmolality on the growth and recombinant tPA production of CHO cells. *Biotechnol Bioeng* **52**, 152–160.
- 114 Zhu MM, Goyal A, Rank DL, Gupta SK, Boom T Vanden & Lee SS (2008) Effects of Elevated pCO<sub>2</sub> and Osmolality on Growth of CHO Cells and Production of Antibody-Fusion Protein B1: A Case Study. *Biotechnol Prog* **21**, 70–77.
- 115 O'Connor KC & Papoutsakis ET (1992) Agitation effects on microcarrier and suspension CHO cells. *Biotechnol Tech* **6**, 323–328.
- 116 Chen A, Chitta R, Chang D & Amanullah A (2009) Twenty-four well plate miniature bioreactor system as a scale-down model for cell culture process development. *Biotechnol Bioeng* **102**, 148–160.
- 117 Janakiraman V, Kwiatkowski C, Kshirsagar R, Ryll T & Huang Y-M (2015) Application of high-throughput mini-bioreactor system for systematic scale-down modeling, process characterization, and control strategy development. *Biotechnol Prog* **31**, 1623–1632.
- 118 Legmann R, Schreyer HB, Combs RG, McCormick EL, Russo AP & Rodgers ST (2009) A predictive high-throughput scale-down model of monoclonal antibody production in CHO cells. *Biotechnol Bioeng* **104**, 1107–1120.



- 119 Restelli V, Wang M-D, Huzel N, Ethier M, Perreault H & Butler M (2006) The effect of dissolved oxygen on the production and the glycosylation profile of recombinant human erythropoietin produced from CHO cells. *Biotechnol Bioeng* **94**, 481–494.
- 120 Dreesen IAJ & Fussenegger M (2011) Ectopic expression of human mTOR increases viability, robustness, cell size, proliferation, and antibody production of chinese hamster ovary cells. *Biotechnol Bioeng* **108**, 853–866.
- 121 Fussenegger M, Mazur X & Bailey JE (1997) A novel cytostatic process enhances the productivity of Chinese hamster ovary cells. *Biotechnol Bioeng* **55**, 927–39.
- 122 Mazur X, Fussenegger M, Renner WA & Bailey JE (1998) Higher Productivity of Growth-Arrested Chinese Hamster Ovary Cells Expressing the Cyclin-Dependent Kinase Inhibitor p27. *Biotechnol Prog* **14**, 705–713.
- 123 Gorman CM, Howard BH & Reeves R (1983) Expression of recombinant plasmids in mammalian cells is enhanced by sodium butyrate. *Nucleic Acids Res* **11**, 7631–7648.
- 124 Yoon SK, Hwang SO & Lee GM (2004) Enhancing Effect of Low Culture Temperature on Specific Antibody Productivity of Recombinant Chinese Hamster Ovary Cells: Clonal Variation. *Biotechnol Prog* **20**, 1683–1688.
- 125 Jefferis R (2008) Glycosylation of Recombinant Antibody Therapeutics. *Biotechnol Prog* **21**, 11–16.
- 126 Natsume A, Niwa R & Satoh M (2009) Improving effector functions of antibodies for cancer treatment: Enhancing ADCC and CDC. *Drug Des Devel Ther* **3**, 7–16.
- 127 Walsh G & Jefferis R (2006) Post-translational modifications in the context of therapeutic proteins. *Nat Biotechnol* **24**, 1241–1252.
- 128 Nezlin R & Ghetie V (2004) Interactions of Immunoglobulins Outside the Antigen-Combining Site. In *Advances in Immunology* pp. 155–215.

- 129 Youings A, Chang SC, Dwek RA & Scragg IG (1996) Site-specific glycosylation of human immunoglobulin G is altered in four rheumatoid arthritis patients. *Biochem J* **314** ( Pt 2, 621–30.
- 130 Jacobs PP & Callewaert N (2009) N-glycosylation engineering of biopharmaceutical expression systems. *Curr Mol Med* **9**, 774–800.
- 131 Bosques CJ, Collins BE, Meador JW, Sarvaiya H, Murphy JL, DelloRusso G, Bulik DA, Hsu I-H, Washburn N, Sipsey SF, Myette JR, Raman R, Shriver Z, Sasisekharan R & Venkataraman G (2010) Chinese hamster ovary cells can produce galactose- $\alpha$ -1,3-galactose antigens on proteins. *Nat Biotechnol* **28**, 1153–1156.
- 132 Larsen RD, Rivera-Marrero CA, Ernst LK, Cummings RD & Lowe JB (1990) Frameshift and nonsense mutations in a human genomic sequence homologous to a murine UDP-Gal:beta-D-Gal(1,4)-D-GlcNAc alpha(1,3)-galactosyltransferase cDNA. *J Biol Chem* **265**, 7055–61.
- 133 Lee EU, Roth J & Paulson JC (1989) Alteration of terminal glycosylation sequences on N-linked oligosaccharides of Chinese hamster ovary cells by expression of beta-galactoside alpha 2,6-sialyltransferase. *J Biol Chem* **264**, 13848–55.
- 134 Campbell C & Stanley P (1983) Regulatory mutations in CHO cells induce expression of the mouse embryonic antigen SSEA-1. *Cell* **35**, 303–309.
- 135 Walsh G (2010) Post-translational modifications of protein biopharmaceuticals. *Drug Discov Today* **15**, 773–780.
- 136 Feige MJ & Hendershot LM (2011) Disulfide bonds in ER protein folding and homeostasis. *Curr Opin Cell Biol* **23**, 167–175.
- 137 Hossler P, Khattak SF & Li ZJ (2009) Optimal and consistent protein glycosylation in mammalian cell culture. *Glycobiology* **19**, 936–49.
- 138 Ceaglio N, Etcheverrigaray M, Kratje R & Oggero M (2008) Novel long-lasting interferon alpha derivatives designed by glycoengineering. *Biochimie* **90**, 437–449.

- 139 Umaña P, Jean-Mairet J, Moudry R, Amstutz H & Bailey JE (1999) Engineered glycoforms of an antineuroblastoma IgG1 with optimized antibody-dependent cellular cytotoxic activity. *Nat Biotechnol* **17**, 176–80.
- 140 Davies J, Jiang L, Pan L-Z, LaBarre MJ, Anderson D & Reff M (2001) Expression of GnTIII in a recombinant anti-CD20 CHO production cell line: Expression of antibodies with altered glycoforms leads to an increase in ADCC through higher affinity for FC $\gamma$ RIII. *Biotechnol Bioeng* **74**, 288–294.
- 141 Yamane-Ohnuki N, Kinoshita S, Inoue-Urakubo M, Kusunoki M, Iida S, Nakano R, Wakitani M, Niwa R, Sakurada M, Uchida K, Shitara K & Satoh M (2004) Establishment of FUT8 knockout Chinese hamster ovary cells: an ideal host cell line for producing completely defucosylated antibodies with enhanced antibody-dependent cellular cytotoxicity. *Biotechnol Bioeng* **87**, 614–22.
- 142 Mori K, Kuni-Kamochi R, Yamane-Ohnuki N, Wakitani M, Yamano K, Imai H, Kanda Y, Niwa R, Iida S, Uchida K, Shitara K & Satoh M (2004) Engineering Chinese hamster ovary cells to maximize effector function of produced antibodies using FUT8 siRNA. *Biotechnol Bioeng* **88**, 901–8.
- 143 Chenu S, Grégoire A, Malykh Y, Visvikis A, Monaco L, Shaw L, Schauer R, Marc A & Goergen J-L (2003) Reduction of CMP-N-acetylneuraminic acid hydroxylase activity in engineered Chinese hamster ovary cells using an antisense-RNA strategy. *Biochim Biophys Acta - Gen Subj* **1622**, 133–144.
- 144 Borys MC, Dalal NG, Abu-Absi NR, Khattak SF, Jing Y, Xing Z & Li ZJ (2010) Effects of culture conditions on N-glycolylneuraminic acid (Neu5Gc) content of a recombinant fusion protein produced in CHO cells. *Biotechnol Bioeng* **105**, n/a-n/a.
- 145 Kumar V, Abbas AK, Aster JC & Robbins SL (2012) *Robbins basic pathology*, 9th ed Elsevier/Saunders, Philadelphia, PA.

- 146 Norbury C & Nurse P (1992) Animal Cell Cycles and Their Control. *Annu Rev Biochem* **61**, 441–468.
- 147 Bertoli C, Skotheim JM & de Bruin RAM (2013) Control of cell cycle transcription during G1 and S phases. *Nat Rev Mol Cell Biol* **14**, 518–528.
- 148 Coutts AS & Weston L (eds.) (2016) *Cell Cycle Oscillators*, 1st ed. Springer New York, New York, NY.
- 149 Stark GR & Taylor WR (2006) Control of the G2/M transition. *Mol Biotechnol* **32**, 227–48.
- 150 Morgan DO (1995) Principles of CDK regulation. *Nature* **374**, 131–4.
- 151 Vermeulen K, Van Bockstaele DR & Berneman ZN (2003) The cell cycle: a review of regulation, deregulation and therapeutic targets in cancer. *Cell Prolif* **36**, 131–49.
- 152 Ma HT & Poon RYC (2011) How protein kinases co-ordinate mitosis in animal cells. *Biochem J* **435**, 17–31.
- 153 He G, Siddik ZH, Huang Z, Wang R, Koomen J, Kobayashi R, Khokhar AR & Kuang J (2005) Induction of p21 by p53 following DNA damage inhibits both Cdk4 and Cdk2 activities. *Oncogene* **24**, 2929–2943.
- 154 Buselmaier W (2007) *Biologie für Mediziner* Springer Berlin Heidelberg.
- 155 Nigg EA (2001) Mitotic kinases as regulators of cell division and its checkpoints. *Nat Rev Mol Cell Biol* **2**, 21–32.
- 156 Renner WA, Lee KH, Hatzimanikatis V, Bailey JE & Eppenberger HM (1995) Recombinant cyclin E expression activates proliferation and obviates surface attachment of chinese hamster ovary (CHO) cells in protein-free medium. *Biotechnol Bioeng* **47**, 476–482.
- 157 Carvalhal A V., Marcelino I & Carrondo MJT (2003) Metabolic changes during cell growth inhibition by p27 overexpression. *Appl Microbiol Biotechnol* **63**, 164–173.
- 158 Arden N & Betenbaugh MJ (2004) Life and death in mammalian cell culture: strategies for apoptosis inhibition. *Trends Biotechnol* **22**, 174–180.

- 159 Krampe B & Al-Rubeai M (2010) Cell death in mammalian cell culture: molecular mechanisms and cell line engineering strategies. *Cytotechnology* **62**, 175–88.
- 160 Sunstrom N-AS, Gay RD, Wong DC, Kitchen NA, DeBoer L & Gray PP (2000) Insulin-Like Growth Factor-I and Transferrin Mediate Growth and Survival of Chinese Hamster Ovary Cells. *Biotechnol Prog* **16**, 698–702.
- 161 Zanghi JA, Renner WA, Bailey JE & Fussenegger M (2000) The Growth Factor Inhibitor Suramin Reduces Apoptosis and Cell Aggregation in Protein-Free CHO Cell Batch Cultures. *Biotechnol Prog* **16**, 319–325.
- 162 Chang KH, Kim KS & Kim JH (1999) N-acetylcysteine increases the biosynthesis of recombinant EPO in apoptotic Chinese hamster ovary cells. *Free Radic Res* **30**, 85–91.
- 163 Oh HK, So MK, Yang J, Yoon HC, Ahn JS, Lee JM, Kim JT, Yoo JU & Byun TH (2008) Effect of N-Acetylcystein on Butyrate-Treated Chinese Hamster Ovary Cells To Improve the Production of Recombinant Human Interferon- $\beta$ -1a. *Biotechnol Prog* **21**, 1154–1164.
- 164 Cost GJ, Freyvert Y, Vafiadis A, Santiago Y, Miller JC, Rebar E, Collingwood TN, Snowden A & Gregory PD (2010) BAK and BAX deletion using zinc-finger nucleases yields apoptosis-resistant CHO cells. *Biotechnol Bioeng* **105**, 330–340.
- 165 Meents H, Enenkel B, Eppenberger HM, Werner RG & Fussenegger M (2002) Impact of coexpression and coamplification of sICAM and antiapoptosis determinants bcl-2/bcl-x(L) on productivity, cell survival, and mitochondria number in CHO-DG44 grown in suspension and serum-free media. *Biotechnol Bioeng* **80**, 706–16.
- 166 Becker J, Hackl M, Rupp O, Jakobi T, Schneider J, Szczepanowski R, Bekel T, Borth N, Goesmann A, Grillari J, Kaltschmidt C, Noll T, Pühler A, Tauch A & Brinkrolf K (2011) Unraveling the Chinese hamster ovary cell line transcriptome by next-generation sequencing. *J Biotechnol* **156**, 227–235.
- 167 Hammond S, Swanberg JC, Kaplarevic M & Lee KH (2011) Genomic sequencing and analysis of a Chinese hamster ovary cell line using Illumina sequencing technology. *BMC*

*Genomics* **12**, 67.

- 168 Le H, Chen C & Goudar CT (2015) An evaluation of public genomic references for mapping RNA-Seq data from Chinese hamster ovary cells. *Biotechnol Bioeng* **112**, 2412–2416.
- 169 Rupp O, Becker J, Brinkrolf K, Timmermann C, Borth N, Pühler A, Noll T & Goesmann A (2014) Construction of a Public CHO Cell Line Transcript Database Using Versatile Bioinformatics Analysis Pipelines. *PLoS One* **9**, e85568.
- 170 Charaniya S, Karypis G & Hu W-S (2009) Mining transcriptome data for function-trait relationship of hyper productivity of recombinant antibody. *Biotechnol Bioeng* **102**, 1654–1669.
- 171 Kantardjieff A, Jacob NM, Yee JC, Epstein E, Kok Y-J, Philp R, Betenbaugh M & Hu W-S (2010) Transcriptome and proteome analysis of Chinese hamster ovary cells under low temperature and butyrate treatment. *J Biotechnol* **145**, 143–159.
- 172 Fomina-Yadlin D, Mujacic M, Maggiora K, Quesnell G, Saleem R & McGrew JT (2015) Transcriptome analysis of a CHO cell line expressing a recombinant therapeutic protein treated with inducers of protein expression. *J Biotechnol* **212**, 106–115.
- 173 Pan X, Alsayyari AA, Dalm C, Hageman JA, Wijffels RH, Martens DE, Wijffels H, Martens DE, Wijffels RH, Martens DE, Wijffels H, Martens DE, Wijffels RH, Martens DE, Wijffels H, Martens DE, Wijffels RH, Martens DE, Wijffels H, Martens DE, Wijffels RH & Martens DE (2019) Transcriptome Analysis of CHO Cell Size Increase During a Fed-Batch Process. *Biotechnol J* **14**, 1–12.
- 174 Capella Roca B, Doolan P, Barron N, O’Neill F & Clynes M (2020) Altered gene expression in CHO cells following polyamine starvation. *Biotechnol Lett* **42**, 927–936.
- 175 Shen D, Kiehl TR, Khattak SF, Li ZJ, He A, Kayne PS, Patel V, Neuhaus IM & Sharfstein ST (2010) Transcriptomic responses to sodium chloride-induced osmotic stress: A study of industrial fed-batch CHO cell cultures. *Biotechnol Prog* **26**, NA-NA.

- 176 Doolan P, Meleady P, Barron N, Henry M, Gallagher R, Gammell P, Melville M, Sinacore M, McCarthy K, Leonard M, Charlebois T & Clynes M (2010) Microarray and proteomics expression profiling identifies several candidates, including the valosin-containing protein (VCP), involved in regulating high cellular growth rate in production CHO cell lines. *Biotechnol Bioeng* **106**, n/a-n/a.
- 177 Nissom PM, Sanny A, Kok YJ, Hiang YT, Chuah SH, Shing TK, Lee YY, Wong KTK, Hu W, Sim MYG & Philp R (2006) Transcriptome and Proteome Profiling to Understanding the Biology of High Productivity CHO Cells. *Mol Biotechnol* **34**, 125–140.
- 178 Jamnikar U, Nikolic P, Belic A, Blas M, Gaser D, Francky A, Laux H, Blejec A, Baebler S & Gruden K (2015) Transcriptome study and identification of potential marker genes related to the stable expression of recombinant proteins in CHO clones. *BMC Biotechnol* **15**, 98.
- 179 Baek E, Lee JS & Lee GM (2018) Untangling the mechanism of 3-methyladenine (3-MA) in enhancing the specific productivity: Transcriptome analysis of recombinant CHO cells treated with 3-MA. *Biotechnol Bioeng*, 0–2.
- 180 Hudder A, Nathanson L & Deutscher MP (2003) Organization of Mammalian Cytoplasm. *Mol Cell Biol* **23**, 9318–9326.
- 181 Ross JL, Ali MY & Warshaw DM (2008) Cargo transport: molecular motors navigate a complex cytoskeleton. *Curr Opin Cell Biol* **20**, 41–47.
- 182 Paavilainen VO, Bertling E, Falck S & Lappalainen P (2004) Regulation of cytoskeletal dynamics by actin-monomer-binding proteins. *Trends Cell Biol* **14**, 386–394.
- 183 Stamnes M (2002) Regulating the actin cytoskeleton during vesicular transport. *Curr Opin Cell Biol* **14**, 428–433.
- 184 Dinnis DM, Stansfield SH, Schlatter S, Smales CM, Alete D, Birch JR, Racher AJ, Marshall CT, Nielsen LK & James DC (2006) Functional proteomic analysis of GS-NS0 murine myeloma cell lines with varying recombinant monoclonal antibody production rate.

- Biotechnol Bioeng* **94**, 830–841.
- 185 Chung JY, Lim SW, Hong YJ, Hwang SO & Lee GM (2004) Effect of doxycycline-regulated calnexin and calreticulin expression on specific thrombopoietin productivity of recombinant chinese hamster ovary cells. *Biotechnol Bioeng* **85**, 539–546.
- 186 Peng R-W & Fussenegger M (2009) Molecular engineering of exocytic vesicle traffic enhances the productivity of Chinese hamster ovary cells. *Biotechnol Bioeng* **102**, 1170–1181.
- 187 Pieper LA, Strotbek M, Wenger T, Olayioye MA & Hausser A (2017) ATF6 $\beta$ -based fine-tuning of the unfolded protein response enhances therapeutic antibody productivity of Chinese hamster ovary cells. *Biotechnol Bioeng* **114**, 1310–1318.
- 188 Passarella S, Atlante A, Valenti D & de Bari L (2003) The role of mitochondrial transport in energy metabolism. *Mitochondrion* **2**, 319–343.
- 189 Carinhas N, Duarte TM, Barreiro LC, Carrondo MJT, Alves PM & Teixeira AP (2013) Metabolic signatures of GS-CHO cell clones associated with butyrate treatment and culture phase transition. *Biotechnol Bioeng* **110**, 3244–3257.
- 190 Templeton N, Dean J, Reddy P & Young JD (2013) Peak antibody production is associated with increased oxidative metabolism in an industrially relevant fed-batch CHO cell culture. *Biotechnol Bioeng* **110**, 2013–24.
- 191 Warburg O (1956) On the Origin of Cancer Cells. *Science (80- )* **123**, 309–314.
- 192 Hartley F, Walker T, Chung V & Morten K (2018) Mechanisms driving the lactate switch in Chinese hamster ovary cells. *Biotechnol Bioeng* **115**, 1890–1903.
- 193 Xu S, Jiang R, Mueller R, Hoesli N, Kretz T, Bowers J & Chen H (2018) Probing lactate metabolism variations in large-scale bioreactors. *Biotechnol Prog* **34**, 756–766.
- 194 Mulukutla BC, Yongky A, Grimm S, Daoutidis P & Hu W-S (2015) Multiplicity of steady states in glycolysis and shift of metabolic state in cultured mammalian cells. *PLoS One*



- 10**, e0121561.
- 195 Mulukutla BC, Gramer M & Hu W-S (2012) On metabolic shift to lactate consumption in fed-batch culture of mammalian cells. *Metab Eng* **14**, 138–49.
- 196 Zagari F, Jordan M, Stettler M, Broly H & Wurm FM (2013) Lactate metabolism shift in CHO cell culture: the role of mitochondrial oxidative activity. *N Biotechnol* **30**, 238–45.
- 197 Glacken MW (1988) Catabolic Control of Mammalian Cell Culture. *Nat Biotechnol* **6**, 1041–1050.
- 198 Donnelly M & Scheffler IE (1976) Energy metabolism in respiration-deficient and wild type chinese hamster fibroblasts in culture. *J Cell Physiol* **89**, 39–51.
- 199 Neermann J & Wagner R (1996) Comparative analysis of glucose and glutamine metabolism in transformed mammalian cell lines, insect and primary liver cells. *J Cell Physiol* **166**, 152–169.
- 200 Mitchell P (1961) Coupling of phosphorylation to electron and hydrogen transfer by a chemi-osmotic type of mechanism. *Nature* **191**, 144–8.
- 201 Hinkle PC (2005) P/O ratios of mitochondrial oxidative phosphorylation. *Biochim Biophys Acta - Bioenerg* **1706**, 1–11.
- 202 Nath S & Villadsen J (2015) Oxidative phosphorylation revisited. *Biotechnol Bioeng* **112**, 429–437.
- 203 Fang J, Hsu BYL, MacMullen CM, Poncz M, Smith TJ & Stanley CA (2002) Expression, purification and characterization of human glutamate dehydrogenase (GDH) allosteric regulatory mutations. *Biochem J* **363**, 81–7.
- 204 Frieden C (1965) Glutamate Dehydrogenase. VI. Survey of Purine Nucleotide and Other Effects on the Enzyme from Various Sources. *J Biol Chem* **240**, 2028–35.
- 205 Herzig S & Shaw RJ (2018) AMPK: guardian of metabolism and mitochondrial homeostasis. *Nat Rev Mol Cell Biol* **19**, 121–135.

- 206 Carling D, Zammit VA & Hardie DG (1987) A common bicyclic protein kinase cascade inactivates the regulatory enzymes of fatty acid and cholesterol biosynthesis. *FEBS Lett* **223**, 217–222.
- 207 Carling D (2004) The AMP-activated protein kinase cascade – a unifying system for energy control. *Trends Biochem Sci* **29**, 18–24.
- 208 Corton JM, Gillespie JG & Hardie DG (1994) Role of the AMP-activated protein kinase in the cellular stress response. *Curr Biol* **4**, 315–324.
- 209 Gwinn DM, Shackelford DB, Egan DF, Mihaylova MM, Mery A, Vasquez DS, Turk BE & Shaw RJ (2008) AMPK Phosphorylation of Raptor Mediates a Metabolic Checkpoint. *Mol Cell* **30**, 214–226.
- 210 Marsin A-S, Bertrand<sup>†</sup> L, Rider MH, Deprez J, Beauloye C, Vincent<sup>‡</sup> MF, Van den Berghe<sup>‡</sup> G, Carling D & Hue L (2000) Phosphorylation and activation of heart PFK-2 by AMPK has a role in the stimulation of glycolysis during ischaemia. *Curr Biol* **10**, 1247–1255.
- 211 Mihaylova MM, Vasquez DS, Ravnskjaer K, Denechaud P-D, Yu RT, Alvarez JG, Downes M, Evans RM, Montminy M & Shaw RJ (2011) Class IIa Histone Deacetylases Are Hormone-Activated Regulators of FOXO and Mammalian Glucose Homeostasis. *Cell* **145**, 607–621.
- 212 Bungard D, Fuerth BJ, Zeng P-Y, Faubert B, Maas NL, Viollet B, Carling D, Thompson CB, Jones RG & Berger SL (2010) Signaling Kinase AMPK Activates Stress-Promoted Transcription via Histone H2B Phosphorylation. *Science (80- )* **329**, 1201–1205.
- 213 Vander Heiden MG, Cantley LC & Thompson CB (2009) Understanding the Warburg effect: the metabolic requirements of cell proliferation. *Science* **324**, 1029–33.
- 214 Pegg AE (2009) Mammalian polyamine metabolism and function. *IUBMB Life* **61**, 880–894.
- 215 Nitta T, Igarashi K & Yamamoto N (2002) Polyamine Depletion Induces Apoptosis through Mitochondria-Mediated Pathway. *Exp Cell Res* **276**, 120–128.

- 216 Schuber F (1989) Influence of polyamines on membrane functions. *Biochem J* **260**, 1–10.
- 217 Bettuzzi S, Davalli P, Astancolle S, Pinna C, Roncaglia R, Boraldi F, Tiozzo R, Sharrard M & Corti A (1999) Coordinate changes of polyamine metabolism regulatory proteins during the cell cycle of normal human dermal fibroblasts. *FEBS Lett* **446**, 18–22.
- 218 Kramer DL, Chang BD, Chen Y, Diegelman P, Alm K, Black AR, Roninson IB & Porter CW (2001) Polyamine depletion in human melanoma cells leads to G1 arrest associated with induction of p21WAF1/CIP1/SDI1, changes in the expression of p21-regulated genes, and a senescence-like phenotype. *Cancer Res* **61**, 7754–62.
- 219 Morgan JE, Blankenship JW & Matthews HR (1987) Polyamines and acetylpolyamines increase the stability and alter the conformation of nucleosome core particles. *Biochemistry* **26**, 3643–3649.
- 220 Lu SC (2000) S-Adenosylmethionine. *Int J Biochem Cell Biol* **32**, 391–395.
- 221 Avila MAMA, García-Trevijano ER, Lu SC, Corrales FJ, Mato JM, García-Trevijano ER, Lu SC, Corrales FJ & Mato JM (2004) Methylthioadenosine. *Int J Biochem Cell Biol* **36**, 2125–2130.
- 222 Cantoni GL (1951) Methylation of nicotinamide with soluble enzyme system from rat liver. *J Biol Chem* **189**, 203–16.
- 223 Finkelstein JD & Martin JJ (1986) Methionine metabolism in mammals. Adaptation to methionine excess. *J Biol Chem* **261**, 1582–7.
- 224 Lu S (1998) Regulation of Hepatic Glutathione Synthesis. *Semin Liver Dis* **18**, 331–343.
- 225 Cai J, Mao Z, Hwang JJ & Lu SC (1998) Differential expression of methionine adenosyltransferase genes influences the rate of growth of human hepatocellular carcinoma cells. *Cancer Res* **58**, 1444–50.
- 226 Pascale RM, Simile MM, Seddaiu MA, Daino L, Vinci MA, Pinna G, Bennati S, Gaspa L & Feo F (1993) Chemoprevention of rat liver carcinogenesis by S-adenosyl-L-methionine:

- is DNA methylation involved? *Basic Life Sci* **61**, 219–237.
- 227 Pegg AE (1988) Polyamine metabolism and its importance in neoplastic growth and a target for chemotherapy. *Cancer Res* **48**, 759–74.
- 228 Hibasami H, Borchardt RT, Chen SY, Coward JK & Pegg AE (1980) Studies of inhibition of rat spermidine synthase and spermine synthase. *Biochem J* **187**, 419–428.
- 229 Alm K & Oredsson SM (2000) The Organization of Replicon Clusters Is Not Affected by Polyamine Depletion. *J Struct Biol* **131**, 1–9.
- 230 Wojtowicz W & Mlynarz P (2016) Metabolomics and fluxomics in biotechnology: current trends. *BioTechnologia* **2**, 137–144.
- 231 Stephanopoulos G (1999) Metabolic Fluxes and Metabolic Engineering. *Metab Eng* **1**, 1–11.
- 232 Dickson AJ (2014) Enhancement of production of protein biopharmaceuticals by mammalian cell cultures: the metabolomics perspective. *Curr Opin Biotechnol* **30**, 73–79.
- 233 Nyberg GB, Balcarcel RR, Follstad BD, Stephanopoulos G & Wang DI (1999) Metabolism of peptide amino acids by Chinese hamster ovary cells grown in a complex medium. *Biotechnol Bioeng* **62**, 324–35.
- 234 Ahn WS & Antoniewicz MR (2013) Parallel labeling experiments with [1,2-(13)C]glucose and [U-(13)C]glutamine provide new insights into CHO cell metabolism. *Metab Eng* **15**, 34–47.
- 235 Crown SB & Antoniewicz MR (2013) Parallel labeling experiments and metabolic flux analysis: Past, present and future methodologies. *Metab Eng* **16**, 21–32.
- 236 Winter G & Krömer JO (2013) Fluxomics - connecting 'omics analysis and phenotypes. *Environ Microbiol* **15**, 1901–1916.

- 237 Selvarasu S, Ho YS, Chong WPK, Wong NSC, Yusufi FNK, Lee YY, Yap MGS & Lee D-Y (2012) Combined in silico modeling and metabolomics analysis to characterize fed-batch CHO cell culture. *Biotechnol Bioeng* **109**, 1415–1429.
- 238 Chong WPK, Goh LT, Reddy SG, Yusufi FNK, Lee DY, Wong NSC, Heng CK, Yap MGS & Ho YS (2009) Metabolomics profiling of extracellular metabolites in recombinant Chinese Hamster Ovary fed-batch culture. *Rapid Commun Mass Spectrom* **23**, 3763–3771.
- 239 Sellick CA, Croxford AS, Maqsood AR, Stephens GM, Westerhoff H V., Goodacre R & Dickson AJ (2015) Metabolite profiling of CHO cells: Molecular reflections of bioprocessing effectiveness. *Biotechnol J* **10**, 1434–1445.
- 240 Dietmair S, Timmins NE, Gray PP, Nielsen LK & Krömer JO (2010) Towards quantitative metabolomics of mammalian cells: Development of a metabolite extraction protocol. *Anal Biochem* **404**, 155–164.
- 241 Vuckovic D (2012) Current trends and challenges in sample preparation for global metabolomics using liquid chromatography–mass spectrometry. *Anal Bioanal Chem* **403**, 1523–1548.
- 242 Yamamoto K & Niwa A (1993) Amino acid and vitamin requirements in mammalian cultured cells. *Amino Acids* **5**, 1–16.
- 243 Eagle H (1955) Nutrition Needs of Mammalian Cells in Tissue Culture. *Science (80- )* **122**, 501–504.
- 244 Eagle H (1955) The minimum vitamin requirements of the L and HeLa cells in tissue culture, the production of specific vitamin deficiencies, and their cure. *J Exp Med* **102**, 595–600.
- 245 Eagle H (1959) Amino acid metabolism in mammalian cell cultures. *Science* **130**, 432–7.
- 246 Ehrensvar G, Fischer A & Stjernholm R (1949) Protein metabolism of tissue cells in vitro; the chemical nature of some obligate factors of tissue cell nutrition. *Acta Physiol Scand* **18**, 218–30.

- 247 Gstraunthaler G (2003) Alternatives to the use of fetal bovine serum: serum-free cell culture. *ALTEX* **20**, 275–81.
- 248 van der Valk J, Brunner D, De Smet K, Fex Svenningsen Å, Honegger P, Knudsen LE, Lindl T, Noraberg J, Price A, Scarino ML & Gstraunthaler G (2010) Optimization of chemically defined cell culture media – Replacing fetal bovine serum in mammalian in vitro methods. *Toxicol Vitro* **24**, 1053–1063.
- 249 Murakami H, Masui H, Sato GH, Sueoka N, Chow TP & Kano-Sueoka T (1982) Growth of hybridoma cells in serum-free medium: ethanolamine is an essential component. *Proc Natl Acad Sci U S A* **79**, 1158–62.
- 250 Pumper RW (1958) Adaptation of tissue culture cells to a serum-free medium. *Science* **128**, 363.
- 251 Bottenstein JE & Sato GH (1979) Growth of a rat neuroblastoma cell line in serum-free supplemented medium. *Proc Natl Acad Sci* **76**, 514–517.
- 252 Hayashi I & Sato GH (1976) Replacement of serum by hormones permits growth of cells in a defined medium. *Nature* **259**, 132–4.
- 253 Ham RG (1965) Clonal Growth of Mammalian Cells in a Chemically Defined, Synthetic Medium. *Proc Natl Acad Sci U S A* **53**, 288–93.
- 254 Keen MJ & Rapson NT (1995) Development of a serum-free culture medium for the large scale production of recombinant protein from a Chinese hamster ovary cell line. *Cytotechnology* **17**, 153–63.
- 255 Zang M, Trautmann H, Gandor C, Messi F, Asselbergs F, Leist C, Fiechter A & Reiser J (1995) Production of Recombinant Proteins in Chinese Hamster Ovary Cells Using A Protein-Free Cell Culture Medium. *Nat Biotechnol* **13**, 389–392.
- 256 Fletcher T (2005) Designing Culture Media for Recombinant Protein Production A Rational Approach. *Bioprocess Int* **January**, 2–6.

- 257 Xie L & Wang DIC (1994) Stoichiometric analysis of animal cell growth and its application in medium design. *Biotechnol Bioeng* **43**, 1164–1174.
- 258 Castro PL, Hayter P, Ison A & Bull A (1992) Application of a statistical design to the optimization of culture medium for recombinant interferon-gamma production by Chinese hamster ovary cells. *Appl Microbiol Biotechnol* **38**, 84–90.
- 259 Reinhart D, Damjanovic L, Kaisermayer C & Kunert R (2015) Benchmarking of commercially available CHO cell culture media for antibody production. *Appl Microbiol Biotechnol* **99**, 4645–4657.
- 260 Floris P, McGillicuddy N, Morrissey B, Albrecht S, Kaisermayer C, Hawe D, Riordan L, Lindeberg A, Forestell S & Bones J (2019) A LC–MS/MS platform for the identification of productivity markers in industrial mammalian cell culture media. *Process Biochem* **86**, 136–143.
- 261 Atanassov CL, Seiler N & Rebel G (1998) Reduction of ammonia formation in cell cultures by l-alanyl-l-glutamine requires optimization of the dipeptide concentration. *J Biotechnol* **62**, 159–162.
- 262 Imamoto Y, Tanaka H, Takahashi K, Konno Y & Suzawa T (2013) Advantages of AlaGln as an additive to cell culture medium: use with anti-CD20 chimeric antibody-producing POTELLIGENT™ CHO cell lines. *Cytotechnology* **65**, 135–43.
- 263 Franek F, Eckschlager T & Katinger H (2003) Enhancement of Monoclonal Antibody Production by Lysine-Containing Peptides. *Biotechnol Prog* **19**, 169–174.
- 264 Franěk F & Šrámková K (1996) Protection of B lymphocyte hybridoma against starvation-induced apoptosis: survival-signal role of some amino acids. *Immunol Lett* **52**, 139–144.
- 265 Franek F & Katinger H (2002) Specific Effects of Synthetic Oligopeptides on Cultured Animal Cells. *Biotechnol Prog* **18**, 155–158.
- 266 Rubio-Aliaga I & Daniel H (2008) Peptide transporters and their roles in physiological processes and drug disposition. *Xenobiotica* **38**, 1022–1042.

- 267 Menvielle JP, Safini N, Tisminetzky SG & Skoko N (2013) Dual Role of Dextran Sulfate 5000 Da as Anti-Apoptotic and Pro-Autophagy Agent. *Mol Biotechnol* **54**, 711–720.
- 268 Hyoung Park J, Sin Lim M, Rang Woo J, Won Kim J & Min Lee G (2016) The molecular weight and concentration of dextran sulfate affect cell growth and antibody production in CHO cell cultures. *Biotechnol Prog* **32**, 1113–1122.
- 269 Kim CL, Jung MY, Kim YS, Jang JW & Lee GM (2018) Improving the production of recombinant human bone morphogenetic protein-4 in Chinese hamster ovary cell cultures by inhibition of undesirable endocytosis. *Biotechnol Bioeng* **115**, 2565–2575.
- 270 Baek E, Kim CL, Kim MG, Lee JS & Lee GM (2016) Chemical inhibition of autophagy: Examining its potential to increase the specific productivity of recombinant CHO cell lines. *Biotechnol Bioeng* **113**, 1953–1961.
- 271 Nasser SS, Ghaffari N, Braasch K, Jardon MA, Butler M, Kennard M, Gopaluni B & Piret JM (2014) Increased CHO cell fed-batch monoclonal antibody production using the autophagy inhibitor 3-MA or gradually increasing osmolality. *Biochem Eng J* **91**, 37–45.
- 272 Park JH, Noh SM, Woo JR, Kim JW & Lee GM (2016) Valeric acid induces cell cycle arrest at G1 phase in CHO cell cultures and improves recombinant antibody productivity. *Biotechnol J* **11**, 487–96.
- 273 Balcarcel RR & Stephanopoulos G (2001) Rapamycin reduces hybridoma cell death and enhances monoclonal antibody production. *Biotechnol Bioeng* **76**, 1–10.
- 274 Du Z, Treiber D, McCarter JD, Fomina-Yadlin D, Saleem RA, McCoy RE, Zhang Y, Tharmalingam T, Leith M, Follstad BD, Dell B, Grisim B, Zupke C, Heath C, Morris AE & Reddy P (2015) Use of a small molecule cell cycle inhibitor to control cell growth and improve specific productivity and product quality of recombinant proteins in CHO cell cultures. *Biotechnol Bioeng* **112**, 141–155.
- 275 Takagi Y, Kikuchi T, Wada R & Omasa T (2017) The enhancement of antibody concentration and achievement of high cell density CHO cell cultivation by adding



- nucleoside. *Cytotechnology* **69**, 511–521.
- 276 Xu P, Xu S, He C & Khetan A (2020) Applications of small molecules in modulating productivity and product quality of recombinant proteins produced using cell cultures. *Biotechnol Adv* **43**, 107577.
- 277 Wessman SJ & Levings RL (1999) Benefits and risks due to animal serum used in cell culture production. *Dev Biol Stand* **99**, 3–8.
- 278 Eagle H (1955) The specific amino acid requirements of a mammalian cell (strain L) in tissue culture. *J Biol Chem* **214**, 839–52.
- 279 Barrett S & Jacobia S (2011) CELL CULTURE MEDIUM COMPRISING SMALL PEPTIDES. .
- 280 Buchholz J, Schwentner A, Brunnenkan B, Gabris C, Grimm S, Gerstmeir R, Takors R, Eikmanns BJ & Blombach B (2013) Platform Engineering of *Corynebacterium glutamicum* with Reduced Pyruvate Dehydrogenase Complex Activity for Improved Production of L-Lysine, L-Valine, and 2-Ketoisovalerate. *Appl Environ Microbiol* **79**, 5566–5575.
- 281 Henderson JW & Brooks A (2010) *Improved amino acid methods using Agilent ZORBAX Eclipse Plus C18 columns for a variety of Agilent LC instrumentation and separation goals* Santa Clara, CA.
- 282 Teleki A, Sánchez-Kopper A & Takors R (2015) Alkaline conditions in hydrophilic interaction liquid chromatography for intracellular metabolite quantification using tandem mass spectrometry. *Anal Biochem* **475**, 4–13.
- 283 Feith A, Teleki A, Graf M, Favilli L & Takors R (2019) HILIC-Enabled <sup>13</sup>C Metabolomics Strategies: Comparing Quantitative Precision and Spectral Accuracy of QTOF High- and QQQ Low-Resolution Mass Spectrometry. *Metabolites* **9**, 63.
- 284 Cserjan-Puschmann M, Kramer W, Duerschmid E, Striedner G & Bayer K (1999) Metabolic approaches for the optimisation of recombinant fermentation processes. *Appl Microbiol Biotechnol* **53**, 43–50.

- 285 Kanehisa M & Goto S (2000) KEGG: kyoto encyclopedia of genes and genomes. *Nucleic Acids Res* **28**, 27–30.
- 286 Hefzi H, Ang KS, Hanscho M, Bordbar A, Ruckerbauer D, Lakshmanan M, Orellana CA, Baycin-Hizal D, Huang Y, Ley D, Martinez VS, Kyriakopoulos S, Jiménez NE, Zielinski DC, Quek L-E, Wulff T, Arnsdorf J, Li S, Lee JS, Paglia G, Loira N, Spahn PN, Pedersen LE, Gutierrez JM, King ZA, Lund AM, Nagarajan H, Thomas A, Abdel-Haleem AM, Zanghellini J, Kildegaard HF, Voldborg BG, Gerdtzen ZP, Betenbaugh MJ, Palsson BO, Andersen MR, Nielsen LK, Borth N, Lee D-Y & Lewis NE (2016) A Consensus Genome-scale Reconstruction of Chinese Hamster Ovary Cell Metabolism. *Cell Syst* **3**, 434-443.e8.
- 287 Quek L-E, Dietmair S, Krömer JO & Nielsen LK (2010) Metabolic flux analysis in mammalian cell culture. *Metab Eng* **12**, 161–171.
- 288 Sheikh K, Förster J & Nielsen LK (2008) Modeling Hybridoma Cell Metabolism Using a Generic Genome-Scale Metabolic Model of *Mus musculus*. *Biotechnol Prog* **21**, 112–121.
- 289 Martens DE (2007) Metabolic Flux Analysis of Mammalian Cells. In pp. 275–299.
- 290 Cherlet M & Marc A (1998) Intracellular pH Monitoring as a Tool for the Study of Hybridoma Cell Behavior in Batch and Continuous Bioreactor Cultures. *Biotechnol Prog* **14**, 626–638.
- 291 Bulté DB, Gómez C, Palomares LA & Ramírez OT (2018) Overexpression of the mitochondrial pyruvate carrier increases CHO cell and recombinant protein productivity and reduces lactate production. In *Cell Culture Engineering XVI*.
- 292 Kilburn DG, Lilly MD & Webb FC (1969) The energetics of mammalian cell growth. *J Cell Sci* **4**, 645–54.
- 293 Locasale JW & Cantley LC (2011) Metabolic flux and the regulation of mammalian cell growth. *Cell Metab* **14**, 443–51.

- 294 Schaub J, Clemens C, Schorn P, Hildebrandt T, Rust W, Mennerich D, Kaufmann H & Schulz TW (2010) CHO gene expression profiling in biopharmaceutical process analysis and design. *Biotechnol Bioeng* **105**, 431–438.
- 295 Templeton N, Smith KD, McAtee-Pereira AG, Dorai H, Betenbaugh MJ, Lang SE & Young JD (2017) Application of <sup>13</sup>C flux analysis to identify high-productivity CHO metabolic phenotypes. *Metab Eng* **43**, 218–225.
- 296 Zhang H, Wang H, Liu M, Zhang T, Zhang J, Wang X & Xiang W (2013) Rational development of a serum-free medium and fed-batch process for a GS-CHO cell line expressing recombinant antibody. *Cytotechnology* **65**, 363–78.
- 297 Handlogten MW, Lee-O'Brien A, Roy G, Levitskaya S V., Venkat R, Singh S & Ahuja S (2018) Intracellular response to process optimization and impact on productivity and product aggregates for a high-titer CHO cell process. *Biotechnol Bioeng* **115**, 126–138.
- 298 Junghans L, Teleki A, Wijaya AW, Becker M, Schweikert M & Takors R (2019) From nutritional wealth to autophagy: In vivo metabolic dynamics in the cytosol, mitochondrion and shuttles of IgG producing CHO cells. *Metab Eng* **54**, 145–159.
- 299 Templeton N, Xu S, Roush DJ & Chen H (2017) <sup>13</sup>C metabolic flux analysis identifies limitations to increasing specific productivity in fed-batch and perfusion. *Metab Eng* **44**, 126–133.
- 300 Pfizenmaier J, Junghans L, Teleki A & Takors R (2016) Hyperosmotic stimulus study discloses benefits in ATP supply and reveals miRNA/mRNA targets to improve recombinant protein production of CHO cells. *Biotechnol J* **11**, 1037–47.
- 301 Sha S, Bhatia H & Yoon S (2018) An RNA-seq based transcriptomic investigation into the productivity and growth variants with Chinese hamster ovary cells. *J Biotechnol* **271**, 37–46.
- 302 Nematpour F, Mahboudi F, Khalaj V, Vaziri B, Ahmadi S, Ahmadi M, Ebadat S & Davami F (2017) Optimization of monoclonal antibody expression in CHO cells by employing

- epigenetic gene regulation tools. *TURKISH J Biol* **41**, 622–628.
- 303 Wippermann A, Rupp O, Brinkrolf K, Hoffrogge R & Noll T (2015) The DNA methylation landscape of Chinese hamster ovary (CHO) DP-12 cells. *J Biotechnol* **199**, 38–46.
- 304 Feichtinger J, Hernández I, Fischer C, Hanscho M, Auer N, Hackl M, Jadhav V, Baumann M, Krempl PM, Schmidl C, Farlik M, Schuster M, Merkel A, Sommer A, Heath S, Rico D, Bock C, Thallinger GG & Borth N (2016) Comprehensive genome and epigenome characterization of CHO cells in response to evolutionary pressures and over time. *Biotechnol Bioeng* **113**, 2241–2253.
- 305 Harreither E, Hackl M, Pichler J, Shridhar S, Auer N, Łabaj PP, Scheideler M, Karbiener M, Grillari J, Kreil DP & Borth N (2015) Microarray profiling of preselected CHO host cell subclones identifies gene expression patterns associated with in-creased production capacity. *Biotechnol J* **10**, 1625–1638.
- 306 Dhiman H, Gerstl MP, Ruckerbauer D, Hanscho M, Himmelbauer H, Clarke C, Barron N, Zanghellini J & Borth N (2019) Genetic and Epigenetic Variation across Genes Involved in Energy Metabolism and Mitochondria of Chinese Hamster Ovary Cell Lines. *Biotechnol J* **14**, 1800681.
- 307 Pfizenmaier-Wu JI (2017) Metabolic and transcriptomic response to hyperosmotic stimulus reveals strategies for optimization of antibody producing Chinese hamster ovary cells. *Von Der Fak Biotech Verfahrens-, Energie-*, 217.
- 308 Hoffman JL (1986) Chromatographic analysis of the chiral and covalent instability of S-adenosyl-L-methionine. *Biochemistry* **25**, 4444–9.
- 309 Morana A, Stiuso P, Colonna G, Lamberti M, Carteni M & De Rosa M (2002) Stabilization of S-adenosyl-L-methionine promoted by trehalose. *Biochim Biophys Acta* **1573**, 105–8.
- 310 Lankau T, Kuo TN & Yu CH (2017) Computational Study of the Degradation of S - Adenosyl Methionine in Water. *J Phys Chem A* **121**, 505–514.

- 311 Subhi AL, Diegelman P, Porter CW, Tang B, Lu ZJ, Markham GD & Kruger WD (2003) Methylthioadenosine Phosphorylase Regulates Ornithine Decarboxylase by Production of Downstream Metabolites. *J Biol Chem* **278**, 49868–49873.
- 312 Hevia H, Varela-Rey M, Corrales FJ, Berasain C, Martínez-Chantar ML, Latasa MU, Lu SC, Mato JM, García-Trevijano ER & Avila MA (2004) 5'-methylthioadenosine modulates the inflammatory response to endotoxin in mice and in rat hepatocytes. *Hepatology* **39**, 1088–1098.
- 313 Verhagen N, Teleki A, Heinrich C, Schilling M, Unsöld A & Takors R (2020) S-adenosylmethionine and methylthioadenosine boost cellular productivities of antibody forming Chinese hamster ovary cells. *Biotechnol Bioeng* **117**, 3239–3247.
- 314 Sunley K & Butler M (2010) Strategies for the enhancement of recombinant protein production from mammalian cells by growth arrest. *Biotechnol Adv* **28**, 385–394.
- 315 Al-Rubeai M, Emery AN, Chalder S & Jan DC (1992) Specific monoclonal antibody productivity and the cell cycle-comparisons of batch, continuous and perfusion cultures. *Cytotechnology* **9**, 85–97.
- 316 Hammond S & Lee KH (2012) RNA interference of cofilin in Chinese hamster ovary cells improves recombinant protein productivity. *Biotechnol Bioeng* **109**, 528–535.
- 317 Nishimiya D, Mano T, Miyadai K, Yoshida H & Takahashi T (2013) Overexpression of CHOP alone and in combination with chaperones is effective in improving antibody production in mammalian cells. *Appl Microbiol Biotechnol* **97**, 2531–2539.
- 318 Furukawa K & Ohsuye K (1999) Enhancement of Productivity of Recombinant  $\alpha$ -Amidating Enzyme by Low Temperature Culture. In *Animal Cell Technology: Basic & Applied Aspects* pp. 153–157. Kluwer Academic Publishers, Dordrecht.
- 319 Prabhu A, Gadre R & Gadgil M (2018) Zinc supplementation decreases galactosylation of recombinant IgG in CHO cells. *Appl Microbiol Biotechnol* **102**, 5989–5999.

- 320 Coronel J, Klausing S, Heinrich C, Noll T, Figueredo-Cardero A & Castilho LR (2016) Valeric acid supplementation combined to mild hypothermia increases productivity in CHO cell cultivations. *Biochem Eng J* **114**, 101–109.
- 321 Ahn Y-H, Han K, Yoon SK & Song J (1999) Effect of Glycine Betaine as Osmoprotectant on the Production of Erythropoietin by CHO Cells in Hyperosmotic Serum Free Media Culture. In *Animal Cell Technology: Basic & Applied Aspects* pp. 247–250. Kluwer Academic Publishers, Dordrecht.
- 322 Afgan E, Baker D, Batut B, van den Beek M, Bouvier D, Čech M, Chilton J, Clements D, Coraor N, Grüning BA, Guerler A, Hillman-Jackson J, Hiltmann S, Jalili V, Rasche H, Soranzo N, Goecks J, Taylor J, Nekrutenko A & Blankenberg D (2018) The Galaxy platform for accessible, reproducible and collaborative biomedical analyses: 2018 update. *Nucleic Acids Res* **46**, W537–W544.
- 323 Langmead B & Salzberg S (2013) Bowtie2. *Nat Methods* **9**, 357–359.
- 324 Anders S, Pyl PT & Huber W (2015) HTSeq-A Python framework to work with high-throughput sequencing data. *Bioinformatics* **31**, 166–169.
- 325 Love MI, Huber W & Anders S (2014) Moderated estimation of fold change and dispersion for RNA-seq data with DESeq2. *Genome Biol* **15**, 550.
- 326 Gentleman RC, Carey VJ, Bates DM, Bolstad B, Dettling M, Dudoit S, Ellis B, Gautier L, Ge Y, Gentry J, Hornik K, Hothorn T, Huber W, Iacus S, Irizarry R, Leisch F, Li C, Maechler M, Rossini AJ, Sawitzki G, Smith C, Smyth G, Tierney L, Yang JYH & Zhang J (2004) Bioconductor: open software development for computational biology and bioinformatics. *Genome Biol* **5**, R80.
- 327 Benjamini Y & Hochberg Y (1995) Controlling the False Discovery Rate: A Practical and Powerful Approach to Multiple Testing. *J R Stat Soc Ser B* **57**, 289–300.
- 328 Fischer S, Handrick R & Otte K (2015) The art of CHO cell engineering: A comprehensive retrospect and future perspectives. *Biotechnol Adv* **33**, 1878–1896.

- 329 Katz U (1995) Cellular water content and volume regulation in animal cells. *Cell Biochem Funct* **13**, 189–193.
- 330 Lang F, Busch GL, Ritter M, Völkl H, Waldegger S, Gulbins E & Häussinger D (1998) Functional significance of cell volume regulatory mechanisms. *Physiol Rev* **78**, 247–306.
- 331 Sun Z, Zhou R, Liang S, McNeeley KM & Sharfstein ST (2008) Hyperosmotic Stress in Murine Hybridoma Cells: Effects on Antibody Transcription, Translation, Posttranslational Processing, and the Cell Cycle. *Biotechnol Prog* **20**, 576–589.
- 332 Khoo SHG & Al-Rubeai M (2009) Detailed understanding of enhanced specific antibody productivity in NSO myeloma cells. *Biotechnol Bioeng* **102**, 188–199.
- 333 Delanote V, Vandekerckhove J & Gettemans J (2005) Plastins: versatile modulators of actin organization in (patho)physiological cellular processes. *Acta Pharmacol Sin* **26**, 769–79.
- 334 Kim C, Cho Y, Kang C, Kim MG, Lee H, Cho E & Park D (2005) Filamin is essential for shedding of the transmembrane serine protease, epithin. *EMBO Rep* **6**, 1045–1051.
- 335 Chen L, Johnson RC & Milgram SL (1998) P-CIP1, A Novel Protein That Interacts with the Cytosolic Domain of Peptidylglycine  $\alpha$ -Amidating Monooxygenase, Is Associated with Endosomes. *J Biol Chem* **273**, 33524–33532.
- 336 Hofmann WA, Stojiljkovic L, Fuchsova B, Vargas GM, Mavrommatis E, Philimonenko V, Kyselá K, Goodrich JA, Lessard JL, Hope TJ, Hozak P & de Lanerolle P (2004) Actin is part of pre-initiation complexes and is necessary for transcription by RNA polymerase II. *Nat Cell Biol* **6**, 1094–1101.
- 337 Philimonenko V V., Zhao J, Iben S, Dingová H, Kyselá K, Kahle M, Zentgraf H, Hofmann WA, de Lanerolle P, Hozák P & Grummt I (2004) Nuclear actin and myosin I are required for RNA polymerase I transcription. *Nat Cell Biol* **6**, 1165–1172.
- 338 Sasaki Y, Itoh F, Kobayashi T, Kikuchi T, Suzuki H, Toyota M & Imai K (2002) Increased expression of T-fimbrin gene after DNA damage in CHO cells and inactivation of T-

- fimbrin by CpG methylation in human colorectal cancer cells. *Int J Cancer* **97**, 211–216.
- 339 Hughes CA & Bennett V (1995) Adducin: a Physical Model with Implications for Function in Assembly of Spectrin-Actin Complexes. *J Biol Chem* **270**, 18990–18996.
- 340 Edwards RA & Bryan J (1995) Fascins, a family of actin bundling proteins. *Cell Motil Cytoskeleton* **32**, 1–9.
- 341 Moseley JB, Bartolini F, Okada K, Wen Y, Gundersen GG & Goode BL (2007) Regulated Binding of Adenomatous Polyposis Coli Protein to Actin. *J Biol Chem* **282**, 12661–12668.
- 342 Mimori-Kiyosue Y, Shiina N & Tsukita S (2000) Adenomatous Polyposis Coli (APC) Protein Moves along Microtubules and Concentrates at Their Growing Ends in Epithelial Cells. *J Cell Biol* **148**, 505–518.
- 343 Hauge H, Patzke S & Aasheim H-C (2007) Characterization of the FAM110 gene family. *Genomics* **90**, 14–27.
- 344 De Petro G, Copeta A & Barlati S (1994) Urokinase-Type and Tissue-Type Plasminogen Activators as Growth Factors of Human Fibroblasts. *Exp Cell Res* **213**, 286–294.
- 345 Shetty S, Gyetko MR & Mazar AP (2005) Induction of p53 by Urokinase in Lung Epithelial Cells. *J Biol Chem* **280**, 28133–28141.
- 346 Li W, Liang Y, Yang B, Sun H & Wu W (2015) Downregulation of ARNT2 promotes tumor growth and predicts poor prognosis in human hepatocellular carcinoma. *J Gastroenterol Hepatol* **30**, 1085–1093.
- 347 Shiokawa D & Tanuma S (2001) Characterization of Human DNase I Family Endonucleases and Activation of DNase  $\gamma$  during Apoptosis †. *Biochemistry* **40**, 143–152.
- 348 Normanno N, De Luca A, Bianco C, Strizzi L, Mancino M, Maiello MR, Carotenuto A, De Feo G, Caponigro F & Salomon DS (2006) Epidermal growth factor receptor (EGFR) signaling in cancer. *Gene* **366**, 2–16.



- 349 Chen K, Li D, Li H, Li B, Wang R, Jiang L, Huang L, Xu X, Li J, Teng F, Jiang C, Gu H & Fang J (2019) Improved recombinant protein production by regulation of transcription and protein transport in Chinese hamster ovary cells. *Biotechnol Lett* **41**, 719–732.
- 350 Liu L, Kim H, Casta A, Kobayashi Y, Shapiro LS & Christiano AM (2014) Hairless is a histone H3K9 demethylase. *FASEB J* **28**, 1534–1542.
- 351 Herranz N, Dave N, Millanes-Romero A, Pascual-Reguant L, Morey L, Díaz VM, Lórenz-Fonfría V, Gutierrez-Gallego R, Jerónimo C, Iturbide A, Di Croce L, García de Herreros A & Peiró S (2016) Lysyl oxidase-like 2 (LOXL2) oxidizes trimethylated lysine 4 in histone H3. *FEBS J* **283**, 4263–4273.
- 352 Thompson PM, Gotoh T, Kok M, White PS & Brodeur GM (2003) CHD5, a new member of the chromodomain gene family, is preferentially expressed in the nervous system. *Oncogene* **22**, 1002–1011.
- 353 Li G, Li H, Tan Y, Hao N, Yang X, Chen K & Ouyang P (2020) Improved S-adenosyl-l-methionine production in *Saccharomyces cerevisiae* using tofu yellow serofluid. *J Biotechnol* **309**, 100–106.
- 354 Kildegaard HF, Baycin-Hizal D, Lewis NE & Betenbaugh MJ (2013) The emerging CHO systems biology era: harnessing the 'omics revolution for biotechnology. *Curr Opin Biotechnol* **24**, 1102–7.
- 355 Wurm FM & Hacker D (2011) First CHO genome. *Nat Biotechnol* **29**, 718–720.
- 356 Ahn WS & Antoniewicz MR (2011) Metabolic flux analysis of CHO cells at growth and non-growth phases using isotopic tracers and mass spectrometry. *Metab Eng* **13**, 598–609.
- 357 Hu Y & Zhu T (2014) Cell growth and size homeostasis in silico. *Biophys J* **106**, 991–7.
- 358 Lloyd D & Murray DB (2000) Redox Cycling of Intracellular Thiols: State Variables for Ultradian, Cell Division Cycle and Circadian Cycles? In *The Redox State and Circadian Rhythms* pp. 85–94. Springer Netherlands, Dordrecht.

- 359 Verhagen N, Zieringer J & Takors R (2020) Methylthioadenosine (MTA) boosts cell-specific productivities of Chinese hamster ovary cultures: dosage effects on proliferation, cell cycle and gene expression. *FEBS Open Bio* **10**, 2791–2804.
- 360 Matuszczyk J-C, Teleki A, Pfizenmaier J & Takors R (2015) Compartment-specific metabolomics for CHO reveals that ATP pools in mitochondria are much lower than in cytosol. *Biotechnol J* **10**, 1639–1650.
- 361 Teleki A, Rahnert M, Bungart O, Gann B, Ochrombel I & Takors R (2017) Robust identification of metabolic control for microbial L-methionine production following an easy-to-use puristic approach. *Metab Eng* **41**, 159–172.
- 362 Zimmermann M, Sauer U & Zamboni N (2014) Quantification and Mass Isotopomer Profiling of  $\alpha$ -Keto Acids in Central Carbon Metabolism. *Anal Chem* **86**, 3232–3237.
- 363 Schaub J, Mauch K & Reuss M (2008) Metabolic flux analysis in Escherichia coli by integrating isotopic dynamic and isotopic stationary  $^{13}\text{C}$  labeling data. *Biotechnol Bioeng* **99**, 1170–85.
- 364 Maier K, Hofmann U, Reuss M & Mauch K (2008) Identification of metabolic fluxes in hepatic cells from transient  $^{13}\text{C}$ -labeling experiments: Part II. Flux estimation. *Biotechnol Bioeng* **100**, 355–370.
- 365 Schmidt K, Carlsen M, Nielsen J & Villadsen J (1997) Modeling isotopomer distributions in biochemical networks using isotopomer mapping matrices. *Biotechnol Bioeng* **55**, 831–840.
- 366 Nicolae A, Wahrheit J, Bahnemann J, Zeng A-P & Heinzle E (2014) Non-stationary  $^{13}\text{C}$  metabolic flux analysis of Chinese hamster ovary cells in batch culture using extracellular labeling highlights metabolic reversibility and compartmentation. *BMC Syst Biol* **8**, 50.
- 367 Antoniewicz MR, Kelleher JK & Stephanopoulos G (2006) Determination of confidence intervals of metabolic fluxes estimated from stable isotope measurements. *Metab Eng*

- 8, 324–337.
- 368 Metallo CM, Walther JL & Stephanopoulos G (2009) Evaluation of <sup>13</sup>C isotopic tracers for metabolic flux analysis in mammalian cells. *J Biotechnol* **144**, 167–174.
- 369 Hosios AM & Vander Heiden MG (2018) The redox requirements of proliferating mammalian cells. *J Biol Chem* **293**, 7490–7498.
- 370 Pan X, Dalm C, Wijffels RH & Martens DE (2017) Metabolic characterization of a CHO cell size increase phase in fed-batch cultures. *Appl Microbiol Biotechnol* **101**, 8101–8113.
- 371 Furuya E & Uyeda K (1980) An activation factor of liver phosphofructokinase. *Proc Natl Acad Sci* **77**, 5861–5864.
- 372 Passonneau J V. & Lowry OH (1964) The role of phosphofructokinase in metabolic regulation. *Adv Enzyme Regul* **2**, 265–274.
- 373 Mansour TE (1963) Studies on Heart Phosphofructokinase. Purification, Inhibition, and Activation. *J Biol Chem* **238**, 2285–2292.
- 374 Moreadith RW & Lehninger AL (1984) Purification, kinetic behavior, and regulation of NAD(P)<sup>+</sup> malic enzyme of tumor mitochondria. *J Biol Chem* **259**, 6222–7.
- 375 Vizán P, Alcarraz-Vizán G, Díaz-Moralli S, Solovjeva ON, Frederiks WM & Cascante M (2009) Modulation of pentose phosphate pathway during cell cycle progression in human colon adenocarcinoma cell line HT29. *Int J cancer* **124**, 2789–96.
- 376 Sengupta N, Rose ST & Morgan JA (2011) Metabolic flux analysis of CHO cell metabolism in the late non-growth phase. *Biotechnol Bioeng* **108**, 82–92.
- 377 Tuttle S, Stamato T, Perez ML & Biaglow J (2000) Glucose-6-phosphate dehydrogenase and the oxidative pentose phosphate cycle protect cells against apoptosis induced by low doses of ionizing radiation. *Radiat Res* **153**, 781–7.
- 378 Balsa E, Perry EA, Bennett CF, Jedrychowski M, Gygi SP, Doench JG & Puigserver P (2020) Defective NADPH production in mitochondrial disease complex I causes inflammation

and cell death. *Nat Commun* **11**, 2714.

379 Handlogten MW, Zhu M & Ahuja S (2018) Intracellular response of CHO cells to oxidative stress and its influence on metabolism and antibody production. *Biochem Eng J* **133**, 12–20.

380 Raina A, Tuomi K & Pajula R-L (1982) Inhibition of the synthesis of polyamines and macromolecules by 5'-methylthioadenosine and 5'-alkylthiotubercidins in BHK21 cells. *Biochem J* **204**, 697–703.

381 Pegg AE, Borchardt RT & Coward JK (1981) Effects of inhibitors of spermidine and spermine synthesis on polyamine concentrations and growth of transformed mouse fibroblasts. *Biochem J* **194**, 79–89.

## 6 Appendix

### 6.1 Supplementary Material: Manuscript 1

#### Supplementary Material 1

Model Name: CHO\_FBA\_v1

Date: Dec 10, 2018 1:05:33 PM

----- REACTION -----

Identifier	Equation	Compartment
2OXOADOXm	$\text{NAD} + \text{CoA} + 2\text{-Oxoadipate} \Rightarrow \text{NADH} + \text{CO}_2 + \text{Glutaryl-CoA}$	Mitochondria
3DSPHR	$3\text{-Dehydrosphinganine} + \text{NADPH} \Rightarrow \text{NADP} + \text{Sphinganine}$	Cytosol
3HAO	$\text{O}_2 + 3\text{-Hydroxyanthranilate} \Rightarrow 2\text{-Amino-3-carboxymuconate semialdehyde}$	Cytosol
3SALATAi	$3\text{-sulfinato-L-alaninate} + 2\text{-Oxoglutarate} \Rightarrow 3\text{-Sulfinoxyruvate} + \text{L-Glutamate}$	Cytosol
3SPYRSP	$3\text{-Sulfinoxyruvate} + \text{H}_2\text{O} \Rightarrow \text{Pyruvate}$	Cytosol
ACACT1r2*	$\text{Acetyl-CoA} = \text{CoA} + \text{Acetoacetyl-CoA}$	Cytosol
ACACT1rm	$2*\text{Acetyl-CoA} = \text{CoA} + \text{Acetoacetyl-CoA}$	Mitochondria
ACCOAC	$\text{Acetyl-CoA} + \text{ATP} + \text{H}_2\text{O} + \text{CO}_2 \Rightarrow \text{ADP} + \text{Malonyl-CoA} + \text{Orthophosphate}$	Cytosol
ACITL	$\text{CoA} + \text{ATP} + \text{Citrate} \Rightarrow \text{Acetyl-CoA} + \text{ADP} + \text{Orthophosphate} + \text{Oxaloacetate}$	Cytosol
ACOATA	$\text{ACP} + \text{Acetyl-CoA} \Rightarrow \text{Acetyl-ACP} + \text{CoA}$	Cytosol
ACONTm	$\text{Citrate} = \text{Isocitrate}$	Mitochondria
ADK1	$\text{ATP} + \text{AMP} = 2*\text{ADP}$	Cytosol
ADK3	$\text{AMP} + \text{GTP} = \text{ADP} + \text{GDP}$	Cytosol
ADKd	$\text{dAMP} + \text{dATP} = 2*\text{dADP}$	Cytosol
AKGDM	$\text{NAD} + 2\text{-Oxoglutarate} + \text{CoA} \Rightarrow \text{NADH} + \text{CO}_2 + \text{Succinyl-CoA}$	Mitochondria
ALATA_LL	$\text{L-Alanine} + 2\text{-Oxoglutarate} = \text{Pyruvate} + \text{L-Glutamate}$	Cytosol
ALATA_Lm	$\text{L-Alanine} + 2\text{-Oxoglutarate} = \text{Pyruvate} + \text{L-Glutamate}$	Mitochondria
AM6SAD2	$2\text{-Aminomuconate semialdehyde} + \text{H}_2\text{O} + \text{NAD} = 2\text{-Aminomuconate} + \text{NADH}$	Cytosol
AMCOXO	$2\text{-Aminomuconate} + \text{H}_2\text{O} + \text{NADPH} \Rightarrow 2\text{-Oxoadipate} + \text{NADP} + \text{NH}_4$	Cytosol
AMPDA	$\text{AMP} + \text{H}_2\text{O} \Rightarrow \text{IMP} + \text{NH}_4$	Cytosol
ARG	$\text{L-Arginine} + 2\text{-Oxoglutarate} \Rightarrow \text{Urea} + 2*\text{L-Glutamate}$	Cytosol
ASNN	$\text{L-Asparagine} + \text{H}_2\text{O} \Rightarrow \text{L-Aspartate} + \text{NH}_4$	Cytosol
ASPCTr	$\text{L-Aspartate} + \text{Carbamoyl phosphate} = \text{Orthophosphate} + \text{N-Carbamoyl-L-aspartate}$	Cytosol
ASPTA	$\text{L-Aspartate} + 2\text{-Oxoglutarate} = \text{Oxaloacetate} + \text{L-Glutamate}$	Cytosol
ASPTAm	$\text{L-Aspartate} + 2\text{-Oxoglutarate} = \text{Oxaloacetate} + \text{L-Glutamate}$	Mitochondria
BCAT1	$4*\text{NAD} + 2\text{-Oxoglutarate} + \text{L-Valine} + \text{ADP} \Rightarrow \text{CO}_2 + \text{L-Glutamate} + \text{Succinate} + 4*\text{NADH} + \text{ATP}$	Cytosol
Biomass_pmol_cell	$7.32\text{E-}2*\text{L-Alanine} + 4.6\text{E-}2*\text{L-Arginine} + 4.38\text{E-}2*\text{L-Aspartate} + 3.51\text{E-}2*\text{L-Asparagine} + 1.77\text{E-}2*\text{L-Cysteine} + 3.93\text{E-}2*\text{L-Glutamine} + 4.71\text{E-}2*\text{L-Glutamate} + 6.56\text{E-}2*\text{Glycine} + 1.74\text{E-}2*\text{L-Histidine} + 3.59\text{E-}2*\text{L-Isoleucine} + 6.88\text{E-}2*\text{L-Leucine} + 6.95\text{E-}2*\text{L-Lysine} + 1.68\text{E-}2*\text{L-Methionine} + 2.67\text{E-}2*\text{L-Phenylalanine} + 3.82\text{E-}2*\text{L-Proline} + 5.25\text{E-}2*\text{L-Serine} + 4.71\text{E-}2*\text{L-Threonine} + 5.37\text{E-}3*\text{L-Tryptophan} + 2.22\text{E-}2*\text{L-Tyrosine} + 5.08\text{E-}2*\text{L-Valine} + 3.40\text{E-}2*\text{alpha-D-Glucose} + 1.83\text{E-}3*\text{dAMP} + 1.22\text{E-}3*\text{dCMP} + 1.22\text{E-}3*\text{dGMP} + 1.83\text{E-}3*\text{dTMP} + 4.03\text{E-}3*\text{ATP} + 6.71\text{E-}3*\text{CMP} + 7.56\text{E-}3*\text{GMP} + 4.03\text{E-}3*\text{UMP} + 2.20\text{E-}3*\text{Cholesterol} + 8.42\text{E-}3*\text{Phosphatidylcholine} + 3.17\text{E-}3*\text{Phosphatidylethanolamine} + 1.22\text{E-}3*\text{1-Phosphatidyl-D-myo-inositol} + 3.66\text{E-}4*\text{Phosphatidylserine} + 1.22\text{E-}4*\text{Phosphatidylglycerol} + 3.66\text{E-}4*\text{Cardiolipin} + 9.67\text{E-}4*\text{Sphingomyelin} \Rightarrow \text{X} + 4.03\text{E-}3*\text{ADP}$	Cytosol
C14STRc	$4,4\text{-Dimethyl-5alpha-cholesta-8,14,24-trien-3beta-ol} + \text{NADPH} = 14\text{-Demethylsterol} + \text{NADP}$	Cytosol
C3STDH1Pc	$4\text{alpha-Methylzymosterol-4-carboxylate} + \text{NADP} = 3\text{-Keto-4-methylzymosterol} + \text{CO}_2 + \text{NADPH}$	Cytosol

## Appendix

---

C3STKR2c zymosterol\_intermediate\_2 + NADPH => Zymosterol + NADP Cytosol  
 C4STMO1c 14-Demethylstanosterol + 3\*NADPH + 3\*O2 => 4alpha-Methylzymosterol-4-carboxylate + 4\*H2O + 3\*NADP Cytosol  
 C4STMO2Pc 3-Keto-4-methylzymosterol + NADP + O2 => CO2 + NADPH + zymosterol\_intermediate\_2 Cytosol  
 CBPS 2\*H2O + 2\*ATP + CO2 + L-Glutamine => 2\*ADP + Orthophosphate + L-Glutamate + Carbamoyl\_phosphate Cytosol  
 CDIPTr\_cho CDP-diacylglycerol + myo-Inositol = CMP + 1-Phosphatidyl-D-myo-inositol Cytosol  
 CDS\_choCTP + Phosphatidate => CDP-diacylglycerol + Diphosphate Cytosol  
 CEPTC\_cho 1,2-Diacyl-sn-glycerol + CDP-choline => Phosphatidylcholine + CMP Cytosol  
 CEPTE\_cho 1,2-Diacyl-sn-glycerol + CDP-ethanolamine => Phosphatidylethanolamine + CMP Cytosol  
 CHLP H2O + Choline\_phosphate => Orthophosphate + Choline Cytosol  
 CHLPCTD ADP + CDP-choline => CTP + ATP + Choline\_phosphate Cytosol  
 CSm H2O + Acetyl-CoA + Oxaloacetate => + CoA + Citrate Mitochondria  
 CTPS2 ATP + UTP + L-Glutamine + H2O => ADP + Orthophosphate + CTP + L-Glutamate Cytosol  
 CYSO L-Cysteine + O2 => 3-sulfinato-L-alaninate Cytosol  
 CYTK1 ATP + CMP = ADP + CDP Cytosol  
 CYTK10 CMP + dGTP = CDP + dGDP Cytosol  
 CYTK11 dCMP + dGTP = dCDP + dGDP Cytosol  
 CYTK12 dCMP + dCTP = 2\*dCDP Cytosol  
 DGK1 ATP + dGMP = ADP + dGDP Cytosol  
 DHCR243r Desmosterol + FADH2 => Cholesterol + FAD Cytosol  
 DHCRD1\_cho Dihydroceramide + NADP => N-Acylsphingosine + NADPH Cytosol  
 DHCRD2\_cho Dihydroceramide + FAD => N-Acylsphingosine + FADH2 Cytosol  
 DHFR NADP + Tetrahydrofolate = NADPH + Dihydrofolate Cytosol  
 DHORTS N-Carbamoyl-L-aspartate = H2O + (S)-Dihydroorotate Cytosol  
 DMATTc Dimethylallyl\_diphosphate + Isopentenyl\_diphosphate => Geranyl\_diphosphate + Diphosphate Cytosol  
 DPMVDc(R)-5-Diphosphomevalonate + ATP => ADP + CO2 + Isopentenyl\_diphosphate + Orthophosphate Cytosol  
 DSAT\_cho Acyl-CoA + Sphinganine => CoA + Dihydroceramide Cytosol  
 DTMPK ATP + dTMP = ADP + dTDP Cytosol  
 EBP1c Zymosterol => 5alpha-Cholesta-7,24-dien-3beta-ol Cytosol  
 ECOAH1m (S)-3-Hydroxybutanoyl-CoA = H2O + Crotonoyl-CoA Mitochondria  
 ENO D-Glycerate\_2-phosphate = H2O + Phosphoenolpyruvate Cytosol  
 ETC\_1 NADH + 1.5\*ADP + O2 => NAD + 1.5\*ATP + H2O Mitochondria  
 ETC\_2 FADH2 + 1.2\*ADP + O2 => FAD + 1.2\*ATP + H2O Mitochondria  
 ETHAK ATP + Ethanolamine => ADP + Ethanolamine\_phosphate Cytosol  
 FA16BS Acetyl-ACP + 4.67\*Malonyl-CoA + 9.34\*NADPH => 4.67\*CO2 + 4.67\*CoA + 4.67\*H2O + 9.34\*NADP + Hexadecanoyl-ACP Cytosol  
 FA180ACPH H2O + Octadecanoyl-ACP => ACP + Octadecanoic\_acid Cytosol  
 FACOAL160i Hexadecanoic acid + CoA + ATP => AMP + Diphosphate + Palmitoyl-CoA Cytosol  
 FAS180ACP Malonyl-CoA + 2\*NADPH + Hexadecanoyl-ACP => CO2 + CoA + H2O + 2\*NADP + Octadecanoyl-ACP Cytosol  
 FBA alpha-D-Fructose\_1,6-bisphosphate = Glycerone\_phosphate + 3-Phospho-D-glycerate Cytosol  
 FKYNH H2O + L-Formylkynurenine => Formate + L-Kynurenine Cytosol  
 FOLR2 NADPH + Folate => NADP + Dihydrofolate Cytosol  
 FTHFDH 10-Formyltetrahydrofolate + NADP + H2O = Tetrahydrofolate + CO2 + NADPH Cytosol  
 FUMc H2O + Fumarate = L-Malate Cytosol  
 FUMm H2O + Fumarate = L-Malate Mitochondria  
 G3PD1 NADH + Glycerone\_phosphate = NAD + sn-Glycerol 3-phosphate Cytosol

## Appendix

---

G5SADr L-Glutamate\_5-semialdehyde = (S)-1-Pyrroline-5-carboxylate + H2O Cytosol  
G5SADrm L-Glutamate\_5-semialdehyde = (S)-1-Pyrroline-5-carboxylate + H2O Mitochondria  
G6PDH2r NADP + alpha-D-Glucose\_6-phosphate = NADPH + D-Glucono-1,5-lactone\_6-phosphate  
Cytosol  
GALU UTP + alpha-D-Glucose\_1-phosphate = Diphosphate + UDP-glucose Cytosol  
GAPD NAD + Orthophosphate + 3-Phospho-D-glycerate = NADH + 3-Phospho-D-glyceroyl\_phosphate  
Cytosol  
GHMT2r L-Serine + Tetrahydrofolate = H2O + Glycine + 5,10-Methylenetetrahydrofolate Cytosol  
GK1 ATP + GMP = ADP + GDP Cytosol  
GLUDxm L-Glutamate + H2O + NAD = 2-Oxoglutarate + NADH + NH4 Mitochondria  
GLUN L-Glutamine + H2O => L-Glutamate + NH4 Mitochondria  
GLUTCOADHm FAD + Glutaryl-CoA => FADH2 + CO2 + Crotonoyl-CoA Mitochondria  
GMPS2 XMP + ATP + L-Glutamine + H2O => GMP + AMP + Diphosphate + L-Glutamate Cytosol  
GND NADP + 6-Phospho-D-gluconate => NADPH + CO2 + D-Ribulose\_5-phosphate Cytosol  
GRTTc Geranyl\_diphosphate + Isopentenyl\_diphosphate => trans,trans-Farnesyl\_diphosphate + Diphosphate  
Cytosol  
HACD1m NADH + Acetoacetyl-CoA = NAD + (S)-3-Hydroxybutanoyl-CoA Mitochondria  
HAL L-Histidine + NADH + Tetrahydrofolate => 5,10-Methylenetetrahydrofolate + L-Glutamate + H2O +  
NAD Cytosol  
HEX1 ATP + alpha-D-Glucose => ADP + alpha-D-Glucose\_6-phosphate Cytosol  
HKYNH H2O + 3-Hydroxy-L-kynurenine => L-Alanine + 3-Hydroxyanthranilate Cytosol  
HMGCOArc S-3-Hydroxy-3-methylglutaryl-CoA + 2\*NADPH => CoA + (R)-Mevalonate + 2\*NADP  
Cytosol  
HMGCOAsi Acetoacetyl-CoA + Acetyl-CoA + H2O => CoA + S-3-Hydroxy-3-methylglutaryl-CoA  
Cytosol  
HXACPHY Hexadecanoyl-ACP + H2O => Hexadecanoic acid + ACP Cytosol  
HXPRT Hypoxanthine + 5-Phospho-alpha-D-ribose\_1-diphosphate => IMP + Diphosphate Cytosol  
ICDHxm NAD + Isocitrate => NADH + 2-Oxoglutarate + CO2 Mitochondria  
IMPD H2O + IMP + NAD = NADH + XMP Cytosol  
INSK ATP + Inosine => ADP + IMP Cytosol  
IPDDI Isopentenyl\_diphosphate = Dimethylallyl\_diphosphate Cytosol  
IgG\_Martens 40\*ATP + L-Serine + 0.85\*L-Threonine + 0.77\*L-Valine + 0.69\*L-Lysine + 0.69\*L-Proline +  
0.62\*Glycine + 0.62\*L-Leucine + 0.62\*L-Glutamine + 0.54\*L-Alanine + 0.53\*L-Glutamate + 0.52\*L-Aspartate +  
0.46\*L-Asparagine + 0.38\*L-Phenylalanine + 0.37\*L-Isoleucine + 0.32\*L-Tyrosine + 0.31\*L-Cysteine + 0.24\*L-  
Arginine + 0.18\*L-Tryptophan + 0.17\*L-Histidine + 0.13\*L-Methionine => IgG1 + 40\*ADP + 40\*Orthophosphate  
Cytosol  
KYN3OX O2 + NADP + L-Kynurenine => NADP + H2O + 3-Hydroxy-L-kynurenine Cytosol  
LDH\_L NADH + Pyruvate = NAD + L-Lactate Cytosol  
LNS14DMc Lanosterol + 3\*NADPH + 3\*O2 => 4,4-Dimethyl-5alpha-cholesta-8,14,24-trien-3beta-ol +  
Formate + 4\*H2O + 3\*NADP Cytosol  
LNSTLSc (S)-2,3-Epoxysqualene => Lanosterol Cytosol  
LSTO1c 5alpha-Cholesta-7,24-dien-3beta-ol + NADPH + O2 => 7-Dehydrodesmosterol + 2\*H2O + NADP  
Cytosol  
M ATP => ADP Cytosol  
MDH NAD + L-Malate = NADH + Oxaloacetate Cytosol  
MDHm NAD + L-Malate = NADH + Oxaloacetate Mitochondria  
ME1m L-Malate + NAD = Pyruvate + CO2 + NADH Mitochondria  
ME2 L-Malate + NADP => Pyruvate + CO2 + NADPH Cytosol  
MEVK1c ATP + (R)-Mevalonate => (R)-5-Phosphomevalonate + ADP Cytosol  
MTHFC H2O + 5,10-Methenyltetrahydrofolate = 10-Formyltetrahydrofolate Cytosol  
MTHFD NADP + 5,10-Methylenetetrahydrofolate = NADPH + 5,10-Methenyltetrahydrofolate Cytosol  
NDPK1 ATP + GDP = ADP + GTP Cytosol

## Appendix

---

NDPK1m      ATP + GDP = ADP + GTP      Mitochondria  
 NDPK2      ATP + UDP = ADP + UTP      Cytosol  
 NDPK3      ATP + CDP = ADP + CTP      Cytosol  
 NDPK4      ATP + dTDP = ADP + dTTP      Cytosol  
 NDPK5      ATP + dGDP = ADP + dGTP      Cytosol  
 NDPK7      ATP + dCDP = ADP + dCTP      Cytosol  
 NDPK8      ATP + dADP = ADP + dATP      Cytosol  
 OMPDC      Orotidine 5'-phosphate => CO2 + UMP      Cytosol  
 ORPT      5-Phospho-alpha-D-ribose\_1-diphosphate + Orotate = Diphosphate + Orotidine 5'-phosphate  
             Cytosol  
 P5CRxm      NADH + (S)-1-Pyrroline-5-carboxylate = NAD + L-Proline      Mitochondria  
 PCLAD      2-Amino-3-carboxymuconate\_semialdehyde => CO2 + 2-Aminomuconate\_semialdehyde      Cytosol  
 PDHm      NAD + CoA + Pyruvate => NADH + CO2 + Acetyl-CoA      Mitochondria  
 PETHCT      CTP + Ethanolamine\_phosphate => Diphosphate + CDP-ethanolamine      Cytosol  
 PFK      ATP + alpha-D-Fructose\_6-phosphate => ADP + alpha-D-Fructose\_1,6-bisphosphate      Cytosol  
 PGCD      NAD + 3-Phospho-D-glycerate => NADH + 3-Phosphonoxypruvate      Cytosol  
 PGI      alpha-D-Glucose\_6-phosphate = alpha-D-Fructose\_6-phosphate      Cytosol  
 PGK      ADP + 3-Phospho-D-glyceroyl\_phosphate = ATP + D-Glycerate\_3-phosphate      Cytosol  
 PGL      H2O + D-Glucono-1,5-lactone\_6-phosphate => 6-Phospho-D-gluconate      Cytosol  
 PGM      D-Glycerate\_3-phosphate = D-Glycerate\_2-phosphate      Cytosol  
 PGMT      alpha-D-Glucose\_1-phosphate = alpha-D-Glucose\_6-phosphate      Cytosol  
 PGPPT\_cho      sn-Glycerol 3-phosphate + CDP-diacylglycerol => CMP + Phosphatidylglycerol      Cytosol  
 PMEVKc (R)-5-Phosphomevalonate + ATP => (R)-5-Diphosphomevalonate + ADP      Cytosol  
 PPAP\_cho      Phosphatidate + H2O => 1,2-Diacyl-sn-glycerol + Orthophosphate      Cytosol  
 PPM      alpha-D-Ribose 1-phosphate = D-Ribose 5-phosphate      Cytosol  
 PPi\_Hydro      Diphosphate = 2\*Orthophosphate      Cytosol  
 PRO1xm      NAD + L-Proline => (S)-1-Pyrroline-5-carboxylate + NADH      Mitochondria  
 PROD2      FAD + L-Proline => (S)-1-Pyrroline-5-carboxylate + FADH2      Cytosol  
 PROD2m      FAD + L-Proline =>(S)-1-Pyrroline-5-carboxylate + FADH2      Mitochondria  
 PRPPS      ATP + D-Ribose\_5-phosphate = AMP + 5-Phospho-alpha-D-ribose\_1-diphosphate      Cytosol  
 PSERT      3-Phosphonoxypruvate + L-Glutamate => O-Phospho-L-serine + 2-Oxoglutarate      Cytosol  
 PSP\_L      H2O + O-Phospho-L-serine => Orthophosphate + L-Serine      Cytosol  
 PSSA1\_cho      Phosphatidylcholine + L-Serine = Choline + Phosphatidylserine      Cytosol  
 PUNP5      Orthophosphate + Inosine = alpha-D-Ribose\_1-phosphate + Hypoxanthine      Cytosol  
 PYK      ADP + Phosphoenolpyruvate => ATP + Pyruvate      Cytosol  
 R00851      sn-Glycerol 3-phosphate + Acyl-CoA => 1-Acyl-sn-glycerol 3-phosphate + CoA      Cytosol  
 R01083      N6-(1,2-Dicarboxyethyl)-AMP => Fumarate + AMP      Cytosol  
 R01135      GTP + IMP + L-Aspartate => GDP + Orthophosphate + N6-(1,2-Dicarboxyethyl)-AMP      Cytosol  
 R01866      (S)-Dihydroorotate + NADP => Orotate + NADPH      Cytosol  
 R02030      Phosphatidylglycerol + CDP-diacylglycerol => Cardiolipin + CMP      Cytosol  
 R02241      1-Acyl-sn-glycerol 3-phosphate + Acyl-CoA => Phosphatidate + CoA      Cytosol  
 RE0453Cd      ATP + dTDP = dADP + dTTP      Cytosol  
 RE2410C7      Dehydrodesmosterol + NADPH => Desmosterol + NADP      Cytosol  
 RE3347CF      FAD + NADH = FADH2 + NAD      Cytosol  
 RNDR2      Thioredoxin + GDP => H2O + Thioredoxin disulfide + dGDP      Cytosol  
 RNDR3      Thioredoxin + CDP => H2O + Thioredoxin disulfide + dCDP      Cytosol  
 RNDR4      Thioredoxin + UDP => H2O + Thioredoxin disulfide + dUDP      Cytosol  
 RPE      D-Ribulose\_5-phosphate = D-Xylulose\_5-phosphate      Cytosol  
 RPI      D-Ribulose\_5-phosphate = D-Ribose\_5-phosphate      Cytosol  
 SERPT      Palmitoyl-CoA + L-Serine = 3-Dehydrosphinganine + CO2 + CoA      Cytosol  
 SMS\_cho      N-Acylsphingosine + Phosphatidylcholine => 1,2-Diacyl-sn-glycerol + Sphingomyelin  
             Cytosol



## Appendix

---

SQLEc NADPH + O2 + Squalene => (S)-2,3-Epoxy-squalene + H2O+ NADP Cytosol  
 SQLSc 2\*trans,trans-Farnesyl\_diphosphate + NADPH => NADP + 2\*Diphosphate + Squalene Cytosol  
 SUCD1 FAD + Succinate = FADH2 + Fumarate Cytosol  
 SUCD1mFAD + Succinate = FADH2 + Fumarate Mitochondria  
 SUCOAS1m Succinyl-CoA + Orthophosphate + GDP = CoA + Succinate + GTP Mitochondria  
 TALA 3-Phospho-D-glycerate + Sedoheptulose\_7-phosphate = alpha-D-Fructose\_6-phosphate + D-Erythrose\_4-phosphate Cytosol  
 TKT1 D-Ribose\_5-phosphate + D-Xylulose\_5-phosphate = 3-Phospho-D-glycerate + Sedoheptulose\_7-phosphate Cytosol  
 TKT2 D-Xylulose\_5-phosphate + D-Erythrose\_4-phosphate = 3-Phospho-D-glycerate + alpha-D-Fructose\_6-phosphate Cytosol  
 TMDS dUMP + 5,10-Methylenetetrahydrofolate => Dihydrofolate + dTMP Cytosol  
 TPI 3-Phospho-D-glycerate = Glycerone phosphate Cytosol  
 TRDR NADPH + Thioredoxin disulfide => NADP + Thioredoxin Cytosol  
 TRPO2 O2 + L-Tryptophan => L-Formylkynurenine Cytosol  
 UMPK ATP + UMP = ADP + UDP Cytosol  
 UMPK3 UTP + UMP = 2\*UDP Cytosol  
 URIDK2 ATP + dUMP = ADP + dUDP Cytosol  
 r0060 L-Serine => Pyruvate + NH4 Cytosol  
 r0074 L-Glutamate + NADH = L-Glutamate\_5-semialdehyde + NAD + H2O Cytosol  
 r0074m L-Glutamate + NADH => L-Glutamate\_5-semialdehyde + NAD + H2O Mitochondria  
 r0512 Dihydrofolate + NAD = Folate + NADH Cytosol

----- TRANSPORT -----

Identifier	Equation	Compartment
2OXOADPTm	2-Oxoadipate_Cytosol + 2-Oxoglutarate_Mitochondria = 2-Oxoadipate_Mitochondria + 2-Oxoglutarate_Cytosol	Mitochondria - Cytosol
AASS	2*CoA_Mitochondria + 3*NAD_Mitochondria + 2*2-Oxoglutarate_Cytosol + L-Lysine_Cytosol => 2*L-Glutamate_Cytosol + 2*Acetyl-CoA_Mitochondria + 2*CO2_Cytosol + 3*NADH_Mitochondria	Mitochondria - Cytosol
ASPLUM	L-Glutamate_Cytosol + L-Aspartate_Mitochondria = L-Glutamate_Mitochondria + L-Aspartate_Cytosol	Mitochondria - Cytosol
ATPTm	ADP_Cytosol + ATP_Mitochondria => ATP_Cytosol + ADP_Mitochondria	Mitochondria - Cytosol
Alam	L-Alanine_Mitochondria = L-Alanine_Cytosol	Mitochondria - Cytosol
BCAT2	2-Oxoglutarate_Cytosol + 2*ATP_Cytosol + 3*CoA_Mitochondria + L-Leucine_Cytosol + 2*NAD_Cytosol => 2*ADP_Cytosol + 3*Acetyl-CoA_Mitochondria + L-Glutamate_Cytosol + 2*NADH_Cytosol	Mitochondria - Cytosol
BCAT3	2-Oxoglutarate_Cytosol + CoA_Mitochondria + L-Isoleucine_Cytosol + 3*NAD_Cytosol => Acetyl-CoA_Mitochondria + L-Glutamate_Cytosol + 3*NADH_Cytosol	Mitochondria - Cytosol
CITtam	Citrate_Mitochondria + L-Malate_Cytosol => Citrate_Cytosol + L-Malate_Mitochondria	Mitochondria - Cytosol
CO2m	CO2_Mitochondria = CO2_Cytosol	Mitochondria - Cytosol
Ex_CO2	CO2_Cytosol = CO2_external	Cytosol - external
Ex_Choline	Choline_Cytosol = Choline_external	Cytosol - external
Ex_D-Glucose	alpha-D-Glucose_Cytosol = D-Glucose_external	Cytosol - external
Ex_Ethanolamine	Ethanolamine_Cytosol = Ethanolamine_external	Cytosol - external
Ex_Formate	Formate_Cytosol = Formate_external	Cytosol - external
Ex_Glycine	Glycine_Cytosol = Glycine_external	Cytosol - external
Ex_H2O	H2O_Cytosol = H2O_external	Cytosol - external
Ex_Hypoxanthine	Hypoxanthine_Cytosol = Hypoxanthine_external	Cytosol - external

## Appendix

---

Ex\_L-Alanine L-Alanine\_Cytosol = L-Alanine\_external Cytosol - external  
 Ex\_L-Arginine L-Arginine\_Cytosol = L-Arginine\_external Cytosol - external  
 Ex\_L-Asparagine L-Asparagine\_Cytosol = L-Asparagine\_external Cytosol - external  
 Ex\_L-Aspartate L-Aspartate\_Cytosol = L-Aspartate\_external Cytosol - external  
 Ex\_L-Cysteine L-Cysteine\_Cytosol = L-Cysteine\_external Cytosol - external  
 Ex\_L-Glutamate L-Glutamate\_Cytosol = L-Glutamate\_external Cytosol - external  
 Ex\_L-Glutamine L-Glutamine\_Cytosol = L-Glutamine\_external Cytosol - external  
 Ex\_L-Histidine L-Histidine\_Cytosol = L-Histidine\_external Cytosol - external  
 Ex\_L-Isoleucine L-Isoleucine\_Cytosol = L-Isoleucine\_external Cytosol - external  
 Ex\_L-Lactate L-Lactate\_Cytosol = L-Lactate\_external Cytosol - external  
 Ex\_L-Leucine L-Leucine\_Cytosol = L-Leucine\_external Cytosol - external  
 Ex\_L-Lysine L-Lysine\_Cytosol = L-Lysine\_external Cytosol - external  
 Ex\_L-Methionine L-Methionine\_Cytosol = L-Methionine\_external Cytosol - external  
 Ex\_L-Phenylalanine L-Phenylalanine\_Cytosol = L-Phenylalanine\_external Cytosol - external  
 Ex\_L-Proline L-Proline\_Cytosol = L-Proline\_external Cytosol - external  
 Ex\_L-Serine L-Serine\_Cytosol = L-Serine\_external Cytosol - external  
 Ex\_L-Threonine L-Threonine\_Cytosol = L-Threonine\_external Cytosol - external  
 Ex\_L-Tryptophan L-Tryptophan\_Cytosol = L-Tryptophan\_external Cytosol - external  
 Ex\_L-Tyrosine L-Tyrosine\_Cytosol = L-Tyrosine\_external Cytosol - external  
 Ex\_L-Valine L-Valine\_Cytosol = L-Valine\_external Cytosol - external  
 Ex\_NH4 NH4\_Cytosol = NH4\_external Cytosol - external  
 Ex\_O2 O2\_Cytosol = O2\_external Cytosol - external  
 Ex\_myo-Inositol myo-Inositol\_Cytosol = myo-Inositol\_external Cytosol - external  
 External\_Pi Orthophosphate\_Cytosol=Orthophosphate\_external Cytosol - external  
 GLNtm L-Glutamine\_Cytosol => L-Glutamine\_Mitochondria Mitochondria - Cytosol  
 GLUt2m L-Glutamate\_Cytosol = L-Glutamate\_Mitochondria Mitochondria - Cytosol  
 H2Om H2O\_Mitochondria = H2O\_Cytosol Mitochondria - Cytosol  
 LTAE CoA\_Mitochondria + NAD\_Cytosol + L-Threonine\_Cytosol => Acetyl-CoA\_Mitochondria +  
 Glycine\_Cytosol + NADH\_Cytosol Mitochondria - Cytosol  
 MALtm Orthophosphate\_Mitochondria + L-Malate\_Cytosol = Orthophosphate\_Cytosol + L-  
 Malate\_Mitochondria Mitochondria - Cytosol  
 MAT 2\*ATP\_Cytosol + L-Methionine\_Cytosol + NAD\_Mitochondria + L-Serine\_Cytosol + 2-  
 Oxoglutarate\_Cytosol + Tetrahydrofolate\_Cytosol=> 5,10-Methylenetetrahydrofolate\_Cytosol +  
 NADH\_Mitochondria + Pyruvate\_Cytosol + Succinate\_Cytosol + 2\*ADP\_Cytosol + L-Glutamate\_Cytosol  
 Mitochondria - Cytosol  
 NH4m NH4\_Mitochondria = NH4\_Cytosol Mitochondria - Cytosol  
 O2m O2\_Mitochondria = O2\_Cytosol Mitochondria - Cytosol  
 PROtm L-Proline\_Cytosol = L-Proline\_Mitochondria Mitochondria - Cytosol  
 PYRtm Pyruvate\_Cytosol = Pyruvate\_Mitochondria Mitochondria - Cytosol  
 TAT1 2-Oxoglutarate\_Cytosol + L-Tyrosine\_Cytosol + ATP\_Cytosol + 2\*CoA\_Mitochondria => CO2\_Cytosol +  
 L-Glutamate\_Cytosol + 2\*Acetyl-CoA\_Mitochondria + Fumarate\_Cytosol + ADP\_Cytosol Mitochondria - Cytosol  
 TAT2 2-Oxoglutarate\_Cytosol + NADH\_Cytosol + L-Phenylalanine\_Cytosol + ATP\_Cytosol +  
 2\*CoA\_Mitochondria => CO2\_Cytosol + L-Glutamate\_Cytosol + NAD\_Cytosol + 2\*Acetyl-CoA\_Mitochondria +  
 Fumarate\_Cytosol + ADP\_Cytosol Mitochondria - Cytosol  
 mu 1\*X\_Cytosol=>1\*X\_external Cytosol - external  
 qmab 1\*IgG1\_Cytosol=>1\*IgG1\_external Cytosol - external  
 r0911 L-Glutamate\_Mitochondria + L-Proline\_Cytosol = L-Glutamate\_Cytosol + L-Proline\_Mitochondria  
 Mitochondria - Cytosol  
 r1290 FADH2\_Mitochondria + FAD\_Cytosol = FADH2\_Cytosol + FAD\_Mitochondria Mitochondria - Cytosol  
 tATP ATP\_external = ATP\_Cytosol Cytosol - external  
 tCMP CMP\_external = CMP\_Cytosol Cytosol - external  
 tCardiolipin Cardiolipin\_external = Cardiolipin\_Cytosol Cytosol - external

tCholes 1\*Cholesterol\_Cytosol=>1\*Cholesterol\_external Cytosol - external  
tCholesterol Cholesterol\_external = Cholesterol\_Cytosol Cytosol - external  
tGMP GMP\_external = GMP\_Cytosol Cytosol - external  
tPRT PRT\_external => L-Proline\_Cytosol + L-Tyrosine\_Cytosol Cytosol - external  
tPhosphatidylcholine Phosphatidylcholine\_external = Phosphatidylcholine\_Cytosol Cytosol - external  
tPhosphatidylglycerol Phosphatidylglycerol\_external = Phosphatidylglycerol\_Cytosol Cytosol - external  
tPhosphatidylinositol 1-Phosphatidyl-D-myo-inositol\_external = 1-Phosphatidyl-D-myo-inositol\_Cytosol  
Cytosol - external  
tPhosphatidylserine Phosphatidylserine\_external = Phosphatidylserine\_Cytosol Cytosol - external  
tSphingomyelin Sphingomyelin\_external = Sphingomyelin\_Cytosol Cytosol - external  
tUMP UMP\_external = UMP\_Cytosol Cytosol - external  
tUrea 1\*Urea\_Cytosol=>1\*Urea\_external Cytosol - external  
tdAMP dAMP\_external = dAMP\_Cytosol Cytosol - external  
tdCMP dCMP\_external = dCMP\_Cytosol Cytosol - external  
tdGMP dGMP\_external = dGMP\_Cytosol Cytosol - external  
tdTMP dTMP\_external = dTMP\_Cytosol Cytosol - external

----- POLYMERISATION -----

Identifier	Equation	Compartment
Acyl-CoA_Syn	2*Octadecanoic_acid+ATP+CoA=Acyl-CoA+AMP	Cytosol
Glyc_Syn	100*UDP-glucose=Glycogen+100*UDP	Cytosol

----- BALANCED COMPOUNDS -----

(R)-5-Diphosphomevalonate Cytosol  
(R)-5-Phosphomevalonate Cytosol  
(R)-Mevalonate Cytosol  
(S)-1-Pyrroline-5-carboxylate Cytosol  
(S)-1-Pyrroline-5-carboxylate Mitochondria  
(S)-2,3-Epoxy-squalene Cytosol  
(S)-3-Hydroxybutanoyl-CoA Mitochondria  
(S)-Dihydroorotate Cytosol  
1,2-Diacyl-sn-glycerol Cytosol  
1-Acyl-sn-glycerol\_3-phosphate Cytosol  
1-Phosphatidyl-D-myo-inositol Cytosol  
10-Formyltetrahydrofolate Cytosol  
14-Demethylsterol Cytosol  
2-Amino-3-carboxymuconate\_semialdehyde Cytosol  
2-Aminomuconate Cytosol  
2-Aminomuconate\_semialdehyde Cytosol  
2-Oxadipate Mitochondria  
2-Oxadipate Cytosol  
2-Oxoglutarate Cytosol  
2-Oxoglutarate Mitochondria  
3-Dehydrospinganine Cytosol  
3-Hydroxy-L-kynurenine Cytosol  
3-Hydroxyanthranilate Cytosol  
3-Keto-4-methylzymosterol Cytosol  
3-Phospho-D-glycerate Cytosol  
3-Phospho-D-glyceroyl\_phosphate Cytosol

---

3-Phosphonooxypyruvate	Cytosol
3-Sulfinopyruvate	Cytosol
3-sulfinato-L-alaninate	Cytosol
4,4-Dimethyl-5alpha-cholesta-8,14,24-trien-3beta-ol	Cytosol
4alpha-Methylzymosterol-4-carboxylate	Cytosol
5,10-Methenyltetrahydrofolate	Cytosol
5,10-Methylenetetrahydrofolate	Cytosol
5-Phospho-alpha-D-ribose_1-diphosphate	Cytosol
5alpha-Cholesta-7,24-dien-3beta-ol	Cytosol
6-Phospho-D-gluconate	Cytosol
7-Dehydrodesmosterol	Cytosol
ACP	Cytosol
ADP	Cytosol
ADP	Mitochondria
AMP	Cytosol
ATP	Cytosol
ATP	Mitochondria
Acetoacetyl-CoA	Cytosol
Acetoacetyl-CoA	Mitochondria
Acetyl-ACP	Cytosol
Acetyl-CoA	Cytosol
Acetyl-CoA	Mitochondria
Acyl-CoA	Cytosol
CDP	Cytosol
CDP-choline	Cytosol
CDP-diacylglycerol	Cytosol
CDP-ethanolamine	Cytosol
CMP	Cytosol
CO2	Mitochondria
CO2	Cytosol
CTP	Cytosol
Carbamoyl_phosphate	Cytosol
Cardiolipin	Cytosol
Cholesterol	Cytosol
Choline	Cytosol
Choline_phosphate	Cytosol
Citrate	Cytosol
Citrate	Mitochondria
CoA	Cytosol
CoA	Mitochondria
Crotonoyl-CoA	Mitochondria
D-Erythrose_4-phosphate	Cytosol
D-Glucono-1,5-lactone_6-phosphate	Cytosol
D-Glycerate_2-phosphate	Cytosol
D-Glycerate_3-phosphate	Cytosol
D-Ribose_5-phosphate	Cytosol
D-Ribulose_5-phosphate	Cytosol
D-Xylulose_5-phosphate	Cytosol
Desmosterol	Cytosol
Dihydroceramide	Cytosol
Dihydrofolate	Cytosol
Dimethylallyl_diphosphate	Cytosol

Diphosphate Cytosol  
 Ethanolamine Cytosol  
 Ethanolamine\_phosphate Cytosol  
 FAD Cytosol  
 FAD Mitochondria  
 FADH2 Cytosol  
 FADH2 Mitochondria  
 Folate Cytosol  
 Formate Cytosol  
 Fumarate Cytosol  
 Fumarate Mitochondria  
 GDP Cytosol  
 GDP Mitochondria  
 GMP Cytosol  
 GTP Cytosol  
 GTP Mitochondria  
 Geranyl\_diphosphate Cytosol  
 Glutaryl-CoA Mitochondria  
 Glycerone\_phosphate Cytosol  
 Glycine Cytosol  
 Glycogen Cytosol  
 H2O Cytosol  
 H2O Mitochondria  
 Hexadecanoic\_acid Cytosol  
 Hexadecanoyl-ACP Cytosol  
 Hypoxanthine Cytosol  
 IMP Cytosol  
 IgG1 Cytosol  
 Inosine Cytosol  
 Isocitrate Mitochondria  
 Isopentenyl\_diphosphate Cytosol  
 L-Alanine Cytosol  
 L-Alanine Mitochondria  
 L-Arginine Cytosol  
 L-Asparagine Cytosol  
 L-Aspartate Cytosol  
 L-Aspartate Mitochondria  
 L-Cysteine Cytosol  
 L-Formylkynurenine Cytosol  
 L-Glutamate Cytosol  
 L-Glutamate Mitochondria  
 L-Glutamate\_5-semialdehyde Cytosol  
 L-Glutamate\_5-semialdehyde Mitochondria  
 L-Glutamine Cytosol  
 L-Glutamine Mitochondria  
 L-Histidine Cytosol  
 L-Isoleucine Cytosol  
 L-Kynurenine Cytosol  
 L-Lactate Cytosol  
 L-Leucine Cytosol  
 L-Lysine Cytosol  
 L-Malate Cytosol

L-Malate	Mitochondria
L-Methionine	Cytosol
L-Phenylalanine	Cytosol
L-Proline	Cytosol
L-Proline	Mitochondria
L-Serine	Cytosol
L-Threonine	Cytosol
L-Tryptophan	Cytosol
L-Tyrosine	Cytosol
L-Valine	Cytosol
Lanosterol	Cytosol
Malonyl-CoA	Cytosol
N-Acylsphingosine	Cytosol
N-Carbamoyl-L-aspartate	Cytosol
N6-(1,2-Dicarboxyethyl)-AMP	Cytosol
NAD	Mitochondria
NAD	Cytosol
NADH	Mitochondria
NADH	Cytosol
NADP	Cytosol
NADPH	Cytosol
NH <sub>4</sub>	Cytosol
NH <sub>4</sub>	Mitochondria
O-Phospho-L-serine	Cytosol
O <sub>2</sub>	Cytosol
O <sub>2</sub>	Mitochondria
Octadecanoic_acid	Cytosol
Octadecanoyl-ACP	Cytosol
Orotate	Cytosol
Orotidine_5'-phosphate	Cytosol
Orthophosphate	Cytosol
Orthophosphate	Mitochondria
Oxaloacetate	Cytosol
Oxaloacetate	Mitochondria
Palmitoyl-CoA	Cytosol
Phosphatidate	Cytosol
Phosphatidylcholine	Cytosol
Phosphatidylethanolamine	Cytosol
Phosphatidylglycerol	Cytosol
Phosphatidylserine	Cytosol
Phosphoenolpyruvate	Cytosol
Pyruvate	Cytosol
Pyruvate	Mitochondria
S-3-Hydroxy-3-methylglutaryl-CoA	Cytosol
Sedoheptulose_7-phosphate	Cytosol
Sphinganine	Cytosol
Sphingomyelin	Cytosol
Squalene	Cytosol
Succinate	Cytosol
Succinate	Mitochondria
Succinyl-CoA	Mitochondria
Tetrahydrofolate	Cytosol

Thioredoxin Cytosol  
 Thioredoxin\_disulfide Cytosol  
 UDP Cytosol  
 UDP-glucose Cytosol  
 UMP Cytosol  
 UTP Cytosol  
 Urea Cytosol  
 X Cytosol  
 XMP Cytosol  
 Zymosterol Cytosol  
 alpha-D-Fructose\_1,6-bisphosphate Cytosol  
 alpha-D-Fructose\_6-phosphate Cytosol  
 alpha-D-Glucose Cytosol  
 alpha-D-Glucose\_1-phosphate Cytosol  
 alpha-D-Glucose\_6-phosphate Cytosol  
 alpha-D-Ribose\_1-phosphate Cytosol  
 dADP Cytosol  
 dAMP Cytosol  
 dATP Cytosol  
 dCDP Cytosol  
 dCMP Cytosol  
 dCTP Cytosol  
 dGDP Cytosol  
 dGMP Cytosol  
 dGTP Cytosol  
 dTDP Cytosol  
 dTMP Cytosol  
 dTTP Cytosol  
 dUDP Cytosol  
 dUMP Cytosol  
 myo-Inositol Cytosol  
 sn-Glycerol\_3-phosphate Cytosol  
 trans,trans-Farnesyl\_diphosphate Cytosol  
 zymosterol\_intermediate\_2 Cytosol

## 6.2 Supplementary Material: Manuscript 3

**Table 8. S1.** List of differential expressed genes (FDR adjusted p-values  $\leq 0.05$  and a  $\log_2$ -fold-change  $\geq |1|$ ) between MTA treated cells and REF at different sampling points.

Cultivation time	Gene name	Encoded protein	$\log_2$ FC	$p_{adj}$
60 h	LOC100758641	Unknown loci	-1.5462	2.09E-11
72 h	Apc2	Adenomatous polyposis coli protein 2	-2.0147	2.05E-05
	Il11	Interleukin-11	1.7590	9.04E-03
	LOC100752010	Unknown loci	-1.8965	3.28E-44
	LOC100752547	Unknown loci	-1.7611	6.47E-61
	LOC100752904	Unknown loci	-2.8233	6.96E-52
	LOC100754104	Unknown loci	-2.1791	1.22E-03
	LOC100757772	Unknown loci	-2.0797	4.80E-03
	LOC100758641	Unknown loci	-2.2051	3.56E-57
	LOC100759078	Unknown loci	2.6407	8.35E-06
	LOC100763833	Unknown loci	1.3991	1.06E-22
	LOC107979446	Unknown loci	-1.5823	2.07E-04
	LOC113834379	Unknown loci	2.4872	2.37E-12
84 h	Abhd6	Monoacylglycerol lipase ABHD6	1.6150	3.39E-14
	Apc2	Adenomatous polyposis coli protein 2	-2.6685	1.19E-11
	Aqp1	Aquaporin-1	1.6270	4.92E-07
	Arnt2	Aryl hydrocarbon receptor nuclear translocator 2	2.0281	1.81E-03
	Atf5	Cyclic AMP-dependent transcription factor ATF-5	-1.3981	1.00E-11
	Cd53	Leukocyte surface antigen CD53	1.2726	1.66E-02
	Dnase1l3	Deoxyribonuclease gamma	1.7149	2.64E-06
	Egfr	Epidermal growth factor receptor	1.9483	4.93E-02
	Fam110c	Protein FAM110C	3.3351	3.89E-02
	Hr	Lysine-specific demethylase hairless	1.7904	3.55E-11
	Il11	Interleukin-11	1.6337	1.34E-02
	Il17f	Interleukin-17F	1.3734	2.01E-02
	Lcp1	Plastin-2	1.3012	1.63E-02
	LOC100752010	Unknown loci	-1.8313	5.22E-41
	LOC100752320	Unknown loci	2.4102	2.92E-03
	LOC100752547	Unknown loci	-1.8263	4.61E-72
	LOC100752904	Unknown loci	-2.7420	5.12E-50
	LOC100754451	Unknown loci	1.7129	6.84E-04
	LOC100757491	Unknown loci	-1.4832	3.13E-03
	LOC100757772	Unknown loci	-2.1447	9.61E-04
LOC100758065	Unknown loci	-1.7437	6.51E-04	



Appendix

	LOC100758641	Unknown loci	-1.8581	5.61E-31
	LOC100759078	Unknown loci	3.2187	7.24E-13
	LOC100763833	Unknown loci	1.3429	1.39E-16
	LOC100768011	Unknown loci	2.1813	1.33E-03
	LOC100772574	Unknown loci	1.8754	7.70E-05
	LOC103159878	Unknown loci	1.6027	2.92E-03
	LOC103160179	Unknown loci	1.5442	7.70E-05
	LOC103163365	Unknown loci	1.6926	2.19E-06
	LOC107979406	Unknown loci	2.0241	1.36E-02
	LOC107979446	Unknown loci	-1.7874	1.07E-09
	LOC113830954	Unknown loci	-1.5141	2.98E-04
	LOC113831402	Unknown loci	-1.5335	2.21E-06
	LOC113834379	Unknown loci	3.3442	2.24E-26
	Lpin3	Phosphatidate phosphatase LPIN3	1.4621	1.52E-04
	Oasl	2'-5'-oligoadenylate synthase-like protein 2	1.6231	7.03E-08
	Osr1	Protein odd-skipped-related 1	1.6940	4.93E-02
	Plau	Urokinase-type plasminogen activator	1.6420	1.84E-06
	Rassf6	Ras association domain-containing protein 6	3.0480	3.42E-05
	Sh2d1b	SH2 domain-containing protein 1B	2.6888	2.47E-02
	St14	Suppressor of tumorigenicity 14 protein homolog	1.7150	2.25E-06
	St8sia6	Alpha-2,8-sialyltransferase 8F	2.5774	5.18E-02
96 h	37135	unclassified gene	1.6601	3.44E-05
	Abhd6	Monoacylglycerol lipase ABHD6	1.5517	6.14E-13
	Acsf6	Long-chain-fatty-acid--CoA ligase 6	1.4768	2.77E-02
	Add2	beta-adducin	1.9814	4.20E-63
	Adgrd1	Adhesion G-protein coupled receptor D1	1.9627	2.90E-09
	Akr1d1	Aldo-keto reductase family 1 member D1	3.0345	6.37E-07
	Aqp1	Aquaporin-1	1.9092	2.58E-27
	Arnt2	Aryl hydrocarbon receptor nuclear translocator 2	2.4951	1.73E-09
	Btbd16	BTB/POZ domain-containing protein 16	2.6161	1.53E-03
	Cacnb4	Voltage-dependent L-type calcium channel subunit beta-4	1.4605	6.18E-07
	Caps2	Calcyphosin-2	1.9403	2.23E-04
	Cd53	Leukocyte surface antigen CD53	1.7555	1.06E-27
	Cdkl4	Cyclin-dependent kinase-like 4	2.3503	1.41E-02
	Dnase1l3	Deoxyribonuclease gamma	1.9169	1.01E-10
	Egfr	Epidermal growth factor receptor	1.9510	2.04E-02
	Fam110c	Protein FAM110C	3.9865	1.10E-03
	Fbln5	Fibulin-5	2.3963	4.75E-08
	Fcer2	Low affinity immunoglobulin epsilon Fc receptor	2.3978	1.84E-02
	Fgf22	Fibroblast growth factor 22	-2.3868	5.67E-04

Appendix

Fscn1	Fascin	2.0475	5.63E-03
Fubp1	Far upstream element-binding protein 1	-1.3968	3.20E-18
Gda	Guanine deaminase	2.5229	7.09E-03
Grap2	GRB2-related adaptor protein 2	3.1363	4.42E-04
Hr	Lysine-specific demethylase hairless	2.2624	1.08E-28
Il17f	Interleukin-17F	1.5799	9.27E-08
Il7r	Interleukin-7 receptor	1.7915	1.08E-13
Lama3	Laminin subunit alpha-3	1.8936	2.84E-02
Lama4	Laminin subunit alpha-4	3.2260	2.04E-07
Lcp1	Plastin-2	1.8680	3.54E-32
LOC100752320	Unknown loci	2.6816	5.68E-05
LOC100754451	Unknown loci	2.1444	7.02E-12
LOC100758264	Unknown loci	2.6336	1.91E-07
LOC100759078	Unknown loci	3.1636	2.42E-11
LOC100761810	Unknown loci	1.8829	2.51E-05
LOC100765213	Unknown loci	2.4075	8.59E-04
LOC100767707	Unknown loci	1.6958	8.07E-04
LOC100768011	Unknown loci	1.9758	1.21E-02
LOC100768431	Unknown loci	2.0809	6.29E-06
LOC100769250	Unknown loci	2.1826	8.94E-03
LOC100771813	Unknown loci	1.5230	9.47E-03
LOC100772574	Unknown loci	2.5184	1.49E-17
LOC100773221	Unknown loci	3.1006	6.35E-05
LOC103159534	Unknown loci	3.1549	4.40E-02
LOC103159864	Unknown loci	1.7840	1.11E-09
LOC103160097	Unknown loci	2.7651	1.37E-04
LOC103160117	Unknown loci	1.8504	2.63E-08
LOC103160179	Unknown loci	1.8616	5.64E-16
LOC103161069	Unknown loci	1.9762	6.04E-06
LOC103161216	Unknown loci	2.5399	5.21E-04
LOC103161664	Unknown loci	1.5320	2.58E-14
LOC103162509	Unknown loci	3.7144	5.03E-06
LOC103163365	Unknown loci	1.5129	1.37E-02
LOC103163978	Unknown loci	2.4338	1.28E-03
LOC103164035	Unknown loci	1.8408	1.01E-03
LOC103164463	Unknown loci	2.7724	7.76E-22
LOC107977260	Unknown loci	1.5847	3.33E-02
LOC107977336	Unknown loci	2.7754	5.18E-02
LOC107977412	Unknown loci	1.8604	5.23E-04
LOC107978123	Unknown loci	4.2850	8.60E-03
LOC107979406	Unknown loci	2.1857	1.43E-03
LOC107979531	Unknown loci	3.7050	2.20E-02

Appendix

	LOC107979868	Unknown loci	1.9182	3.52E-07
	LOC107979936	Unknown loci	3.0577	3.81E-06
	LOC113830872	Unknown loci	1.7550	3.65E-03
	LOC113834379	Unknown loci	2.8868	3.86E-17
	LOC113834741	Unknown loci	1.6853	8.49E-04
	LOC113835325	Unknown loci	2.6836	1.54E-02
	Loxl2	Lysyl oxidase homolog 2	1.3176	2.60E-06
	Lpin3	Phosphatidate phosphatase LPIN3	1.5952	6.91E-09
	Mpeg1	Macrophage-expressed gene 1 protein	2.2254	8.00E-04
	Neurl3	E3 ubiquitin-protein ligase NEURL3	1.4171	1.25E-07
	Oasl	2'-5'-oligoadenylate synthase-like protein 2	1.5642	9.50E-07
	Olfml2b	Olfactomedin-like protein 2B	2.1188	6.12E-09
	Pglyrp2	N-acetylmuramoyl-L-alanine amidase	3.1533	2.50E-02
	Pik3r5	Phosphoinositide 3-kinase regulatory subunit 5	1.9506	3.16E-04
	Plau	Urokinase-type plasminogen activator	2.2809	2.16E-32
	Ppm1h	Protein phosphatase 1H	2.0878	8.26E-03
	Rassf6	Ras association domain-containing protein 6	2.8067	1.23E-04
	Sema4d	Semaphorin-4D	1.5042	1.25E-03
	Sema4f	Semaphorin-4F	3.2138	3.52E-05
	Sh2d1b	SH2 domain-containing protein 1B	2.8037	7.95E-03
	Slc17a6	Vesicular glutamate transporter 2	2.3757	6.18E-07
	Spn	Leukosialin	3.3465	1.82E-03
	Spp1	Osteopontin	1.9261	1.40E-04
	St14	Suppressor of tumorigenicity 14 protein homolog	2.2368	1.39E-22
	St8sia6	Alpha-2,8-sialyltransferase 8F	3.2315	6.91E-05
	Tcea2	Transcription elongation factor A protein 2	-1.7638	8.29E-03
	Tmprss11f	Transmembrane protease serine 11F	2.0498	2.38E-12
144 h	Add2	beta-adducin	1.6707	1.88E-07
	Adgrd1	Adhesion G-protein coupled receptor D1	1.9219	1.88E-11
	Akr1d1	Aldo-keto reductase family 1 member D1	3.6322	1.20E-05
	Aqp1	Aquaporin-1	2.0311	1.01E-48
	Chd5	Chromodomain-helicase-DNA-binding protein 5	1.4287	1.84E-02
	Dpysl3	Dihydropyrimidinase-related protein 3	3.5452	5.24E-03
	Fbn1	Fibrillin-1	2.1766	1.90E-02
	Il7r	Interleukin-7 receptor	1.7037	7.07E-05
	Lcp1	Plastin-2	1.7737	1.55E-25
	LOC100765213	Unknown loci	3.1663	5.46E-03
	LOC100769250	Unknown loci	2.9004	1.34E-07
	LOC100771813	Unknown loci	2.2455	1.39E-18
	LOC100771938	Unknown loci	3.9692	1.84E-02

Appendix

LOC100772574	Unknown loci	2.9161	2.07E-32
LOC103160179	Unknown loci	1.8126	1.61E-13
LOC103160858	Unknown loci	2.3540	4.56E-06
LOC103161069	Unknown loci	2.2406	1.64E-11
LOC103163104	Unknown loci	2.8482	4.73E-04
LOC103163978	Unknown loci	2.6849	2.17E-04
LOC103164463	Unknown loci	1.9957	5.22E-02
LOC107977412	Unknown loci	1.7400	1.98E-02
LOC107978048	Unknown loci	3.4223	1.48E-04
LOC107978123	Unknown loci	4.2591	1.07E-03
LOC107978153	Unknown loci	3.9118	1.32E-02
LOC107979254	Unknown loci	2.9282	1.77E-03
LOC107979493	Unknown loci	2.8049	2.84E-02
LOC107979936	Unknown loci	2.4581	1.39E-04
Loxl2	Lysyl oxidase homolog 2	1.3890	1.82E-11
Mmp2	72 kDa type IV collagenase	2.3902	2.12E-04
Mpeg1	Macrophage-expressed gene 1 protein	1.8577	6.15E-03
Pdzrn3	E3 ubiquitin-protein ligase PDZRN3	2.0603	1.31E-02
Pecam1	Platelet endothelial cell adhesion molecule	1.2802	3.92E-03
Pglyrp2	N-acetylmuramoyl-L-alanine amidase	3.2871	1.98E-02
Pik3cg	Phosphatidylinositol 4,5-bisphosphate 3-kinase catalytic subunit gamma isoform	1.7025	3.13E-02
Plac1	Placenta-specific protein 1	1.4593	1.88E-07
Plau	Urokinase-type plasminogen activator	2.1120	2.88E-20
Sema4d	Semaphorin-4D	1.8857	6.55E-09
St14	Suppressor of tumorigenicity 14 protein homolog	2.0575	1.45E-12
Tmc1	Transmembrane channel-like protein 1	-1.9236	1.75E-03
Tmprss11f	Transmembrane protease serine 11F	2.0424	3.24E-04
Trem14	Trem-like transcript 4 protein	2.9737	3.23E-03

**Appendix S1.** Transcriptome analysis. Sample description, mapping statistics and counts.

Available online: [doi:10.1002/2211-5463.13019](https://doi.org/10.1002/2211-5463.13019)

## 6.3 Supplementary Material: Manuscript 4

### Supplemental Material 2

#### Optimizer

	Ref - growth	MTA - growth
Number of data fitted	210	210
Number of flux parameter	8	8
$\chi^2(0.95)$	236.159	236.159
$\chi^2$ (optimizer)	176.74	191.89

$$SSR = \frac{(x^{sim} - x^{exp})^2}{\sigma^2}$$

## Key Fluxes

REFERENCE				
Flux ID	Reaction	optimized	LB (95%)	UB (95%)
ppp1	G6P --> P5P + CO2	0.00458	0.00325	0.00600
phdgh	GAP --> Ser	0.00109	0.00056	0.00169
fGlyco	Glyco --> G6P	0.01973	0.01440	0.02427
pepck	OAA --> PEP + CO2	0.01888	0.01873	0.01906
alt	Pyr + Glu <-> Ala + aKG	0.035	0.02650	0.04655
me	Mal <-> Pyr + CO2	0.06585	0.04741	0.07770
mem	Mal_m <-> Pyr_m + CO2	-0.005	-0.03600	0.01100
astm	Asp_m + aKG_m <-> OAA_m + Glu_m	-0.00192	-0.00206	-0.00179
MTA48				
Flux ID	Reaction	optimized	LB (95%)	UB (95%)
ppp1	G6P --> P5P + CO2	0.09898	0.09060	0.10698
phdgh	GAP --> Ser	0.000678	0.00037	0.00118
fGlyco	Glyco --> G6P	0	0.00000	0.00300
pepck	OAA --> PEP + CO2	0.02441	0.01576	0.03600
alt	Pyr + Glu <-> Ala + aKG	0.01207	0.01100	0.01480
me	Mal <-> Pyr + CO2	0.03483	0.02300	0.04232
mem	Mal_m <-> Pyr_m + CO2	-0.007627	-0.01880	-0.00050
astm	Asp_m + aKG_m <-> OAA_m + Glu_m	-0.007373	-0.00970	-0.00485

## Fluxes detail

	Flux ID	Reaction	REFERENCE		MTA48		Welsch Test	
			mean	std	mean	std	MTA48	SIG/NON SIG
Extracellular rates	tAla	Ala <-> Ala_ex	0.102	0.00168	0.13848	0.01056	0.0275	SIG
	tAsn	Asn_ex -> Asn	0.29232	0.03288	0.29064	0.01872	0.9435	NON-SIG
	tAsp	Asp <-> Asp_ex	0.01944	0.00288	0.0156	0.00168	0.1400	NON-SIG
	tCO2	CO2 -> CO2_ex	9.8628	4.08312	8.172	0.92376	0.5566	NON-SIG
	tGlc	Glc -> G6P	2.67744	0.60888	2.8332	0.1392	0.7079	NON-SIG
	tGln	Gln_ex -> Gln	0.22152	0.01176	0.15552	0.02712	0.0608	NON-SIG
	tGlu	Glu <-> Glu_ex	0.13104	0.0096	0.10656	0.006	0.0332	SIG
	tLac	Lac <-> Lac_ex	3.09144	0.564	3.04704	0.09912	0.5158	NON-SIG
	tSer	Ser_ex -> Ser	0.16248	0.02664	0.10872	0.00456	0.7113	NON-SIG
Biomass growth reactions	acl	Cit --> OAA + AcCoA	0.20328	0.01296	0.14976	0.054	0.2370	NON-SIG
	muAcCoA	AcCoA -> AcCoA_X	0.20328	0.01296	0.14976	0.054	0.2370	NON-SIG
	muAla	Ala -> Ala_X	0.01152	0.00312	0.03624	0.0132	0.0874	NON-SIG
	muAsn	Asn -> Asn_X	0.02376	0.00144	0.01752	0.00624	0.2335	NON-SIG
	muAsp	Asp -> Asp_X	0.03864	0.0024	0.02856	0.01032	0.2412	NON-SIG
	muG6P	G6P -> G6P_X	0.02376	0.00144	0.01752	0.00624	0.0626	NON-SIG
	muGAP	GAP -> GAP_X	0.01008	0.00072	0.00744	0.00264	0.0645	NON-SIG
	muGln	Gln -> Gln_X	0.054	0.00168	0.01944	0.00696	0.0140	SIG
	muGlu	Glu -> Glu_X	0.03168	0.00192	0.02328	0.0084	0.0625	NON-SIG
	muP5P	P5P -> P5P_X	0.0192	0.0012	0.01416	0.00504	0.0629	NON-SIG
	muSer	Ser -> Ser_X	0.03624	0.0024	0.02664	0.0096	0.0635	NON-SIG
EMP	fGlyco	Glyco -> G6P	0.47352	0.10896	0.024	0.024	0.0199	SIG
	pgi	G6P <-> F6P	3.01728	0.61944	0.49392	0.222	0.0221	SIG
	pfk	F6P <-> FbP	3.07776	0.61872	2.0484	0.1524	0.1910	NON-SIG
	fbpa	FbP <-> GAP + DHAP	3.07776	0.61872	2.0484	0.1524	0.1910	NON-SIG
	tpi	DHAP <-> GAP	3.07776	0.61872	2.0484	0.1524	0.1910	NON-SIG
	gapdh	GAP <-> 3PG	6.17592	1.23744	4.86672	0.28848	0.3942	NON-SIG

Appendix

	eno	3PG <-> PEP	6.14976	1.23744	4.84704	0.28848	0.3942	NON-SIG
	pkm	PEP -> Pyr	6.60288	1.23744	5.43288	0.35544	0.4538	NON-SIG
	ldh	Pyr <-> Lac	3.09144	0.564	3.04704	0.09912	0.5158	NON-SIG
<b>PPP</b>	G6Pdh	G6P -> P5P + CO2	0.10992	0.03192	2.34576	0.17136	0.0020	SIG
	tk1	2*P5P <-> S7P + GAP	0.03024	0.01056	0.77712	0.05712	0.0020	SIG
	tald	E4P + P5P <-> F6P + GAP	0.03024	0.01056	0.77712	0.05712	0.0020	SIG
	tk2	S7P + GAP <-> E4P + F6P	0.03024	0.01056	0.77712	0.05712	0.0020	SIG
<b>Mitochondrial shuttles</b>	AGC	Glu + Asp_m --> Glu_m + Asp	0.31488	0.03312	0.44136	0.0552	0.4766	NON-SIG
	CIC	Cit_m + Mal --> Cit + Mal_m	0.20328	0.01296	0.14976	0.054	0.2370	NON-SIG
	DIC	Mal_m <-> Mal	1.19352	0.34992	1.0368	0.29784	0.5963	NON-SIG
	GC	Glu_m <-> Glu	0.89304	0.20472	0.34824	0.0552	0.0119	SIG
	MPC	Pyr --> Pyr_m	4.40424	1.40448	2.93832	0.42648	0.5143	NON-SIG
	OGC	Mal + aKG_m <-> Mal_m + aKG	-0.5832	0.20664	0.08712	0.07224	0.0160	SIG
	mAla	Ala <-> Ala_m	0.72648	0.204	0.13512	0.04848	0.0256	SIG
	mAsn	Asn <-> Asn_m	0.2688	0.03288	0.27336	0.01968	0.4380	NON-SIG
	mCO2	CO2_m <-> CO2	7.71936	4.0932	4.4796	0.98472	0.9863	NON-SIG
<b>Citric acid cycle</b>	pdh	Pyr_m -> AcCoA_m	3.31296	1.36056	1.96176	0.30792	0.7350	NON-SIG
	csyn	AcCoA + OAA -> Cit	3.31296	1.36056	1.96176	0.30792	0.7350	NON-SIG
	idh	Cit_m <-> aKG_m + CO2_m	3.10968	1.3608	1.812	0.31272	0.7655	NON-SIG
	adh	aKG_m <-> Fum_m + CO2_m	3.11472	1.36104	1.81776	0.3168	0.8893	NON-SIG
	mdh	Mal_m <-> OAA_m	1.66104	1.39152	1.20096	0.44136	0.6153	NON-SIG
	fus	Fum <-> Mal	3.11472	1.36104	1.81776	0.3168	0.8893	NON-SIG
	mdhc	OAA <-> Mal	0.00696	0.036	-0.03912	0.22176	0.9419	NON-SIG



<b>anaplerotic</b>	pc	Pyr_m <-> OAA_m	1.698	0.28704	0.9288	0.30768	0.0326	SIG
	me	Mal <-> Pyr + CO2	1.5804	0.2844	0.7608	0.2088	0.0276	SIG
	mem	Mal_m <-> Pyr_m + CO2_m	-0.12	0.0144	-0.18312	0.08088	0.3147	NON-SIG
	pepck	OAA <-> PEP + CO2	0.45312	0.0036	0.58584	0.2076	0.3836	NON-SIG
<b>Amino acids metabolism</b>	gs	Gln -> Glu	0.16752	0.01176	0.13584	0.02784	0.2111	NON-SIG
	gdh	aKG_m <-> Glu_m	0.10224	0.03672	0.06	0.0408	0.1239	NON-SIG
	phdgh	3PG -> Ser	0.02616	0.01272	0.01968	0.00864	0.5183	NON-SIG
	sds	Ser -> Pyr	0.1524	0.02952	0.10176	0.01368	0.7332	NON-SIG
	asns	Asn_m <-> Asp_m	0.2688	0.03288	0.27336	0.01968	0.4380	NON-SIG
	ast	Asp + aKG <-> OAA + Glu	0.2568	0.03336	0.39696	0.05616	0.1500	NON-SIG
	astm	Asp_m + aKG_m <-> OAA_m + Glu_m	-0.04608	0.00312	-0.168	0.0516	0.0150	SIG
	alt	Pyr + Glu <- > Ala + aKG	0.84	0.204	0.30984	0.04536	0.0481	SIG
	altm	Ala_m + aKG_m <-> Pyr_m + Glu_m	0.72648	0.204	0.13512	0.04848	0.0256	SIG

**NADH NADPH**

Production	Ref	MTA
NADPH	1.80024	5.45232
NADPH_err	0.29148	0.40132
NADH(c)	6.17592	4.90584
NADH(c)_err	1.23744	0.36386565
NADH(m)	7.88544	4.83072
NADH(m)_err	2.37498	0.62686

### **Supplemental Material 3**

\*\*\*\* HEADER \*\*\*\*

Method:FBA

Mode: CPLEX

Model: Nielsen\_CHO\_FBA\_simplified

Version: 4.3.0-SNAPSHOT

Date: 3/6/2020 - 8:05

Comment:

Objective: 1.0\*m\_NADPH 1.4037589999999995

Constraints:

-1.0\*"Ex\_D-Glucose" = 0.11284  
1.0\*Ex\_Glycine <= 0.007123  
1.0\*Ex\_Glycine >= 0.005828  
1.0\*Ex\_Hypoxanthine = 0.0  
1.0\*"Ex\_L-Alanine" <= 0.013079  
1.0\*"Ex\_L-Alanine" >= 0.010701  
-1.0\*"Ex\_L-Arginine" <= 0.00476  
-1.0\*"Ex\_L-Arginine" >= 0.00389  
-1.0\*"Ex\_L-Asparagine" <= 0.01907  
-1.0\*"Ex\_L-Asparagine" >= 0.01561  
-1.0\*"Ex\_L-Aspartate" <= 0.0047  
-1.0\*"Ex\_L-Aspartate" >= 0.00384  
-1.0\*"Ex\_L-Cysteine" <= 0.00452  
-1.0\*"Ex\_L-Cysteine" >= 0.0037  
1.0\*"Ex\_L-Glutamate" <= 0.008557  
1.0\*"Ex\_L-Glutamate" >= 0.007001  
-1.0\*"Ex\_L-Glutamine" <= 0.04954  
-1.0\*"Ex\_L-Glutamine" >= 0.04054  
-1.0\*"Ex\_L-Histidine" <= 0.00207  
-1.0\*"Ex\_L-Histidine" >= 0.00169  
-1.0\*"Ex\_L-Isoleucine" <= 0.00547  
-1.0\*"Ex\_L-Isoleucine" >= 0.00448  
1.0\*"Ex\_L-Lactate" <= 0.224561  
1.0\*"Ex\_L-Lactate" >= 0.183732  
-1.0\*"Ex\_L-Leucine" <= 0.00861  
-1.0\*"Ex\_L-Leucine" >= 0.00704  
-1.0\*"Ex\_L-Lysine" <= 0.00689  
-1.0\*"Ex\_L-Lysine" >= 0.00564  
-1.0\*"Ex\_L-Methionine" <= 0.00414  
-1.0\*"Ex\_L-Methionine" >= 0.00339  
-1.0\*"Ex\_L-Phenylalanine" <= 0.00347  
-1.0\*"Ex\_L-Phenylalanine" >= 0.00284  
-1.0\*"Ex\_L-Proline" <= 0.00349  
-1.0\*"Ex\_L-Proline" >= 0.00286  
-1.0\*"Ex\_L-Serine" <= 0.01893  
-1.0\*"Ex\_L-Serine" >= 0.01548  
-1.0\*"Ex\_L-Threonine" <= 0.00543  
-1.0\*"Ex\_L-Threonine" >= 0.00445  
-1.0\*"Ex\_L-Tryptophan" <= 0.00103  
-1.0\*"Ex\_L-Tryptophan" >= 8.4E-4  
1.0\*"Ex\_L-Tyrosine" = 0.0

```
-1.0*"Ex_L-Valine" <= 0.00519
-1.0*"Ex_L-Valine" >= 0.00425
1.0*tATP = 0.0
1.0*tCMP = 0.0
1.0*tCardiolipin = 0.0
1.0*tCholes = 0.0
1.0*tCholesterol = 0.0
1.0*tGMP = 0.0
1.0*tPhosphatidylglycerol = 0.0
1.0*tPhosphatidylinositol = 0.0
1.0*tPhosphatidylserine = 0.0
1.0*tSphingomyelin = 0.0
Equation: 0.11*D-Glucose + 0.91*H2O + 0.76E-2*O2 + 0.47E-2*L-Arginine + 0.19E-1*L-Asparagine + 0.47E-2*L-
Aspartate + 0.45E-2*L-Cysteine + 0.49E-1*L-Glutamine + 0.2E-2*L-Histidine + 0.54E-2*L-Isoleucine + 0.86E-2*L-
Leucine + 0.68E-2*L-Lysine + 0.41E-2*L-Methionine + 0.34E-2*L-Phenylalanine + 0.34E-2*L-Proline + 0.18E-1*L-
Serine + 0.54E-2*L-Threonine + 0.1E-2*L-Tryptophan + 0.51E-2*L-Valine + 0.23E-1*Orthophosphate =
0.72*CO2 + 0.1E-2*Formate + 0.18*L-Lactate + 0.2*NH4 + 0.58E-2*Glycine + 0.1E-1*L-Alanine + 0.7E-2*L-
Glutamate + 0.47E-2*Urea
**** EOF HEADER ****

**** Flux ****
2OXOADOXm 0.00103
2OXOADPTm 0.00103
3DSPHR 0.0
3HAO 0.00103
3SALATAi 0.00452
3SPYRSP0.00452
AASS 0.00689
ACACT1r0.0
ACACT1rm -0.00103
ACCOAC 0.0
ACITL 0.0
ACOATA 0.0
ACONTm 0.09142799999999995
ADK1 0.0
ADK3 0.0
ADKd 0.0
AKGDm 0.144287
ALATA_L-0.373008999999999987
ALATA_Lm 0.36333799999999999
AM6SAD0.00103
AMCOXO 0.00103
AMPDA 0.23334699999999997
ARG 0.00476
ASNN 0.01907
ASPCTr 0.0
ASPLUm 0.53367599999999998
ASPTA 0.324098999999999986
ASPTAm -0.53367599999999998
ATPtM 0.144287
Acyl-CoA_Syn 0.0
Alam -0.36333799999999999
```

## Appendix

---

BCAT1	0.00519	
BCAT2	0.00861	
BCAT3	0.00547	
Biomass_pmol_cell		0.0
C14STRc	0.0	
C3STDH1Pc	0.0	
C3STKR2c	0.0	
C4STMO1c	0.0	
C4STMO2Pc	0.0	
CBPS	0.0	
CDIPTr_cho	0.0	
CDS_cho	0.0	
CEPTC_cho	0.0	
CEPTE_cho	0.0	
CHLP	0.0	
CHLPCTD	0.0	
CITtam	0.0	
CO2m	-0.3554109999999999	
CSm	0.09142799999999995	
CTPS2	0.0	
CYSO	0.00452	
CYTK1	0.0	
CYTK10	0.0	
CYTK11	0.0	
CYTK12	0.0	
DGK1	0.0	
DHCR243r	0.0	
DHCRD1_cho	0.0	
DHCRD2_cho	0.0	
DHFR	0.0	
DHORTS	0.0	
DMATTc	0.0	
DPMVDc	0.0	
DSAT_cho	0.0	
DTMPK	0.0	
EBP1c	0.0	
EOAH1m	-0.00103	
ENO	0.11284	
ETC_1	0.0	
ETC_2	0.0	
ETHAK	0.0	
Ex_CO2	0.7277199999999999	
Ex_Choline	0.0	
Ex_D-Glucose	-0.11284	
Ex_Ethanolamine	0.0	
Ex_Formate	0.00103	
Ex_Glycine	0.005828	
Ex_H2O	-0.9194179999999997	
Ex_Hypoxanthine	0.0	
Ex_L-Alanine	0.010701	
Ex_L-Arginine	-0.00476	
Ex_L-Asparagine	-0.01907	

---

Ex_L-Aspartate	-0.0047
Ex_L-Cysteine	-0.00452
Ex_L-Glutamate	0.007001
Ex_L-Glutamine	-0.04954
Ex_L-Histidine	-0.00207
Ex_L-Isoleucine	-0.00547
Ex_L-Lactate	0.183732
Ex_L-Leucine	-0.00861
Ex_L-Lysine	-0.00689
Ex_L-Methionine	-0.00414
Ex_L-Phenylalanine	-0.00347
Ex_L-Proline	-0.00349
Ex_L-Serine	-0.01893
Ex_L-Threonine	-0.00543
Ex_L-Tryptophan	-0.00103
Ex_L-Tyrosine	0.0
Ex_L-Valine	-0.00519
Ex_NH4	0.20092999999999997
Ex_O2	-0.0076100000000000004
Ex_myo-Inositol	0.0
External_Pi	-0.0237800000000000023
FA16BS	0.0
FA180ACPH	0.0
FACOAL160i	0.0
FAS180ACP	0.0
FBA	0.0
FKYNH	0.00103
FOLR2	0.0
FTHFDH	0.0066079999999999999
FUMc	0.24614699999999998
FUMm	0.144287
G3PD1	0.0
G5SADr	-0.00349
G5SADrm	0.0
G6PDH2r	0.33852
GALU	0.0
GAPD	0.11284
GHMT2r	3.979999999999999E-4
GK1	0.0
GLNtm	0.04954
GLUDxm	-0.11644899999999997
GLUN	0.04954
GLUTCOADHm	0.00103
GLUt2m	-0.5293269999999999
GMPS2	0.0
GND	0.33852
GRTTc	0.0
Glyc_Syn	0.0
H2Om	-0.169836
HACD1m	-0.00103
HAL	0.00207
HEX1	0.11284

---

HKYNH 0.00103  
HMGCOARc 0.0  
HMGCOASi 0.0  
HXACPHY 0.0  
HXPRT 0.0  
ICDHxm 0.0914279999999995  
IMPD 0.0  
INSK 0.0  
IPDDI 0.0  
IgG 0.0  
KYN3OX 0.00103  
LDH\_L 0.183732  
LNS14DMc 0.0  
LNSTLSc 0.0  
LSTO1c 0.0  
LTAE 0.00543  
M 0.0  
MALtm -0.144287  
MAT 0.00414  
MDH -0.32409899999999986  
MDHm 0.6251039999999998  
ME1m -0.6251039999999998  
ME2 0.7145329999999999  
MEVK1c 0.0  
MTHFC 0.006607999999999999  
MTHFD 0.006607999999999999  
NDPK1 0.23334699999999997  
NDPK1m -0.144287  
NDPK2 0.0  
NDPK3 0.0  
NDPK4 0.0  
NDPK5 0.0  
NDPK7 0.0  
NDPK8 0.0  
NH4m -0.06690899999999997  
O2m 0.0  
OMPDC 0.0  
ORPT 0.0  
P5CRxm 0.17805399999999999  
PCLAD 0.00103  
PDHm 0.031917999999999946  
PETHCT 0.0  
PFK 0.0  
PGCD 0.0  
PGI -0.22568  
PGK 0.11284  
PGL 0.33852  
PGM 0.11284  
PGMT 0.0  
PGPPT\_cho 0.0  
PMEVKc 0.0  
PPAP\_cho 0.0

---

PPM 0.0  
PPi\_Hydro 0.0  
PRO1xm 0.0  
PROD2 0.00349  
PROD2m 0.1780539999999999  
PROtm 0.0  
PRPPS 0.0  
PSERT 0.0  
PSP\_L 0.0  
PSSA1\_cho 0.0  
PUNP5 0.0  
PYK 0.11284  
PYRtm 0.29368399999999995  
R00851 0.0  
R01083 0.23334699999999997  
R01135 0.23334699999999997  
R01866 0.0  
R02030 0.0  
R02241 0.0  
RE0453C0.0  
RE2410C0.0  
RE3347C-0.3361909999999999  
RNDR2 0.0  
RNDR3 0.0  
RNDR4 0.0  
RPE 0.22568  
RPI 0.11284  
SERPT 0.0  
SMS\_cho 0.0  
SQLEc 0.0  
SQLSc 0.0  
SUCD1 0.00933  
SUCD1m 0.144287  
SUCOAS1m 0.144287  
TALA 0.11284  
TAT1 0.0  
TAT2 0.00347  
TKT1 0.11284  
TKT2 0.11284  
TMDS 0.0  
TPI 0.0  
TRDR 0.0  
TRPO2 0.00103  
UMPK 0.0  
UMPK3 0.0  
URIDK2 0.0  
m\_NADPH 1.40375899999999995  
mu 0.0  
qmab 0.0  
r0060 0.014391999999999999  
r0074 -0.00349  
r0074m 0.0

r0512 0.0  
 r0911 0.0  
 r1290 0.3233709999999999  
 tATP 0.0  
 tCMP 0.0  
 tCardiolipin 0.0  
 tCholes 0.0  
 tCholesterol 0.0  
 tGMP 0.0  
 tPhosphatidylcholine 0.0  
 tPhosphatidylglycerol 0.0  
 tPhosphatidylinositol 0.0  
 tPhosphatidylserine 0.0  
 tSphingomyelin 0.0  
 tUMP 0.0  
 tUrea 0.00476  
 tdAMP 0.0  
 tdCMP 0.0  
 tdGMP 0.0  
 tdTMP 0.0  
 \*\*\*\* EOF Flux \*\*\*\*

NADPH

Identifier	Rate	Rate x Stoichiometric Factor	Contribution [%]	Properties
FTHFDH	0.007	0.007	0.47	Properties
G6PDH2r	0.339	0.339	24.098	Properties
GND	0.339	0.339	24.098	Properties
ME2	0.715	0.715	50.864	Properties
MTHFD	0.007	0.007	0.47	Properties

OK



## 6.4 Original Publications

The following manuscripts were published in peer-reviewed journals and reproduced with permission of the authors (copyright holders).

Verhagen N, Wijaya AW, Teleki A, et al. Comparison of L-tyrosine containing dipeptides reveals maximum ATP availability for L-prolyl-L-tyrosine in CHO cells. *Eng Life Sci.* 2020; 1-11.

N.V. is the main author who conceived the first version of the manuscript, designed and conducted the experimental part and data analysis

N.V. and A.T. designed and conducted metabolomic measurements

A.W.W. conducted FBA analysis

A.T. and A.W.W. co-authored the manuscript

R.T. supervised the studies and co-authored the manuscript

Verhagen N, Teleki A, Heinrich C, Schilling M, Unsöld A, Takors R. S-adenosylmethionine and methylthioadenosine boost cellular productivities of antibody forming Chinese hamster ovary cells. *Biotechnology and Bioengineering.* 2020; 1-9.

N.V. is the main author who conceived the first version of the manuscript, designed and conducted the experimental part and data analysis

N.V. and A.T. developed and conducted extracellular MTA measurements

A.T. co-authored the manuscript

R.T. supervised the studies and co-authored the manuscript

Verhagen N, Zieringer J, Takors R. Methylthioadenosine (MTA) boosts cell-specific productivities of Chinese hamster ovary cultures: dosage effects on proliferation, cell cycle and gene expression. FEBS Open Bio. 2020; 1-14.

N.V. is the main author who conceived the first version of the manuscript, designed and conducted the experimental part and data analysis

J.Z. analyzed transcriptome data and co-authored the manuscript

N.V. and J.Z. interpreted transcriptome data

R.T. supervised the studies and co-authored the manuscript



## RESEARCH ARTICLE

# Comparison of L-tyrosine containing dipeptides reveals maximum ATP availability for L-prolyl-L-tyrosine in CHO cells

Natascha Verhagen<sup>1</sup> | Andy Wiranata Wijaya<sup>1</sup> | Attila Teleki<sup>1</sup> |  
Muhammad Fadhlullah<sup>1</sup> | Andreas Unsöld<sup>2</sup> | Martin Schilling<sup>3</sup> |  
Christoph Heinrich<sup>4</sup> | Ralf Takors<sup>1</sup>

<sup>1</sup> Institute of Biochemical Engineering, University of Stuttgart, Stuttgart, Germany

<sup>2</sup> Boehringer Ingelheim Pharma GmbH & Co. KG, Biberach, Germany

<sup>3</sup> Evonik Nutrition and Care GmbH, Darmstadt, Germany

<sup>4</sup> Xell AG, Bielefeld, Germany

## Correspondence

Prof. Dr.-Ing Ralf Takors, University of Stuttgart, Institute of Biochemical Engineering, Allmandring 31, 70563 Stuttgart, Germany.  
Email: [ralf.takors@ibvt.uni-stuttgart.de](mailto:ralf.takors@ibvt.uni-stuttgart.de)

## Funding information

Bundesministerium für Bildung und Forschung (BMBF), Grant/Award Number: 031L0077A

## Abstract

Increasing markets for biopharmaceuticals, including monoclonal antibodies, have triggered a permanent need for bioprocess optimization. Biochemical engineering approaches often include the optimization of basal and feed media to improve productivities of Chinese hamster ovary (CHO) cell cultures. Often, L-tyrosine is added as dipeptide to deal with its poor solubility at neutral pH. Showcasing IgG1 production with CHO cells, we investigated the supplementation of three L-tyrosine (TYR, Y) containing dipeptides: glycyl-L-tyrosine (GY), L-tyrosyl-L-valine (YV), and L-prolyl-L-tyrosine (PY). While GY and YV led to almost no phenotypic and metabolic differences compared to reference samples, PY significantly amplified TYR uptake thus maximizing related catabolic activity. Consequently, ATP formation was roughly four times higher upon PY application than in reference samples.

## KEYWORDS

dipeptides, flux balance analysis, CHO, media optimization, monoclonal antibody

## 1 | INTRODUCTION

Chinese hamster ovary (CHO) cells are important hosts for recombinant protein production and are the preferred system for monoclonal antibody production [1]. Early bioprocesses relied on the use of animal-derived sera like FBS to

meet the growth and productivity needs of those cells [2]. However, the use of such sera is no longer favored because of the inherent risk of viral contamination [3] and typically high lot-to-lot variations, potentially affecting bioprocess performance and product quality [4,5].

Chemically defined (CD) media were introduced about five decades ago and predominately consisted of essential L-amino acids (Eagle's media [6]; F12 media [7]). At a concentration of about 2 mg/mL in water at room temperature and neutral pH, L-tyrosine (TYR) has the lowest solubility of all essential amino acids. Accordingly, only small amounts of TYR can be added to basal and feed media

**Abbreviations:** CAC, citric acid cycle; CHO, Chinese hamster ovary; EMP, Embden-Meyerhof Parnas; FBA, flux balance analysis; GY, glycyl-L-tyrosine; mAB, monoclonal antibody; MAS, malate-aspartate shuttle; NADH, nicotinamide adenine dinucleotide; PY, L-prolyl-L-tyrosine; REF, reference; TYR, L-tyrosine; VCD, viable cell density; YV, L-tyrosyl-L-valine

This is an open access article under the terms of the [Creative Commons Attribution-NonCommercial-NoDerivs](https://creativecommons.org/licenses/by-nc-nd/4.0/) License, which permits use and distribution in any medium, provided the original work is properly cited, the use is non-commercial and no modifications or adaptations are made.

© 2020 The Authors. *Engineering in Life Sciences* published by Wiley-VCH Verlag GmbH & Co. KGaA

to avoid unwanted media precipitation, thereby trying to ensure process stability [5]. Non-wanted TYR insolubility could be prevented by feeding TYR with high pH because the latter greatly increases TYR solubility. However, pH control, salt concentration, and precipitation in the bioreactor are potential problems that can occur with such an approach. A safer and more robust approach is the replacement of single TYR by TYR-containing, chemically defined dipeptides, which can increase solubility up to 250-fold at neutral pH [8].

The industrial performance of CHO cells using specific TYR dipeptides was examined by Kang et al. [5], who demonstrated that substituting free amino acids with L-tyrosyl-L-lysine (YK), L-tyrosyl-L-histidine (LH), L-tyrosyl-L-alanine (YA), and L-tyrosyl-L-valine (YV) decreased secretion of lactate and ammonium by-products. Sánchez-Kopper et al. (2016) [9] showed that dipeptides such as L-alanyl-L-tyrosine (AY), glycyl-L-tyrosine (GY), and L-prolyl-L-tyrosine (PY) are taken up by CHO cells and cleaved intracellularly before entering catabolic and anabolic pathways. Furthermore, recent patents [10] demonstrate industrial interest in protecting the use of TYR-containing dipeptides in feed media.

In this study, we focus on the use of TYR-dipeptides as additional feeding compounds. We investigated the impact of related dipeptides on cellular metabolism. While the potential of TYR-containing dipeptides has been shown by the above studies, little is known about the metabolic consequences resulting from their consumption. Showcasing IgG1 production with CHO cells, our investigation focused on the metabolic impact of dipeptide bolus feeding. We chose GY, YV, and PY as our model dipeptides. Phenotypic tests were complemented by quantitative metabolomics and flux analysis to decipher differences caused by dipeptides compared to cells lacking dipeptides in their feed. Whereas GY and YV did not significantly alter metabolism, PY increased the ATP supply, which represents a promising optimization target for future studies.

## 2 | MATERIALS AND METHODS

### 2.1 | Seed train, shake flask cultivation, and addition of dipeptides

The following dipeptides containing TYR were supplied by Evonik Nutrition and Care GmbH (Darmstadt, Germany): glycyl-L-tyrosine (GY), L-prolyl-L-tyrosine (PY), and L-tyrosyl-L-valine (YV). The IgG1-producing CHO suspension cell line BIBH1 (provided by Boehringer Ingelheim Pharma GmbH & Co. KG, Biberach, Germany) was grown in chemically defined TC-42 medium (Xell

### PRACTICAL APPLICATION

L-Tyrosine (TYR) is an essential amino acid for mammalian cells and shows poor solubility in cell culture media at neutral pH. Accordingly, TYR-containing dipeptides are commonly used that offer improved cellular supply. Here, we investigate the application of three L-tyrosine containing dipeptides showcasing the production of IgG1 with Chinese hamster ovary (CHO) cells. L-Prolyl-L-tyrosine (PY) caused the highest intracellular ATP availability that is an important property for all experimentalists in this field.

AG, Bielefeld, Germany) supplemented with 4 mM L-glutamine (Carl Roth GmbH & Co. KG, Karlsruhe, Germany), 200 nM methotrexate (Sigma-Aldrich, Steinheim, Germany), and 0.1 g/L geneticin (Fisher-Scientific, Schwerte, Germany). Seed train and experiments were performed in pre-sterilized disposable shake flasks (Corning Inc., New York, USA) in a humidified and incubated rotary shaker (Infors HT Minitron, Infors GmbH, Einsbach, Germany) at 37°C, 150 rpm with 50 mm displacement, and 5% CO<sub>2</sub>. Stock solutions of TYR-based dipeptides were solved at neutral pH and introduced at the beginning of cultivation (0.05 mM). Furthermore, daily additions (0.05 mmol) of dipeptides were performed from 48 to 120 h of cultivation. In reference cell cultures, sterilized water was used to mimic the additional liquid volume in experimental cultures. Cultivation was performed with biological duplicates in two independent experiments.

### 2.2 | Extracellular analysis

Samples were taken at least once a day during cultivation. Viable cell density and viability were determined using trypan blue staining and a Cedex XS cell counter (Innovatis AG, Bielefeld, Germany). The extracellular concentrations of D-glucose (D-glc) and L-lactate (L-lac) were determined using a Labotrace automatic analyzer (Trace Analytics GmbH, Braunschweig, Germany). The concentration of produced IgG was determined with an ELISA [11]. All sampling and measurement procedures were performed with three technical replicates. The extracellular concentrations of all proteinogenic amino acids with the exception of L-cysteine were quantified using reversed-phase chromatography (Agilent 1200 Series, Agilent Technologies, Waldbronn, Ger-

many) with a precolumn fluorometric derivatization step using ortho-phthalaldehyde (OPA)/9-fluorenylmethyl chloroformate (FMOC) [12,13]. The internal standard  $\gamma$ -aminobutyric acid (GABA) was added to all standard-based external calibration levels and the analyzed samples.

### 2.3 | Intracellular analysis

For each intracellular sample,  $1.6 \times 10^7$  cells were harvested, gently centrifuged (10 min,  $300 \times g$ ,  $4^\circ\text{C}$ ), washed, and quenched in liquid nitrogen. Washing steps were performed three times using ice-cold isotonic PBS solution to remove all extracellular compounds attached to the cells. Samples were taken after 60, 72, 76, 84, 96, 108, and 120 h of cultivation. Pre-processed cell pellets were stored at  $-70^\circ\text{C}$ . The intracellular metabolome was extracted from defined pellets using an adapted cold methanol/chloroform extraction method [9]. An ice-cold 1:2  $\text{CHCl}_3$ :MeOH solution was added to cells followed by ice-cold  $\text{CHCl}_3$  solution and finally by ice-cold water, with 5 min of vortexing after each addition. Resulting suspensions were incubated for 1 h at  $4^\circ\text{C}$  in a rotary overhead-shaker. Phase separation was afterward achieved by centrifugation for 10 min at  $3200 \times g$  and  $0^\circ\text{C}$ . The upper aqueous phase was separated and stored at  $-70^\circ\text{C}$  for further analysis. Dipeptide, amino acid, and central metabolite concentrations were determined on an HPLC system (Agilent 1200 Series) coupled with an Agilent 6410B triple quadrupole tandem mass spectrometer (QQQ-MS/MS, Agilent Technologies, Waldbronn, Germany). The LC-MS method was based on a bicratic (two-phase) zwitterionic hydrophilic interaction chromatography (ZIC-pHILIC) under alkaline mobile phase conditions without any derivatization [14,15]. Targeted metabolites were detected with high selectivity with pre-optimized precursor-to-product ion transitions and associated MS/MS settings in multiple reaction monitoring (MRM) mode. Absolute quantifications were performed by adapted standard-based external calibrations with constant addition of global internal standards ( $50 \mu\text{M}$  L-norvaline and GABA). Data were analyzed using MassHunter B.06.00 Analysis software.

Intracellular pools of AxP nucleotides were determined using an ion-pair-reversed-phase chromatography method with a HPLC system (Agilent 1200 Series) [16]. Underivatized samples were detected via UV light (diode array detector). Quantifications were performed by external standard calibration and selected samples were spiked with AMP, ADP, and ATP (internal calibration) to evaluate the influence of the sample matrix.

### 2.4 | Cell-specific rate estimations

Cell-specific rates of changes in extracellular metabolites were used as constraints when performing flux balance analysis (FBA). Cell-specific exo-metabolic rates were estimated from extracellular metabolite concentrations and viable cell density over time. Using Equations 1 and 2 and linear regression, growth rate and specific exo-metabolome uptake and secretion rates were estimated.

$$\frac{dC_x}{dt} = \mu C_x \Rightarrow \ln(C_x) = \mu(t - t_0) + \ln(C_0) \quad (1)$$

$$\frac{dC_i}{dt} = q_i C_x \Rightarrow C_i = \left(\frac{q_i}{\mu}\right) C_x - C_{i,0} \quad (2)$$

### 2.5 | Flux balance analysis

The metabolic model used in this study is a simplified genome-based model derived from the following sources: KEGG [17], CHOMINE [18], and *Mus musculus* GeM [19]. The detailed metabolic model is presented in Supporting Information S1. This model includes the central carbon metabolic pathway (consisting of the Embden-Meyerhof Parnas [EMP; glycolysis], pentose phosphate pathway [PPP], citric acid cycle [CAC], and anaerobic reactions), the biosynthesis of essential biomass precursors (fatty acids, steroids, glycogen, and nucleotides), and amino acid catabolism. The biomass composition required to model cell growth uses values reported by Sheikh et al. [20], whereas antibody composition is based on Martens [21]. Dipeptide cleavage occurs intracellularly following findings reported by Sánchez-Kopper et al. [9].

FBA was used to predict the fate of intracellular dipeptides and determine their role in CHO metabolism. FBA was performed using Insilico Discovery (Insilico Biotechnology, Stuttgart, Germany). FBA was carried out during the exponential growth phase, when the highest amount of dipeptide consumption occurs. Multiple assumptions were made for FBA. First, FBA was performed under a metabolic steady state with a constant growth rate and specific rates of change in D-glucose, L-lactate, L-glutamine, and L-asparagine levels. Additionally, the P/O ratio of nicotinamide adenine dinucleotide (NADH) and flavin adenine dinucleotide ( $\text{FADH}_2$ ) oxidation was assumed to be 1.5 and 1.2 mol ATP per mol of the nucleotide, respectively. FBA was performed using growth rate and extracellular metabolome uptake/secretion rates as constraints. The objective function of FBA was to maximize the model-predicted growth rate.

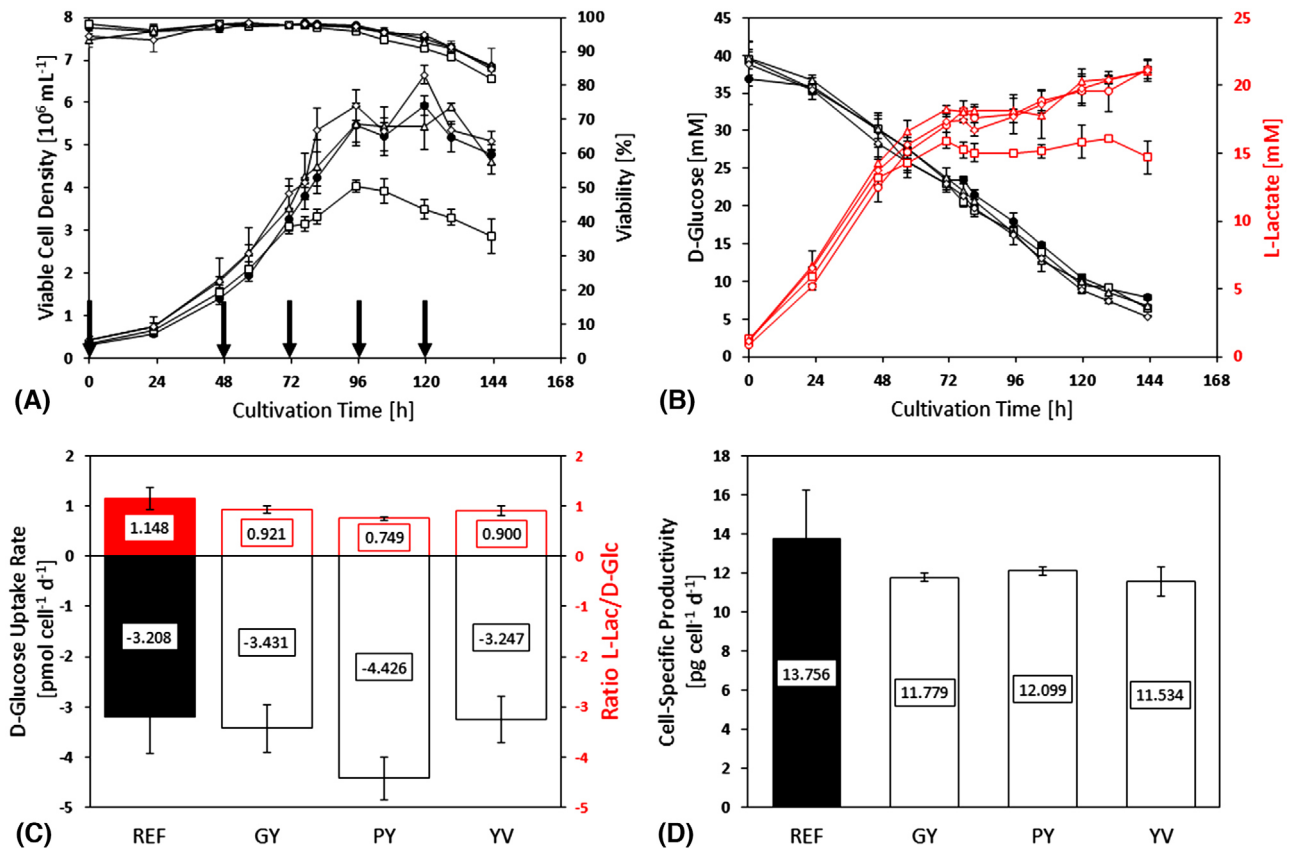


**FIGURE 1** (A) Time courses of viable cell density [ $10^6 \text{ cells mL}^{-1}$ ] and viability [%] and (B) time courses of extracellular D-glucose (black) and L-lactate (red) concentrations [mM] of dipeptide supplemented cells (GY  $\Delta$ , PY  $\square$ , YV  $\diamond$ ) and reference (REF  $\bullet$ ). Arrows indicate time points at which dipeptides or water were added. (C) Cell-specific rates of the exponential phase are calculated in [ $\mu\text{mol cell}^{-1} \text{ d}^{-1}$ ] for D-glucose consumption (black) and D-glucose-to-L-lactate-ratio (red). (D) Cell-specific productivity [ $\text{pg cell}^{-1} \text{ d}^{-1}$ ] of dipeptide supplemented cells (GY, PY, YV) and the reference (REF) in the exponential phase. Error bars show standard deviations of biological duplicates

Three simulations were performed for experimental and control cultures (REF, GY, PY, and YV) to obtain the maximum, minimum, and median rate predictions. Maximum (best-case scenario) and minimum predictions were simulated using the maximum or minimum uptake and secretion rates, respectively. For median estimation, maximum and minimum settings were applied as constraints. Upper and lower confidence intervals were calculated using twice the standard error of the predictions (i.e., 95% confidence level).

### 3 | RESULTS

#### 3.1 | The addition of L-prolyl-L-tyrosine alters cell growth and metabolism

Initially, TYR-containing dipeptides were added to a final concentration of 0.5 mM to cell culture medium used to cultivate CHO BIBH1 cells for IgG1-antibody production.

Fresh additions of TYR-containing dipeptides (0.05 mmol) took place after 48, 72, 96, and 120 h of cultivation (indicated by arrows in Figure 1). The addition of L-prolyl-L-tyrosine (PY) significantly reduced viable cell density (VCD), unlike the addition of glycyl-L-tyrosine (GY) and L-tyrosyl-L-valine (YV). Cells receiving regular additions of PY only reached a maximum viable cell density of  $(4.030 \pm 0.153) \times 10^6 \text{ cells/mL}$ , which was approximately two-thirds of the viable cell densities of GY, YV, and reference (REF) cultures.

PY addition affected antibody titer (Supporting Information S2, Figure S1) whereas cell-specific antibody productivity was similar for all experimental conditions. Specific D-glucose consumption rates were highest after PY addition during the exponential phase. Furthermore, cells that grew in medium with PY showed reduced L-lactate formation reflected in the low ratio of D-glucose consumption to L-lactate secretion (PY:  $0.749 \pm 0.030 \text{ mol}_{\text{D-Glucose}}/\text{mol}_{\text{L-Lactate}}$ ; REF:  $1.148 \pm 0.161 \text{ mol}_{\text{D-Glucose}}/\text{mol}_{\text{L-Lactate}}$ ; Figure 1).

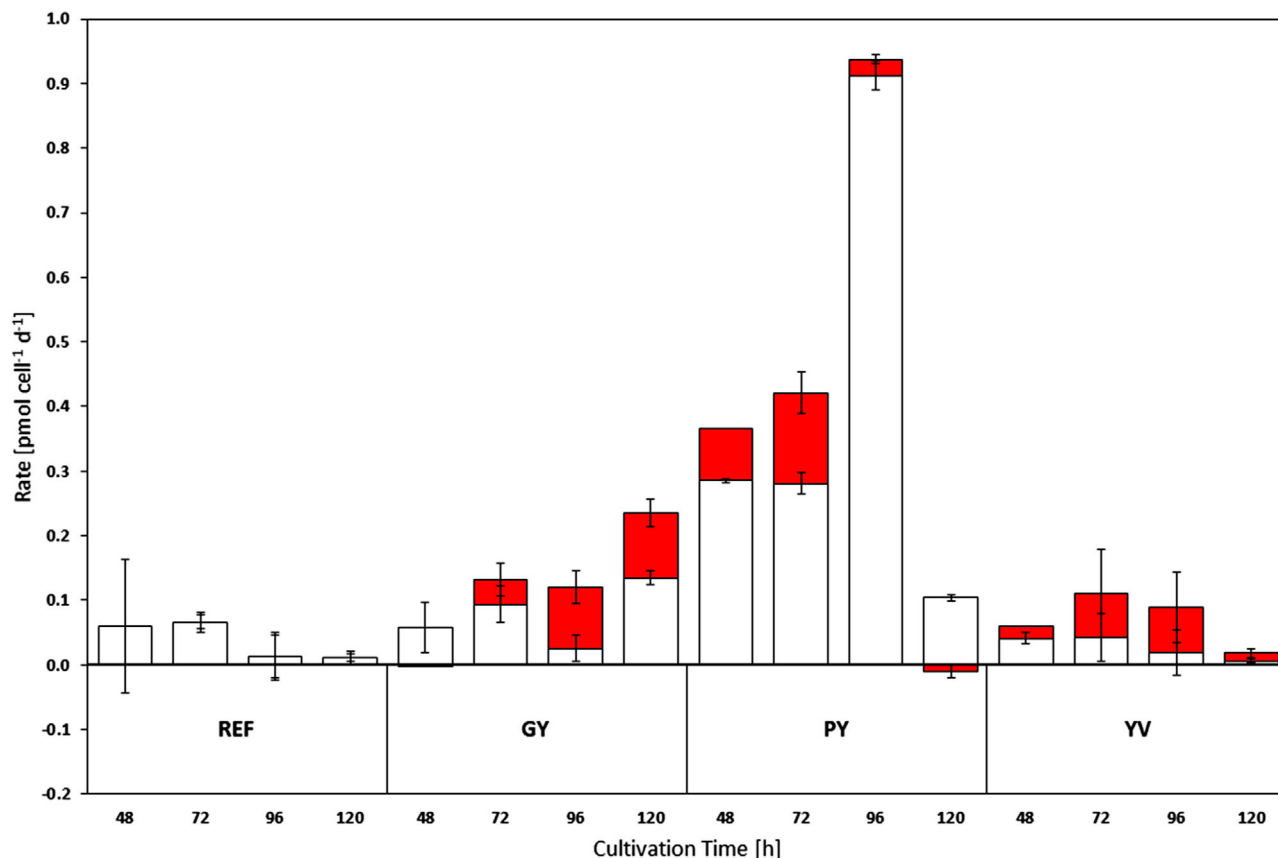


FIGURE 2 TYR uptake and release rates [pmol cell<sup>-1</sup> d<sup>-1</sup>] via dipeptides addition compared to reference cultures (REF) after 48, 72, 96, and 120 h of cultivation. Columns indicate the total levels of dipeptide uptake consisting of retained (white) and released (red) parts of TYR. Error bars show standard deviations of biological duplicates

### 3.2 | Dipeptide uptake depends on composition and causes metabolic changes

Uptake dynamics of TYR at different cultivation time points (48, 72, 96, and 120 h) are displayed in Figure 2. PY addition led to the largest total TYR uptake rates (indicated by the entire columns) and the largest fractions of TYR that remained intracellular (white columns) after 48, 72, and 96 h of cultivation. Remarkably, each addition of a TYR-containing dipeptide increased TYR uptake compared to reference cultures. However, some TYR from the decomposed dipeptide was always secreted (indicated by the red bar).

Small intracellular pools of dipeptides measured in intracellular extracts indicate the uptake of all dipeptides by cells. Intracellular fluctuations reflect extracellular bolus feeding. Repeated dipeptide addition to the medium (48, 72, 96, and 120 h) increased extracellular concentrations and consequently increased intracellular pool sizes of the intact dipeptides thereafter. Besides GY and YV,

extracellular PY is depleted at 72 and 96 h demonstrating the faster uptake of PY (Supporting Information S2, Figure S2).

Uptake rates of the essential amino acid L-glutamine were similar in PY ( $-1.297 \pm 0.047$  pmol cell<sup>-1</sup> d<sup>-1</sup>), GY ( $-1.243 \pm 0.170$  pmol cell<sup>-1</sup> d<sup>-1</sup>), and REF ( $-1.373 \pm 0.042$  pmol cell<sup>-1</sup> d<sup>-1</sup>) conditions but differed under YV conditions ( $-1.028 \pm 0.038$  pmol cell<sup>-1</sup> d<sup>-1</sup>). In contrast, sizes of intracellular L-glutamine pools differed. Compared to REF cultures, YV addition increased the L-glutamine pool while GY addition diminished the L-glutamine pool and PY addition nearly depleted the L-glutamine pool (Figure 3).

As outlined in Figure 2, cells always consumed the surplus of TYR provided by dipeptide addition and retained different fractions of that TYR. The additional TYR provided by PY affected the energetic status of the cells and increased ATP pool sizes beginning from 72 h after cultivation (Figure 4). Simultaneously, AMP pool sizes decreased after dipeptide addition.

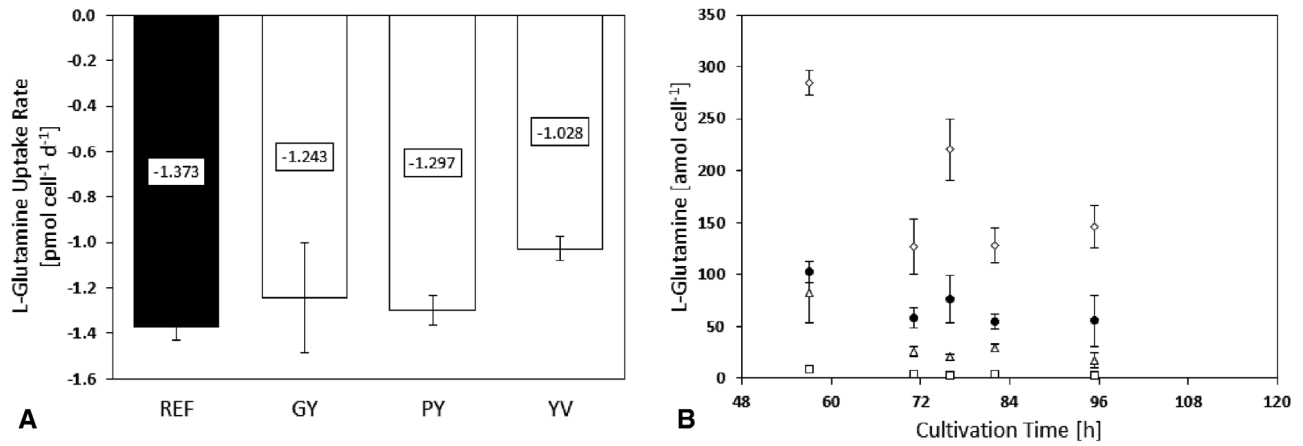


FIGURE 3 L-Glutamine consumption rates [pmol cell<sup>-1</sup> d<sup>-1</sup>] (A) and intracellular pool sizes [amol cell<sup>-1</sup>] (B) of dipeptide-supplemented cells (GY  $\Delta$ , PY  $\square$ , YV  $\diamond$ ) and reference cells (REF  $\bullet$ ). Negative values indicate an uptake. Error bars show standard deviations of biological duplicates

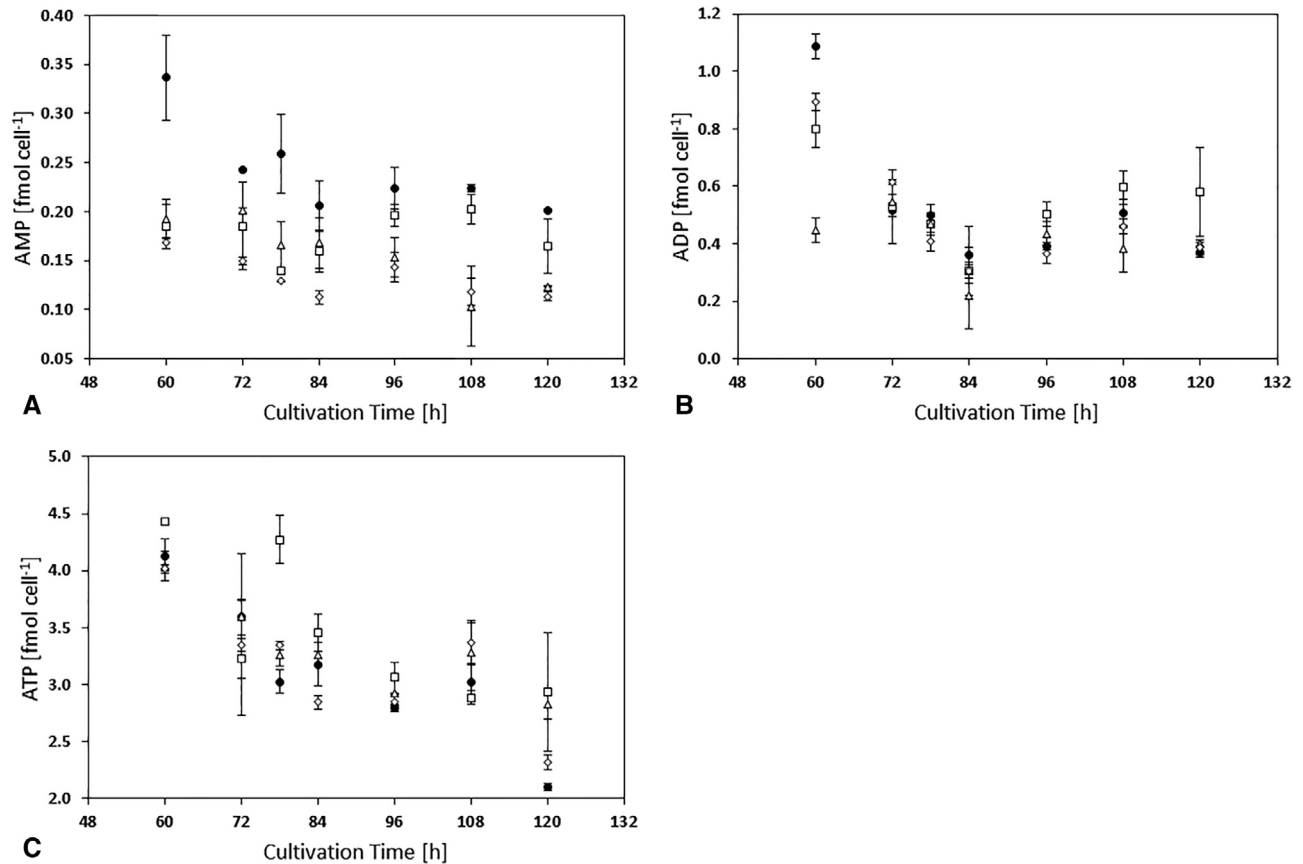
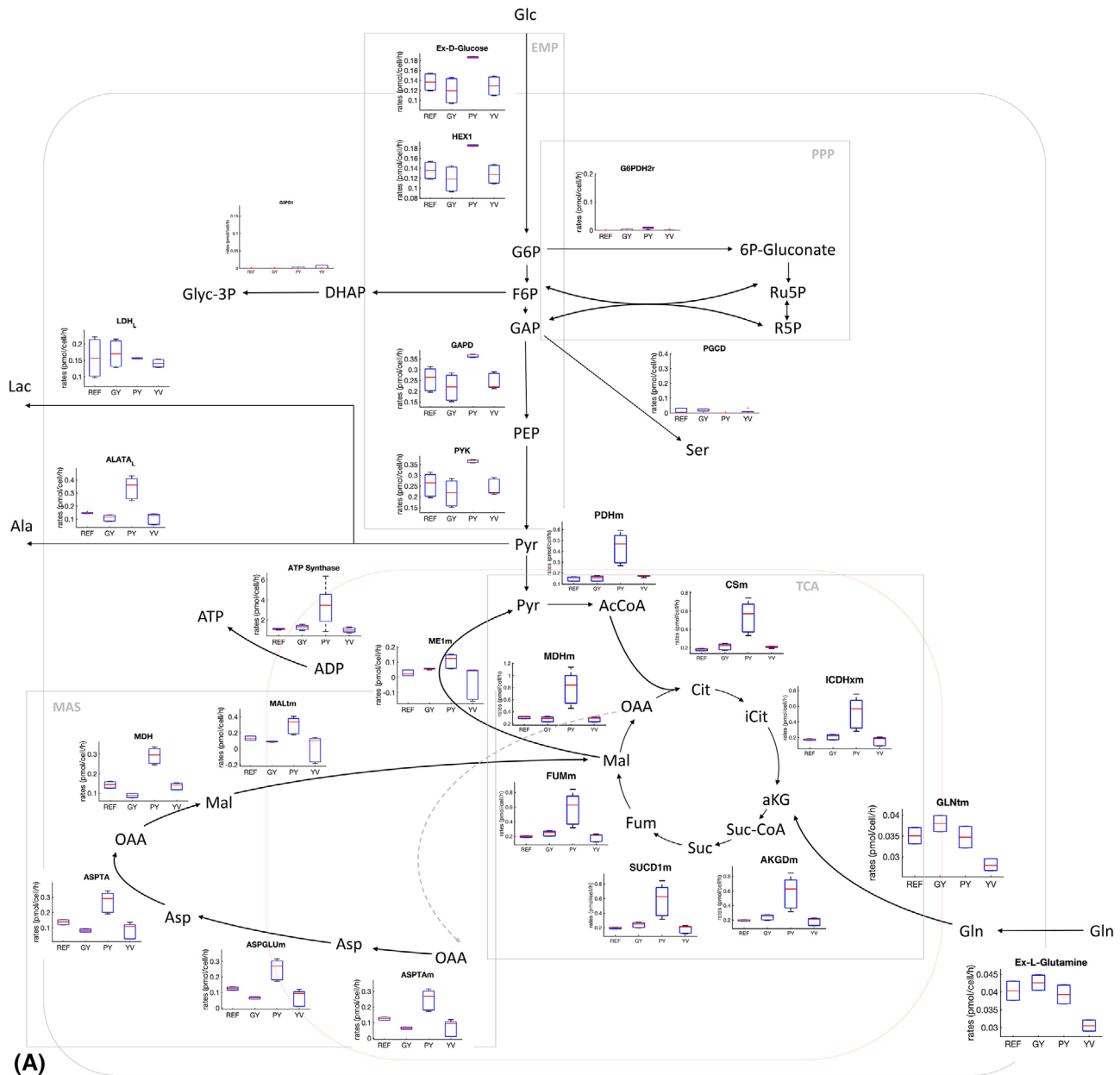


FIGURE 4 Intracellular pools of AMP (A), ADP (B), and ATP (C) [fmol cell<sup>-1</sup>] of dipeptide supplemented cells (GY  $\Delta$ , PY  $\square$ , YV  $\diamond$ ) and reference cells (REF  $\bullet$ ). Error bars show standard deviations of biological duplicates





**FIGURE 5** (A) Central carbon metabolism flux distribution during exponential growth phase as determined FBA. The boxplot indicates the flux of each reaction with samples arranged in the sequence REF-GY-PY-TY from left to right; (B) Cytosolic NADH production and consumption. Cytosolic NADH is produced predominantly by the EMP pathway. Additionally, NADH/NAD conversion can occur via lactate dehydrogenase (LDH) and/or the malate-aspartate shuttle (MAS). The pie chart indicates fractional amounts, not absolute amounts

### 3.3 | In silico analysis of the effects of TYR-containing dipeptides on metabolic activities of CHO cells

Figure 5 shows the flux distributions obtained using FBA. FBA was performed during the exponential growth phase (0–96 h of cultivation) where the TYR-containing dipeptides were supplemented to the cultures. Due to the higher D-glucose uptake rate and similar L-lactate secretion rate in PY cultures, it is expected that more

glycolytic carbon was channeled to mitochondria in PY cultures compared to other cultures. The fraction of carbon diverted to the PPP, L-serine biosynthesis, and glycerophospholipid biosynthesis is negligible since cellular requirements for purine and glycerophospholipids are low. Moreover, L-serine was also available in the cultivation media.

Accordingly, the estimated citric acid cycle (CAC) flux of PY cultures was about three times higher than in the other cultures.

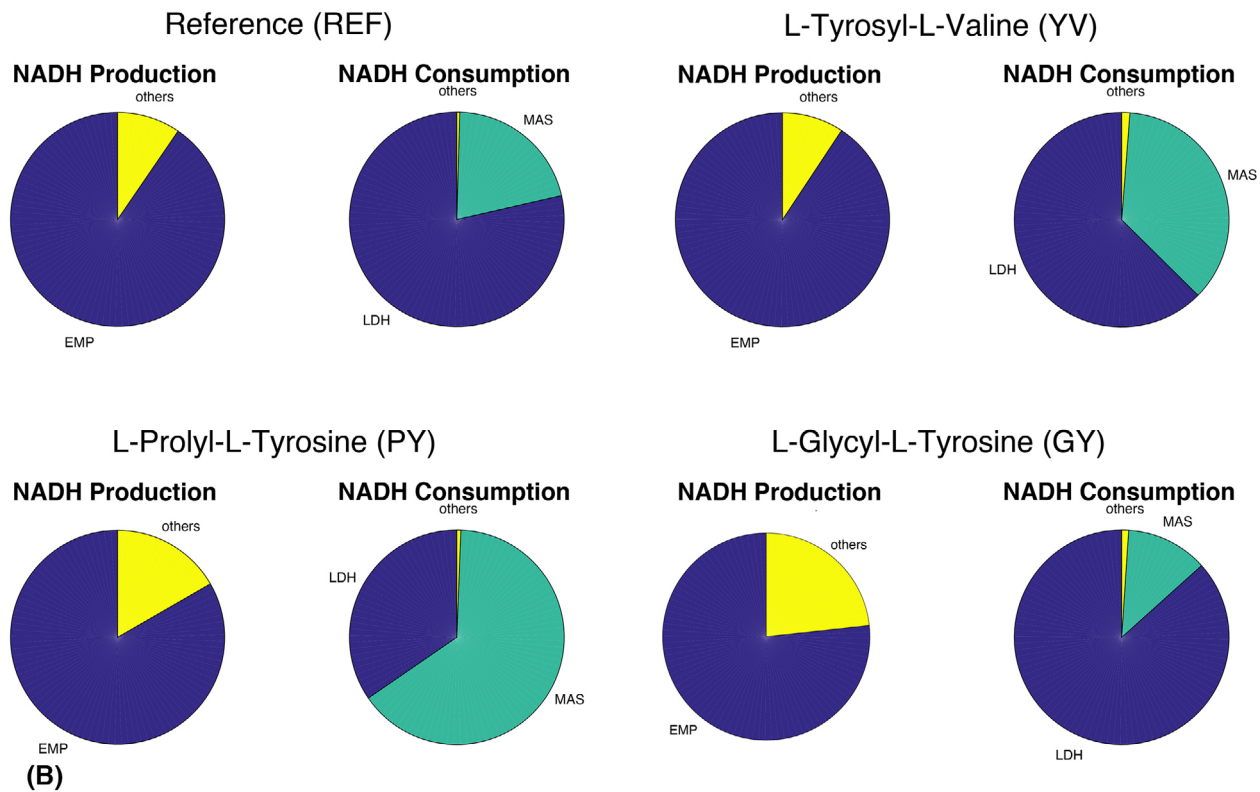


FIGURE 5 Continued

Higher glycolytic flux in PY cultures increased production of cytosolic nicotinamide adenine dinucleotide (NADH). Since the activity of NADH-consuming lactate dehydrogenase was low, NADH was transferred to mitochondria to fuel oxidative phosphorylation. NADH enters mitochondria via the malate–aspartate shuttle (MAS). In our *in silico* analysis (Figure 5), MAS activity in the PY cultures was  $0.29 \text{ pmol}_{\text{NADH}} \text{ cell}^{-1} \text{ h}^{-1}$  and responsible for 65% of cytosolic NADH while MAS activity in REF, YV, and GY cultures yielded 21%, 36%, and 13% cytosolic NADH, respectively. Additionally, FBA predictions revealed that incoming carbon from L-glutamine catabolism did not significantly affect the total CAC flux.

In addition to alleviated D-glucose uptake rates, PY cultures also showed elevated essential amino acid consumption (Supporting Information S2, Figure S3). Considering that cells grew at equal rates in all cultures, the increased amino acid uptake of PY cells is predicted to provide additional ATP. Different dipeptide uptake rates were observed in cultures leading to different fractions of catabolized TYR in FBA calculations (Figure 6). Figure 7 displays the correlation between TYR-containing dipeptide uptake and TYR fraction metabolism in cells. Additionally, a saturating uptake kinetic is observed, hinting at a maximum internal TYR metabolism.

## 4 | DISCUSSION

Dipeptides are promising supplements for cell culture media in order to compensate for low solubility and stability of individual amino acids. Previous studies have demonstrated that peptide addition may have diverse effects on cellular performance, motivating further tests to elucidate the underlying mechanisms [5,9]. The initial goal of this study was to identify TYR-containing dipeptides that can increase the maximum supply of TYR to cells through cell culture medium. Our experimental findings support the hypothesis that the metabolic effects of TYR depend on the molecular structure of the TYR-containing dipeptide. More specifically, L-prolyl-L-tyrosine (PY) alters cellular metabolism, unlike glycyl-L-tyrosine (GY) and L-tyrosyl-L-valine (YV).

The data support the potential for different uptake mechanisms and kinetics of TYR-containing dipeptides [9]. Moreover, the investigation of intracellular dipeptide pools showed that PY, GY, and YV were taken up as intact dipeptides (Supporting Information S2, Figure S2). Once they entered the cell, the dipeptides were either rapidly degraded, metabolized, or exported. Based on recent CHO genome sequencing and annotation studies, the importers PepT1 and PepT2 may be responsible for dipeptide uptake [18], however, such identification does not yet explain the dipeptide type-dependent differences.

**FIGURE 6** ATP flow in reference and PY cultures. The percentage indicates the portion produced or consumed by cellular metabolism

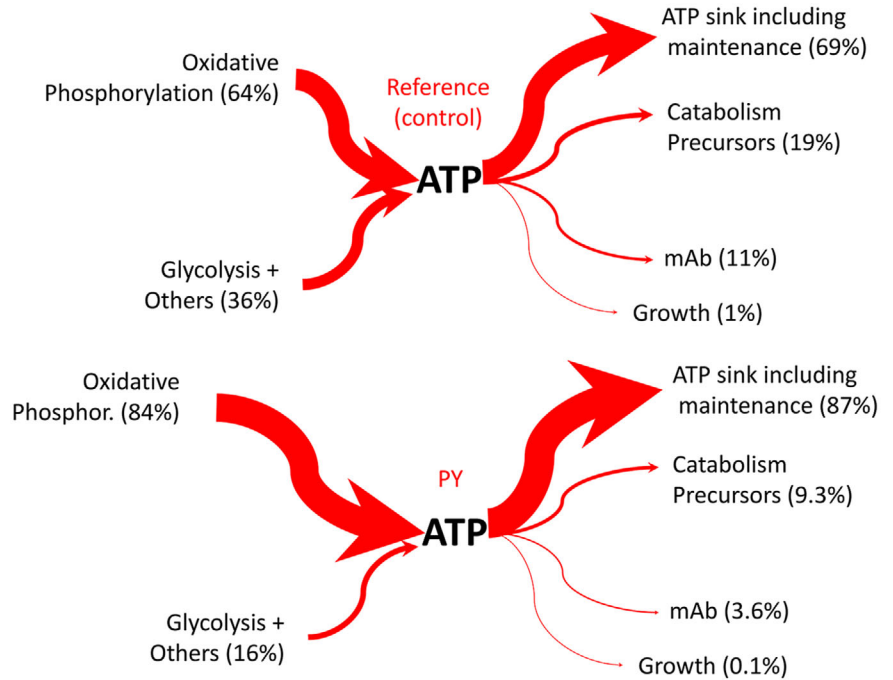
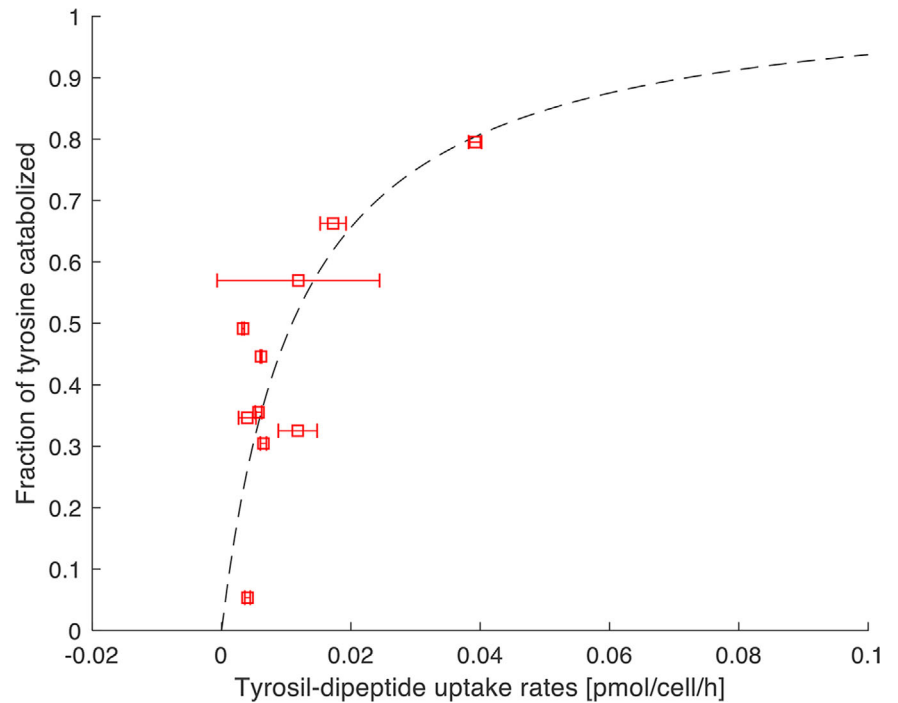


**FIGURE 7** The correlation of TYR-containing dipeptides uptake rates with the fraction of TYR metabolized. This correlation forms saturating kinetics indicating that there is a maximal TYR metabolism



PY showed the strongest impact of all tested dipeptides on CHO metabolism and caused decreased growth, increased D-glucose uptake, and reduced overflow metabolism (Figure 1). Moreover, PY supplementation also altered CAC activity, intracellular ATP pools (Figure 4 and 5), and depleted the L-glutamine pool (Figure 3).

The dipeptide PY possibly works as a signal molecule (demonstrated for amino acids by Franek and Sramkova)

inducing a reprogramming of the cellular metabolism [22]. An altered intracellular pH ( $pH_i$ ) may contribute especially to reduced VCD and modified enzyme activities. In this experiment, our data did not encourage a changed  $pH_i$  as we observed enhanced D-glc uptake [23]. Additionally, the data set is not sufficient to reveal this effect as intracellular data of L-lac,  $NH_4^+$ , and  $pH_i$  were not applicable in this setting and were not within the scope of this study.

Nevertheless, addition of PY possibly triggers signaling pathway that contribute to decreased VCD and enhanced ATP formation.

Our FBA results suggest that CAC activity was increased in PY-treated cultures based on relatively low L-lactate formation relative to the D-glucose consumed. Moreover, D-glucose uptake rates of PY-treated cultures were approximately 30% higher compared to other cultures and mitochondrial malate-aspartate shuttle (MAS) activity was tripled in PY cultures compared to the reference (REF) culture. Such phenomenon can be interpreted as cellular responses to increased NADH supply in the cytosol while MAS activity reflects increases in glycolytic activity and reductions in L-lactate formation. MAS, a known indirect transporter of NADH from the cytosol to mitochondria, shuffles excess cytosolic NADH into the mitochondrion to fuel respiration and ATP formation. These metabolic changes resulted in an approximately four times higher ATP formation in PY culture compared to the others.

For our FBA model, only three TYR sinks are possible: (i) TYR utilization for building macromolecules like cellular proteins or mAB, (ii) TYR export, and (iii) TYR catabolism. Interestingly enough, we identified sink (iii) as the dominant fate of TYR, thus TYR was predominately used for ATP formation, beginning with its deamination using  $\alpha$ -ketoglutarate ( $\alpha$ KG) as amino acceptor. Next, the remaining carbon backbone is converted into fumarate and acetyl-CoA in mitochondria, thus fueling the CAC and supporting respiration. To generate sufficient  $\alpha$ KG supply for such scenarios, one of two routes may be engaged, either through quick deamination of L-glutamate, the product of  $\alpha$ KG amination, to create a steady-state cycle or the replenishment of  $\alpha$ KG by the sequential deamination of L-glutamine. The observation of diminishing levels of intracellular  $\alpha$ KG and extracellular L-glutamine pools favors the second scenario. Notably, GY and YV consumption did not result in similar trends of intracellular  $\alpha$ KG and extracellular L-glutamine levels compared to PY consumption. Instead, upon GY or YV consumption, L-glutamine pools remained steady or were even elevated and  $\alpha$ KG levels showed no decrease.

Becker et al. [24] demonstrated that the cell-specific mAB productivity  $q_{mAB}$  rises in D-glucose-limited perfusion cultures when ATP formation via respiration is increased [24]. However, those results are not strictly applicable to our study as our cells were analyzed under D-glucose-saturated conditions. Accordingly, our observations should be compared to those of Bulté et al. [25] who observed increased CAC activity without rising  $q_{mAB}$  [25]. Apparently, ATP supply does not limit mAB production under D-glucose-saturating conditions.

Mammalian cells are well known for their high ATP requirements to meet maintenance demands. Killburn

et al. [26] estimated this ATP requirement to be larger than 65% of total ATP [26]. Consequently, D-glucose-limited cells, including those in perfusion cultures, may be in an ATP-limited condition such that an additional ATP supply fuels maintenance demands, establishes ion gradients [27] and boosts anabolic mAB formation. In contrast, D-glucose-saturated cells are likely to satisfy ATP maintenance demands, allowing for the use of excess ATP for the formation of recombinant proteins like mAB production. However, such demands are fairly low, only requiring about 11% of total ATP in the reference cultures (Figure 6). As indicated, ATP demands in reference cultures were estimated as 69% of total ATP, in line with the findings of Killburn et al. [26].

## 5 | CONCLUDING REMARKS

In conclusion, we demonstrated that TYR-containing dipeptides influence CHO cell metabolism in different ways depending on their specific amino acid combination. While the dipeptides glycyl-L-tyrosine (GY) and L-tyrosyl-L-valine (YV) showed minimal impact on cellular metabolism, L-prolyl-L-tyrosine (PY) increased L-glutamine usage and increased ATP availability in the cells. Strictly speaking, the FBA approach cannot distinguish between rising ATP demands for maintenance or improved ATP availability beyond what is required for maintenance. Additional  $^{13}\text{C}$  flux studies may help to decipher the maintenance versus excess question experimentally. Our evidence of increased ATP pools in PY cultures favors the presence of improved ATP supply with unchanged maintenance demands. As next step, this exploitation potential could be used to transfer the additional energy into improved product formation. Input parameters like proper D-glucose limitation in combination with different PY feed scenarios should be tested to further optimize production performance.

## NOMENCLATURE

$C_i$ [mmol/L]	Extracellular concentration of metabolite $i$
$C_x$ [cell/L]	Viable Cell Density (VCD)
$q_i$ [pmol/cell/h]	Extracellular production/consumption rate of $i$
$\mu$ [ $\text{h}^{-1}$ ]	cell-specific growth rate

## ACKNOWLEDGMENTS

The authors gratefully acknowledge the funding by the Bundesministerium für Bildung und Forschung (BMBF), (Funding Number 031L0077A).

## CONFLICT OF INTEREST

The authors have declared no conflict of interest.

## ORCID

Andy Wiranata Wijaya  <https://orcid.org/0000-0001-9388-7357>

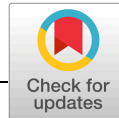
## REFERENCES

- Birch, J. R., Racher, A. J. Antibody production. *Adv. Drug. Deliv. Rev.* 2006, 58, 671–685.
- Gstraunthaler, G. Alternatives to the use of fetal bovine serum: serum-free cell culture. *ALTEX Altern. Anim. Exp.* 2003, 20, 275–281.
- Wessman, S. J., Levings, R. L. Benefits and risks due to animal serum used in cell culture production. *Dev. Biol. Stand.* 1999, 99, 3–8.
- van der Valk, J., Brunner, D., De Smet, K., Svenningsen, Å. F. et al. Optimization of chemically defined cell culture media—replacing fetal bovine serum in mammalian in vitro methods. *Toxicol. in Vitro* 2010, 24, 1053–1063.
- Kang, S., Mullen, J., Miranda, L. P., Deshpande, R. Utilization of tyrosine-and histidine-containing dipeptides to enhance productivity and culture viability. *Biotechnol. Bioeng.* 2012, 109, 2286–2294.
- Eagle, H. The specific amino acid requirements of a mammalian cell (strain L) in tissue culture. *J. biol. Chem.* 1955, 214, 839–852.
- Ham, R. G. Clonal growth of mammalian cells in a chemically defined, synthetic medium. *PNAS* 1965, 53, 288.
- Fürst, P. Old and new substrates in clinical nutrition. *J. Nutr.* 1998, 128, 789–796.
- Sánchez-Kopper, A., Becker, M., Pfizenmaier, J., Kessler, C. et al. Tracking dipeptides at work-uptake and intracellular fate in CHO culture. *AMB Express* 2016, 6, 48.
- Barrett and Jacobia (2011) EP 2 561 065 B1. Munich: European Patent Office.
- Pfizenmaier, J., Matuszczyk, J. C., Takors, R. Changes in intracellular ATP-content of CHO cells as response to hyperosmolality. *Biotechnol. Prog.* 2015, 31, 1212–1216.
- Buchholz, J., Schwentner, A., Brunnenkan, B., Gabris, C. et al. Platform engineering of *Corynebacterium glutamicum* with reduced pyruvate dehydrogenase complex activity for improved production of L-lysine, L-valine, and 2-ketoisovalerate. *Appl. Environ. Microbiol.* 2013, 79, 5566–5575.
- Henderson, J. W., Brooks, A. Improved amino acid methods using Agilent ZORBAX Eclipse Plus C18 columns for a variety of Agilent LC instrumentation and separation goals. Agilent Technologies, Santa Clara, CA 2010.
- Teleki, A., Sánchez-Kopper, A., Takors, R. Alkaline conditions in hydrophilic interaction liquid chromatography for intracellular metabolite quantification using tandem mass spectrometry. *Anal. Biochem.* 2015, 475, 4–13.
- Feith, A., Teleki, A., Graf, M., Favilli, L. et al. HILIC-enabled (13)C metabolomics strategies: comparing quantitative precision and spectral accuracy of QTOF High- and QQQ low-resolution mass spectrometry. *Metabolites* 2019, 9, 63.
- Cserjan-Puschmann, M., Kramer, W., Duerrschmid, E., Striedner, G. et al. Metabolic approaches for the optimisation of recombinant fermentation processes. *Appl. Microbiol. Biotechnol.* 1999, 53, 43–50.
- Kanehisa, M., Goto, S. KEGG: Kyoto encyclopedia of genes and genomes. *Nucleic. Acids. Res.* 2000, 28, 27–30.
- Hefzi, H., Ang, K. S., Hanscho, M., Bordbar, A. et al. A consensus genome-scale reconstruction of Chinese hamster ovary cell metabolism. *Cell Syst.* 2016, 3, 434–443.
- Quek, L. E., Dietmair, S., Krömer, J. O., Nielsen, L. K. Metabolic flux analysis in mammalian cell culture. *Metab. Eng.* 2010, 12, 161–171.
- Sheikh, K., Förster, J., Nielsen, L. K. Modeling hybridoma cell metabolism using a generic genome-scale metabolic model of *Mus musculus*. *Biotechnol. Prog.* 2005, 21, 112–121.
- Martens, D. E. Metabolic flux analysis of mammalian cells. *Syst. Biol.* 2007, 275–299.
- Franěk, F., Šrámková, K. Protection of B lymphocyte hybridoma against starvation-induced apoptosis: survival-signal role of some amino acids. *Immunol. Lett.* 1996, 52, 139–144.
- Cherlet, M., Marc, A. Intracellular pH monitoring as a tool for the study of hybridoma cell behavior in batch and continuous bioreactor cultures. *Biotechnol. Prog.* 1998, 14(4), 626–638.
- Becker, M., Junghans, L., Teleki, A., Bechmann, J. et al. Perfusion cultures require optimum respiratory ATP supply to maximize cell-specific and volumetric productivities. *Biotechnol. Bioeng.* 2019, 116, 951–960.
- Bulté, D., Palomares, L. A., Ramírez, O. T., Gómez, C. Overexpression of the mitochondrial pyruvate carrier increases CHO cell and recombinant protein productivity and reduces lactate production. In “Cell Culture Engineering XVI”, A. Robinson, PhD, Tulane University R. Venkat, PhD, MedImmune E. Schaefer, ScD, J&J Janssen Eds, ECI Symposium Series, (2018).
- Kilburn, D. G., Lilly, M. D., Webb, F. C. The energetics of mammalian cell growth. *J. Cell Sci.* 1969, 4, 645–654.
- Locasale, J. W., Cantley, L. C. Metabolic flux and the regulation of mammalian cell growth. *Cell Metab.* 2011, 14, 443–451.

## SUPPORTING INFORMATION

Additional supporting information may be found online in the Supporting Information section at the end of the article.

**How to cite this article:** Verhagen N, Wijaya AW, Teleki A, et al. Comparison of L-tyrosine containing dipeptides reveals maximum ATP availability for L-prolyl-L-tyrosine in CHO cells. *Eng Life Sci.* 2020;1-11. <https://doi.org/10.1002/elsc.202000017>



## ARTICLE

# S-adenosylmethionine and methylthioadenosine boost cellular productivities of antibody forming Chinese hamster ovary cells

Natascha Verhagen<sup>1</sup> | Attila Teleki<sup>1</sup> | Christoph Heinrich<sup>2</sup> | Martin Schilling<sup>3</sup> | Andreas Unsöld<sup>4</sup> | Ralf Takors<sup>1</sup>

<sup>1</sup>Institute of Biochemical Engineering, University of Stuttgart, Allmandring, Stuttgart, Germany

<sup>2</sup>Xell AG, Bielefeld, Germany

<sup>3</sup>Evonik Nutrition & Care GmbH, Darmstadt, Germany

<sup>4</sup>Boehringer Ingelheim Pharma GmbH & Co. KG, Biberach, Germany

**Correspondence**

Ralf Takors, Institute of Biochemical Engineering, University of Stuttgart, Allmandring 31, 70569 Stuttgart, Germany. Email: [ralf.takors@ibvt.uni-stuttgart.de](mailto:ralf.takors@ibvt.uni-stuttgart.de)

**Funding information**

Bundesministerium für Bildung und Forschung, Grant/Award Number: 031L0077A

**Abstract**

The improvement of cell specific productivities for the formation of therapeutic proteins is an important step towards intensified production processes. Among others, the induction of the desired production phenotype via proper media additives is a feasible solution provided that said compounds adequately trigger metabolic and regulatory programs inside the cells. In this study, S-(5'-adenosyl)-L-methionine (SAM) and 5'-deoxy-5'-(methylthio)adenosine (MTA) were found to stimulate cell specific productivities up to approx. 50% while keeping viable cell densities transiently high and partially arresting the cell cycle in an anti-IL-8-producing CHO-DP12 cell line. Noteworthy, MTA turned out to be the chemical degradation product of the methyl group donor SAM and is consumed by the cells.

**KEYWORDS**

5'-deoxy-5'-(methylthio)adenosine (MTA), cell cycle arrest, cell specific productivity, Chinese hamster ovary (CHO) cell, medium optimization, S-(5'-adenosyl)-L-methionine (SAM)

## 1 | INTRODUCTION

Therapeutic proteins such as monoclonal antibodies (mAb) dominate the global market for biopharmaceuticals and are mostly produced in Chinese hamster ovary (CHO) cells (Walsh, 2018). The last decades of biomanufacturing witnessed a steady rise of product titers in conventional fed-batch modes reaching 5–8 g/L in 12–14 days process time (Reinhart, Damjanovic, Kaisermayer, & Kunert, 2015; Schaub et al., 2010; Wurm, 2004). However, those volumetric productivity improvements predominately mirror elevated viable cell densities rather than the equal rise of cell specific productivities (CSPs). The latter however, is of outstanding importance when the next generation of intensified bioprocesses should be realized, in particular when using perfusion processes (Becker, Junghans, Teleki, Bechmann, & Takors, 2019; Templeton, Smith, et al., 2017; Zhang et al., 2013).

Consequently, novel approaches are needed that boost CSPs for pharmaceutical proteins. As a prerequisite, detailed understanding of the roles of interacting partners in the complex regulatory patterns of CHO metabolism is necessary. As a result of this, novel switches to enhance CSPs may be derived. Promising studies focused on metabolism (Handlogten et al., 2018; Junghans et al., 2019; Templeton, Xu, Roush, & Chen, 2017), transcription (Pfizenmaier, Junghans, Teleki, & Takors, 2016; Sha, Bhatia, & Yoon, 2018), and on epigenetics. Epigenetic adaption mechanisms that is histone modification via acetylation and DNA methylation are basic features of CHO cell adaption. Nematpour et al. (2017) showed that stabilized acetylation by inhibition of histone deacetylases with medium additives enhanced mAb productivity in CHO cells. Furthermore, DNA methylation which links genetics with transcriptomics (Wippermann, Rupp, Brinkrolf, Hoffrogge, & Noll, 2015) was revealed to be the main

This is an open access article under the terms of the Creative Commons Attribution License, which permits use, distribution and reproduction in any medium, provided the original work is properly cited.

© 2020 The Authors. *Biotechnology and Bioengineering* Published by Wiley Periodicals LLC

reason for particular downregulation and upregulation patterns found in high-producer cell lines (Feichtinger et al., 2016; Harreither et al., 2015). Recent studies of Dhiman et al. (2019) demonstrated that more than half of the analyzed nuclear genes are susceptible to methylation. Consequently, the addition of molecules interacting with epigenetic regulation mechanisms offers the intrinsic potential to improve CSPs.

In this context, the cosubstrate *S*-(5'-adenosyl)-*L*-methionine (SAM) was chosen as a medium additive whose structure was discovered in the early 1950s (Cantoni, 1951). SAM may be involved in aminopropylation (polyamine synthesis), trans-methylation and -sulfuration underlining its crucial role for cellular growth and regulation. Accordingly, SAM limitation may affect gene expression, membrane fluidity, and glutathione availability reflecting its roles in DNA methylation, methylation of phospholipids, and trans-sulfuration, respectively (Finkelstein, 1990; Mato, Alvarez, Ortiz, & Pajares, 1997). Metabolically, the methyl group donor SAM is created by methionine adenosyltransferase (MAT) using adenosine triphosphate (ATP) and *L*-methionine as substrates. In CHO, the latter needs to be supplemented in the medium. In methylation reactions, SAM is de-methylated to *S*-(5'-adenosyl)-*L*-homocysteine (SAH) further de-adenylated to homocysteine, re-methylated to methionine, and finally re-adenosylated to SAM again (SAM cycle; Finkelstein, 1990; Mato et al., 1997). Accordingly, the cycle not only regenerates the key methyl donor SAM, it also provides important precursors: Homocysteine serves as a precursor for glutathione synthesis (Lu, 1998) which is an important antioxidant in cells. By analogy, SAM enters the polyamine synthesis (Finkelstein, 1990). Investigations on liver disease demonstrated that extracellular SAM influences the cellular glutathione level. Likely, SAM is taken up by the cells (Mato et al., 1997) which may explain why SAM-treated liver cells showed decreased growth rate, prevented the development of liver cancer (Cai, Mao, Hwang, & Lu, 1998; Pascale et al., 1993) and disclosed antiapoptotic mechanisms (Ansorena, 2002).

Summarizing, SAM is a crucial cosubstrate that serves as a key methyl donor thereby linking metabolism with cellular regulation and epigenetics. Consequently, it offers the intrinsic potential to function as an additive that boosts CSPs in CHO cells.

## 2 | MATERIALS AND METHODS

### 2.1 | Seed train, shake flask cultivation, and addition of SAM, 5'-deoxy-5'-(methylthio)adenosine (MTA), and *L*-homoserine lactone hydrochloride (HSL)

The following additives are products of Sigma-Aldrich (Steinheim, Germany): SAM, MTA, and HSL. The anti-IL-8-producing CHO-DP12 cell line (ATCC® CRL 12445™) adapted to grow in suspension was cultivated in chemically defined TC-42 medium (Xell AG, Bielefeld, Germany) supplemented with 4 mM *L*-glutamine (Carl Roth GmbH & Co. KG, Karlsruhe, Germany) and 200 nM methotrexate (Sigma-Aldrich, Steinheim, Germany). Seed train and experiments were performed in pre-sterilized disposable shake flasks (Corning Inc., NY) in a humidified rotary

shaker (Infors HT Minitron, Infors GmbH, Einsbach, Germany) at 37°C, 150 rpm with 50 mm displacement, and 5% CO<sub>2</sub>. The additives SAM, MTA, and HSL were introduced after 48 hr of cultivation. In reference cell cultures, sterilized water was used to mimic the additional liquid volume in experimental cultures. Cultivation was performed with biological duplicates or quadruplicates.

### 2.2 | Extracellular analysis

Samples were taken at least once a day. Viable cell density, viability, and average cell diameter were determined using trypan blue staining using a Cedex XS cell counter (Innovatis AG, Bielefeld, Germany) for read out. The extracellular concentrations of *D*-glucose and *L*-lactate were determined using a Labotrace automatic analyzer (Trace Analytics GmbH, Braunschweig, Germany). The product concentration of immunoglobulin G (IgG) was determined applying enzyme-linked immunosorbent assay (ELISA; Pfizenmaier, Matuszczyk, & Takors, 2015). Each sampling and measurement procedure was performed in replicates.

### 2.3 | SAM and MTA determination

The amount of SAM and MTA was quantified on an Agilent 1200 Series HPLC system coupled with an Agilent 6410B triple quadrupole tandem mass spectrometer (QQQ-MS/MS; Agilent Technologies, Waldbronn, Germany). The LC-MS/MS method was based on a bicratic zwitterionic hydrophilic interaction chromatography (ZIC-pHILIC) under alkaline mobile phase conditions (10 mM ammonium acetate, pH 9.2) without prior derivatization (Feith, Teleki, Graf, Favilli, & Takors, 2019; Teleki, Sánchez-Kopper, & Takors, 2015). Targeted analytes were detected with high selectivity in multiple reaction monitoring (MRM) mode using pre-optimized precursor-to-product ion transitions and MS/MS parameters. Absolute quantification was performed by adapted standard-based external calibration with constant addition of global internal standards (*L*-norvaline and  $\gamma$ -aminobutyric acid) in diluted samples (1:8). Data were analyzed using MassHunter B.06.00 Analysis software.

### 2.4 | Cell cycle analysis

Cell cycle analysis was performed with an adapted method (Pfizenmaier-Wu, 2017).  $10 \times 10^6$  cells were harvested and washed with ice-cold phosphate-buffered saline (PBS). After washing, the cells were immediately fixed with ice-cold fixation buffer (70% EtOH, 30% PBS [vol/vol]) and stored at -20°C until further analysis. The staining procedure started with gently thawing and resuspending of the cells. Then, cells were washed twice with PBS, resuspended in staining solution (propidium iodide and RNase A in PBS) and incubated for 10 min at 37°C in the dark. Samples stayed on ice until cell cycle analysis. The BD Accuri™ C6 Plus flow cytometer was used with 610/20 nm filter and detected 50,000 events per sample. Data were analyzed with BD Csample software.

## 2.5 | Statistical methods

Error bars show standard deviations that were calculated based on four or two biological replicates (considering the technical replicates). Unpaired one-sided Student's *t* test was performed to investigate the data for statistical significance (\*\**p* = .001, \*\**p* = .01, \**p* = .05).

## 3 | RESULTS

### 3.1 | SAM addition boosted CSP while repressing growth

After 48 hr cultivation time, SAM was added reaching a concentration of 250  $\mu\text{M}$ . Notably, REF received the equivalent volume of water to prevent any bias due to medium dilution. The SAM-treated cultures reduced maximum viable cell density (VCD) and growth rate (between 48 and 120 hr) by 10% and 18% compared with REF, respectively (Figure 1). However, high cell viabilities remained.

Although, SAM supplemented cells showed lower VCD than REF they reached more than 50% higher antibody titer (SAM:  $192.73 \pm 18.24$  mg/L and REF:  $123.39 \pm 12.63$  mg/L). The increased titer (>48 hr) transformed to increased CSP between 0 and 120 hr: SAM supplemented cells produced  $9.81 \pm 0.89$  pg/day whereas the reference only showed  $6.24 \pm 0.51$  pg/day. This corresponds to a 57% increase in CSP (Figure 2) after SAM addition.

### 3.2 | SAM degradation was not affected by the presence of cells

To investigate the effects of SAM addition and uptake extracellular SAM concentrations were monitored in the medium. The anticipated

SAM "uptake" coincided with equally fast degradation rates observed in cell-free cultivation medium under similar conditions (medium + SAM + cells,  $11.54 \pm 0.32$   $\mu\text{M/hr}$ ; medium + SAM,  $10.95 \pm 0.30$   $\mu\text{M/hr}$ ). Consequently, the direct cellular uptake of SAM seemed unlikely. To better understand SAM degradation, MTA as literature described degradation product was measured in the medium (Hoffman, 1986; Morana et al., 2002). Indeed, MTA was detectable in medium with and without cells but not in the reference (water addition). MTA concentration increased over time in medium without cells. In contrast, cell culture studies only showed high MTA levels at the beginning which decreased during the cultivation (Figure 3).

### 3.3 | SAM and its degradation products MTA and HSL

To check whether MTA is the inducer of the growth and IL-8 production phenotype, SAM and the degradation products MTA and HSL were studied in supplementation tests. The addition of substrates occurred after 48 hr of cultivation with a final concentration of 250  $\mu\text{M}$  (REF was supplied with the same volume of water). The addition resulted in maximum VCDs ( $10^6$  cells/ml) of SAM  $7.085 \pm 0.326$ , MTA  $5.512 \pm 0.203$ , HSL  $8.216 \pm 0.780$ , and REF  $8.961 \pm 0.576$ . As indicated in Figure 4, SAM and MTA supplementation caused reduced growth during 60–120 hr leading to a growth rate of  $0.022 \pm 0.002$   $\text{hr}^{-1}$  and  $0.017 \pm 0.001$   $\text{hr}^{-1}$ , respectively. However, there was no effect on the growth phenotype after HSL addition ( $0.028 \pm 0.002$   $\text{hr}^{-1}$ ) compared with the reference ( $0.028 \pm 0.001$   $\text{hr}^{-1}$ ).

Antibody titers were differently affected by the supplemented additives. Cultivations with SAM or MTA addition showed increased titers (SAM:  $165.17 \pm 7.53$  mg/L and MTA:  $167.72 \pm 15.77$  mg/L) whereas experiments with HSL (HSL:  $125.94 \pm 23.30$  mg/L) and the reference (REF:  $132.11 \pm 9.61$  mg/L) showed no improvements.

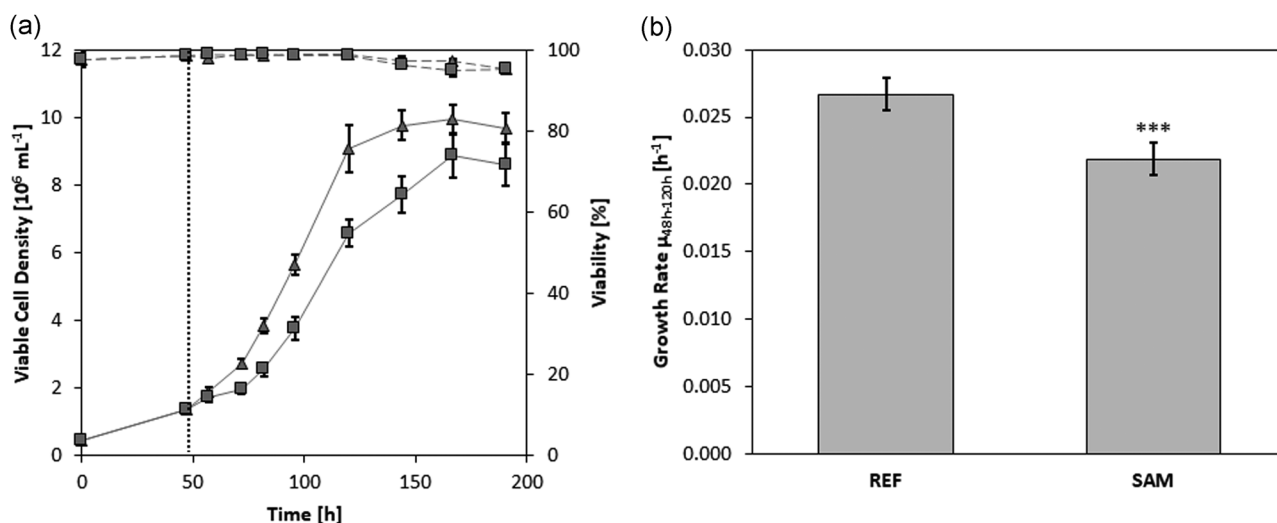


**FIGURE 1** (a) Time courses of viable cell density ( $10^6/\text{ml}$ ) and viability (%) of S-(5'-adenosyl)-L-methionine (SAM) supplemented cells (□) and reference (REF, Δ). SAM was added at 48 hr cultivation time. (b) Growth rate per hour ( $\text{hr}^{-1}$ ) regarding the time interval 48–120 hr. Error bars show standard deviations of biological quadruplicates and technical replicates. Significance was tested with one-sided *t*-test. \*\*\**p* = .001



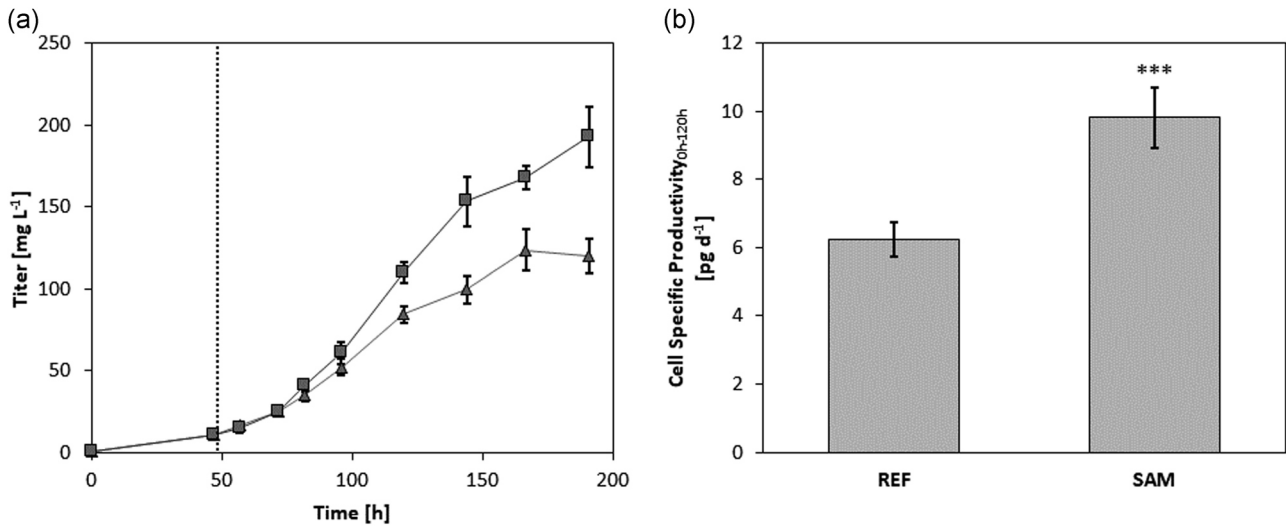


**FIGURE 2** (a) Time courses of the antibody titer (mg/L) of *S*-(5'-adenosyl)-L-methionine (SAM) supplemented cells (□) and reference (REF, Δ). SAM was added after 48 hr cultivation time. (b) Cell specific productivity (pg/day) for the time interval 0–120 hr. Error bars show standard deviations of biological quadruplicates and technical replicates. Significance was tested with one-sided *t*-test. \*\*\**p* = .001

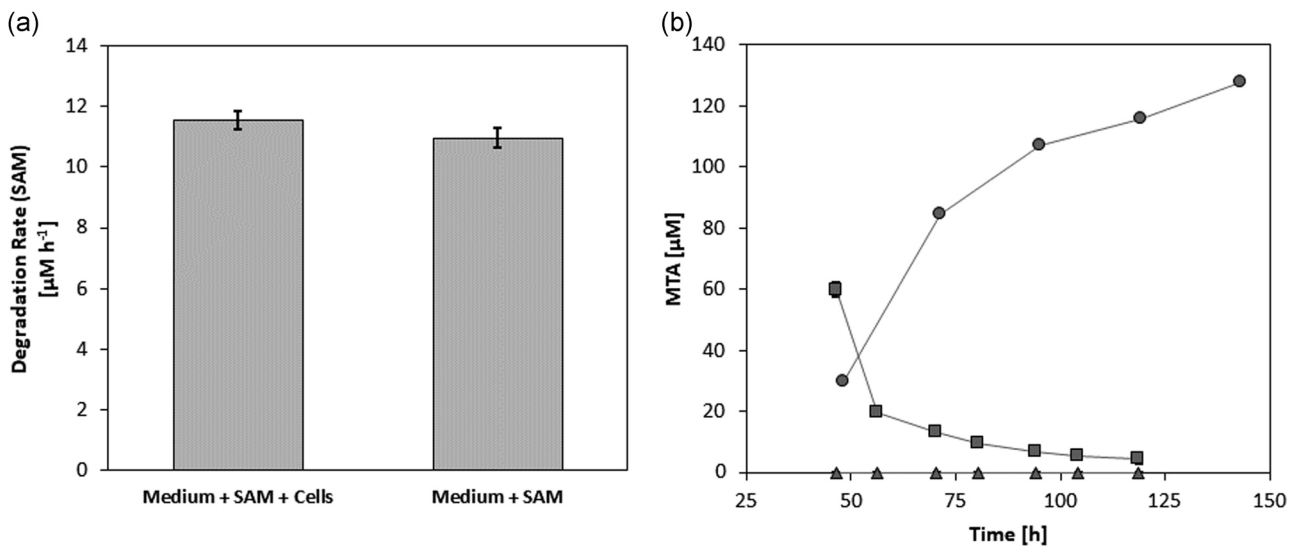


**FIGURE 3** (a) Degradation rate (μM/hr) of *S*-(5'-adenosyl)-L-methionine (SAM) in medium at 37°C, 5% CO<sub>2</sub>, and 150 rpm with and without cells. (b) Time courses of 5'-(methylthio)adenosine (MTA) concentration (μM) in the medium of SAM supplemented cells (□), reference (REF, Δ) and medium + SAM without cells (○). Error bars show standard deviations of biological duplicates

Accordingly, CSPs (Figure 5) of the first 120 hr revealed increased CSPs after the addition of SAM or MTA (SAM:  $11.02 \pm 1.70$  pg/day and MTA:  $8.73 \pm 0.20$  pg/day). These values corresponded to a 27–60% surplus of production. For comparison, HSL addition did not have an influence compared with the reference (HSL:  $7.15 \pm 0.64$  pg/day and REF  $6.87 \pm 0.43$  pg/day).

### 3.4 | SAM and MTA interact with the cell cycle

Propidium iodide staining revealed differences in the cell cycle phase distribution (Figure 6). All cells started from a common

preculture that was split after 48 hr cultivation before adding SAM, MTA, HSL, or water (REF) as described above. About 12 hr after addition (60 hr cultivation time) SAM supplemented cells accumulated in G2-phase whereas MTA supplemented cells showed an increase in S-phase compared with the reference. Noteworthy, both cultures reduced the fraction of cells in G1-phase. Cells supplemented with HSL behaved like the reference. 12 hr later (72 hr cultivation time), the scenario of SAM-treated cultures had changed. Now, the fraction of cells in G1-phase was even higher than that in G2-phase compared with the reference. Still, MTA-treated cultures revealed alleviated numbers of cells in S-phase and less in G1-phase. After additional 12 hr (84 hr

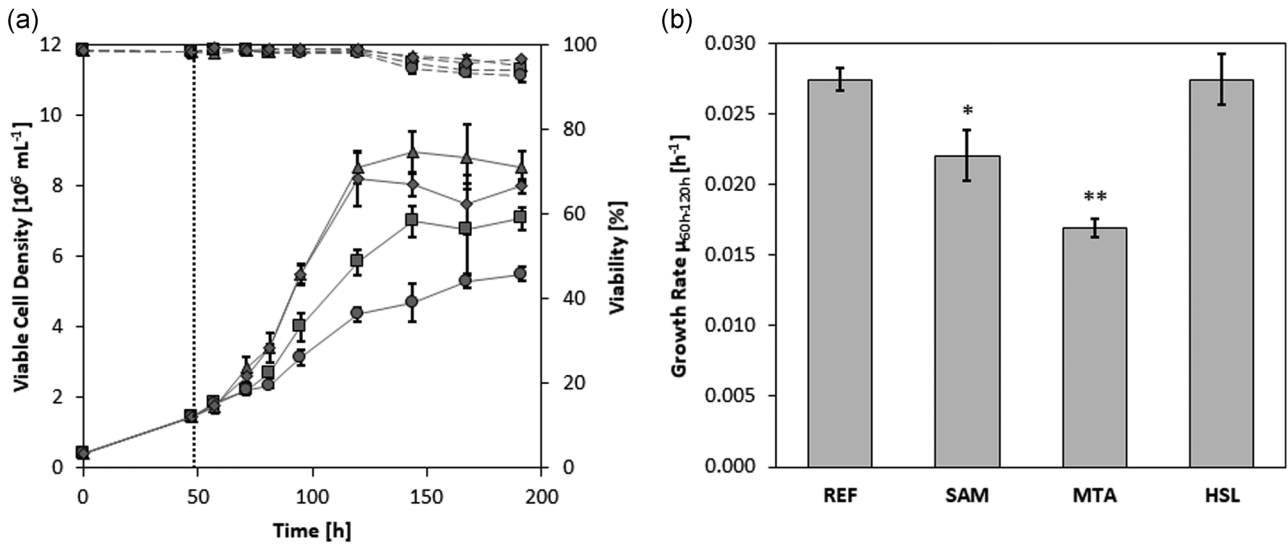


**FIGURE 4** (a) Time courses of viable cell density (10<sup>6</sup>/ml) and viability (%) of *S*-(5′-adenosyl)-L-methionine (SAM, □), 5′-(methylthio) adenosine (MTA, ○), and L-homoserine lactone hydrochloride (HSL, ◇) supplemented cells compared with the reference (REF, Δ). SAM, MTA, or HSL was added at 48 hr. (b) Growth rate (hr<sup>-1</sup>) regarding the time interval 60–120 hr. Error bars show standard deviations of biological duplicates and technical replicates. Significance was tested with one-sided *t*-test. \*\**p* = .01, \**p* = .05

cultivation time) S-phase differences leveled out. Cells that were supplemented with SAM or MTA had more cells in G1-phase but less in G2-phase than the reference.

Additionally, the average cell diameter of all cultures was monitored. Cells supplemented with SAM or MTA revealed a rising average cell diameter of about 10% (SAM + 11.66%; MTA + 13.90%) 36 hr after addition. However, cell size was reduced to the size of the reference culture in the later phase of the cultivation.

#### 4 | DISCUSSION

We added SAM to the medium of CHO cells to interact with the cellular metabolism and with SAM mediated regulation (Finkelstein, 1990; Mato et al., 1997). Clearly, SAM addition decreased the growth rate (Figure 1) which is in agreement with previous findings in liver cells (Cai et al., 1998; Pascale et al., 1993). It may be anticipated that changes in the DNA methylation pattern caused the growth phenotype

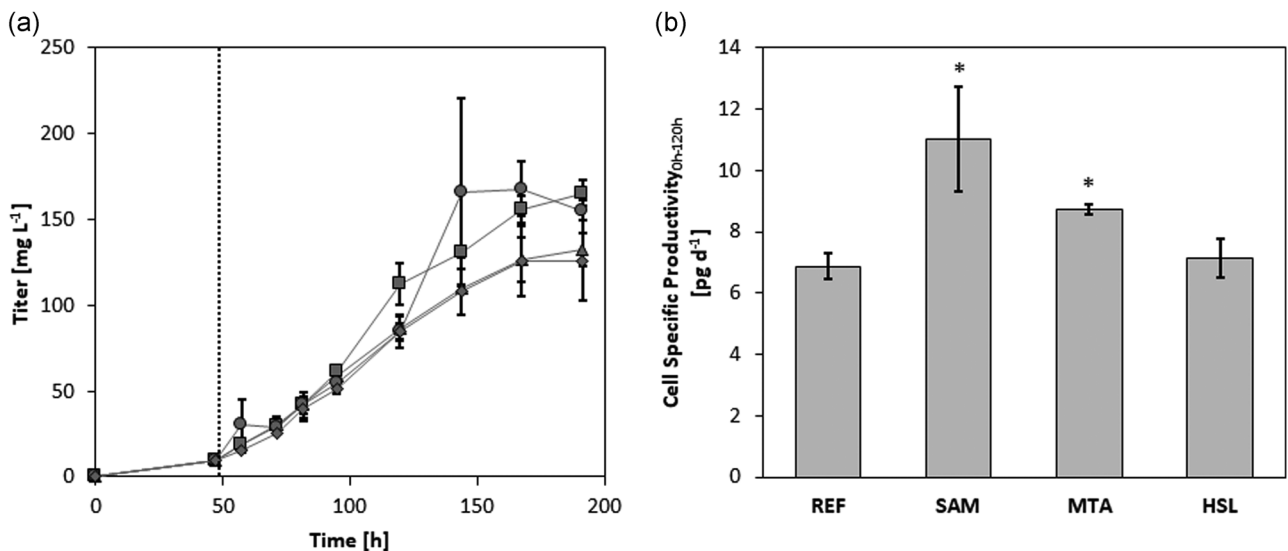


**FIGURE 5** (a) Time courses of antibody titers (mg/L) of *S*-(5′-adenosyl)-L-methionine (SAM, □), 5′-(methylthio)adenosine (MTA, ○), and L-homoserine lactone hydrochloride (HSL, ◇) supplemented cells compared with the reference (REF, Δ). SAM, MTA, or HSL was added after 48 hr cultivation. (b) Cell specific productivity (pg/day) regarding the time interval 0–120 hr. Error bars show standard deviations of biological duplicates and technical replicates. Significance was tested with one-sided *t*-test. \**p* = .05

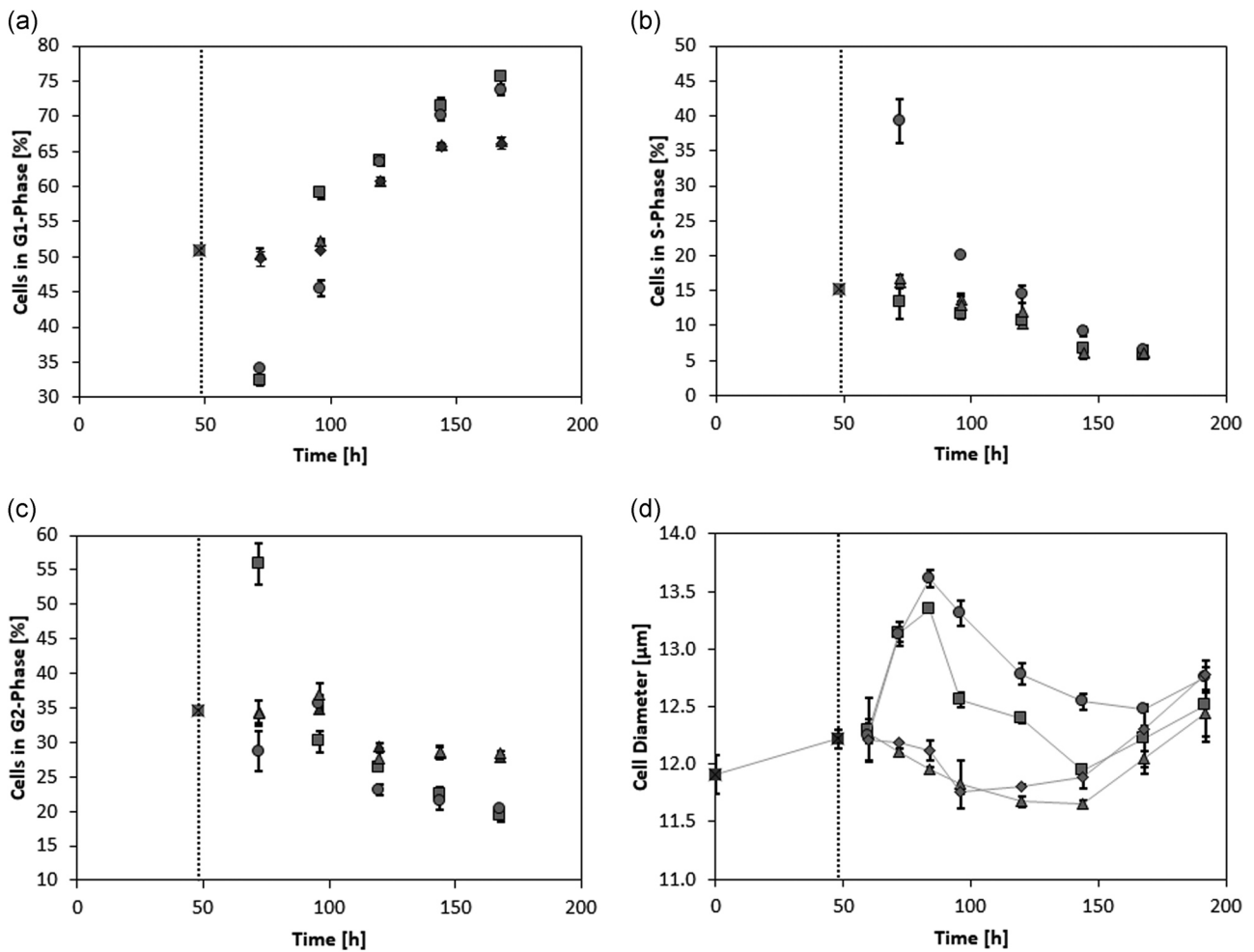


**FIGURE 6** (a–c) Time courses of cell cycle phase distribution (%) and (d) average cell diameter ( $\mu\text{m}$ ) of *S*-(5'-adenosyl)-L-methionine (SAM,  $\square$ ), 5'-(methylthio)adenosine (MTA,  $\circ$ ), and L-homoserine lactone hydrochloride (HSL) supplemented cells ( $\diamond$ ) compared with the reference (REF,  $\Delta$ ) and common preculture (crossed  $\square$ ). Error bars show standard deviations of biological duplicates and technical replicates

(Feichtinger et al., 2016). Unfortunately, the identification of methylation differences with and without SAM addition was not manageable within the scope of the study.

Significantly increased CSP was found in CHO-DP12 cells after SAM addition (Figure 2), although growth rates were reduced. Metabolically, this phenomenon may be understood by assuming that SAM enters the cell boosting the precursor supply of the SAM cycle and/or alleviating the ATP dependent recycling. Mato et al. (1997) anticipated that liver cells take up extracellular SAM. The hypothesis was deduced from rising intracellular glutathione levels. However, Figure 3 reveals that decreasing extracellular SAM levels were observed irrespective of whether cells were present or not. Consequently, the cellular uptake of SAM is unlikely.

A computational study demonstrated that SAM degrades to MTA and HSL in water (Lankau, Kuo, & Yu, 2017). Consequently, we investigated the addition of these degradation products to the media. Whereas HSL did not create any particular phenotype, MTA caused effects very similar to the SAM addition (Figure 4). Noteworthy, MTA natively occurs in mammalian cells as part of the

polyamine biosynthesis (Pegg, 1988; Williams-Ashman, Seidenfeld, & Galletti, 1982). There, SAM is decarboxylated to MTA to access spermidine and spermine. Because high MTA levels inhibit polyamine synthesis MTA is rapidly degraded by 5'-methylthioadenosine phosphorylase. MTA was shown to permeate the cellular membrane. Furthermore, MTA was found to induce particular gene expression patterns, to regulate apoptosis, and to inhibit cell proliferation in hepatocytes, leukemia cells, fibroblasts, and lymphoma cells (Ansorena, 2002; Lee & Cho, 1998; Maher, 1993; Riscoe, Tower, & Ferro, 1984). The latter reflects the inhibition of polyamine synthesis by high MTA levels which reduces cell cycle progression in turn (Oredsson, 2003). Experiments with hepatic cells revealed inhibited DNA synthesis after MTA addition (Pascale, Simile, De Miglio, & Feo, 2002). The reduction of polyamine pathway intermediates such as spermidine after the addition of metabolic inhibitors induced arrest in the cell cycle's S-phase of CHO cells (Alm & Oredsson, 2000).

In agreement with this, we observed the accumulation of cells in S-phase after MTA addition concomitantly with a diminishing number in G1-phase compared with the REF (Figure 6). We hypothesize that

MTA inhibited polyamine synthesis finally creating the observed cytostatic effect (Subhi et al., 2003).

Both, SAM and MTA additions increased CSPs of CHO-DP12 cells (Figure 5). One explanation could be that cell cycle arrest particularly boosted cellular production rates (Fox, Patel, Yap, & Wang, 2004; Hendrick et al., 2001; Kaufmann, Mazur, Fussenegger, & Bailey, 1999; Pfizenmaier et al., 2015). However, those improvements are neither necessarily nor exclusively linked to a single cell cycle phase. Instead, they may benefit from multiple phases (Aggeler, Kapp, Tseng, & Werb, 1982; Al-Rubeai & Emery, 1990; Kim, Kim, & Lee, 2014; Kubbies & Stockinger, 1990; Lloyd, Holmes, Jackson, Emery, & Al-Rubeai, 2000). Accordingly, one may argue whether the improvement of CSP mirrors the benefits of arresting the cell cycle alone. Lloyd et al. (2000) observed CSPs proportional to the cell volume investigating four different CHO cell lines. As cell volume and cell cycle status are linked too, unequivocal conclusions are hard to get. As a result, they concluded that rather cells in S- and G2/M-phase show improved cellular productivity than those in G1-phase. However, this statement somewhat contradicts the findings of other groups (Fox et al., 2004; Hendrick et al., 2001; Kaufmann et al., 1999; Pfizenmaier et al., 2015). In our studies, cell diameters rose after MTA and SAM addition (Figure 6) which agrees with the findings of Lloyd et al. (2000). Strictly speaking, the observation does not exclude potential beneficial effects resulting from cell cycle arrest. In general, cell cycle arrest allows cells to use more energy for recombinant antibody production because biomass formation is hampered (Fussenegger, Mazur, & Bailey, 1997).

Besides the consequences of MTA and SAM on cell cycle and diameter, MTA may interact with a lot of other cell mechanisms (Ansorena, 2002; Lee & Cho, 1998; Maher, 1993; Riscoe et al., 1984). For instance, MTA inactivates SAH hydrolase (Williams-Ashman et al., 1982) leading to increased SAH levels finally resulting in reduced DNA methylation (Iraburu et al., 2002). As methylation is a crucial part of epigenetic regulation (Feichtinger et al., 2016) affecting transcription too (Wippermann et al., 2015) further transcriptional regulation programs are likely to be activated as well. Consequently, the substrate MTA will be further investigated, and its balanced addition is expected to intensify its boosting capability and avoid potential negative effects.

## 5 | CONCLUSION

The study was motivated by the idea to identify novel, non-conventional media components as promising additives to boost CSPs showcasing IgG-1 formation with CHO-DP12 cells. Testing the methyl group donor SAM, a multilevel effector was selected that may interact with different hierarchy levels of cellular regulation concomitantly. SAM addition improved CSPs by approx. 50% arresting the cell cycle and reducing cellular growth at the same time. A similar phenotype occurred when MTA was added which turned out to be the real effector resulting from SAM degradation and can transfer the cellular membrane.

The underlying mechanisms why CSPs are improved are not fully elucidated yet. However, the observations of cell cycle arrest and rising cell volumes support current state-of-the-art understanding but do not disclose key benefits in detail. Further metabolic and transcriptional studies are needed that are beyond the scope of this contribution. Nevertheless, the identification of SAM and MTA as promising media additives to boost CSPs may open the door for the search of other beneficial compounds that trigger cellular performance on multiple levels of metabolism and control.

## ACKNOWLEDGMENTS

The authors gratefully acknowledge the funding by the Bundesministerium für Bildung und Forschung (BMBF, Funding Number 031L0077A). Open access funding enabled and organized by Projekt DEAL.

## CONFLICT OF INTERESTS

The authors declare that there are no conflict of interests.

## ORCID

Natascha Verhagen  <http://orcid.org/0000-0001-9604-8815>

Ralf Takors  <http://orcid.org/0000-0001-5837-6906>

## REFERENCES


- Aggeler, J., Kapp, L., Tseng, S., & Werb, Z. (1982). Regulation of protein secretion in Chinese hamster ovary cells by cell cycle position and cell density. *Experimental Cell Research*, 139(2), 275–283. [https://doi.org/10.1016/0014-4827\(82\)90252-X](https://doi.org/10.1016/0014-4827(82)90252-X)
- Alm, K., & Oredsson, S. M. (2000). The organization of replicon clusters is not affected by polyamine depletion. *Journal of Structural Biology*, 131(1), 1–9. <https://doi.org/10.1006/jsbi.2000.4263>
- Al-Rubeai, M., & Emery, A. N. (1990). Mechanisms and kinetics of monoclonal antibody synthesis and secretion in synchronous and asynchronous hybridoma cell cultures. *Journal of Biotechnology*, 16(1–2), 67–85. [https://doi.org/10.1016/0168-1656\(90\)90066-K](https://doi.org/10.1016/0168-1656(90)90066-K)
- Ansorena, E. (2002). S-adenosylmethionine and methylthioadenosine are antiapoptotic in cultured rat hepatocytes but proapoptotic in human hepatoma cells. *Hepatology*, 35(2), 274–280. <https://doi.org/10.1053/jhep.2002.30419>
- Becker, M., Junghans, L., Teleki, A., Bechmann, J., & Takors, R. (2019). Perfusion cultures require optimum respiratory ATP supply to maximize cell-specific and volumetric productivities. *Biotechnology and Bioengineering*, 116(5), 951–960. <https://doi.org/10.1002/bit.26926>
- Cai, J., Mao, Z., Hwang, J. J., & Lu, S. C. (1998). Differential expression of methionine adenosyltransferase genes influences the rate of growth of human hepatocellular carcinoma cells. *Cancer Research*, 58(7), 1444–1450.
- Cantoni, G. L. (1951). Methylation of nicotinamide with soluble enzyme system from rat liver. *The Journal of Biological Chemistry*, 189(1), 203–216.
- Dhiman, H., Gerstl, M. P., Ruckerbauer, D., Hanscho, M., Himmelbauer, H., Clarke, C., ... Borth, N. (2019). Genetic and epigenetic variation across genes involved in energy metabolism and mitochondria of Chinese hamster ovary cell lines. *Biotechnology Journal*, 14(7), 1800681. <https://doi.org/10.1002/biot.201800681>
- Feichtinger, J., Hernández, I., Fischer, C., Hanscho, M., Auer, N., Hackl, M., ... Borth, N. (2016). Comprehensive genome and epigenome characterization of CHO cells in response to evolutionary pressures and over time. *Biotechnology and Bioengineering*, 113(10), 2241–2253. <https://doi.org/10.1002/bit.25990>

- Feith, A., Teleki, A., Graf, M., Favilli, L., & Takors, R. (2019). Hilic-enabled 13c metabolomics strategies: Comparing quantitative precision and spectral accuracy of qtof high- and qqq low-resolution mass spectrometry. *Metabolites*, 9(4), <https://doi.org/10.3390/metabo9040063>
- Finkelstein, J. D. (1990). Methionine metabolism in mammals. *The Journal of Nutritional Biochemistry*, 1(5), 228–237. [https://doi.org/10.1016/0955-2863\(90\)90070-2](https://doi.org/10.1016/0955-2863(90)90070-2)
- Fox, S. R., Patel, U. A., Yap, M. G. S., & Wang, D. I. C. (2004). Maximizing interferon- $\gamma$  production by Chinese hamster ovary cells through temperature shift optimization: Experimental and modeling. *Biotechnology and Bioengineering*, 85(2), 177–184. <https://doi.org/10.1002/bit.10861>
- Fussenegger, M., Mazur, X., & Bailey, J. E. (1997). A novel cytostatic process enhances the productivity of Chinese hamster ovary cells. *Biotechnology and Bioengineering*, 55(6), 927–939. [https://doi.org/10.1002/\(SICI\)1097-0290\(19970920\)55:6<927::AID-BIT10>3.0.CO;2-4](https://doi.org/10.1002/(SICI)1097-0290(19970920)55:6<927::AID-BIT10>3.0.CO;2-4)
- Handlogten, M. W., Lee-O'Brien, A., Roy, G., Levitskaya, S. V., Venkat, R., Singh, S., & Ahuja, S. (2018). Intracellular response to process optimization and impact on productivity and product aggregates for a high-titer CHO cell process. *Biotechnology and Bioengineering*, 115(1), 126–138. <https://doi.org/10.1002/bit.26460>
- Harreither, E., Hackl, M., Pichler, J., Shridhar, S., Auer, N., Łabaj, P. P., ... Borth, N. (2015). Microarray profiling of preselected CHO host cell subclones identifies gene expression patterns associated with increased production capacity. *Biotechnology Journal*, 10(10), 1625–1638. <https://doi.org/10.1002/biot.201400857>
- Hendrick, V., Winnepeninckx, P., Abdelkafi, C., Vandeputte, O., Cherlet, M., Marique, T., ... Werenne, J. (2001). Increased productivity of recombinant tissular plasminogen activator (t-PA) by butyrate and shift of temperature: A cell cycle phases analysis. *Cytotechnology*, 36(1–3), 71–83. <https://doi.org/10.1023/A:1014088919546>
- Hoffman, J. L. (1986). Chromatographic analysis of the chiral and covalent instability of S-adenosyl-L-methionine. *Biochemistry*, 25(15), 4444–4449. <https://doi.org/10.1021/bi00363a041>
- Iraburu, M., García-Trevijano, E. R., Ansorena, E., Avila, M. A., Mato, J. M., Martínez-Chantar, M. L., ... Huang, Z. Z. (2002). S-adenosylmethionine and methylthioadenosine are antiapoptotic in cultured rat hepatocytes but proapoptotic in human hepatoma cells. *Hepatology*, 35(2), 274–280. <https://doi.org/10.1053/jhep.2002.30419>
- Junghans, L., Teleki, A., Wijaya, A. W., Becker, M., Schweikert, M., & Takors, R. (2019). From nutritional wealth to autophagy: In vivo metabolic dynamics in the cytosol, mitochondrion and shuttles of IgG producing CHO cells. *Metabolic Engineering*, 54, 145–159. <https://doi.org/10.1016/j.ymben.2019.02.005>
- Kaufmann, H., Mazur, X., Fussenegger, M., & Bailey, J. E. (1999). Influence of low temperature on productivity, proteome and protein phosphorylation of CHO cells. *Biotechnology and Bioengineering*, 63(5), 573–582. [https://doi.org/10.1002/\(SICI\)1097-0290\(19990605\)63:5<573::AID-BIT7>3.0.CO;2-Y](https://doi.org/10.1002/(SICI)1097-0290(19990605)63:5<573::AID-BIT7>3.0.CO;2-Y)
- Kim, W. H., Kim, Y. J., & Lee, G. M. (2014). Gadd45-induced cell cycle G2/M arrest for improved transient gene expression in Chinese hamster ovary cells. *Biotechnology and Bioprocess Engineering*, 19(3), 386–393. <https://doi.org/10.1007/s12257-014-0151-0>
- Kubbies, M., & Stockinger, H. (1990). Cell cycle-dependent DHFR and t-PA production in cotransfected, MTX-amplified CHO cells revealed by dual-laser flow cytometry. *Experimental Cell Research*, 188(2), 267–271. [https://doi.org/10.1016/0014-4827\(90\)90169-B](https://doi.org/10.1016/0014-4827(90)90169-B)
- Lankau, T., Kuo, T. N., & Yu, C. H. (2017). Computational study of the degradation of S-adenosyl methionine in water. *The Journal of Physical Chemistry A*, 121(2), 505–514. <https://doi.org/10.1021/acs.jpca.6b09639>
- Lee, S. H., & Cho, Y. D. (1998). Induction of apoptosis in leukemia U937 cells by 5'-deoxy-5'-methylthioadenosine, a potent inhibitor of protein carboxylmethyltransferase. *Experimental Cell Research*, 240(2), 282–292. <https://doi.org/10.1006/excr.1998.4000>
- Lloyd, D. R., Holmes, P., Jackson, L. P., Emery, A. N., & Al-Rubeai, M. (2000). Relationship between cell size, cell cycle and specific recombinant protein productivity. *Cytotechnology*, 34(1–2), 59–70. <https://doi.org/10.1023/A:1008103730027>
- Lu, S. C. (1998). Regulation of hepatic glutathione synthesis. *Seminars in Liver Disease*, 18(4), 331–343. <https://doi.org/10.1055/s-2007-1007168>
- Maher, P. A. (1993). Inhibition of the tyrosine kinase activity of the fibroblast growth factor receptor by the methyltransferase inhibitor 5'-methylthioadenosine. *The Journal of Biological Chemistry*, 268(6), 4244–4249.
- Mato, J., Alvarez, L., Ortiz, P., & Pajares, M. A. (1997). S-adenosylmethionine synthesis: Molecular mechanisms and clinical implications. *Pharmacology & Therapeutics*, 73(3), 265–280. [https://doi.org/10.1016/S0163-7258\(96\)00197-0](https://doi.org/10.1016/S0163-7258(96)00197-0)
- Morana, A., Stiuso, P., Colonna, G., Lamberti, M., Rosa, M. De, & Carteni, M. (2002). Stabilization of S-adenosyl-L-methionine promoted by trehalose. *Biochimica et Biophysica Acta*, 1573, 105–108.
- Nematpour, F., Mahboudi, F., Khalaj, V., Vaziri, B., Ahmadi, S., Ahmadi, M., ... Davami, F. (2017). Optimization of monoclonal antibody expression in CHO cells by employing epigenetic gene regulation tools. *Turkish Journal of Biology*, 41(4), 622–628. <https://doi.org/10.3906/biy-1702-18>
- Oredsson, S. M. (2003). Polyamine dependence of normal cell-cycle progression. *Biochemical Society Transactions*, 31(2), 366–370. <https://doi.org/10.1042/BST0310366>
- Pascale, R. M., Simile, M. M., Seddaiu, M. A., Daino, L., Vinci, M. A., Pinna, G., ... Feo, F. (1993). Chemoprevention of rat liver carcinogenesis by S-adenosyl-L-methionine: Is DNA methylation involved? *Basic Life Sciences*, 61, 219–237. [https://doi.org/10.1007/978-1-4615-2984-2\\_20](https://doi.org/10.1007/978-1-4615-2984-2_20)
- Pascale, R. M., Simile, M. M., De Miglio, M. R., & Feo, F. (2002). Chemoprevention of hepatocarcinogenesis: S-adenosyl-L-methionine. *Alcohol*, 27(3), 193–198. [https://doi.org/10.1016/S0741-8329\(02\)00227-6](https://doi.org/10.1016/S0741-8329(02)00227-6)
- Pegg, A. E. (1988). Polyamine metabolism and its importance in neoplastic growth and as a target for chemotherapy. *Cancer Research*, 48(4), 759–774.
- Pfizenmaier, J., Junghans, L., Teleki, A., & Takors, R. (2016). Hyperosmotic stimulus study discloses benefits in ATP supply and reveals miRNA/mRNA targets to improve recombinant protein production of CHO cells. *Biotechnology Journal*, 11(8), 1037–1047. <https://doi.org/10.1002/biot.201500606>
- Pfizenmaier, J., Matuszczyk, J.-C., & Takors, R. (2015). Changes in intracellular ATP-content of CHO cells as response to hyperosmolality. *Biotechnology Progress*, 31(5), 1212–1216. <https://doi.org/10.1002/btpr.2143>
- Pfizenmaier-Wu, J. I. (2017). *Metabolic and transcriptomic response to hyperosmotic stimulus reveals strategies for optimization of antibody producing Chinese hamster ovary cells*. University of Stuttgart. Retrieved from <https://doi.org/10.18419/opus-9145>
- Reinhart, D., Damjanovic, L., Kaisermayer, C., & Kunert, R. (2015). Benchmarking of commercially available CHO cell culture media for antibody production. *Applied Microbiology and Biotechnology*, 99(11), 4645–4657. <https://doi.org/10.1007/s00253-015-6514-4>
- Riscoe, M. K., Tower, P. A., & Ferro, A. J. (1984). Mechanism of action of 5'-methylthioadenosine in S49 cells. *Biochemical Pharmacology*, 33(22), 3639–3643. [https://doi.org/10.1016/0006-2952\(84\)90150-3](https://doi.org/10.1016/0006-2952(84)90150-3)
- Schaub, J., Clemens, C., Schorn, P., Hildebrandt, T., Rust, W., Mennerich, D., ... Schulz, T. W. (2010). CHO gene expression profiling in biopharmaceutical process analysis and design. *Biotechnology and Bioengineering*, 105(2), 431–438. <https://doi.org/10.1002/bit.22549>
- Sha, S., Bhatia, H., & Yoon, S. (2018). An RNA-seq based transcriptomic investigation into the productivity and growth variants with Chinese hamster ovary cells. *Journal of Biotechnology*, 271(2010), 37–46. <https://doi.org/10.1016/j.jbiotec.2018.02.008>

- Subhi, A. L., Diegelman, P., Porter, C. W., Tang, B., Lu, Z. J., Markham, G. D., & Kruger, W. D. (2003). Methylthioadenosine phosphorylase regulates ornithine decarboxylase by production of downstream metabolites. *Journal of Biological Chemistry*, 278(50), 49868–49873. <https://doi.org/10.1074/jbc.M308451200>
- Teleki, A., Sánchez-Kopper, A., & Takors, R. (2015). Alkaline conditions in hydrophilic interaction liquid chromatography for intracellular metabolite quantification using tandem mass spectrometry. *Analytical Biochemistry*, 475, 4–13. <https://doi.org/10.1016/j.ab.2015.01.002>
- Templeton, N., Smith, K. D., McAtee-Pereira, A. G., Dorai, H., Betenbaugh, M. J., Lang, S. E., & Young, J. D. (2017). Application of <sup>13</sup>C flux analysis to identify high-productivity CHO metabolic phenotypes. *Metabolic Engineering*, 43(December), 218–225. <https://doi.org/10.1016/j.ymben.2017.01.008>
- Templeton, N., Xu, S., Roush, D. J., & Chen, H. (2017). <sup>13</sup>C metabolic flux analysis identifies limitations to increasing specific productivity in fed-batch and perfusion. *Metabolic Engineering*, 44(September), 126–133. <https://doi.org/10.1016/j.ymben.2017.09.010>
- Walsh, G. (2018). Biopharmaceutical benchmarks 2018. *Nature Biotechnology*, 36(12), 1136–1145. <https://doi.org/10.1038/nbt.4305>
- Williams-Ashman, H. G., Seidenfeld, J., & Galletti, P. (1982). Trends in the biochemical pharmacology of 5'-deoxy-5'-methylthioadenosine. *Biochemical Pharmacology*, 31(3), 277–288. [https://doi.org/10.1016/0006-2952\(82\)90171-X](https://doi.org/10.1016/0006-2952(82)90171-X)
- Wippermann, A., Rupp, O., Brinkrolf, K., Hoffrogge, R., & Noll, T. (2015). The DNA methylation landscape of Chinese hamster ovary (CHO) DP-12 cells. *Journal of Biotechnology*, 199, 38–46. <https://doi.org/10.1016/j.jbiotec.2015.02.014>
- Wurm, F. M. (2004). Production of recombinant protein therapeutics in cultivated mammalian cells. *Nature Biotechnology*, 22(11), 1393–1398. <https://doi.org/10.1038/nbt1026>
- Zhang, H., Wang, H., Liu, M., Zhang, T., Zhang, J., Wang, X., & Xiang, W. (2013). Rational development of a serum-free medium and fed-batch process for a GS-CHO cell line expressing recombinant antibody. *Cytotechnology*, 65(3), 363–378. <https://doi.org/10.1007/s10616-012-9488-4>

**How to cite this article:** Verhagen N, Teleki A, Heinrich C, Schilling M, Unsöld A, Takors R. S-adenosylmethionine and methylthioadenosine boost cellular productivities of antibody forming Chinese hamster ovary cells. *Biotechnology and Bioengineering*. 2020;1–9. <https://doi.org/10.1002/bit.27484>

# Methylthioadenosine (MTA) boosts cell-specific productivities of Chinese hamster ovary cultures: dosage effects on proliferation, cell cycle and gene expression

Natascha Verhagen , Julia Zieringer and Ralf Takors

Institute of Biochemical Engineering, University of Stuttgart, Stuttgart, Germany Open access funding enabled and organized by ProjektDEAL.

## Keywords

cell cycle arrest; cell-specific productivity; Chinese hamster ovary cell; medium optimization; methylthioadenosine; transcriptome analysis

## Correspondence

R. Takors, Institute of Biochemical Engineering, University of Stuttgart, Allmandring 31, 70569 Stuttgart, Germany  
E-mail: ralf.takors@ibvt.uni-stuttgart.de

(Received 30 August 2020, revised 19 October 2020, accepted 24 October 2020)

doi:10.1002/2211-5463.13019

A major goal for process and cell engineering in the biopharmaceutical industry is enhancing production through increasing volumetric and cell-specific productivities (CSP). Here, we present 5'-deoxy-5'-(methylthio)adenosine (MTA), the degradation product of S-(5'-adenosyl)-L-methionine (SAM), as a highly attractive native additive which can boost CSP by 79% when added to exponentially growing cells at a concentration of 250–300  $\mu\text{M}$ . Notably, cell viability and cell size remain higher than in non-treated cultures. In addition, cell cycle arrests first in S-, then in G2-phase before levelling out compared to non-treated cultivations. Intensive differential gene analysis reveals that expression of genes for cytoskeleton mediated proteins and vesicle transport is amplified by treatment. Furthermore, the interaction of MTA with cell proliferation additionally stimulated recombinant protein formation. The results may serve as a promising starting point for further developments in process and cell engineering to boost productivity.

Biopharmaceutical markets are dominated by therapeutic proteins, particularly monoclonal antibodies (mAb) which are predominantly produced by CHO cells [1]. In the last decades, significant increase of maximum viable cell density (VCD) improved volumetric productivity and reached titers up to 5–8  $\text{g}\cdot\text{L}^{-1}$  in fed-batch processes [2–4]. Process intensifications are performed to raise production performance. As a prerequisite, increasing CSPs are needed for the next step of process development [5,6].

5'-Deoxy-5'-(methylthio)adenosine (MTA) consists of L-methionine (L-met) and adenosine triphosphate (ATP) and is a naturally occurring molecule in mammalian tissues [7,8]. It is produced from S-(5'-adenosyl)-L-methionine (SAM) in the polyamine synthesis [7] in cells. Production of spermidine and spermine needs the decarboxylation of SAM to MTA that is

rapidly metabolized by 5'-methylthioadenosine phosphorylase to adenine and S-methyl-5-thio-D-ribose 1-phosphate and finally to L-met. The adenine can be used to replenish adenosine monophosphate (AMP), adenosine diphosphate (ADP) and ATP pools. Final recovery of SAM from ATP and L-met closes the SAM cycle [7,9]. Rapid degradation of MTA is crucial because it inhibits spermine synthase, spermidine synthase and ornithine decarboxylase [8,10].

MTA inhibited cell proliferation in hepatocytes, leukemia cells, fibroblasts and lymphoma cells [11–14] that is mainly the consequence of its polyamine synthesis inhibition [15]. A reduction of polyamine intermediates arrested CHO cells in their S-phase [16]. Furthermore, MTA addition inhibited DNA synthesis in hepatic cells [10] but it remained unclear whether MTA or a downstream metabolite is the effector [17].

## Abbreviations

CHO, Chinese hamster ovary; CSP, cell-specific productivity; DEG, differential expressed gene; MTA, 5'-deoxy-5'-(methylthio)adenosine; PC, principal component; REF, reference; SAM, S-(5'-adenosyl)-L-methionine; VCD, viable cell density.

Beside its interaction with polyamine synthesis, MTA demonstrated importance for expression control of genes, cell proliferation inhibition, lymphocyte activation, tumor development and invasiveness, and the regulation of apoptosis [7,9–12,18]. MTA addition induced apoptosis in hepatocarcinoma cells, whereas hepatocytes remained viable and were protected against programmed cell death [11]. Additionally, MTA demonstrated beneficial effects in immune response [19].

Several groups [13,14] observed the inhibition of growth factor-induced protein tyrosine phosphorylation and the increase of intracellular cyclic AMP (cAMP) levels through the inhibition of cAMP-phosphodiesterase by MTA pointing out the interaction with signaling pathways. Furthermore, increased MTA levels inhibited arginine methylation of the STAT1 transcription factor, finally impairing gene transcription [20].

Due to the relation to the SAM cycle, MTA revealed capabilities to inhibit protein methylation pinpointing to its role as post-translational modifier and accordingly as a regulator of cellular signaling and gene expression [12,18,20]. Evidences are given by its direct interaction with methyltransferases and via the indirect inactivation of S-(5'-adenosyl)-L-homocysteine hydrolase [7].

Single MTA addition to the medium increases CSP in CHO cells. Furthermore, cells demonstrated cell cycle arrest and increased cell size [21]. Growth arrest induction is a common strategy to increase CSP [22]. Protein production was increased by effector-induced cell cycle arrest in G1- and S-phase [23,24]. However, cell size controls transitions between cell cycle phases which underlines its importance for proper cell cycling and proliferation [25–27] that correlated with protein production in different cell lines [28]. The complex interactions between cell size, cell growth, and protein production are not fully elucidated, yet. Additionally, genes involved in post-translational steps, secretion and cytoskeleton were reported to enhance CSP [29–31].

Strategies to induce growth arrest for enhancing protein production comprise (a) hypothermia and (b) the addition of effector molecules, e.g. to increase hyperosmolality. Regarding (a), the mechanism of hypothermia is not understood but certainly linked to G1-phase arrest [32] and accompanied by an increased cell size [33,34]. With respect to (b) additives were investigated to modulate cell growth, product stabilization, and to reduce chemical modifications. Examples are sodium butyrate [35], zinc [36], valeric acid [37], glycine betaine [38], valproic acid [39] and sodium chloride [40] among others.

Own studies have already revealed that MTA addition diminished growth, increased CSP, altered cell cycle phases and cell size [21]. Consequently, MTA should be considered as a multi-layer regulator of cell growth, cell cycle, and protein formation that is a highly promising additive for boosting CSP. Accordingly, we conducted experiments with anti-IL-8-producing CHO cells analyzing different levels and intervals of MTA addition and the effect of MTA on transcriptomic level.

## Materials and methods

### Different MTA concentrations and addition time points: Seed train, shake flask cultivation and MTA addition

MTA was a product of Sigma-Aldrich (Steinheim, Germany). The anti-IL-8-producing CHO DP-12 cell line (ATCC® CRL 12445™) adapted to suspension was grown in chemically defined TC-42 medium (Xell AG, Bielefeld, Germany) supplemented with 4 mM L-glutamine (Carl Roth GmbH & Co. KG, Karlsruhe, Germany) and 200 nM methotrexate (Sigma-Aldrich). Seed train and experiments were performed in pre-sterilized disposable shake flasks (Corning Inc., US) in a humidified and incubated rotary shaker (Infors HT Minitron, Infors GmbH, Germany) at 37 °C, 150 rpm with 50 mm displacement and 5% CO<sub>2</sub>. In the experiment with different concentrations, MTA was introduced after 48 h of cultivation in different concentrations (125, 250, 350 and 450 μM). In reference (REF) cell cultures, sterilized water was used to mimic the additional liquid volume in experimental cultures (volume corresponding to the 450 μM addition). In the experiment with different addition time points, MTA was introduced after 48, 84 and 108 h of cultivation in a concentration of 150 pmol·cell<sup>-1</sup>. At every addition time point, all other settings received sterilized water to mimic the additional liquid volume in experimental cultures. Cultivation was performed with biological duplicates.

### Extracellular and cell cycle analysis

Samples were taken at least once a day. Viable cell density (VCD), viability and average cell size were determined using trypan blue staining and a Cedex XS cell counter (Innovatis AG, Bielefeld, Germany). The extracellular concentrations of D-glucose (D-Glc) and L-lactate (L-Lac) were determined using a LaboTRACE automatic analyzer (Trace Analytics GmbH, Braunschweig, Germany). The concentration of secreted antibody was determined with an enzyme-linked immunosorbent assay (ELISA) [41]. All sampling and measurement procedures were performed with three technical replicates. The determination of cell



cycle distribution was performed as described before [21]. All sampling and measurement procedures were performed with two technical replicates.

### Transcriptome analysis

Experimental equipment and settings were used as described above (MTA at 48 h: 250  $\mu\text{M}$ ) in biological triplicates. The isolated RNA was processed by c.ATG. Analysis of raw data was performed on the Galaxy-Server [42], and data were analyzed using the free statistical computing environment R.

### Experiment and sampling for transcriptome analysis and ribonucleic acid (RNA) sequence analysis

Experimental equipment and settings were described in the manuscript. Sampling for transcriptome analysis occurred on 48-h, 60-h, 72-h, 84-h, 96-h and 144-h cultivation time and followed an adapted protocol [40]. A total number of  $2 \times 10^6$  cells were harvested and centrifuged, and supernatant was discarded. Cells were resuspended in RNAProtect Cell Reagent (Qiagen, Hilden, Germany), quickly frozen in liquid nitrogen and stored at  $-70^\circ\text{C}$ . The RNA was isolated with the RNeasy Kit (Qiagen) and QiaShredder (Qiagen). An extra procedure of clean-up to get rid of DNA (Turbo DNase<sup>TM</sup> and Turbo DNase<sup>TM</sup> Buffer, Ambion (Life Technologies, Carlsbad, CA, USA)) and increase the RNA concentration (RNA Clean & Concentrator<sup>TM</sup>, Zymo Research, Irvine, CA, USA) was added. The kits were used as indicated by the manuals. Sequencing of the transcriptome was performed by c.ATG (Tübingen, Germany). Preparation of high-quality mRNA-Seq data was performed using the Illumina TruSeq RNA Sample Preparation Kit. Quality was assessed by an Agilent Fragment Analyzer. Samples with high RNA integrity number (RIN > 8) were selected for library construction using the NEBNext Ultra II Directional RNA Library Prep Kit. Libraries were sequenced as paired-end (50 bp read length) at a depth of 30–40 million reads each.

### Read mapping and gene counting

Read mapping and gene counting was performed on the Galaxy-Server. Sequencing statistics including the quality per base and adapter content assessment of resulting transcriptome sequencing data were checked by FastQC reports. Genes were aligned to the CHO-K1 reference genome (RefSeq: GCF\_000223135.1) (downloaded from <http://www.chogenome.org/>, 07/08/2019) using the RNA sequencing aligner BOWTIE2 v. 2.3.2.2 [43]. On average, the mapping of the reads covers 94.3%. Aligned reads were counted for each gene based on the corresponding annotation available from the CHOgenome webpage for the chosen reference

sequence applying HTSEQ-COUNT v. 0.6.1 [44] in the union mode. On average, 71.0% of the sequenced reads could be assigned uniquely to annotated genes. Sequencing depth was around 33 million reads per sample on average.

### Transcriptome data analysis

Differential gene expression analysis was performed with the R-package DESEQ2 v. 1.26.0 [45] available from Bioconductor [46] (<http://www.bioconductor.org>). Prior to statistical analysis, a non-specific filter was applied to remove low coverage genes with less than one count per million (33 reads on average) in two out of three replicates per condition. Samples were grouped by replicates, and an experimental design was chosen that used sample time and treatment (CPC, REF, MTA) as a combined environmental factor. To normalize the read counts for comparison purposes on sequencing depth and RNA composition, DESeq2 uses the median of ratios method to derive a scaling factor. Dividing the original read counts by the scaling factor normalized count values are generated. To model count-based expression data, DESeq2 uses a negative binomial model as a distribution assumption and fits the expression data for each gene to a generalized linear model (GLM). No outliers were observed in the three biological replicates using Pearson correlation. Resulting *P*-values were adjusted for multiple testing according to [47] to control the false discovery rate (FDR). Genes were identified as significantly differentially expressed by applying FDR adjusted *P*-values < 0.05 and a log<sub>2</sub>-fold-change  $\geq |1|$ . A principal component analysis was used to display the sample to sample distances calculated within the DESeq2 package using the function plotPCA.san available on Github (<https://gist.github.com/sansense/3399064897f1252d31b23ea5178c033c>). Raw counts and processed data can be found in the supplementary information. Data analysis was performed using the free statistical computing environment R v. 3.6.2.

## Results

### The effect of MTA addition depends on its concentration

MTA was added in different concentrations (c1: 150  $\mu\text{M}$ , c2: 250  $\mu\text{M}$ , c3: 350  $\mu\text{M}$ , c4: 450  $\mu\text{M}$ ) to the cells after 48-h cultivation time. All MTA treated cultures showed reduced VCD and growth rate (regarding 48–120 h) dependent on the concentration (Fig. 1). Higher MTA amounts reduced VCD and growth rate stronger than low additions. The lowest concentration c1 led to 30% reduction of growth rate whereas the two highest concentrations c3 and c4 halved it. c2 reduced growth rate by 44%. However, maximum inhibition trends were observed for c3 and c4: The reduction of growth

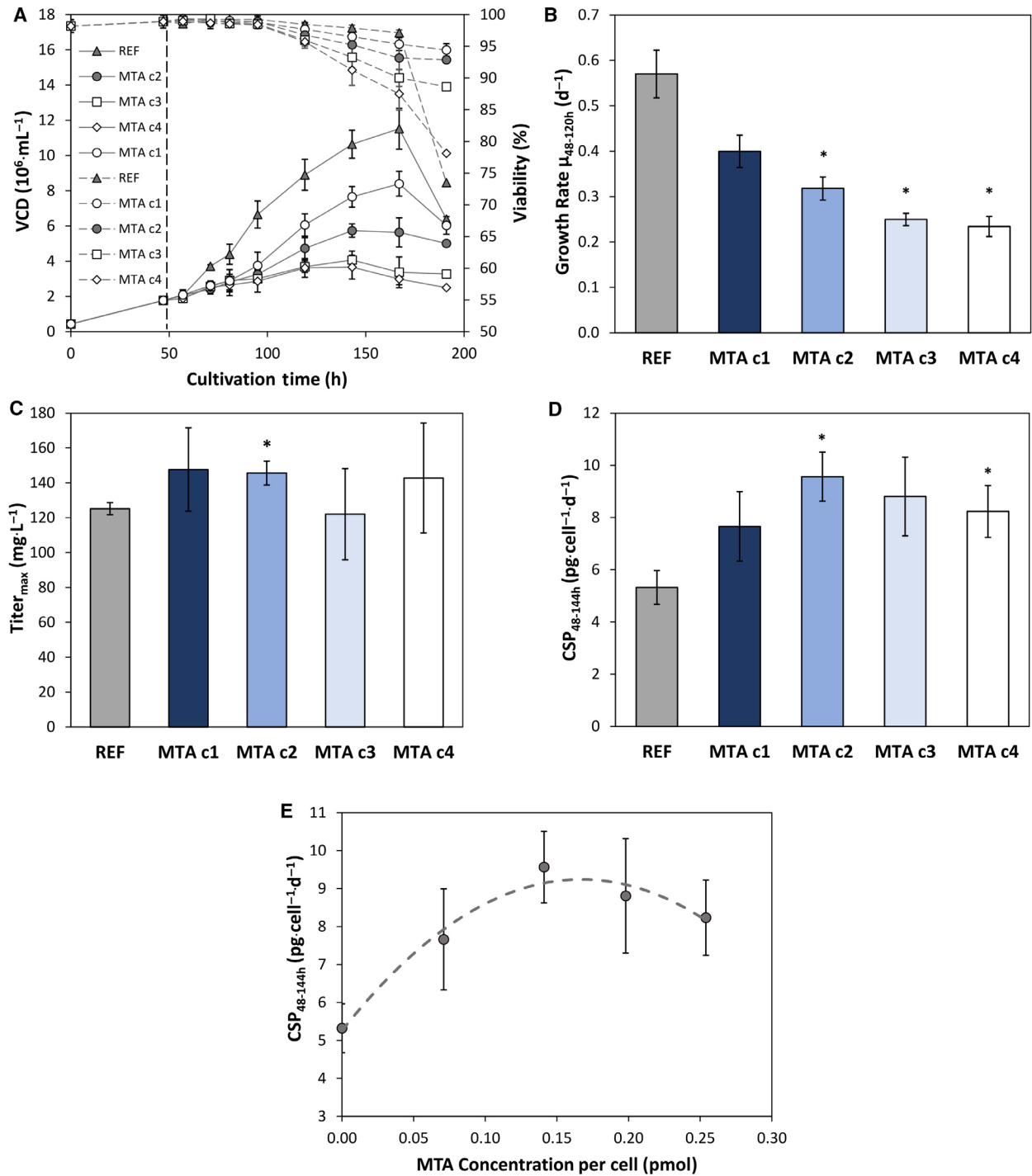


**Fig. 1.** (A) VCD [ $10^6$  cells·mL<sup>-1</sup>] and viability [%] of MTA supplemented cells and reference (REF▲). MTA was added at 48 h in different concentrations: c1 150  $\mu$ M(○), c2 250  $\mu$ M(●), c3 350  $\mu$ M(□), c4 450  $\mu$ M(◇). (B) Growth rate per day [d<sup>-1</sup>] regarding the time interval 48–120 h. (C) Maximum antibody titer [mg·L<sup>-1</sup>]. (D) CSP [pg·cell<sup>-1</sup>·d<sup>-1</sup>] regarding the time interval 48–144 h. (E) CSP [pg·cell<sup>-1</sup>·d<sup>-1</sup>] between 48–144 h plotted against the MTA amount per cell [pmol] at 48 h. Error bars show standard deviations of biological duplicates. Significance (to REF) was tested with a t-test; \* < 0.05.

rate plateaued. Addition of MTA with c1, c2 and c3 demonstrated a higher viability in the last cultivation phase compared to REF. By trend, analysis of maximum product titers unraveled slightly elevated amounts of antibodies for all MTA additions except c3 (Fig. 1). Calculating cell-specific productivities revealed boosted CSPs for all MTA additions between 48–144 h. Concentration c2 showed the best performance (+79.7%) and c1 the lowest (+43.9%). Fitting the CSPs to a 2<sup>nd</sup> order polynomial function reveals optimum MTA addition of 0.167 pmol<sub>MTA</sub>·cell<sup>-1</sup> at 48 h (Fig. 1). The equivalent medium concentration of 295.59  $\mu$ M is close to the tested level of c2 with the highest CSP in the experimental series.

Cell cycle phase distribution revealed the concentration-dependent effect of MTA (Fig. 2). A common preculture split right before MTA (48 h) served as a starting point. Half a day after MTA addition, cells accumulated in G1-phase. 12 h later, i.e. one day after

addition, the number of cells in S-phase increased for the sake of those in G1-phase. At 84 h (36 h after addition) cells in G2-phase dominated and the number of cells in G1-phase kept dropping. Two days after addition the ratios started to normalize. Cultures with c3 and c4 approached REF conditions whereas c1 and c2 kept an elevated fraction of cells in G1-phase. The different MTA concentrations caused diverse effects on cell size. In general, cell size was smallest in REF and largest after c3 and c4 addition. By trend, all MTA treated cells kept enlarged cell size on different levels compared to REF.

### The effect of MTA is time-dependent

In another experimental series, cells received 0.167 pmol<sub>MTA</sub>·cell<sup>-1</sup> after 48, 84 and 108 h (Fig. 3). The rise of VCD slowed down after each MTA addition. Growth reduction was more pronounced the

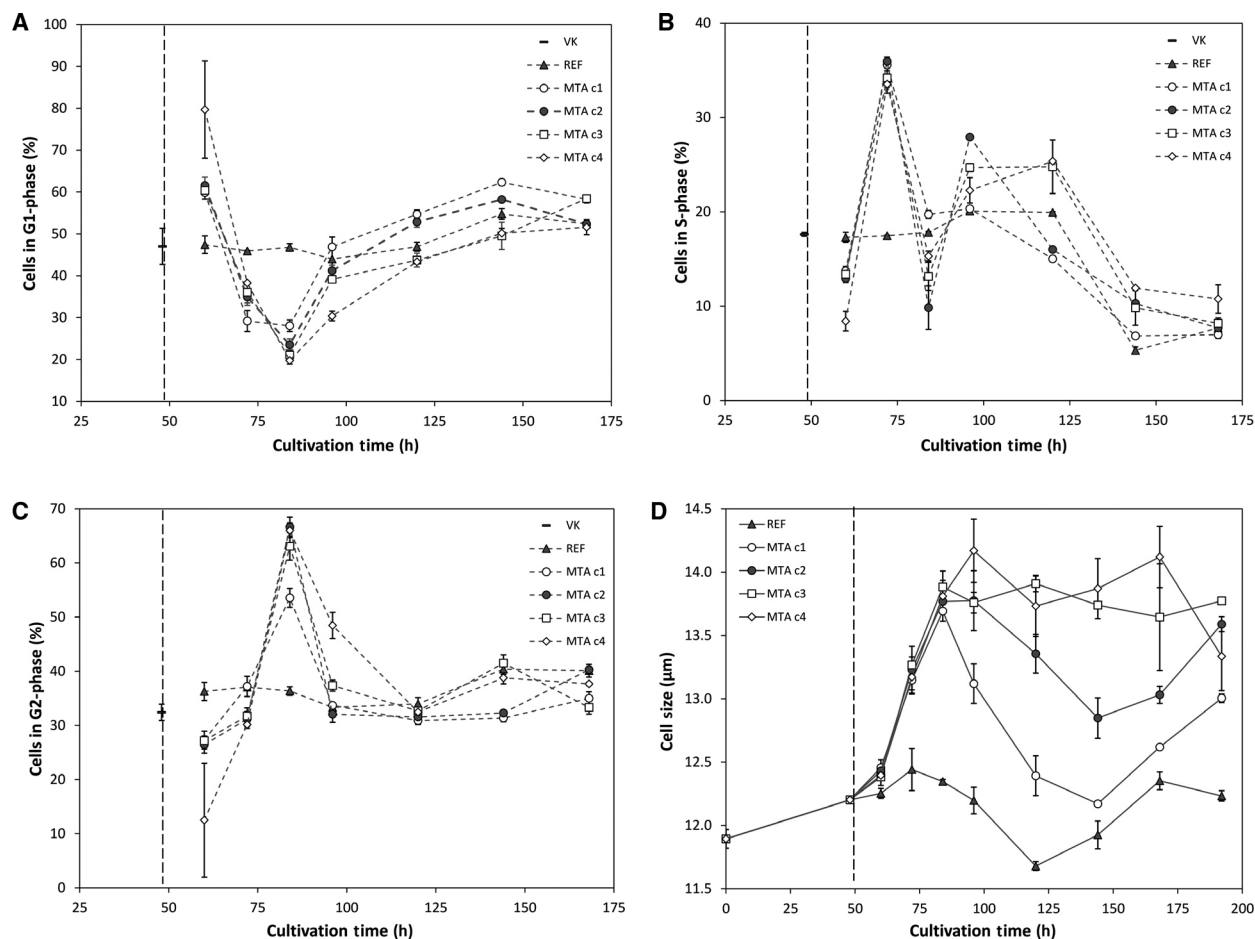


**Fig. 2.** Cell cycle phase distribution (A–C) [%] and average cell size (D) [ $\mu$ m] of MTA supplemented cells, reference (REF▲) and common preculture (▲). MTA was added at 48 h in different concentrations: c1 150  $\mu$ M(O) c2 250  $\mu$ M(●), c3 350  $\mu$ M(□), c4 450  $\mu$ M(◇). Error bars show standard deviations of biological duplicates.

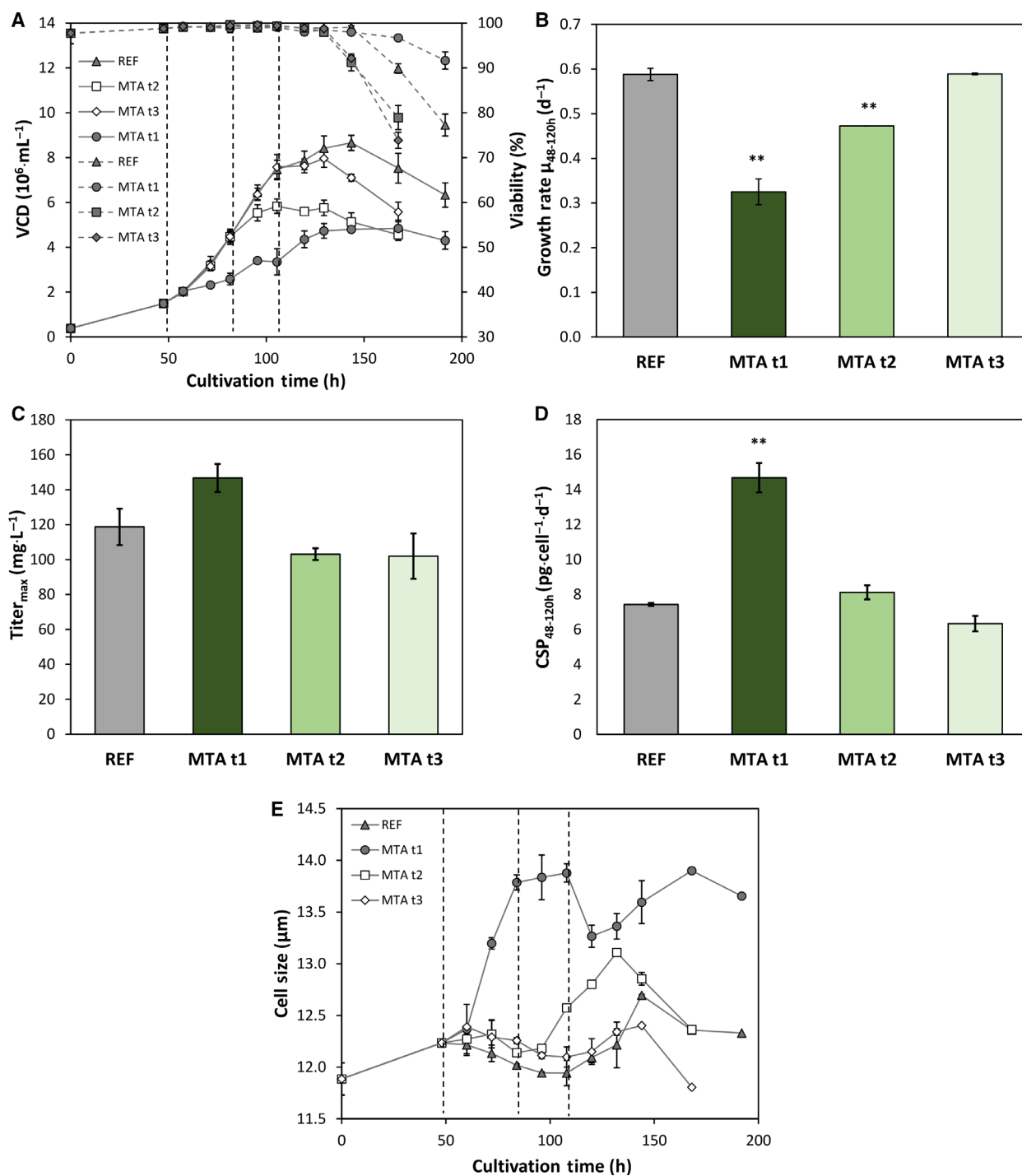


**Fig. 3.** (A) VCD [ $10^6$  cells·mL<sup>-1</sup>] and viability [%] of MTA supplemented cells and reference (REF▲). MTA was added with  $0.167 \text{ pmol}_{\text{MTA}} \text{ per cell}$  at 48, 84 or 108 h: MTA t1 48 h (●), MTA t2 84 h (□), MTA t3 108 h (◇). (B) Growth rate per hour [ $\text{d}^{-1}$ ] regarding the time interval 48–120 h. (C) Maximum antibody titer [ $\text{mg L}^{-1}$ ]. (D) CSP [ $\text{pg}\cdot\text{cell}^{-1}\cdot\text{d}^{-1}$ ] regarding the time interval 48–120 h. (E) Average cell size [ $\mu\text{m}$ ]. Error bars show standard deviations of biological duplicates. Significance (to REF) was tested with  $t$ -test; \*\* < 0.01.

earlier MTA was added with the 48-h-shot showing the slowest post-MTA growth rate. However, the viability of the treated cells remained even higher than

the performance of REF. Regarding growth rate the 48-h-addition caused 44.7% reduction whereas the 84-h-addition only reduced growth by 19.6%. Late

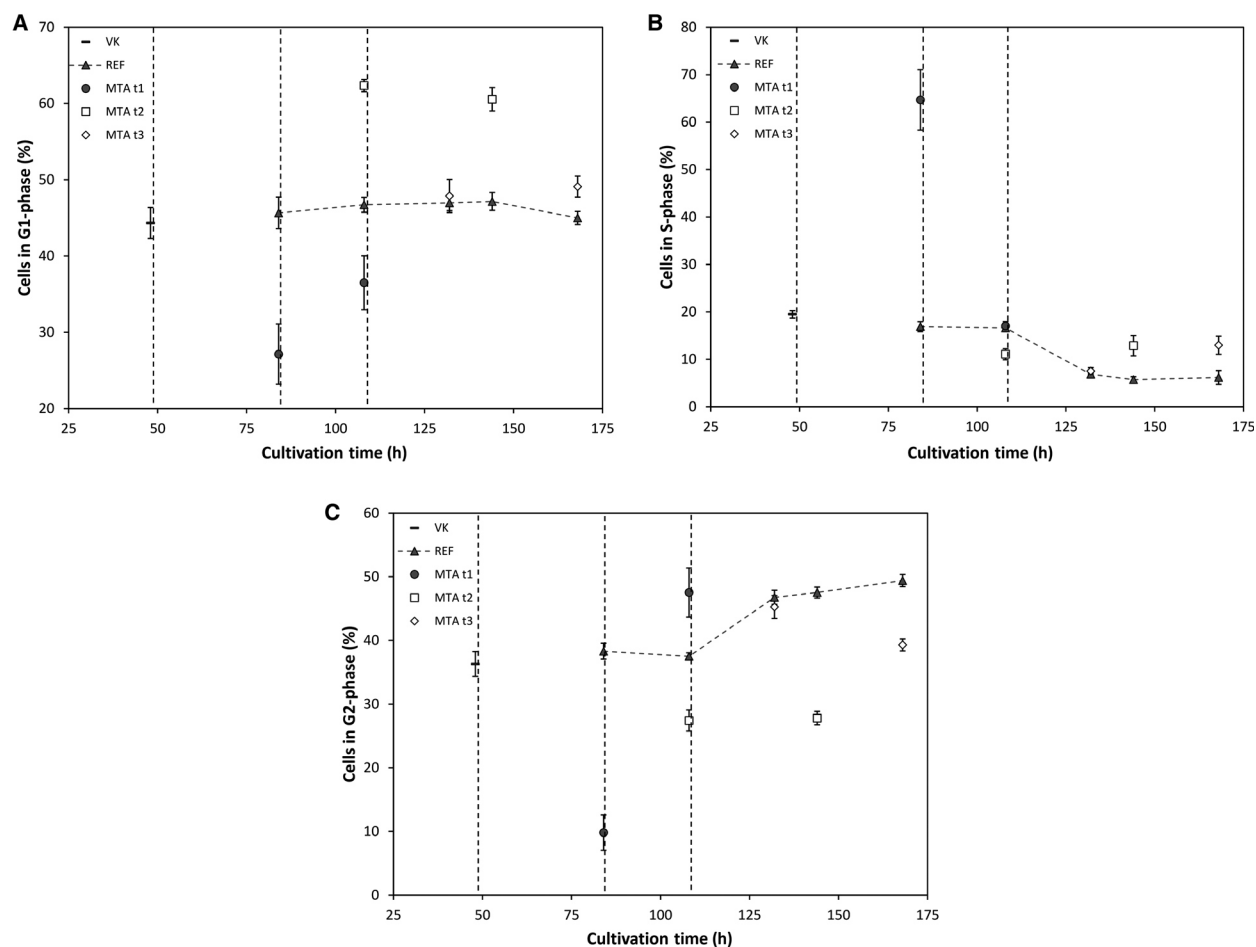


**Fig. 4.** Cell cycle phase distribution (A–C) [%] of MTA supplemented cells, reference (REF▲) and common preculture (VK▲). MTA was added with  $0.167 \text{ pmol}_{\text{MTA}} \text{ per cell}$  at 48, 84 or 108 h: MTA t1 48 h (●), MTA t2 84 h (□), MTA t3 108 h (◇). Error bars show standard deviations of biological duplicates.

addition (108 h) did not cause any growth difference compared to REF. Maximum antibody titers [ $\text{mg} \cdot \text{L}^{-1}$ ] did not increase after MTA additions at 84 and 108 h (Fig. 3) but rose after 48 h. The trend is even more pronounced with respect to CSPs. The 48-h-supplementation almost doubled CSP (+97.4%) compared to REF whereas later MTA treatments showed no effects. By analogy, cell size raises the most when MTA was added at 48 h.

Cell cycle phase distributions and cell sizes are displayed in Fig. 4. Again, highest impact was found for 48-h-cultures whereas later MTA addition did not reveal strong differences compared to REF. Early supplementation caused increasing cell fractions in S-phase and decreasing percentages in G1- and G2-phase 36 h after addition. 60 h after addition, the partition of cells in G2-phase increased and there were still less cells in G1-phase.

### Monitoring transcriptional responses after MTA addition

The impact of MTA on the transcriptome was evaluated via differential gene expression (DEG) analysis based on RNA sequencing. mRNAs of biological triplicates supplemented with MTA were compared at different time points (60, 72, 84, 96, 144 h) to REF. Around 91% of total variance is covered by two principal components (PC) clearly grouping biological triplicates of equal sampling points. Apparently, cultivation time is represented by PC1 and MTA addition by PC2 (Fig. 5). In total, 122 DEGs were identified according to the constraints  $\log_2\text{-fold-change} \geq |1|$  and adjusted  $P\text{-value} \leq 0.05$ . Downregulation of genes occurred mostly 12–36 h after addition (60 h: 1, 72 h: 8, 84 h: 12, 96 h: 3, 144 h: 1) (Fig. 6). Later, i.e. 84 h process time, upregulation of genes dominated DEGs

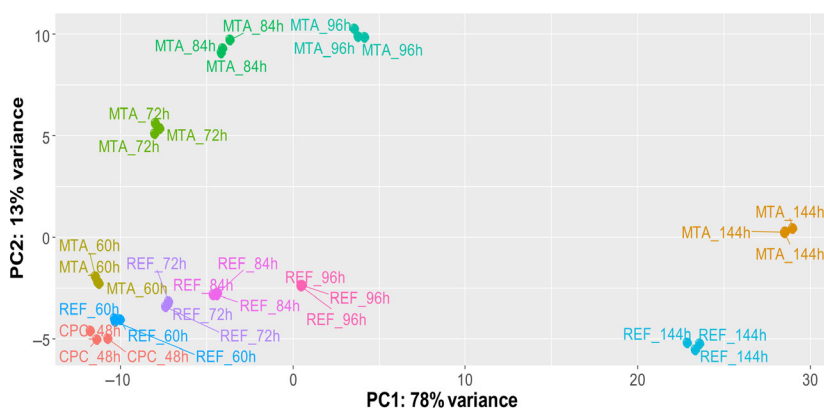


**Fig. 5.** Principal component (PC) analysis of the transcriptome samples taken in the experiment. The two main principal components are cultivation time (PC1) and condition (MTA treatment, PC2). Samples were taken in the common preculture (CPC) at 48-h cultivation time and after MTA addition (final concentration: 250  $\mu$ M) at the cultivation time points 60, 72, 84, 96 and 144 h. Reference (REF) cultures received the equal volume of water to avoid dilution effects.

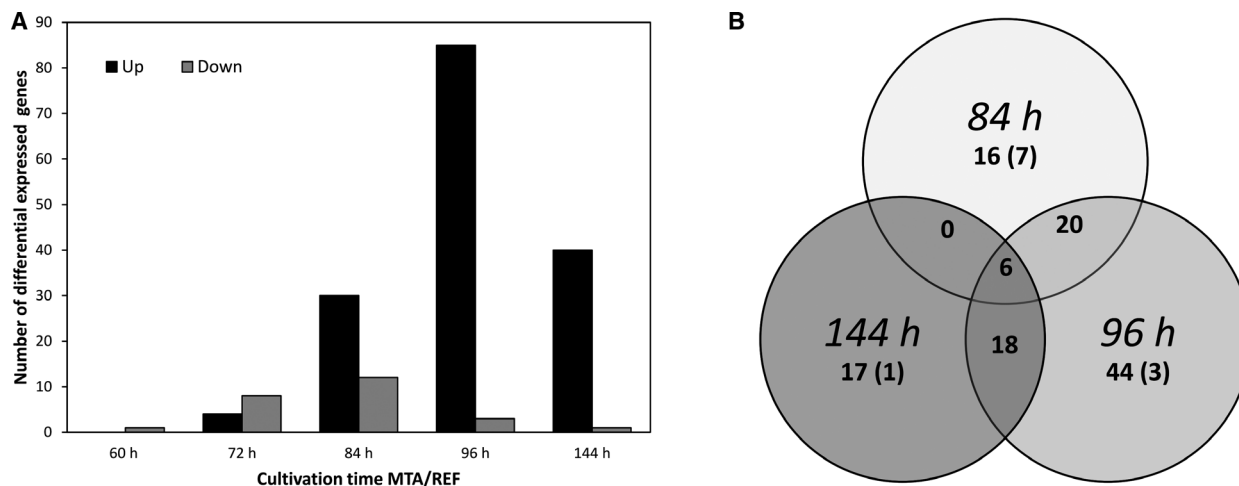


**Fig. 6.** (A) Analysis of differential expressed genes (DEGs) ( $\log_2$ -fold-change  $\geq |1|$  and  $P$ -value  $\leq 0.05$ ) throughout the experiment. MTA supplemented cells (MTA) were compared to REF. Grey bars indicate downregulated and black bars show upregulated genes at different sampling time points. (B) Venn diagram shows overlap of DEGs at 84 h–96 h–144 h. Numbers display all DEGs with the number of downregulated genes in brackets.

by far (60 h: 0, 72 h: 4, 84 h: 30, 96 h: 85, 144 h: 40). The Venn diagram comprising DEGS at 84 h–96 h–144 h reveals 6 commonly upregulated genes compared to REF. All DEGs that were significantly up- or downregulated at more than one sampling time point are listed in Table 1.

Four genes of the six DEGs observed at 84 h–96 h–144 h are annotated: *Aqp1*, *Lcp1*, *Plau* and *St14* whereas two are unknown loci. Aquaporin 1 (*Aqp1*) is a commonly amplified water channel. *Lcp1* codes for plastin, an actin-binding cellular component. Plasminogen activator (*Plau*) and matriptase (*St14*) are serine proteases.

A lot of genes are differentially expressed at two time points after MTA addition. 12 and 24 h after MTA addition (72 h–84 h) two annotated genes are differentially expressed: Adenomatous polyposis coli protein 2 (*APC2*), a gene transcription regulator is

downregulated whereas *Il11* (interleukin-11) is upregulated. 24 and 36 h after MTA addition (84 h–96 h) 13 additional upregulated DEGs were observed: (a) the small G-protein (ras) associated domain-containing protein 6 (*Rassf6*) which is associated with cellular apoptosis, (b) the epidermal growth factor receptor (*Egfr*) involved in proliferation, (c) interleukin-17F (*Il17f*), a pro-inflammatory cytokine, (d) the lysine-specific demethylase hairless (*Hr*), a histone demethylase, (e) deoxyribonuclease gamma (*Dnase1l3*), an enzyme with hydrolytic DNA activity. Nucleus associated upregulated transcripts are: (f) *Arnt2* coding for Aryl hydrocarbon receptor nuclear translocator 2, a transcription factor and (g) the protein FAM110C (*Fam110c*) known for interactions with microtubules and nucleus. Other upregulations are (h) phosphatidate phosphatase LPIN3 (*Lpin3*) involved in lipid synthesis, (i) monoacylglycerol lipase ABHD6 (*Abhd6*) forming

**Table 1.** Selection of differential expressed genes. Downregulated genes are highlighted in grey.

Cultivation time	Gene name	Encoded protein
84 h–96 h–144 h	<i>Plau</i>	Urokinase-type plasminogen activator
	<i>Aqp1</i>	Aquaporin-1
	<i>Lcp1</i>	Plastin-2
	<i>St14</i>	Suppressor of tumorigenicity 14 protein homolog
72 h–84 h	<i>Apc2</i>	Adenomatous polyposis coli protein 2
	<i>Il11</i>	Interleukin-11
84 h–96 h	<i>Rassf6</i>	Ras association domain-containing protein 6
	<i>Abhd6</i>	monoacylglycerol lipase ABHD6
	<i>Hr</i>	Lysine-specific demethylase hairless
	<i>Dnase1l3</i>	Deoxyribonuclease gamma
	<i>Il17f</i>	Interleukin-17F
	<i>Lpin3</i>	Phosphatidate phosphatase LPIN3
	<i>Arnt2</i>	Aryl hydrocarbon receptor nuclear translocator 2
	<i>Sh2d1b</i>	SH2 domain-containing protein 1B
	<i>Fam110c</i>	Protein FAM110C
	<i>Cd53</i>	Leukocyte surface antigen CD53
	<i>Oasl</i>	2'-5'-oligoadenylate synthase-like protein 2
	<i>Egfr</i>	Epidermal growth factor receptor
	<i>St8sia6</i>	Alpha-2,8-sialyltransferase 8F
	96 h–144 h	<i>Add2</i>
<i>Loxl2</i>		Lysyl oxidase homolog 2
<i>Il7r</i>		Interleukin-7 receptor subunit alpha
<i>Tmprss11f</i>		Transmembrane protease serine 11F
<i>Adgrd1</i>		Adhesion G-protein coupled receptor D1
<i>Sema4d</i>		Semaphorin-4D
<i>Akr1d1</i>		Aldo-keto reductase family 1 member D1
<i>Mpeg1</i>		Macrophage-expressed gene 1 protein
<i>Pglyrp2</i>		N-acetylmuramoyl-L-alanine amidase

intraluminal vesicles and (j) the glycosylating protein alpha-2,8-sialyltransferase 8F (*St8sia6*). Genes linked to immune functions are upregulated, including (k) the signaling factor SH2 domain-containing protein 1B (*Sh2d1b*), (l) the tetraspanin leukocyte surface antigen CD53 (*CD53*), and (m) the viral response component 2'-5'-oligoadenylate synthase-like protein 2 (*Oasl*).

## Discussion

### Optimum MTA addition levels during growth are 250–300 $\mu\text{M}$ and stimulate cell cycle arrest, increase cell size and ensure high viability

We investigated concentration and time dependency of MTA addition in CHO cell cultures to elucidate the

impact of these factors on the CSPs. Different effector levels at 48-h cultivation time (Figs 1 and 2) revealed clear concentration dependency. Effects on growth, cell cycle and cell size were affected by different concentrations plateauing > 350  $\mu\text{M}$ . CSP maxed out at about 250–300  $\mu\text{M}$ . Furthermore, the two highest concentrations c3 and c4 even disclosed negative effects as decreasing viability and CSP. Noteworthy, effector levels < 350  $\mu\text{M}$  ensured higher viabilities and higher CSPs than REF.

Similar dependencies of effector levels on CHO growth were observed for catechins trapping cells in S-phase [48]. By analogy, treatment of cells with AMP is concentration-dependent and resulted in S-phase accumulation. As a consequence, CSP increased [49].

Further investigations on optimum MTA additions showed that supplementation during exponential growth is most beneficial (Fig. 3). Coinciding growth-dependent cell size increase may further support the effect. Apparently, the combination of cell cycle arrest, high viability, and increasing cell size defines a key scenario for boosting CSP.

Many studies outlined the boosting effect of temporary cell cycle arrest on CSP although independent of a specific cell cycle phase [24,28,32,41,50,51]. In several CHO cell lines, CSP and cell size correlated [28]. However, cell size increase is linked to cell cycle [25–27] which makes the independent study of each impact hardly possible. Consequently, the combinatorial benefit of cell cycle arrest with increased cell size, still ensuring high cell viability, should be concluded as beneficial for high CSP. Moreover, impaired cell growth yields less biomass formation and allows to use redundant energy and metabolic precursors for protein production [52]. Apparently, MTA initiates the beneficial combination when an optimum effector level of 250–300  $\mu\text{M}$  is installed during exponential growth in the medium.

### Fundamental cell engineering strategies

Cell engineering for improved CSPs focus on engineering apoptosis, metabolism, cell cycle and protein secretion [53]. Transcript studies of low and high producers revealed that high recombinant protein formation negatively correlates with gene expression of cell cycle, metabolic RNA and protein processes [54]. Enhanced gene expression was observed in protein folding, cell survival, cell growth, vesicular trafficking and cytoskeleton organization [55]. As the map of functional gene annotations is still fragmented for CHO, identification of promising novel gene functions is necessary.

### The role of the cytoskeleton part actin for CSP after MTA addition

The water importer aquaporin 1 (encoded by *Aqp1*) was upregulated 84 h–96 h–144 h after MTA addition (Table 1) coinciding with increased cell size (Figs 2 and 3). This observation was seen in stress situations [56,57] (e.g. hyperosmolarity) that caused increased intracellular protein content and CSP [58,59]. In this experiment, the increased need of membrane molecules as glycerolipids could be satisfied by the upregulated phosphatide phosphatase LPIN3 (*Lpin3*) at 84 h–96 h. Co-upregulation of *Lcp1* and *St14* occurred (84 h–96 h–144 h) coding for the actin-associated enzyme plastin and matriptase [60,61]. Noteworthy, actin microfilaments, microtubules and intermediate filaments compose the cytoskeleton which takes over crucial functions for cell shape, protein synthesis [62], transport [63] and secretion [64,65]. Dinnis *et al.*, [66] observed that actin, tubulin, or the actin-binding cofilin demonstrated an important role in protein transport and secretion of high producers. Selection procedures for high producers revealed according to data with enhanced gene expression of actin-related proteins [67]. Recently, Berger *et al.*, [55] identified DEGs involved in cytoskeleton organization and vesicular trafficking as *Rassf9* that is linked to endosome recycling and is a trafficking regulator [68] in high producers. Our studies revealed upregulated genes (84 h–96 h) associated with intraluminal vesicles (monoacylglycerol lipase ABHD6 (*Abhd6*)) and protein processing (glycosylation) (alpha-2,8-sialyltransferase 8F (*St8sia6*)) in the Golgi (Table 1). Actin cooperates with polymerases via pre-initiation complex influencing gene expression [69,70] and is involved in cellular response to DNA damaging agents and toxins in CHO cells [71]. Next to the abovementioned actin-related genes, *Add2* (beta-arcabducin) at 96 h–144 h [72] and *Fscn1* (fascin) at 96 h [73] were upregulated in our data. Right after MTA addition (72 h–84 h) adenomatous polyposis coli protein 2 (*APC2*), a transcription factor linked with actin [74] is downregulated. It is associated with microtubules and interphase [75] as protein FAM110C (*Fam110c*, upregulated at 84 h–96 h) that impairs cell cycle progression [76].

Several gene expressions related to cytoskeleton parts either for transport and secretion or cell growth are differentially regulated in our data highlighting their importance in the CSP enhancing mechanism of MTA.

### Genes encoding for cellular survival, transcriptional regulation and immune system

Plasminogen activator (*Plau*) upregulated at 84 h–96 h–144 h is a growth factor, mitogen and apoptotic reducer [77,78]. Another upregulated gene (84 h–96 h)

associated with cell growth, survival and transcription is the tumor-suppressor ras association domain-containing protein 6 (*Rassf6*) an important regulator of cell cycle arrest and apoptosis and whose upregulated family members were observed in high producers [55,79]. The transcription factor aryl hydrocarbon receptor nuclear translocator 2 (*Arnt2*) correlated with cell proliferation [80] was downregulated at 72 h–84 h. At 84 h–96 h *Dnase113* and *Egfr* were upregulated encoding deoxyribonuclease gamma (*Dnase113*) and epidermal growth factor receptor (EGFR), respectively. *Dnase113* is a apoptosis-related factor [81] whereas EGFR is associated with DNA synthesis and proliferation [82]. *Atf5* (cyclic AMP-dependent transcription factor ATF-5) was upregulated at 84 h which agrees with studies searching for transcription and protein production regulators in CHO cells [83].

Next to growth and cellular survival factors, DEGs for histone proteins influenced transcription and replication [79]. Upregulation occurred for lysine-specific demethylase hairless (*Hr*), a histone demethylase (84 h–96 h), that interacts with cell cycle regulation [84]. Additionally at 96 h–144 h, lysyl oxidase homolog 2 (*Loxl2*) and chromodomain-helicase-DNA-binding protein 5 (*Chd5*), both histone modifying enzymes are upregulated [85,86].

Genes involved in immune functions as SH2 domain-containing protein 1B (*Sh2d1b*), CD53 (*CD53*), viral response component 2'-5'-oligoadenylate synthase-like protein 2 (*Oasl*), interleukin-17F (IL17f) (84 h–96 h) and interleukin-11 (IL11) (72 h–84 h) were upregulated after MTA addition demonstrating a connection to the immune system and its connected signaling pathways [19].

DEGs regarding growth, survival and transcription including DNA modification point out the multi-level effects of MTA that enhanced viability and CSP.

### Concluding remarks

MTA, the degradation product of SAM, boosts CSPs in an anti-IL-8-producing CHO-DP12, presumed that optimum MTA levels of 250–300  $\mu\text{M}$  are installed for exponentially growing cells. Indeed, the rise of VCDs slowed down but CSPs increased up to +97%, even ensuring cell viabilities better than REF. Moreover, titers were comparable to REF in the best MTA addition case. These improvements coincided with cell cycle modulations, i.e. accumulations in S-phase followed by elevated cell numbers in G2-phase which both levelled out during cultivation. DEGs clearly showed upregulations of cytoskeleton, growth, survival and transcription-associated genes as predominant regulation patterns. Although



those DEGs may be qualified as a particular response on MTA next to its function as polyamine synthesis inhibitor that correlate with findings of other independent studies outlining that actin-interacting proteins, cell proliferation and histone proteins are promising candidates for further cell engineering.

With MTA, a native compound is identified that clearly boosts CSPs after 'simple' medium addition. It is the key degradation product of SAM whose price will reduce with its microbial production [87]. MTA initiates regulation programs that deserve further investigations, not only because they may offer even further improvements but also because major findings may be translated to other production cell lines. Apparently, MTA addition positively stimulates cell cycle arrest, cytoskeleton and cell survival genes concomitantly, thereby addressing key topics of current cell line engineering. These findings should be considered for process intensification studies, especially for perfusion processes where improvements of CSPs are an important goal of optimization.

## Acknowledgement

The authors gratefully acknowledge the funding by the Bundesministerium für Bildung und Forschung (BMBF, Funding Number 031L0077A). The authors would like to thank the group of Computational Biology at the Institute of Biochemical Engineering for the use of the Galaxy-Server. Open access funding enabled and organized by ProjektDEAL.

## Conflict of interest

The authors declare no conflict of interest.

## Author contributions

NV and RT designed the experiment. NV conducted the experiments and data analysis. JZ analyzed transcriptome data. NV and JZ interpreted transcriptome data. NV, JZ and RT wrote the manuscript.

## Data accessibility

Processed transcriptome data is accessible in the supplemental part. Further data will be available from the corresponding author upon reasonable request.

## References

- Walsh G (2018) Biopharmaceutical benchmarks 2018. *Nat Biotechnol* **36**, 1136–1145.

- Reinhart D, Damjanovic L, Kaisermayer C and Kunert R (2015) Benchmarking of commercially available CHO cell culture media for antibody production. *Appl Microbiol Biotechnol* **99**, 4645–4657.
- Schaub J, Clemens C, Schorn P, Hildebrandt T, Rust W, Mennerich D, Kaufmann H and Schulz TW (2010) CHO gene expression profiling in biopharmaceutical process analysis and design. *Biotechnol Bioeng* **105**, 431–438.
- Wurm FM (2004) Production of recombinant protein therapeutics in cultivated mammalian cells. *Nat Biotechnol* **22**, 1393–1398.
- Zhang H, Wang H, Liu M, Zhang T, Zhang J, Wang X and Xiang W (2013) Rational development of a serum-free medium and fed-batch process for a GS-CHO cell line expressing recombinant antibody. *Cytotechnology* **65**, 363–378.
- Becker M, Junghans L, Teleki A, Bechmann J and Takors R (2019) Perfusion cultures require optimum respiratory ATP supply to maximize cell-specific and volumetric productivities. *Biotechnol Bioeng* **116**, 951–960.
- Williams-Ashman HG, Seidenfeld J and Galletti P (1982) Trends in the biochemical pharmacology of 5'-deoxy-5'-methylthioadenosine. *Biochem Pharmacol* **31**, 277–288.
- Pegg AE (1988) Polyamine metabolism and its importance in neoplastic growth and as a target for chemotherapy. *Cancer Res* **48**, 759–774.
- Martínez-Chantar ML, Latasa MU, Varela-Rey M, Lu SC, García-Trevijano ER, Mato JM and Avila MA (2003) L-methionine availability regulates expression of the methionine adenosyltransferase 2A gene in human hepatocarcinoma cells. Role of S-adenosylmethionine. *J Biol Chem* **278**, 19885–19890.
- Pascale RM, Simile MM, De Miglio MR and Feo F (2002) Chemoprevention of hepatocarcinogenesis: S-adenosyl-L-methionine. *Alcohol* **27**, 193–198.
- Ansorena E (2002) S-adenosylmethionine and methylthioadenosine are antiapoptotic in cultured rat hepatocytes but proapoptotic in human hepatoma cells. *Hepatology* **35**, 274–280.
- Lee SH and Cho YD (1998) Induction of apoptosis in leukemia U937 cells by 5'-deoxy-5'-methylthioadenosine, a potent inhibitor of protein carboxylmethyltransferase. *Exp Cell Res* **240**, 282–292.
- Maher PA (1993) Inhibition of the tyrosine kinase activity of the fibroblast growth factor receptor by the methyltransferase inhibitor 5'-methylthioadenosine. *J Biol Chem* **268**, 4244–4249.
- Riscoe MK, Tower PA and Ferro AJ (1984) Mechanism of action of 5'-methylthioadenosine in S49 cells. *Biochem Pharmacol* **33**, 3639–3643.
- Oredsson SM (2003) Polyamine dependence of normal cell-cycle progression. *Biochem Soc Trans* **31**, 366–370.

- 16 Alm K and Oredsson SM (2000) The organization of replicon clusters is not affected by polyamine depletion. *J Struct Biol* **131**, 1–9.
- 17 Subhi AL, Diegelman P, Porter CW, Tang B, Lu ZJ, Markham GD and Kruger WD (2003) Methylthioadenosine phosphorylase regulates ornithine decarboxylase by production of downstream metabolites. *J Biol Chem* **278**, 49868–49873.
- 18 Law RE, Stimmel JB, Damore MA, Carter C, Clarke S and Wall R (1992) Lipopolysaccharide-induced NF- $\kappa$ B activation in mouse 70Z/3 pre-B lymphocytes is inhibited by mevinolin and 5'-methylthioadenosine: roles of protein isoprenylation and carboxyl methylation reactions. *Mol Cell Biol* **12**, 103–111.
- 19 Hevia H, Varela-Rey M, Corrales FJ, Berasain C, Martínez-Chantar ML, Latasa MU, Lu SC, Mato JM, García-Trevijano ER and Avila MA (2004) 5'-Methylthioadenosine modulates the inflammatory response to endotoxin in mice and in rat hepatocytes. *Hepatology* **39**, 1088–1098.
- 20 Mowen KA, Tang J, Zhu W, Schurter BT, Shuai K, Herschman HR and David M (2001) Arginine methylation of STAT1 modulates IFN $\alpha$ / $\beta$ -induced transcription. *Cell* **104**, 731–741.
- 21 Verhagen N, Teleki A, Heinrich C, Schilling M, Unsöld A and Takors R (2020) S-adenosylmethionine and methylthioadenosine boost cellular productivities of antibody forming Chinese Hamster ovary cells. *Biotechnol Bioeng* **117**, 3239–3247.
- 22 Sunley K and Butler M (2010) Strategies for the enhancement of recombinant protein production from mammalian cells by growth arrest. *Biotechnol Adv* **28**, 385–394.
- 23 Al-Rubeai M, Emery AN, Chalder S and Jan DC (1992) Specific monoclonal antibody productivity and the cell cycle-comparisons of batch, continuous and perfusion cultures. *Cytotechnology* **9**, 85–97.
- 24 Hendrick V, Winnepenninckx P, Abdelkafi C, Vandeputte O, Cherlet M, Marique T, Renemann G, Loa A, Kretzmer G and Werenne J (2001) Increased productivity of recombinant tissular plasminogen activator (t-PA) by butyrate and shift of temperature: a cell cycle phases analysis. *Cytotechnology* **36**, 71–83.
- 25 Ginzberg MB, Kafri R and Kirschner M (2015) On being the right (cell) size. *Science* **348**, 1245075-1–1245075-7.
- 26 Jorgensen P and Tyers M (2004) How cells coordinate growth and division. *Curr Biol* **14**, 1014–1027.
- 27 Tzur A, Kafri R, LeBleu VS, Lahav G and Kirschner MW (2009) Cell growth and size homeostasis in proliferating animal cells. *Science* **325**, 167–171.
- 28 Lloyd DR, Holmes P, Jackson LP, Emery AN and Al-Rubeai M (2000) Relationship between cell size, cell cycle and specific recombinant protein productivity. *Cytotechnology* **34**, 59–70.
- 29 Hammond S and Lee KH (2012) RNA interference of cofilin in Chinese hamster ovary cells improves recombinant protein productivity. *Biotechnol Bioeng* **109**, 528–535.
- 30 Nishimiya D, Mano T, Miyadai K, Yoshida H and Takahashi T (2013) Overexpression of CHOP alone and in combination with chaperones is effective in improving antibody production in mammalian cells. *Appl Microbiol Biotechnol* **97**, 2531–2539.
- 31 Peng RW, Abellan E and Fussenegger M (2011) Differential effect of exocytic SNAREs on the production of recombinant proteins in mammalian cells. *Biotechnol Bioeng* **108**, 611–620.
- 32 Kaufmann H, Mazur X, Fussenegger M and Bailey JE (1999) Influence of low temperature on productivity, proteome and protein phosphorylation of CHO cells. *Biotechnol Bioeng* **63**, 573–582.
- 33 Furukawa K and Ohsuye K (1999) Enhancement of productivity of recombinant  $\alpha$ -amidating enzyme by low temperature culture. *Cytotechnology* **31**, 85–94.
- 34 Kantardjieff A, Jacob NM, Yee JC, Epstein E, Kok YJ, Philp R, Betenbaugh M and Hu WS (2010) Transcriptome and proteome analysis of Chinese hamster ovary cells under low temperature and butyrate treatment. *J Biotechnol* **145**, 143–159.
- 35 Jiang Z and Sharfstein ST (2008) Sodium butyrate stimulates monoclonal antibody over-expression in CHO cells by improving gene accessibility. *Biotechnol Bioeng* **100**, 189–194.
- 36 Prabhu A, Gadre R and Gadgil M (2018) Zinc supplementation decreases galactosylation of recombinant IgG in CHO cells. *Appl Microbiol Biotechnol* **102**, 5989–5999.
- 37 Coronel J, Klausing S, Heinrich C, Noll T, Figueredo-Cardero A and Castilho LR (2016) Valeric acid supplementation combined to mild hypothermia increases productivity in CHO cell cultivations. *Biochem Eng J* **114**, 101–109.
- 38 Ahn Y-H, Han K, Yoon SK and Song J (1999) Effect of glycine betaine as osmoprotectant on the production of erythropoietin by CHO cells in hyperosmotic serum free media culture. In *Animal Cell Technology: Basic & Applied Aspects* (Kitagawa Y, Matsuda T and Iijima S, eds), pp. 247–250. Kluwer Academic Publishers, Dordrecht.
- 39 Yang WC, Lu J, Nguyen NB, Zhang A, Healy NV, Kshirsagar R, Ryll T and Huang YM (2014) Addition of valproic acid to CHO cell fed-batch cultures improves monoclonal antibody titers. *Mol Biotechnol* **56**, 421–428.
- 40 Pfizenmaier J, Junghans L, Teleki A and Takors R (2016) Hyperosmotic stimulus study discloses benefits in ATP supply and reveals miRNA/mRNA targets to improve recombinant protein production of CHO cells. *Biotechnol J* **11**, 1037–1047.

- 41 Pfizenmaier J, Matuszczyk J-C and Takors R (2015) Changes in intracellular ATP-content of CHO cells as response to hyperosmolality. *Biotechnol Prog* **31**, 1212–1216.
- 42 Afgan E, Baker D, Batut B, Van Den Beek M, Bouvier D, Ech M, Chilton J, Clements D, Coraor N, Grüning BA *et al.* (2018) The Galaxy platform for accessible, reproducible and collaborative biomedical analyses: 2018 update. *Nucleic Acids Res* **46**, W537–W544.
- 43 Langmead B and Salzberg S (2013) Bowtie2. *Nat Methods* **9**, 357–359.
- 44 Anders S, Pyl PT and Huber W (2015) HTSeq-A Python framework to work with high-throughput sequencing data. *Bioinformatics* **31**, 166–169.
- 45 Love MI, Huber W and Anders S (2014) Moderated estimation of fold change and dispersion for RNA-seq data with DESeq2. *Genome Biol* **15**, 1–21.
- 46 Gentleman RC, Carey VJ, Bates DM, Bolstad B, Dettling M, Dudoit S, Ellis B, Gautier L, Ge Y, Gentry J *et al.* (2004) Bioconductor: open software development for computational biology and bioinformatics. *Genome Biol* **5**, R80.1–R80.16.
- 47 Benjamini Y and Hochberg Y (1995) Controlling the false discovery rate: a practical and powerful approach to multiple testing. *J R Stat Soc Ser B* **57**, 289–300.
- 48 Toronjo-Urquiza L, Acosta-Martin AE, James DC, Nagy T and Falconer RJ (2020) The use of catechins in Chinese hamster ovary cell media for the improvement of monoclonal antibody yields and a reduction of acidic species. *Biotechnol Prog* **36**, e2980.
- 49 Zou W, Browne SM and Al-Rubeai M (2019) Physiological alterations of GS-CHO cells in response to adenosine monophosphate treatment. *J Biotechnol* **294**, 49–57.
- 50 Al-Rubeai M and Emery AN (1990) Mechanisms and kinetics of monoclonal antibody synthesis and secretion in synchronous and asynchronous hybridoma cell cultures. *J Biotechnol* **16**, 67–85.
- 51 Kim WH, Kim YJ and Lee GM (2014) Gadd45-induced cell cycle G2/M arrest for improved transient gene expression in Chinese hamster ovary cells. *Biotechnol Bioeng* **19**, 386–393.
- 52 Fussenegger M, Mazur X and Bailey JE (1997) A novel cytoskeletal process enhances the ovary cells. *Biotechnol Bioeng* **55**, 927–939.
- 53 Fischer S, Handrick R and Otte K (2015) The art of CHO cell engineering: a comprehensive retrospect and future perspectives. *Biotechnol Adv* **33**, 1878–1896.
- 54 Sha S, Bhatia H and Yoon S (2018) An RNA-seq based transcriptomic investigation into the productivity and growth variants with Chinese hamster ovary cells. *J Biotechnol* **271**, 37–46.
- 55 Berger A, Le Fourn V, Masternak J, Regamey A, Bodenmann I, Girod P, Mermod N, Girod P and Mermod N (2020) Overexpression of transcription factor Foxa1 and target genes remedies therapeutic protein production bottlenecks in Chinese hamster ovary cells. *Biotechnol Bioeng* **117**, 1101–1116.
- 56 Katz U (1995) Cellular water content and volume regulation in animal cells. *Cell Biochem Funct* **13**, 189–193.
- 57 Lang F, Busch GL, Ritter M, Völkl H, Waldegger S, Gulbins E and Häussinger D (1998) Functional significance of cell volume regulatory mechanisms. *Physiol Rev* **78**, 247–306.
- 58 Sun Z, Zhou R, Liang S, McNeeley KM and Sharfstein ST (2004) Hyperosmotic stress in murine hybridoma cells: effects on antibody transcription, translation, posttranslational processing, and the cell cycle. *Biotechnol Prog* **20**, 576–589.
- 59 Khoo SHG and Al-Rubeai M (2009) Detailed understanding of enhanced specific antibody productivity in NS0 myeloma cells. *Biotechnol Bioeng* **102**, 188–199.
- 60 Delanote V, Vandekerckhove J and Gettemans J (2005) Plastins: versatile modulators of actin organization in (patho)physiological cellular processes. *Acta Pharmacol Sin* **26**, 769–779.
- 61 Kim C, Cho Y, Kang CH, Kim MG, Lee HS, Cho EG and Park D (2005) Filamin is essential for shedding of the transmembrane serine protease, epithin. *EMBO Rep* **6**, 1045–1051.
- 62 Hudder A, Nathanson L and Deutscher MP (2003) Organization of mammalian cytoplasm. *Mol Cell Biol* **23**, 9318–9326.
- 63 Ross JL, Ali MY and Warshaw DM (2008) Cargo transport: molecular motors navigate a complex cytoskeleton. *Curr Opin Cell Biol* **20**, 41–47.
- 64 Paavilainen VO, Bertling E, Falck S and Lappalainen P (2004) Regulation of cytoskeletal dynamics by actin-monomer-binding proteins. *Trends Cell Biol* **14**, 386–394.
- 65 Stamnes M (2002) Regulating the actin cytoskeleton during vesicular transport. *Curr Opin Cell Biol* **14**, 428–433.
- 66 Dinnis DM, Stansfield SH, Schlatter S, Smales CM, Alete D, Birch JR, Racher AJ, Marshall CT, Nielsen LK and James DC (2006) Functional proteomic analysis of GS-NS0 murine myeloma cell lines with varying recombinant monoclonal antibody production rate. *Biotechnol Bioeng* **94**, 830–841.
- 67 Pourcel L, Buron F, Arib G, Le Fourn V, Regamey A, Bodenmann I, Girod P and Mermod N (2020) Influence of cytoskeleton organization on recombinant protein expression by CHO cells. *Biotechnol Bioeng* **117**, 1117–1126.
- 68 Chen L, Johnson RC and Milgram SL (1998) P-CIP1, a novel protein that interacts with the cytosolic domain of peptidylglycine  $\alpha$ -amidating monooxygenase, is

- associated with endosomes. *J Biol Chem* **273**, 33524–33532.
- 69 Hofmann WA, Stojiljkovic L, Fuchsova B, Vargas GM, Mavrommatis E, Philimonenko V, Kysela K, Goodrich JA, Lessard JL, Hope TJ *et al.* (2004) Actin is part of pre-initiation complexes and is necessary for transcription by RNA polymerase II. *Nat Cell Biol* **6**, 1094–1101.
- 70 Philimonenko VV, Zhao J, Iben S, Dingová H, Kyselá K, Kahle M, Zentgraf H, Hofmann WA, de Lanerolle P, Hozák P *et al.* (2004) Nuclear actin and myosin I are required for RNA polymerase I transcription. *Nat Cell Biol* **6**, 1165–1172.
- 71 Sasaki Y, Itoh F, Kobayashi T, Kikuchi T, Suzuki H, Toyota M and Imai K (2002) Increased expression of T-fimbrin gene after DNA damage in CHO cells and inactivation of T-fimbrin by CPG methylation in human colorectal cancer cells. *Int J Cancer* **97**, 211–216.
- 72 Hughes CA and Bennett V (1995) Adducin: a physical model with implications for function in assembly of spectrin-actin complexes. *J Biol Chem* **270**, 18990–18996.
- 73 Edwards RA and Bryan J (1995) Fascins, a family of actin bundling proteins. *Cell Motil Cytoskeleton* **32**, 1–9.
- 74 Moseley JB, Bartolini F, Okada K, Wen Y, Gundersen GG and Goode BL (2007) Regulated binding of adenomatous polyposis coli protein to actin. *J Biol Chem* **282**, 12661–12668.
- 75 Mimori-Kiyosue Y, Shiina N and Tsukita S (2000) Adenomatous polyposis coli (APC) protein moves along microtubules and concentrates at their growing ends in epithelial cells. *J Cell Biol* **148**, 505–517.
- 76 Hauge H, Patzke S and Aasheim HC (2007) Characterization of the FAM110 gene family. *Genomics* **90**, 14–27.
- 77 De Petro G, Copeta A and Barlati S (1994) Urokinase-type and tissue-type plasminogen activators as growth factors of human fibroblasts. *Exp Cell Res* **213**, 286–294.
- 78 Shetty S, Gyetko MR and Mazar AP (2005) Induction of p53 by urokinase in lung epithelial cells. *J Biol Chem* **280**, 28133–28141.
- 79 Charaniya S, Karypis G and Hu WS (2009) Mining transcriptome data for function-trait relationship of hyper productivity of recombinant antibody. *Biotechnol Bioeng* **102**, 1654–1669.
- 80 Li W, Liang Y, Yang B, Sun H and Wu W (2015) Downregulation of ARNT2 promotes tumor growth and predicts poor prognosis in human hepatocellular carcinoma. *J Gastroenterol Hepatol* **30**, 1085–1093.
- 81 Shiokawa D and Tanuma S (2001) Characterization of human DNase I family endonucleases and activation of DNase  $\gamma$  during apoptosis. *Biochemistry* **40**, 143–152.
- 82 Normanno N, De Luca A, Bianco C, Strizzi L, Mancino M, Maiello MR, Carotenuto A, De Feo G, Caponigro F and Salomon DS (2006) Epidermal growth factor receptor (EGFR) signaling in cancer. *Gene* **366**, 2–16.
- 83 Chen K, Li D, Li H, Li B, Wang R, Jiang L, Huang L, Xu X, Li J, Teng F *et al.* (2019) Improved recombinant protein production by regulation of transcription and protein transport in Chinese hamster ovary cells. *Biotechnol Lett* **41**, 719–732.
- 84 Liu L, Kim H, Casta A, Kobayashi Y, Shapiro LS and Christiano AM (2014) Hairless is a histone H3K9 demethylase. *FASEB J* **28**, 1534–1542.
- 85 Herranz N, Dave N, Millanes-Romero A, Pascual-Reguant L, Morey L, Díaz VM, Lórenz-Fonfría V, Gutierrez-Gallego R, Jerónimo C, Iturbide A *et al.* (2016) Lysyl oxidase-like 2 (LOXL2) oxidizes trimethylated lysine 4 in histone H3. *FEBS J* **283**, 4263–4273.
- 86 Thompson PM, Gotoh T, Kok M, White PS and Brodeur GM (2003) CHD5, a new member of the chromodomain gene family, is preferentially expressed in the nervous system. *Oncogene* **22**, 1002–1011.
- 87 Li G, Li H, Tan Y, Hao N, Yang X, Chen K and Ouyang P (2020) Improved S-adenosyl-L-methionine production in *Saccharomyces cerevisiae* using tofu yellow serofluid. *J Biotechnol* **309**, 100–106.

## Supporting information

Additional supporting information may be found online in the Supporting Information section at the end of the article.

**Table S1.** List of differential expressed genes (FDR adjusted p-values  $\leq 0.05$  and a  $\log_2$ -fold-change  $\geq |1|$ ) between MTA treated cells and REF at different sampling points.

**Appendix S1.** Transcriptome analysis. Sample description, mapping statistics and counts.